MODELING AND ANALYSIS OF A DC POWER DISTRIBUTION SYSTEM IN 21ST CENTURY AIRLIFTERS

by

Konstantin P. Louganski

Thesis submitted to the faculty of the
Virginia Polytechnic Institute and State University
in partial fulfillment of the requirements for the degree of

Master of Science
in
Electrical Engineering

Dr. Dusan Borojevic, Chairman
Dr. Fred C. Lee
Dr. Douglas K. Lindner

September 30, 1999
Blacksburg, Virginia

Keywords: power distribution system, multi-level modeling, simulation, small-signal analysis, stability, regenerative energy, three-phase system, starter/generator, power converter, actuator, constant power load

MODELING AND ANALYSIS OF A DC POWER DISTRIBUTION SYSTEM IN 21ST CENTURY AIRLIFTERS

Konstantin P. Louganski

Abstract

A DC power distribution system (PDS) of a transport aircraft was modeled and analyzed using MATLAB/Simulink software. The multi-level modeling concept was used as a modeling approach, which assumes modeling subsystem of the PDS at three different levels of complexity. The subsystem models were implemented in Simulink and combined into the whole PDS model according to certain interconnection rules. Effective modeling of different scenarios of operation was achieved by mixing subsystem models of different levels in one PDS model. Linearized models were obtained from the nonlinear PDS model for stability analysis and control design.

The PDS model was used to examine the system stability and the DC bus power quality under bidirectional power flow conditions. Small-signal analysis techniques were employed to study stability issues resulting from subsystem interactions. The DC bus stability diagram was proposed for predicting stability of the PDS with different types of loads without performing an actual stability test based on regular stability analysis tools. Certain PDS configurations and operational scenarios leading to instability were identified. An analysis of energy transfer in the PDS showed that a large energy storage capacitor in the input filter of a flight control actuator is effective for reduction of the DC bus voltage disturbances produced by regenerative action of the actuator. However, energy storage capacitors do not provide energy savings in the PDS and do not increase its overall efficiency.

Acknowledgments

I would like to thank Dr. Dusan Borojevic for being my advisor and giving me an opportunity to pursue graduate study at Virginia Power Electronics Center (VPEC), presently the Center for Power Electronics Systems (CPES). I appreciate his broad views and enthusiasm in developing this subject, his encouragement and support, and his taking time to guide me through this work.

I would like to thank Dr. Fred C. Lee, director of CPES, for serving as my committee member and for putting so much energy into making CPES one of the best power electronics centers for research and education. It was my pleasure and honor to study and work there.

I would like to thank Dr. Douglas K. Lindner, the major investigator in this sponsored research, for reviewing this thesis and serving as my committee member. His valuable comments and attention to details helped me make this work better.

My special thanks to Mr. Sriram Chandrasekaran, who was always available to provide any help and to share his expertise.

I would like to recognize a contribution of Mr. George Korba and Ms. Catherine Frederick from Lockheed Martin Control Systems in Johnson City, New York, who provided actuator models for use in this research.

Finally, I give thanks to all my friends and family for their encouragement and support during this period of my life.

This work was supported by the Air Force Office of Scientific Research under Grant Number F49620-97-1-0254.

Contents

List of Figures

Chapter 1

Introduction

The “More Electric Initiative” is becoming a leading design concept for future aircrafts. It assumes using electrical energy instead of hydraulic, pneumatic, and mechanical means to power virtually all aircraft subsystems including flight control actuation, environmental control system, and utility functions. The concept offers advantages of reduced overall aircraft weight, reduced need for ground support equipment and maintenance personnel, increased reliability, and reduced susceptibility to battle damage in military applications [1-7]. Hence, all electrically powered subsystems become parts of an electric power distribution system (PDS), which unites all electrical sources and loads of an aircraft by means of a power distribution bus.

A PDS of a more-electric aircraft includes the following elements [2, 6, 7]: internal engine electric starter/generators, integrated power units, solid-state power controllers, electric-driven flight actuators, electric-actuated brakes, electric anti-icing system, fault-tolerant solid-state electrical distribution system, electric aircraft utility functions, electric-driven environmental and engine control. A PDS consists of two independent channels, according to the number of starter/generators in the aircraft. An auxiliary/emergency power unit contains an additional auxiliary starter/generator [6].

The generating system includes starter/generators, power control units, and a generator and system control unit [2]. Either three-phase synchronous machines [2] or switched-reluctance machines [7] may be used as starter/generators in a more-electric aircraft. The power control units are used to transform the “wild frequency” AC power produced by the synchronous

generators into 270V DC power [2]. This power is supplied to the DC power distribution bus, which consists of several different sections. The generator and system control unit controls the generators, power control units, and the DC busses. An auxiliary power unit and battery system provide power for starting the engines and emergency back-up.

Electromechanical (EMA) and electrohydrostatic (EHA) flight actuators are used in a more-electric aircraft instead of traditional hydraulic actuators with a central hydraulic system [2, 7]. The EMA and EHA employ DC brushless motors powered from the 270V DC distribution bus through DC-AC inverters.

Other loads of the PDS include environmental control system loads, utility loads, and avionics. Solid-state DC-DC and DC - AC power converters [2] are used to convert 270V DC power to 115/200V, 400Hz AC power for brushless and induction motor loads and 28V DC power for electronic equipment. According to [22], up to 75% of total PDS load installed in an aircraft will be the constant power type of load.

The following reasons motivated the choice of the 270V DC distribution bus [1]:

- it is a good voltage source for inverters that power motor loads of the aircraft,
- it is easy to provide uninterruptible power on the bus by using a battery back-up,
- regenerative power from electrical actuators can be easily returned to the bus.

At the same time, there are a number of technical issues related to the choice of the 270V DC bus. Among those addressed in [1] are the following:

- system stability,
- power quality on the bus,
- regenerative power flow.

Stability is the most important requirement for a PDS. The issue of stability is closely related to the EMI filter design for subsystems powered through switching power converters. Improper designs of the input filter for such subsystems may result in undesirable interactions [23, 25]. Currently, stability of a PDS in a more-electric aircraft for a particular design is

proposed to be evaluated through computer modeling [1]. Therefore, the importance of development of computer-aided modeling and analysis tools for a PDS cannot be underestimated.

Considerable experience is developed in evaluating stability of subsystem interactions in distributed power systems. Usually, the impedance ratio stability criterion suggested in [23] is used to analyze stability of interactions between two interconnecting subsystems. Stability of a spacecraft DC PDS is addressed in [27]. Stability analysis for a system with a source converter and one or more load converters is given in [26] and [28]. A method of defining the load impedance specifications based on the concept of forbidden region is presented in [29]. All these examples covered relatively simple system configurations, with an ideal voltage source, one source converter, and one or more load converters with resistive loads. The examples represented particular case studies rather than universal analysis tools. The results were obtained by tedious analytical developments for a particular system configuration rather than applying computer-aided analysis techniques to easily reconfigurable global system model.

An effort in modeling and simulation of a more-electric aircraft power system is presented in [24]. The system simulated included a synchronous generator, a diode bridge rectifier, and a resistive load. A circuit-oriented type of simulation software was used. No stability analysis was performed.

It is seen that although some work on modeling, analysis, and simulation of distributed power systems similar to the PDS of a more-electric aircraft has already been done, the issues of stability, DC bus power quality, and regenerative power flow in the PDS of an aircraft have not been addressed comprehensively. Therefore, the following research objectives are proposed:

1. Develop computer-aided analysis tools for modeling and analysis of a PDS in a more-electric transport aircraft.
2. Create nonlinear models of a PDS for large-signal simulations and small-signal analysis.
3. Present examples of using the modeling and simulation tools for analysis of a PDS:
    - stability analysis of a PDS with an electromechanical actuator,
    - stability analysis of a PDS with constant power load and mixed load,

- analysis of the DC bus power quality under bidirectional power flow conditions,
- analysis of ways to optimize regenerative energy flow in the PDS in order to increase its overall efficiency.

In order to achieve the research objectives, a representative power distribution system architecture of a 21st century transport aircraft (Figures 1.1 and 1.2) was developed. The electrical energy sources are two main Starter/Generators (S/G) and a Starter/Generator of an Auxiliary Power Unit (APU). The system loads are two flight control electric actuator systems with electromechanical and electrohydrostatic actuators, Environmental Control System (ECS) motor loads, and utility loads. There is also a battery unit, which can work as either source or load. All the PDS components are connected by a 270V DC bus, which consists of two primary busses and an APU bus. Each subsystem is connected to the power distribution bus through a Bidirectional Power Converter (BDC), which may be DC–DC or Three-Phase–DC type. The Electric Load Management System provides system level control and protective functions.

A prominent feature of this PDS is bidirectional power flow in the DC bus and in many of its subsystems. Normally, the power flows from the sources (generators) to the loads (actuators, ECS, battery, utility loads). However, in certain modes of operation, some loads can work in regenerative mode, thus supplying electric power to the DC distribution bus. For example, a flight control actuator works in regenerative mode when it has to slow down a moving flight control surface, or when the surface is being moved by the air flow. Another example is using the battery as an energy source and the APU starter/generator as a motor to start the APU engine. Bidirectional power flow in the PDS becomes possible because all power converters connecting subsystems to the DC distribution bus possess bidirectional power flow capability.

The regenerative power phenomenon mentioned above has potential advantages since the power regenerated by one subsystem can potentially be used to power the others or be stored in the PDS for future use. However, it also has potential problems because unused regenerative power may create voltage spikes on the DC bus, which may exceed the limits set by the standard. This effect may happen because a load with sufficient power consumption may not be available

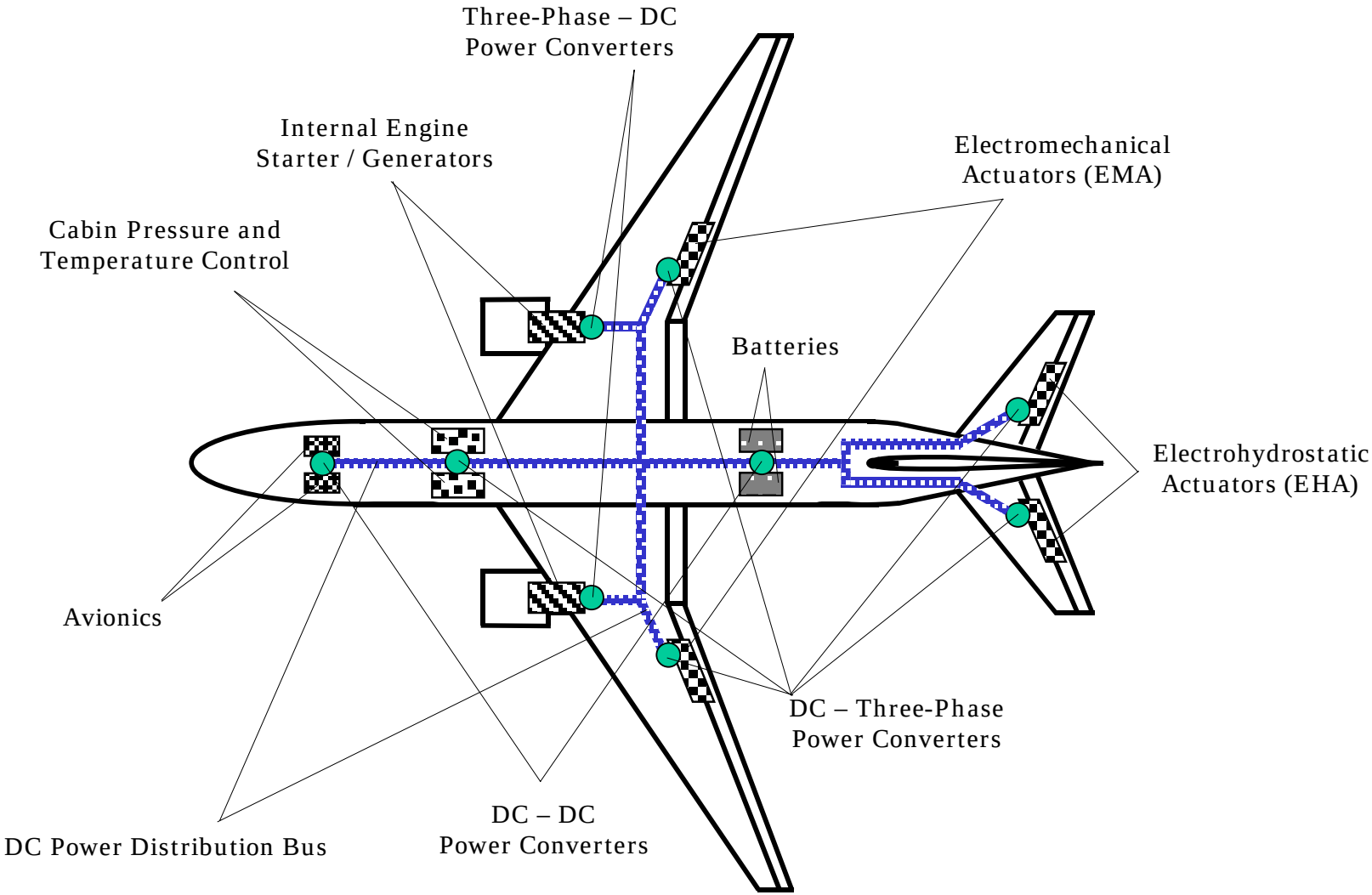

Figure 1.1 Power distribution system of a transport aircraft.

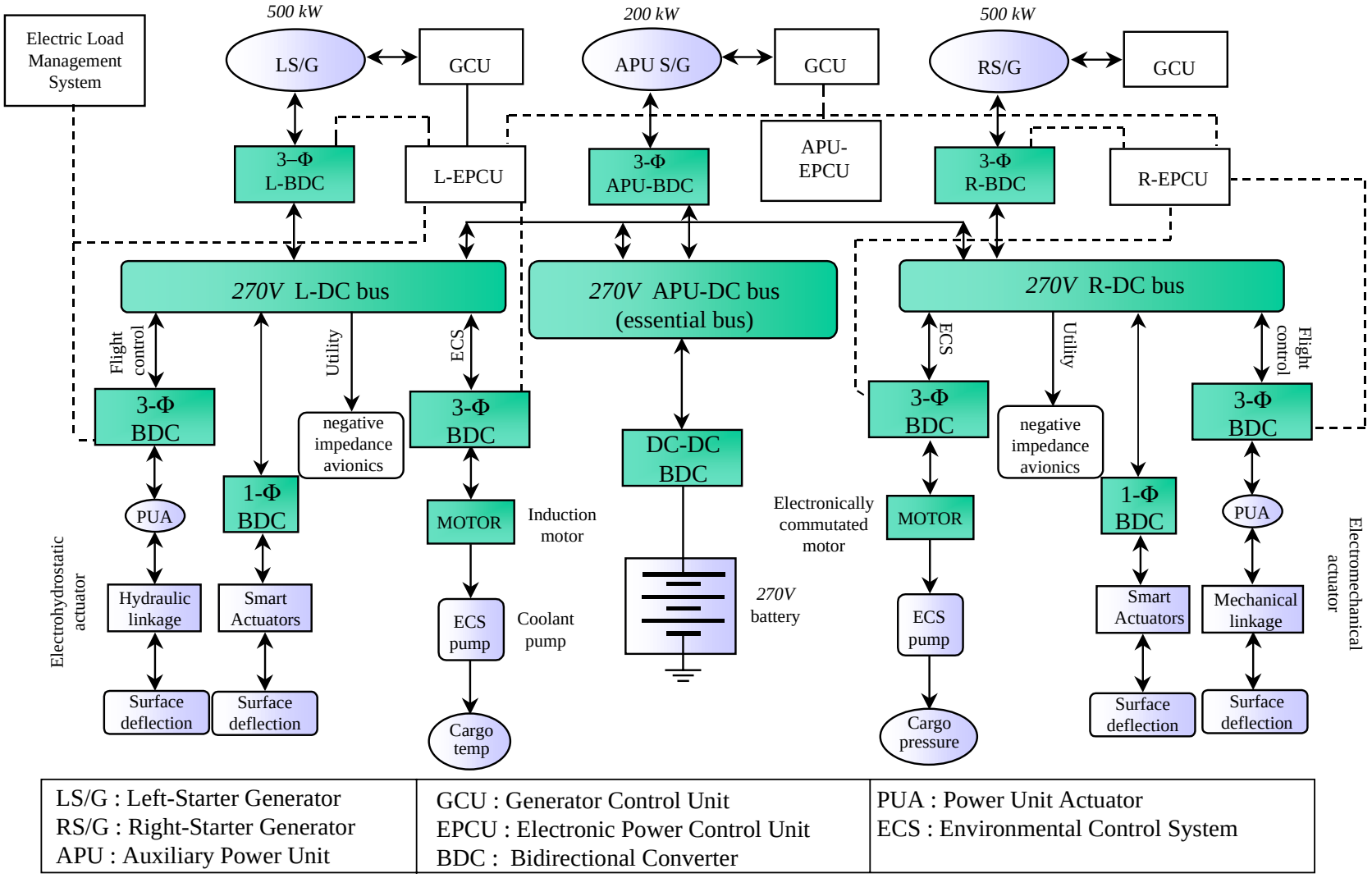

Figure 1.2 Power distribution system architecture.

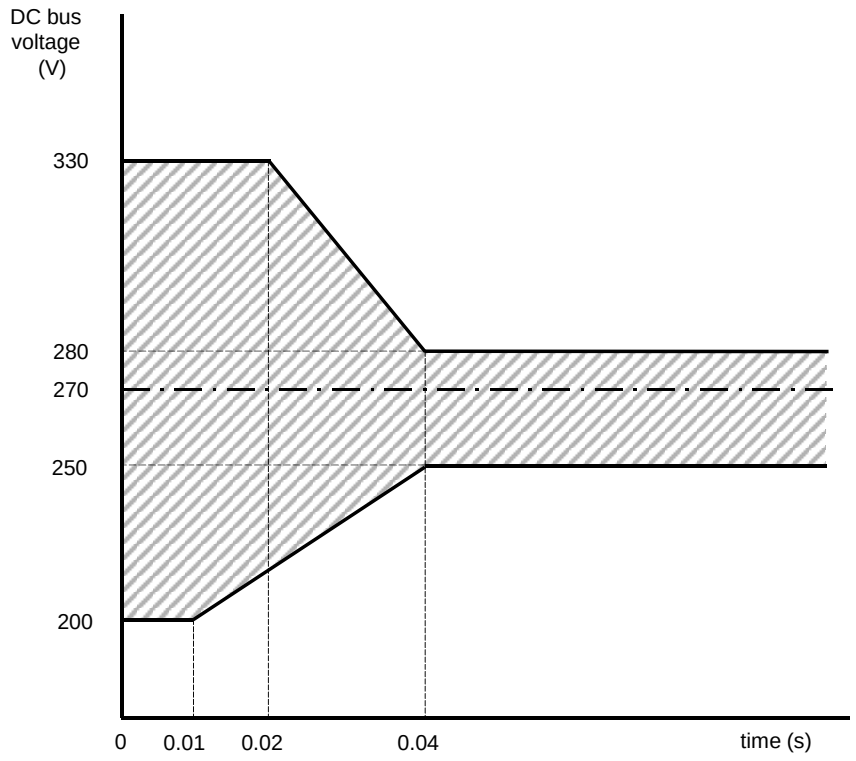

Figure 1.3 DC bus voltage specifications according to MIL-STD-704E.

on the bus at the time of regeneration. Figure 1.3 shows the limits of the DC bus voltage transients set by MIL-STD-704E [8], which specifies power quality characteristics of the DC bus. These transients may affect normal operation of the equipment connected to the bus or even damage it. In order to store the regenerative energy, it is necessary to provide additional energy storage components in the PDS. Since the battery alone charges too slowly to accept transient power spikes generated in certain modes of operation, a significant number of capacitors in the PDS will be needed to fully utilize the regenerative power.

Unlike the current PDS designs based on using components that have minimal interactions, the PDS under investigation consists of highly coupled subsystems closely interacting with each other. This approach brings potential benefits, which include an opportunity for optimization of the whole system that will allow resources of one subsystem such as regenerative energy to be shared with the others. The result would be reduction of the overall weight and cost of the aircraft and increase of the efficiency of its power distribution function.

One possible problem of the PDS with highly coupled subsystems might be a loss of the system stability because of undesirable subsystem interactions. Another possible problem is deterioration of power quality as a result of transient voltage disturbances on the DC bus, especially in regenerative mode of operation. The subsystems constituting the whole PDS must be designed keeping in mind issues of compatibility with the other subsystems. Avoiding undesirable interactions can be achieved by choosing appropriate designs and modes of operation. Therefore, the key to successful subsystem integration into the whole PDS is developing an understanding of possible subsystem interactions.

The objective of this research is to develop nonlinear models of subsystem interactions, especially in the context of bidirectional power flow, to create efficient computational tools for computer-aided analysis of the PDS, and to provide examples of using these tools for robust and energy efficient PDS designs that would take advantage of highly coupled subsystems while avoiding undesirable consequences of subsystem interactions.

Chapter 2

Principles and Techniques of Modeling and Analysis of a DC Power Distribution System

2.1 Multi-Level Modeling of Power Distribution System Components

In order to achieve the research goals, a model of the PDS that allows studying subsystem interactions has to be developed. This model should provide efficient ways for analysis, simulation, optimization, and control system design of subsystems interacting with each other within the PDS. Although good models for all subsystems already exist or can be readily developed with the use of known modeling techniques, simply putting all the subsystem models together would not provide an acceptable solution to the problem. The global system model built this way would be too complicated, with many unnecessary details not helpful for studying subsystem interactions. Since the available system modeling software does have limitations, this model will likely be very computationally intensive, slow, and inefficient, or even inoperative because of numerical convergence problems.

The multi-level modeling concept [30, 31] allows us to overcome this drawback. In this approach, a model reduction procedure is used to obtain models of different level of complexity for each subsystem. Three levels of models are available: a detailed model, a behavioral model, and a reduced order model. For a particular type of analysis, a model of an appropriate level will be chosen for each subsystem.

A detailed model is based on equations derived from the subsystem structure and electrical circuit. For a subsystem whose configuration or topology changes during its operational cycle, there will be a separate set of equations for each configuration. A detailed model reflects both low and high frequency dynamics of the subsystem and may include effects of secondary importance such as parasitics. An example of a detailed model for a switching power converter would be a model that exactly describes all voltage and current waveforms in the circuit produced by the switching action of the semiconductor switches. For switching power converters, a detailed model is often called a "switching" model. A detailed model is very computationally intensive in computer simulations. Since a detailed model often includes discrete and discontinuous functions, it cannot be used for control loop design based on linearization and frequency domain analysis techniques. For this reason, a detailed model is used only in simulations when a detailed study of the subsystem operation is required.

A behavioral model is derived from the detailed model by time averaging of high-frequency periodical waveforms such as switching waveforms [9]. The behavioral model corresponds to a subsystem whose terminal behavior is identical to the original subsystem at frequencies much lower than the switching frequency and excluding the switching ripple in waveforms. The behavioral model preserves nonlinearities and low-frequency dynamics of the original subsystem. It may or may not reflect parasitic effects in the subsystem. Since the high-frequency behavior no longer has to be obtained in the process of numerical integration, the behavioral model is much more computationally efficient than the detailed model. The low-frequency dynamics of the behavioral model is described by continuous functions, which can be linearized and used for control design. A behavioral model of a switching converter is often called an "average" model.

A reduced order model is obtained from a behavioral model by linearizing it at an equilibrium point. Therefore, it is often called a "linearized" model. A large signal model, therefore, is reduced to a small signal model, which is valid only in the vicinity of this operating point. A standard procedure of perturbation and linearization of nonlinear continuous equations of a behavioral model is employed to obtain a linearized model [9]. Most commercial software packages can perform this procedure automatically. A reduced order model allows frequency

domain analysis and design tools to be applied. A reduced order model is often used as a generic model for a subsystem (for example, a source or a load) in cases when having a more detailed model is not essential.

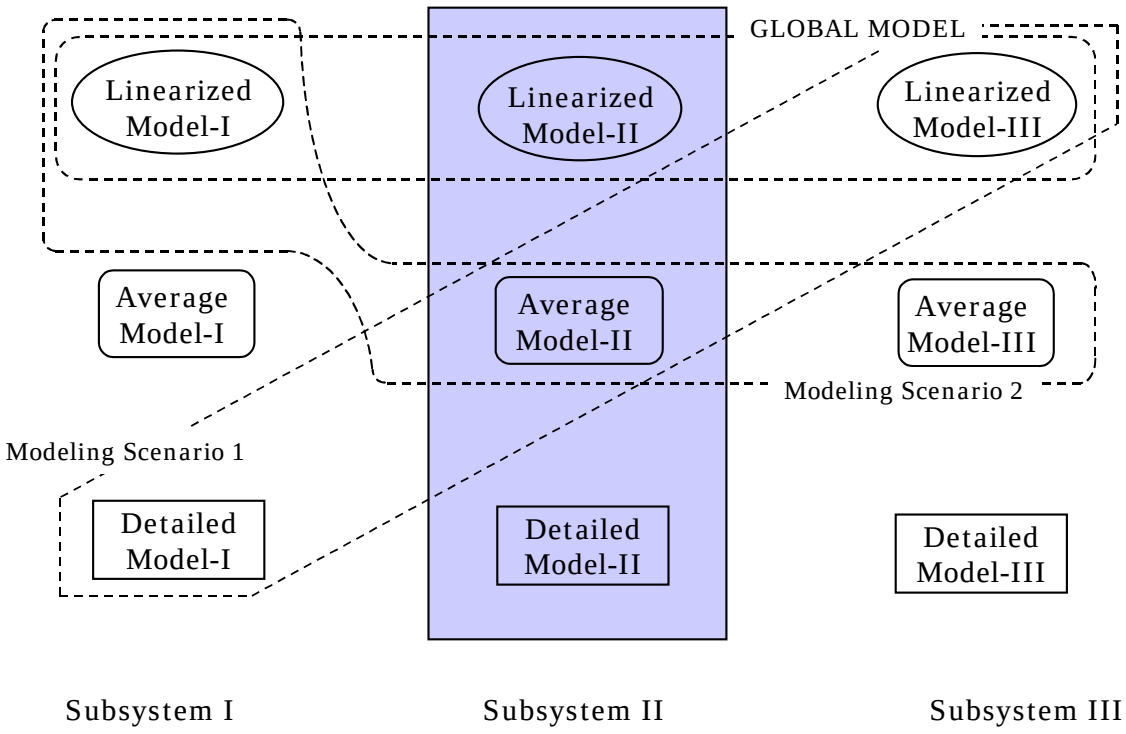

Figure 2.1 Mixed-level modeling concept.

The mixed-level modeling concept provides a convenient way of studying subsystem interactions without making the global model of the system too complicated. As mentioned before, it is neither feasible nor necessary to use detailed models for all subsystems in every scenario. Instead of trying to simulate the whole system "as it is" in all its complexity, we can concentrate our attention on a particular aspect of the system operation that we want to study. This is done by selecting an appropriate level of modeling of the interacting subsystems that would allow capturing the essential features of the phenomenon under investigation. For the rest of the subsystems, reduced level models are used. Figure 2.1 illustrates the usage of this concept. We would use the reduced order model for each subsystem if we wanted to simulate only the global system states. The second scenario could be used to study how the second subsystem interacts with the third subsystem with a contribution from the first subsystem. In this

scenario, we would select the behavioral model of the second and third subsystems and the reduced order model of the first subsystem. The third scenario describes the case when we want to know exactly how the first subsystem responds to the second subsystem with a contribution from the third subsystem. To study this case, we would use the detailed model of the first subsystem, the behavioral model of the second subsystem, and the reduced order model of the third subsystem.

As illustrated above, the mixed-level modeling concept provides an efficient way to investigate all aspects of the system behavior. Instead of having just one global system model, we build particular system models at the levels that suit our needs.

2.2 Power Distribution System Analysis and Simulation Tools

In order to take advantage of the multi-level and mixed-level modeling concepts described above, a computer-aided analysis and simulation tool has to be developed. There are a number of commercial software packages possessing necessary capabilities; most of them are application-specific. The PDS of an aircraft consists of elements with diverse physical nature, both electrical and non-electrical, such as power generators and converters, electromechanical devices, hydraulic and mechanical actuators. This variety calls for a generic modeling and simulation tool that allows diverse physical systems to be modeled in a uniform environment. Based on these considerations, MATLAB/Simulink package was chosen as a software platform. MATLAB is a generic numerical analysis software, which is well suited for system level analysis and simulation [10]. It contains a variety of toolboxes for different types of analysis including optimization and control design. Simulink, a toolbox of MATLAB, is a dynamic system simulation software that provides a convenient graphical user interface for building system models based on their equations [11]. The system stability and transient behavior analyses, which are key issues in studying subsystem interactions, can be conveniently performed using these tools.

The system analysis based on mixed-level modeling concept requires a capability of the software environment to provide an easy way of building simulation models for various system configurations using different level models for the subsystems. This goal is achieved by employing a modular approach for building Simulink models for the subsystems and their parts. Basic models of electric circuit elements and low-level subsystems are designed as modules, which are used as building blocks for creating models of more complicated subsystems and the whole system. Each block has input and output ports, through which it interchanges input and output variables with other blocks connected to it. Generally, each block has its own specific input and output variables, but the majority of variables being exchanged are voltages and currents. Since any subsystem containing an electrical two-port network has both voltages and currents as both inputs and outputs, a special convention for voltage and current variable exchange needs to be made. A convention was made that each block receives its input voltage and output current from the adjacent blocks as its input variables and supplies its input current and output voltage to the adjacent blocks as its output variables. This concept is illustrated in Figure 2.2. All developed Simulink blocks must satisfy this convention, which is known as interconnection rules. This novel modeling concept was developed in this research for greater flexibility in modeling different PDS configurations. Other variables exchanged between the subsystems have similar, although simpler, interconnection rules.

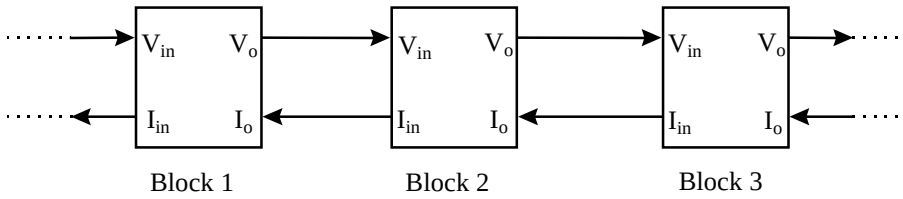

Figure 2.2 Interconnection rules for two-port networks.

Each subsystem, in general, has three types of models as discussed above: detailed, average, and linearized. A general procedure for a subsystem model development includes the following steps:

- partitioning of the subsystem into generic (elementary) blocks,
- developing analytical expressions for each block at both detailed and average model level,
- implementing the models in Simulink, and

- using MATLAB to obtain a linearized model.

An example of partitioning of a system into generic blocks is shown in Figure 2.3. It represents a buck converter with feedback control. The converter is partitioned into the following blocks: input filter, PWM switch, output filter, feedback controller, and blocks for the voltage source and the load. For each of these blocks, a Simulink model is obtained based on their equations. These models are linked into the whole system model according to the interconnection rules as shown in Figure 2.4. The detailed and the average models for the PWM switch will be different, but they will be the same for the other blocks. All these blocks are typical for power converters; therefore, the developed Simulink models can be used as building blocks for building models of different systems.

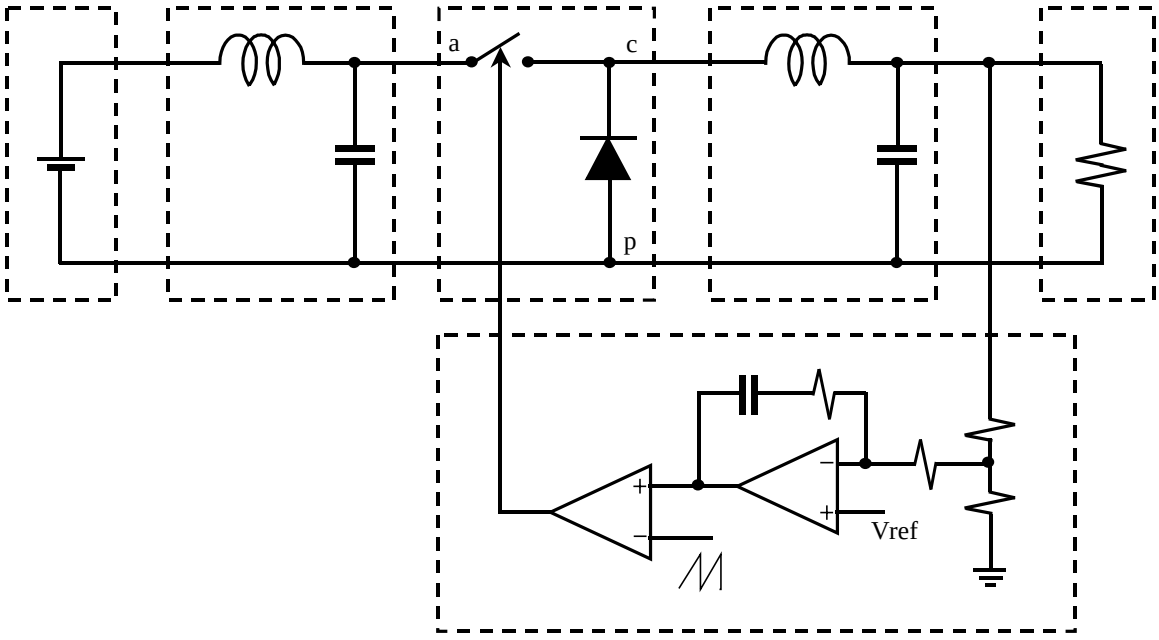

Figure 2.3 Buck converter – partitioning into generic blocks.

A linearized model of a subsystem can be obtained from its average model using MATLAB's Control System Toolbox commands [12]. Usually, a linearized model is obtained for the purpose of control loop design and can be defined within MATLAB, without implementation

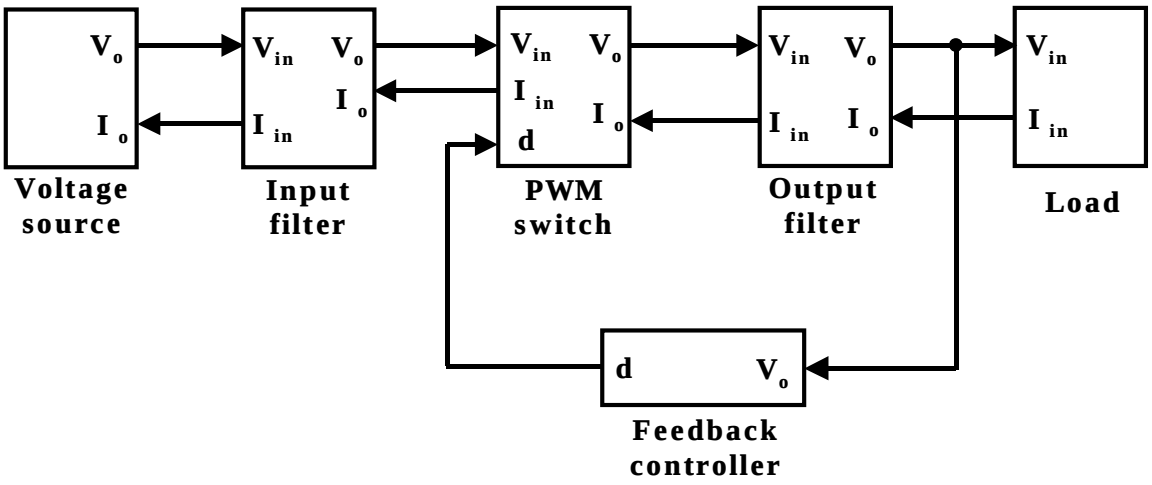

Figure 2.4 Simulink block diagram for the buck converter in Figure 2.3.

in Simulink. A linearized model intended for simulation as a part of the whole system model will be implemented in Simulink.

Chapter 3

Model Development for Power Distribution System Components

3.1 Modeling of Subsystem Elements

As we have seen in the previous section, elementary blocks typical for switching power converters are PWM switches and RLC networks (usually low-pass filters). These elements are two-ports; therefore, the interconnection rules for voltages and currents should be observed. It will be shown below how to use modeling capabilities of Simulink to build models for these elements.

As an example of an RLC network, we will consider a low-pass LC filter (Figure 3.1), which is a generic component of many types of power converters. The circuit is described by equations:

$$\begin{aligned} L\,\frac{di_{in}}{dt} &= v_{in} - v_o - i_{in} R_l \\ C\,\frac{dv_c}{dt} &= i_{in} - i_o \\ v_o &= v_c + R_c (i_{in} - i_o) \end{aligned} \tag{3.1}$$

The “Integrator” block of the built-in Simulink library is used to integrate the state variables of the network while the input and output variables are picked up according to the

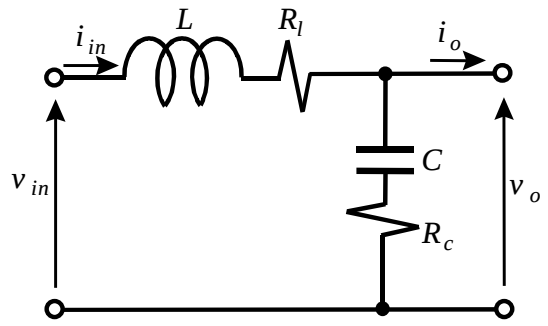

Figure 3.1 Low-pass L-C filter.

interconnection rules. The resulting Simulink model is shown in Figure 3.2. For convenience, it is further enclosed into the "Subsystem" block and used as illustrated in Figure 2.4.

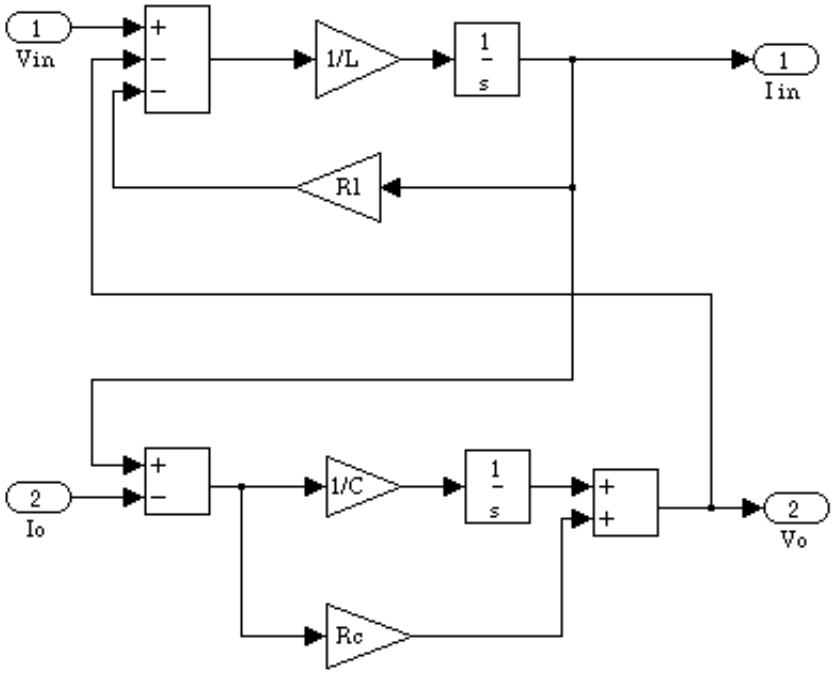

Figure 3.2 Simulink model of the L-C filter.

Another way of building a model for this network is using the "State-space" Simulink block as shown in Figure 3.3 because this filter is a linear system. In order to use this block, it is

necessary to identify state-space matrices for the network by writing its equations in state-space form:

$$\frac{d}{dt}\begin{bmatrix} i_{in} \\ v_c \end{bmatrix} = \begin{bmatrix} -\dfrac{R_c + R_l}{L} & -\dfrac{1}{L} \\ \dfrac{1}{C} & 0 \end{bmatrix}\begin{bmatrix} i_{in} \\ v_c \end{bmatrix} + \begin{bmatrix} \dfrac{1}{L} & -\dfrac{R_c}{L} \\ 0 & -\dfrac{1}{C} \end{bmatrix}\begin{bmatrix} v_{in} \\ i_o \end{bmatrix} \qquad (3.2)$$

$$\begin{bmatrix} i_{in} \\ v_o \end{bmatrix} = \begin{bmatrix} 1 & 0 \\ R_c & 1 \end{bmatrix}\begin{bmatrix} i_{in} \\ v_c \end{bmatrix} + \begin{bmatrix} 0 & 0 \\ 0 & R_c \end{bmatrix}\begin{bmatrix} v_{in} \\ i_o \end{bmatrix}$$

The models in Figures 3.2 and 3.3 are equivalent. The model in Figure 3.2 represents a general approach for model building based on the system equations, which is generally used in this research. The other approach is applicable only to linear systems represented in state-space form. It can be convenient for modeling of high-order systems with a large number of parameters, for which using the previous approach may be too cumbersome. Also, it may be more computationally efficient since it reduces the number of algebraic operations in the process of simulation.

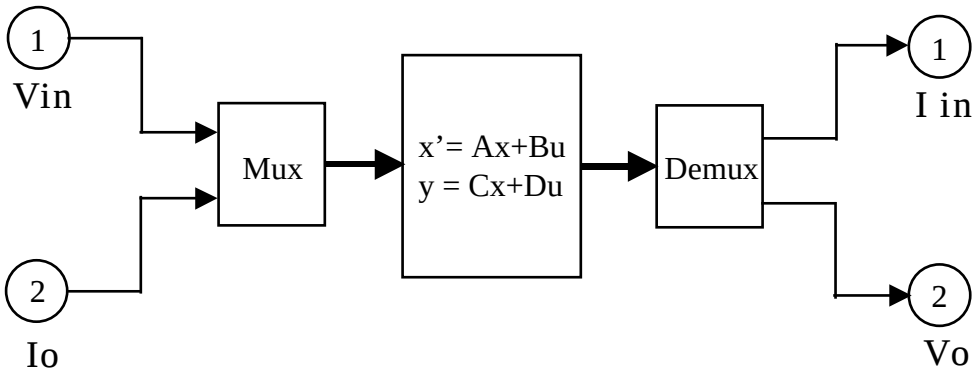

Figure 3.3 Alternative Simulink model of the L-C filter based on state-space representation.

The models for the L-C filter developed above are detailed, average, and linearized at the same time because no switching or nonlinearities are present in the network. The models for the PWM switch that will be considered next are different at detailed and average levels.

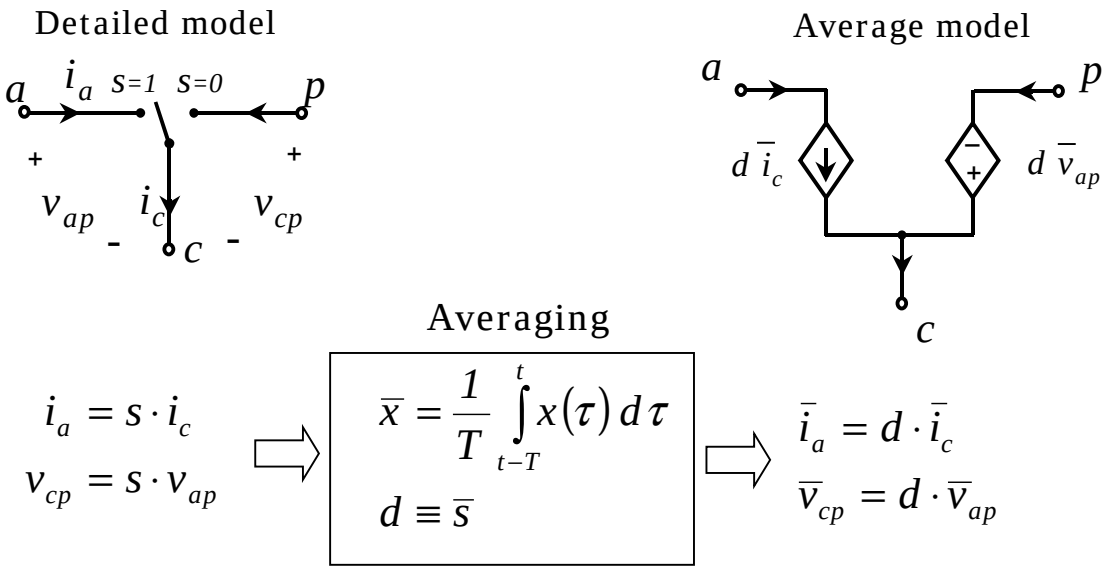

Figure 3.4 Development of detailed and average models for the PWM switch.

The PWM switch configuration used in the buck converter (Figure 2.3) is a two-port switching network with three terminals: active, passive, and common. The switching action of the PWM switch is described by the switching function *s*, which accepts the values of 0 and 1 as shown in Figure 3.4. The terminal behavior of the PWM switch, therefore, is described by the following equations upon which the detailed model of the switch is based:

$$\begin{aligned} i_a &= s \cdot i_c \\ v_{cp} &= s \cdot v_{ap} \end{aligned} \tag{3.3}$$

The switching voltage and current waveforms produced by the PWM switch are averaged by the low-pass filtering action of the input and output filters of the converter as they are seen at the load and source terminals. This filtering action presents a physical basis for using an average model of the switch, which neglects its switching action while preserving quantitative relationships between average values of voltages and currents at its terminals [9]. Mathematically, averaging of a periodical function *x(t)* is defined as

$$\bar{x} = \frac{1}{T}\int_{t-T}^{t} x(\tau)\, d\tau\,, \tag{3.4}$$

where *T* is the period of the function *x(t).*

The operation of averaging, being applied to the discrete switching function *s(t)* with a discrete value of duty cycle *d* for each switching period, results in a continuous duty cycle function *d(t)* and the following equations for the PWM switch, which constitute its average model (Figure 3.4):

$$\begin{aligned} \bar{i}_a &= d \cdot \bar{i}_c \\ \bar{v}_{cp} &= d \cdot \bar{v}_{ap} \end{aligned} \tag{3.5}$$

The Simulink implementations of the detailed and average PWM switch models are shown in Figure 3.5. Besides the terminal voltages and currents, the models have an additional input – the duty cycle command. The detailed model then turns this command into the output voltage and current switching waveforms by comparing it with a ramp generator signal, in a manner very similar to the operation of real PWM modulator circuits. The average Simulink model is based on the average model equations (3.5). Note that the interconnection rules for voltages and currents are observed.

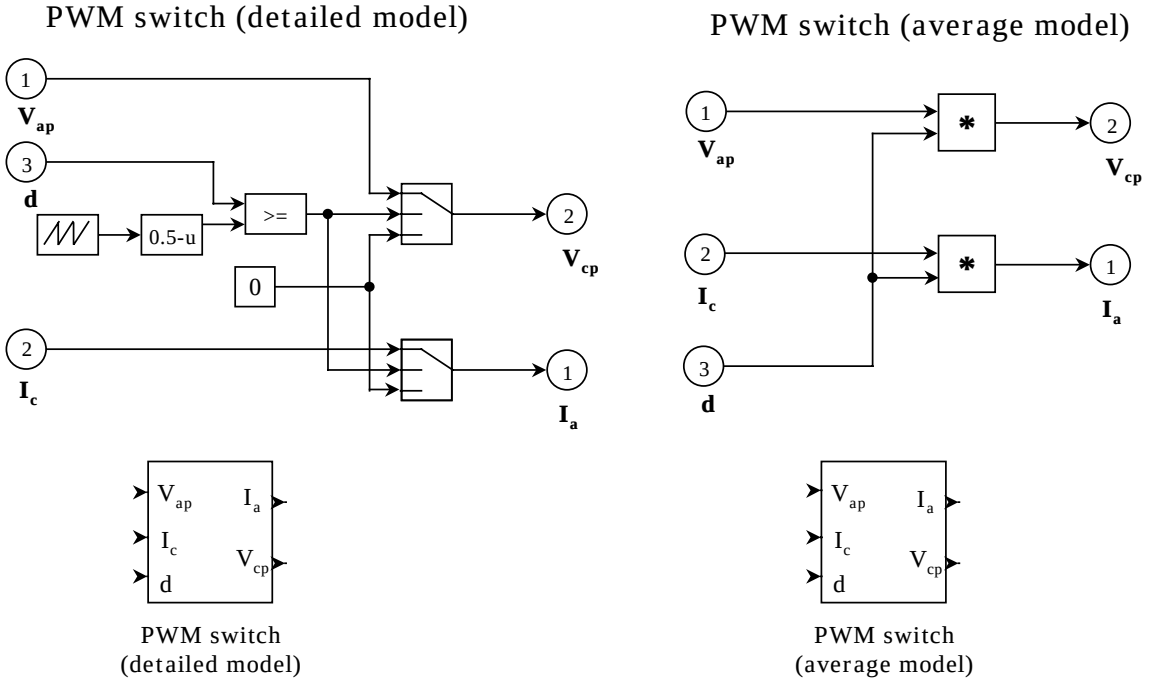

Figure 3.5 Detailed and average Simulink models for the PWM switch.

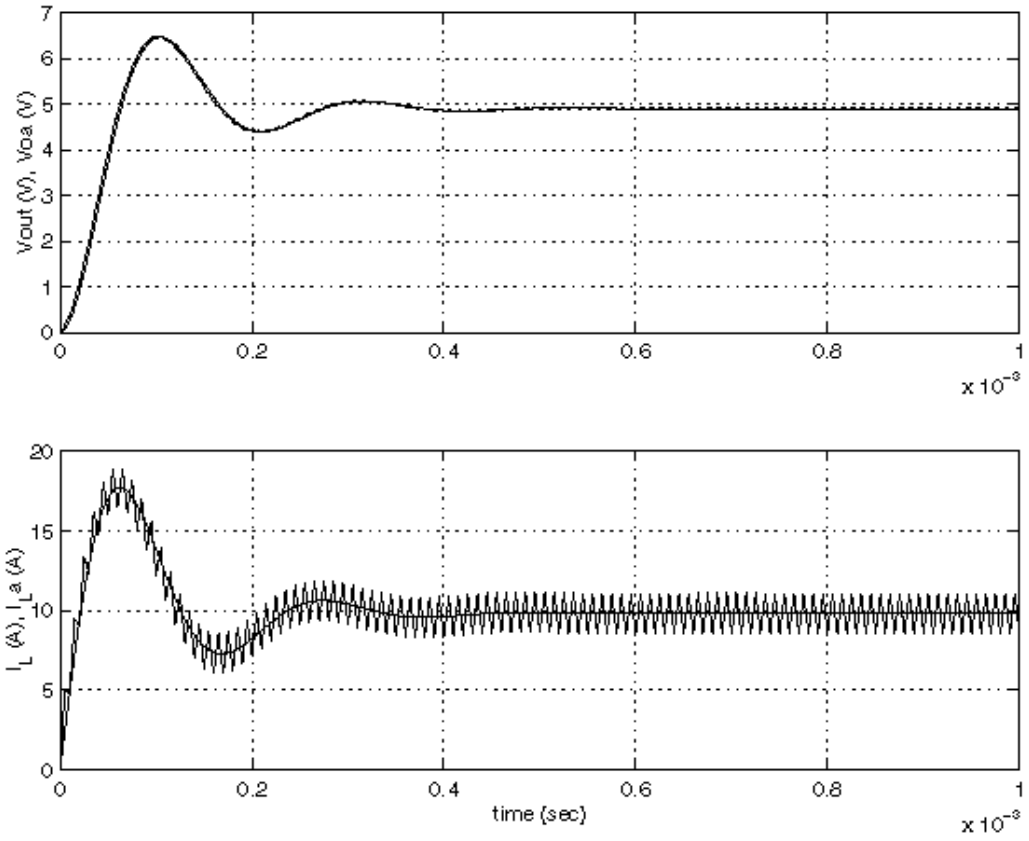

Figure 3.6 Buck converter example of simulation with detailed and average models for the PWM switch.

A Simulink model for the buck converter in Figure 2.4 may employ either detailed or average model for the PWM switch developed above. Both models preserve low-frequency dynamics of the system, but without the switching ripple in the state variables' waveforms if the average model is used. Figure 3.6 illustrates this idea. It shows simulated output filter capacitor voltage and inductor current transients of the buck converter obtained with both detailed and average models of the PWM switch. It is seen that the current response obtained with the average model reflects all the details of the current response obtained with the detailed model except the switching ripple. This is also true for the output voltage waveforms. The switching ripple of the output voltage is so small that both curves look almost identical on the plot.

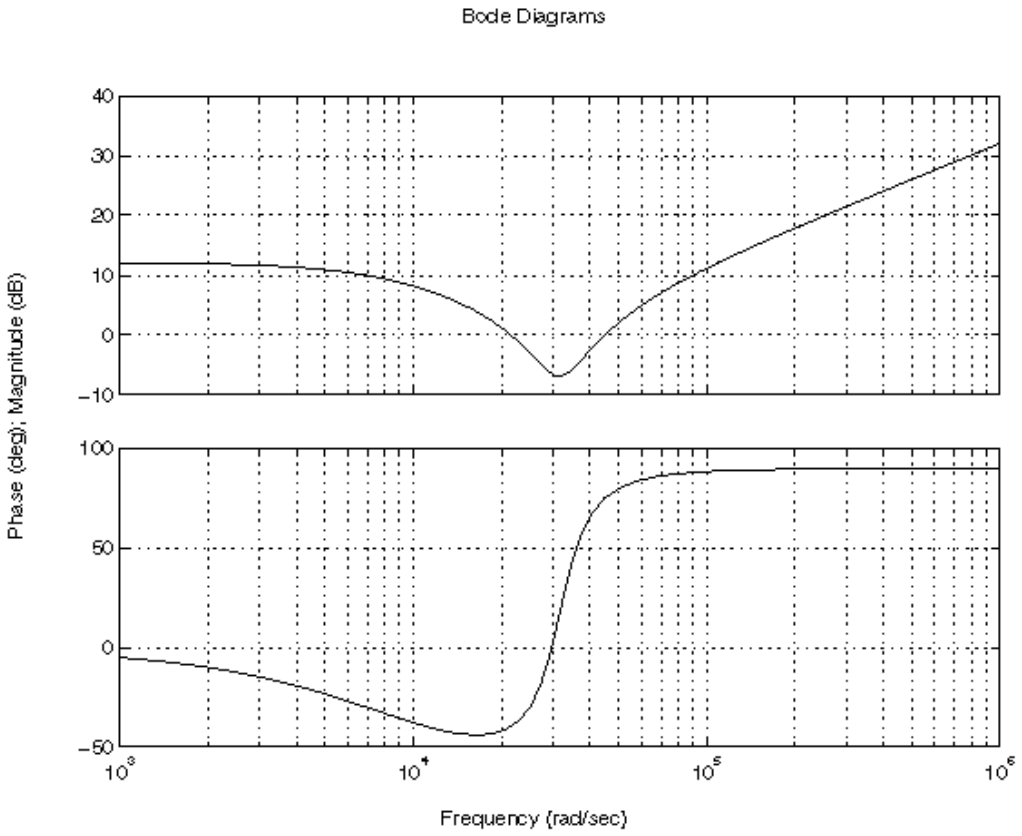

Figure 3.7 Buck converter open loop input impedance.

Although the average model does not show the switching ripple, it provides much faster simulation and an additional opportunity for small-signal analysis and control design using MATLAB's Control System Toolbox [12]. A nonlinear system such as the buck converter described above can be linearized at an equilibrium point, and a number of transfer functions can be obtained. For example, Figure 3.7 shows the input impedance transfer function of the buck converter in open loop configuration obtained by using the Control System Toolbox.

3.2 Modeling of DC-DC Switching Power Converters

3.2.1 DC-DC Buck Converter Modeling

The buck converter topology was already discussed above (Figure 2.3). A complete Simulink model of a buck converter is shown in Figure 3.8. The model features input and output LC filters and an average model of the PWM switch. The converter model can use a different input filter topology with a proper Simulink model. The model has an improved two-pole, two-zero feedback compensator, which provides voltage mode control to the converter. The feedback controller includes the integrator anti-windup feature and provides soft start with the reference voltage rising from zero at the power-up.

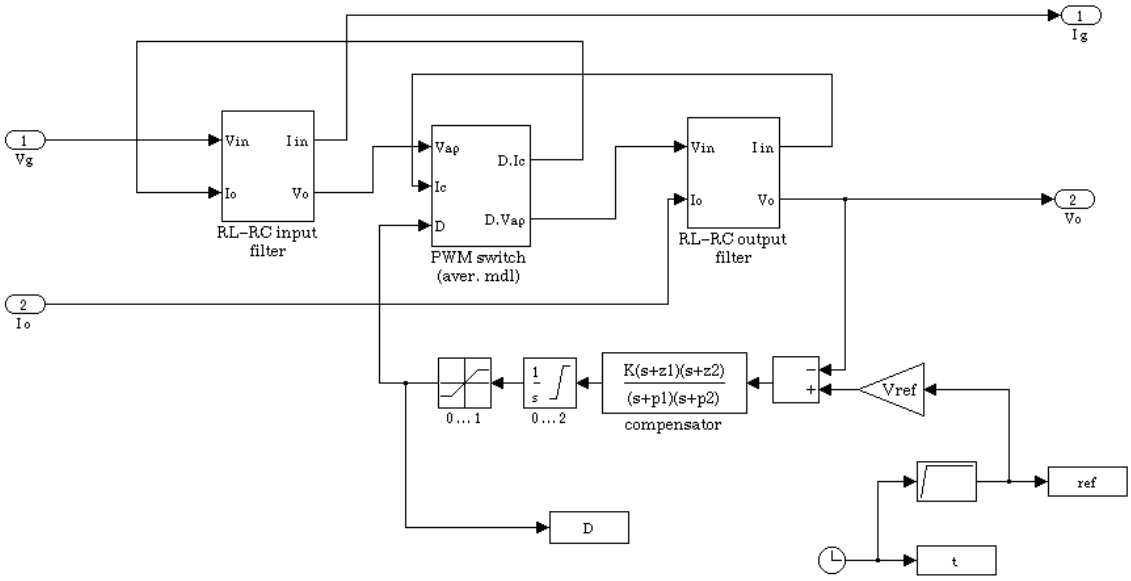

Figure 3.8 Bidirectional buck converter Simulink model.

The model supports bidirectional power flow, i.e. it is valid for power stage topologies that allow reverse output current. The model can be used in the aircraft power distribution system simulations to power low-voltage DC applications such as avionics from 270V DC bus. The model can also be used for bidirectional DC-DC full-bridge buck converter topologies, provided that the lower limit of duty cycle in the feedback loop is set to –1.

3.2.2 DC-DC Boost Converter Modeling

The boost converter has an output filter split by the PWM switch (Figure 3.9); therefore, the power stage model cannot be obtained by interconnecting the existing PWM switch and L-C filter models. A separate Simulink model (Figure 3.11) for the power stage of the boost converter (Figure 3.10) is developed based on the circuit equations:

$$\begin{aligned} L\frac{di_g}{dt} &= v_g - v_o(1-d) - i_g R_l \\ C\frac{dv_c}{dt} &= i_g(1-d) - i_o \\ v_o &= v_c + R_c(i_g(1-d) - i_o) \end{aligned} \tag{3.6}$$

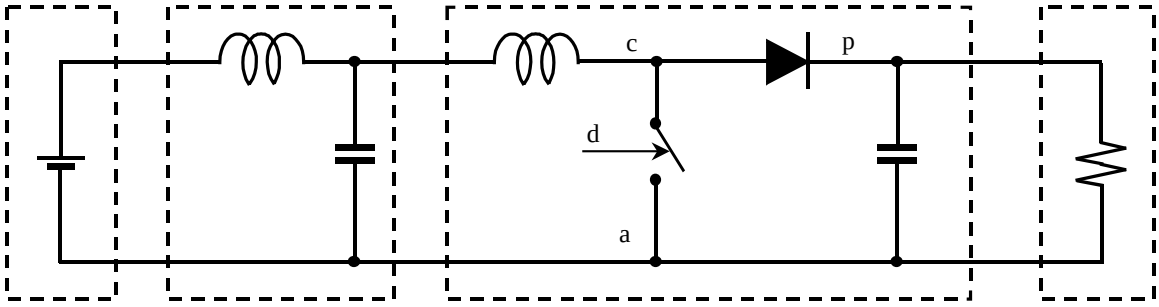

Figure 3.9 Boost converter topology.

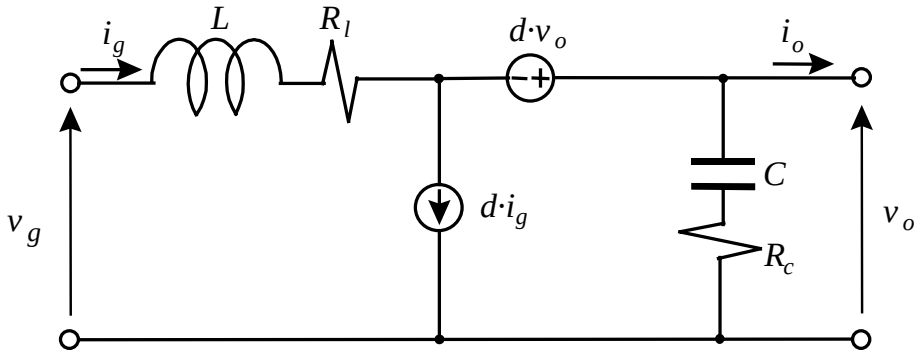

Figure 3.10 Equivalent circuit of the boost converter power stage.

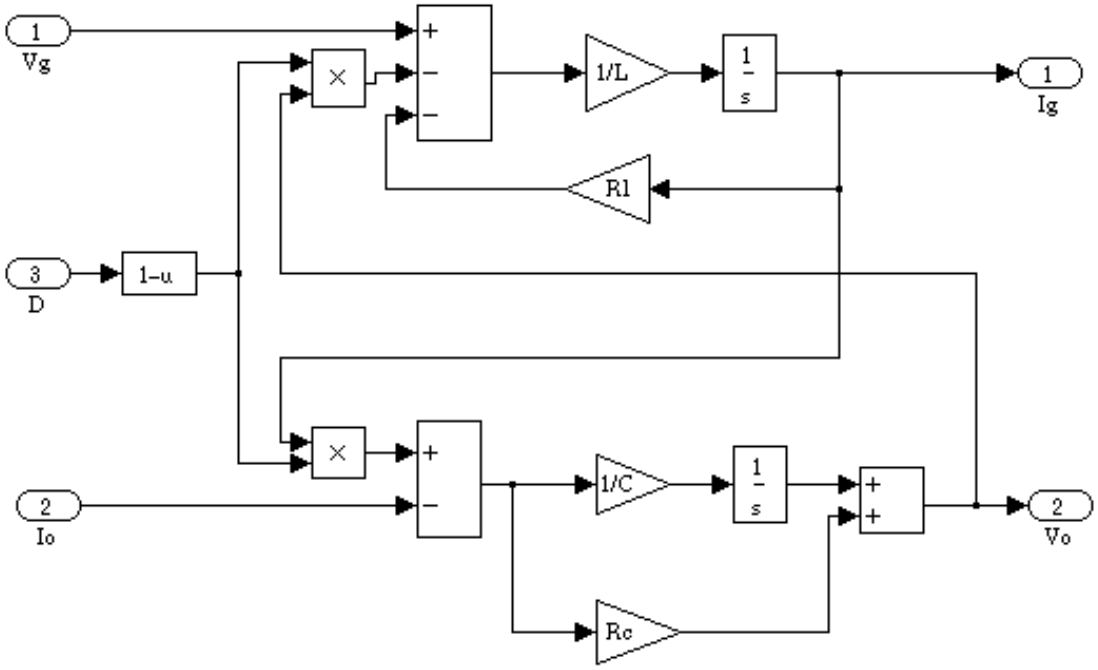

Figure 3.11 Simulink average model for the boost converter power stage.

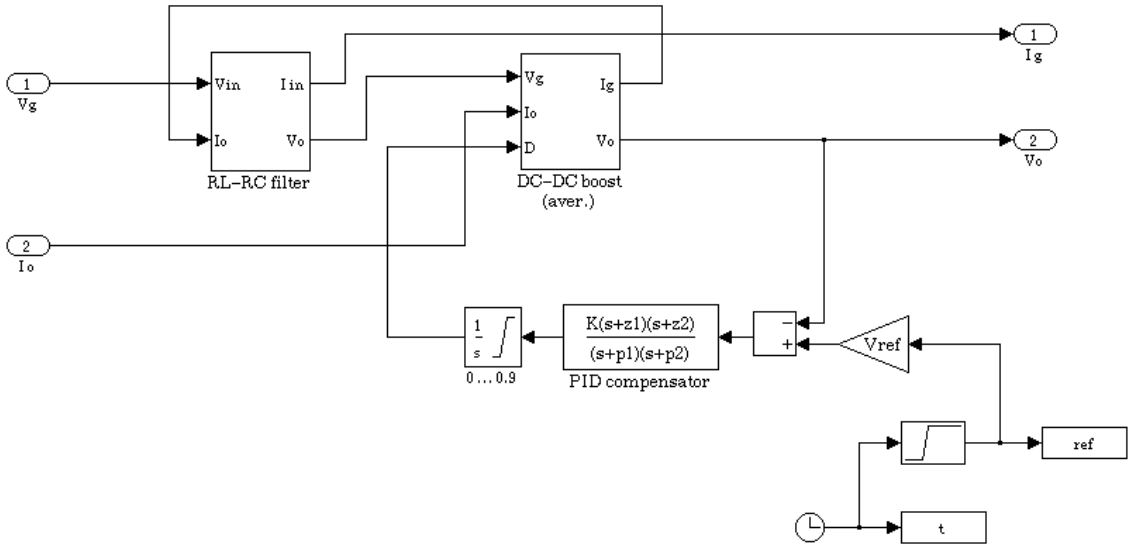

Figure 3.12 Bidirectional closed-loop Simulink model for the boost converter.

A complete model of the boost converter with voltage feedback loop is shown in Figure 3.12. It is composed of the average model of the boost converter power stage, the input filter model, and the feedback controller. The model has a soft start feature. The compensator with anti-windup is very similar to the one used in the buck converter. Of course, the compensator zeros, poles, and gain should be designed individually for a particular converter.

3.3 Modeling of Three-Phase Subsystems

3.3.1 Three-Phase Subsystem Modeling Approach

Three-phase subsystems of the PDS considered in this research include three-phase synchronous motors/generators and three-phase bidirectional converters. We will take a close look at modeling and simulation techniques for a three-phase synchronous starter/generator loaded by a three-phase-to-dc boost rectifier. The models should reflect bidirectional power flow in the subsystems (both generating and motoring) found under different scenarios.

Direct modeling of three-phase systems by writing their circuit equations in the three-phase reference frame is undesirable for several reasons. For a synchronous machine, this would result in equations with time-varying parameters because the self-inductances and mutual inductances of the machine windings depend on the rotor position. For the boost rectifier, even after averaging of the switching ripple, a three-phase model would not allow using the linearization and feedback control design techniques because the steady state waveforms of the system variables are sinusoids, and no operating point could be specified. Simulation of sinusoidal waveforms would require a very small integration step even in steady state operation, which would create computational problems (long simulation time and insufficient memory for storing the simulation history in the workspace).

These problems may be overcome by modeling the subsystems in the synchronously rotating reference frame commonly known as *dq* coordinates. Modeling of the synchronous

machine and the boost rectifier in *dq* coordinates is well covered in literature [13,14]. The synchronous generator and the boost rectifier must be modeled in separate *dq* reference frames according to their modeling approaches. The relationship between a set of *dq* variables and the corresponding set of three-phase *abc* variables is provided by the transformation matrix *T*. Since the three-phase systems studied in this research are balanced, no 0-axis components are present, which allowed using a simplified version of *dq*-transformation:

$$\begin{bmatrix} X_d \\ X_q \end{bmatrix} = T \begin{bmatrix} X_a \\ X_b \\ X_c \end{bmatrix}, \tag{3.7}$$

$$T = \frac{2}{3}\begin{bmatrix} \cos\omega t & \cos(\omega t - \frac{2\pi}{3}) & \cos(\omega t + \frac{2\pi}{3}) \\ -\sin\omega t & -\sin(\omega t - \frac{2\pi}{3}) & -\sin(\omega t + \frac{2\pi}{3}) \end{bmatrix}. \tag{3.8}$$

The inverse transformation from *dq* to *abc* variables is defined as

$$\begin{bmatrix} X_a \\ X_b \\ X_c \end{bmatrix} = T' \begin{bmatrix} X_d \\ X_q \end{bmatrix}, \tag{3.9}$$

$$T' = \begin{bmatrix} \cos\omega t & -\sin\omega t \\ \cos(\omega t - \frac{2\pi}{3}) & -\sin(\omega t - \frac{2\pi}{3}) \\ \cos(\omega t + \frac{2\pi}{3}) & -\sin(\omega t + \frac{2\pi}{3}) \end{bmatrix}. \tag{3.10}$$

To provide a means for *abc-dq* and *dq-abc* transformation of variables during simulation process, two Simulink blocks "ABC-to-DQ" (Figure 3.13) and "DQ-to-ABC" (Figure 3.14) are developed. These blocks must be used with a very small integration step because they contain sinusoidal signal sources. For systems modeled completely in *dq* coordinates without using sinusoidal sources, much larger integration steps may be allowed, which would unleash the full

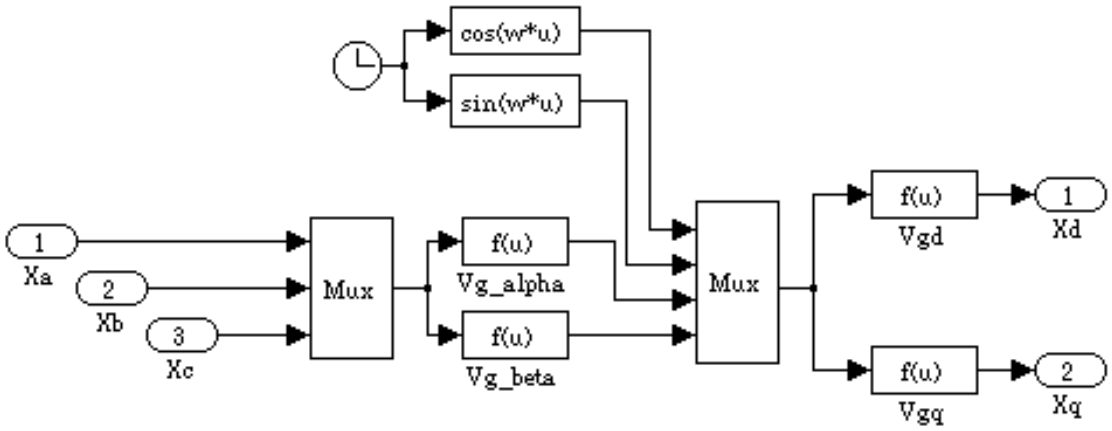

Figure 3.13 ABC-to-DQ transformation Simulink block.

power of robust variable-step integration routines. After the simulation is done, the results in *dq* variables may be converted to *abc* variables using the inverse transformation matrix *T'*. A special MATLAB function "dq2abc" described in Appendix B has been developed for this purpose.

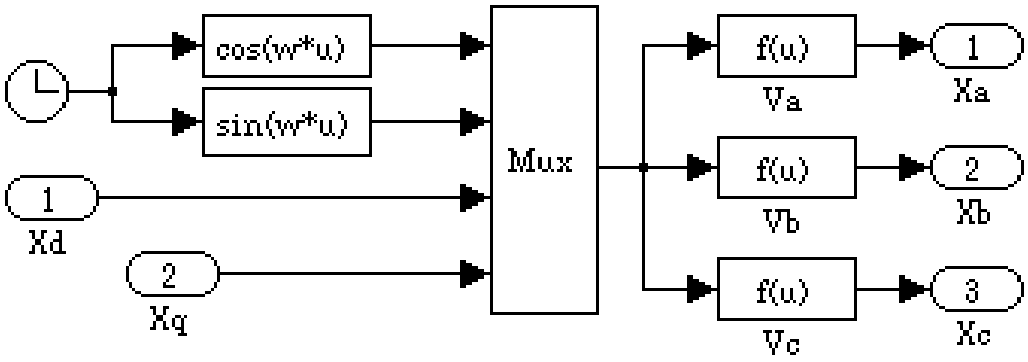

Figure 3.14 DQ-to-ABC transformation Simulink block.

3.3.2 Three-Phase Synchronous Generator Modeling

An equivalent circuit of a synchronous generator with a balanced load is presented in Figure 3.15. As mentioned above, modeling of a synchronous machine in *dq* coordinate frame avoids the problem of time-variance of the winding inductances. It converts the ac system variables into equivalent dc variables, which relate to the magnitude of the sinusoids in the steady state operation and in transients. In addition, the *dq* transformation actually reduces the order of the system (a three-phase system becomes a two-phase system).

The machine is described by the following equations corresponding to the equivalent circuit:

$$
\begin{aligned}
v_d &= (i_{sd} - i_d)R_a \\
v_q &= (i_{sq} - i_q)R_a \\
0 &= R_a i_d - (R_a + R_s)i_{sd} + \omega(L_{ls} + L_{mq})i_{sq} - \omega L_{mq} i_{kq} - (L_{ls} + L_{md})\frac{di_{sd}}{dt} + L_m d\frac{di_{fd}}{dt} + L_{md}\frac{di_{kd}}{dt} \\
0 &= R_a i_q - (R_a + R_s)i_{sq} - \omega(L_{ls} + L_{md})i_{sd} + \omega L_{md} i_{fd} + \omega L_{md} i_{kd} - (L_{ls} + L_{mq})\frac{di_{sq}}{dt} + L_{mq}\frac{di_{kq}}{dt} \qquad (3.11) \\
v_{fd} &= R_{fd} i_{fd} - L_{md}\frac{di_{sd}}{dt} + (L_{lfd} + L_{md})\frac{di_{fd}}{dt} + L_{md}\frac{di_{kd}}{dt} \\
0 &= R_{kd} i_{kd} - L_{md}\frac{di_{sd}}{dt} + (L_{lkd} + L_{md})\frac{di_{kd}}{dt} + L_{md}\frac{di_{fd}}{dt} \\
0 &= R_{kq} - L_{mq}\frac{di_{sq}}{dt} + (L_{lkq} + L_{mq})\frac{di_{kq}}{dt}
\end{aligned}
$$

where

R_s - armature phase resistance,

ω - rotor speed,

v_d - armature *d* axis terminal voltage,

v_q - armature *q* axis terminal voltage,

i_d - armature *d* axis terminal current,

i_q - armature *q* axis terminal current,

i_{sd} - *d* axis phase current,

i_{sq} - *q* axis phase current,

v_{fd} - field winding terminal voltage (reflected to the stator),

i_{fd} - field winding terminal current (reflected to the stator),

i_{kd} - d axis damper winding current (reflected to the stator),

i_{kq} - q axis damper winding current (reflected to the stator),

Λ_d - total armature flux in d axis,

Λ_q - total armature flux in q axis.

In this model, we assume a constant rotor speed. This is justified for studying dynamic behavior of the PDS since changes in the generator load would not likely affect the aircraft engine speed. If it is necessary to include mechanical dynamics into consideration, a mechanical equation of motion should be added to the equations above.

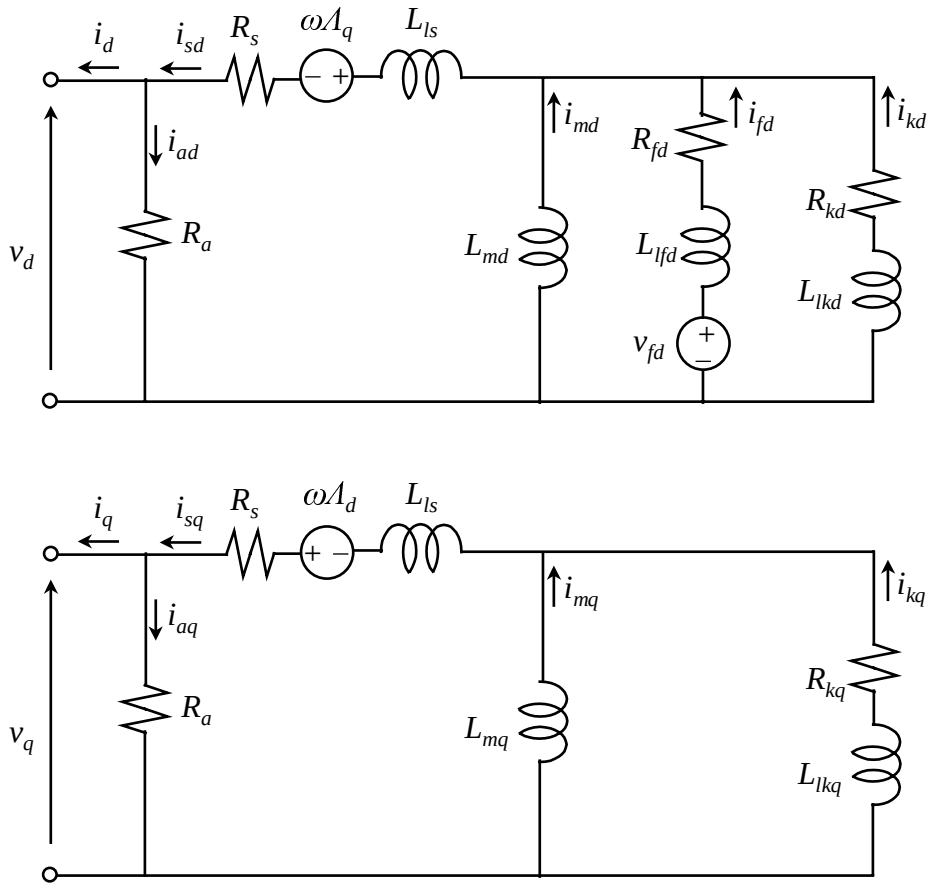

Figure 3.15 Equivalent circuit of a synchronous generator in dq coordinates.

According to the interconnection rules for voltages and currents specified above, a Simulink model for the generator must have a current port as an input and a voltage port as an output. They will be coupled with the boost rectifier's input voltage port and the output current port. The phase currents i_{sd} and i_{sq}, being state variables, cannot be the input variables at the same time. Therefore, a fictitious terminal resistance *Ra* was added to the model. This resistance has a relatively high value and does not affect other variables. It may also account for magnetic losses in the generator.

A Simulink model for this subsystem could be built directly by drawing a block diagram corresponding to the equations (3.11) similarly to the block diagram for the LC filter in Figure 3.2. However, because of complexity of the equations, this approach would be too cumbersome to implement. An alternative approach used in this research uses the "State-space" Simulink block. Equations (3.11) represent a linear system with state variables i_{sd}, i_{sq}, i_{kd}, i_{kq}, i_{fd}, input variables i_d, i_q, v_{fd}, and output variables v_d, v_q. These equations are solved for the state derivatives and represented in state-space form (the details of the solution are given in Appendix C):

$$\begin{aligned} \frac{d}{dt}\begin{bmatrix} i_{sd} \\ i_{sq} \\ i_{kd} \\ i_{kq} \\ i_{fd} \end{bmatrix} &= A_g \begin{bmatrix} i_{sd} \\ i_{sq} \\ i_{kd} \\ i_{kq} \\ i_{fd} \end{bmatrix} + B_g \begin{bmatrix} i_d \\ i_q \\ v_{fd} \end{bmatrix} \\ \begin{bmatrix} v_d \\ v_q \end{bmatrix} &= C_g \begin{bmatrix} i_{sd} \\ i_{sq} \\ i_{kd} \\ i_{kq} \\ i_{fd} \end{bmatrix} + D_g \begin{bmatrix} i_d \\ i_q \\ v_{fd} \end{bmatrix}, \end{aligned} \tag{3.12}$$

where A_g, B_g, C_g, D_g are the state-space matrices.

It can be seen from Equations (3.11) that the output voltage of the synchronous generator significantly depends on its load current. In order to keep the output voltage at a specified level

regardless of load conditions, a voltage feedback loop is introduced into the Simulink model. The feedback provides the rms value of the output voltage calculated from its *dq* components according to the formula:

$$v_{rms} = \frac{1}{\sqrt{2}}\sqrt{v_d^{\,2} + v_q^{\,2}} \tag{3.13}$$

The field winding voltage controller, which is modeled here as a simple gain, uses the output voltage error signal. Since the dc distribution bus voltage is precisely regulated by the boost rectifier, the presence of a small steady-state error in the generator output voltage is not a problem.

The complete Simulink model for the synchronous generator is presented in Figure 3.16. A soft-start feature is added to avoid large transients in the beginning of simulation. The transfer function T_{func} with a very high frequency pole is introduced into the feedback path in order to break an algebraic loop in the model, which may cause numerical problems when the model is used in large system simulations. The transfer function does not affect the model operation otherwise.

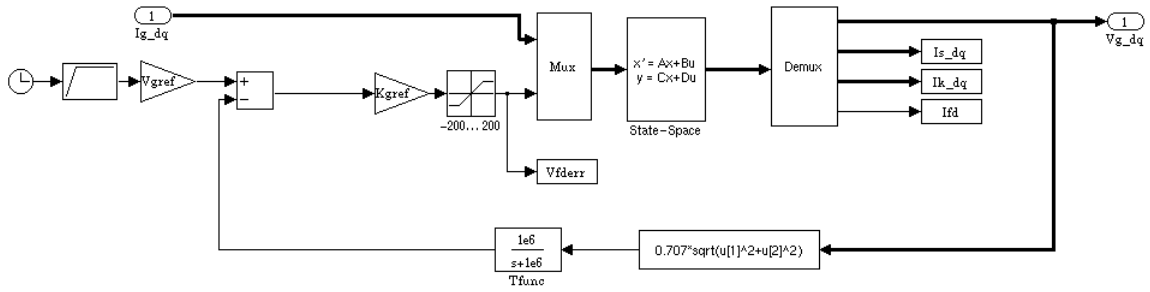

Figure 3.16 Closed-loop Simulink model of the synchronous generator in *dq* coordinates.

3.3.3 Three-Phase Boost Rectifier Modeling

The boost rectifier provides front-end three-phase-to-dc power conversion from the synchronous generator to the dc distribution bus. The rectifier operates with unity power factor and draws sinusoidal currents from the three-phase source. When the output current reverses its direction, the boost rectifier reverses the power flow through it and operates as a voltage source inverter.

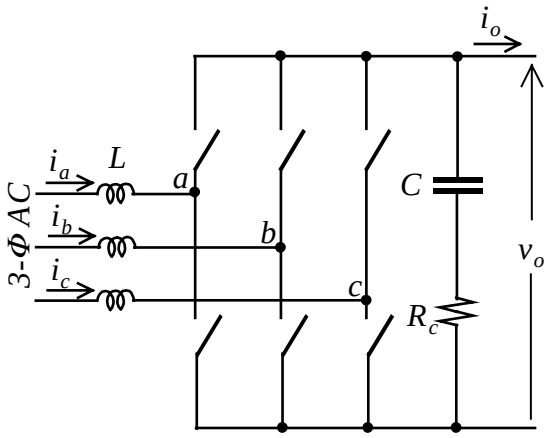

Figure 3.17 Power stage topology of the boost rectifier.

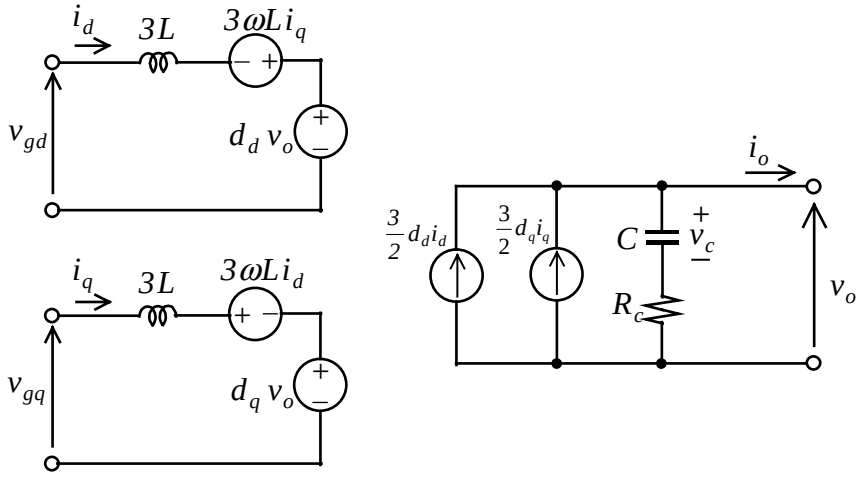

Figure 3.18 Average model of the boost rectifier in *dq* coordinates.

The power stage of the boost rectifier as modeled in this research is shown in Figure 3.17. The output capacitor ESR is taken into consideration in order to reflect the converter dynamics more accurately. By averaging the switching action of the semiconductor switches and applying the *dq* transformation to the resulting average model, a large signal average model in *dq* coordinates is obtained [14,15]. The equivalent circuit is shown in Figure 3.18 and described by equations:

$$\begin{aligned}
\frac{di_d}{dt} &= \frac{1}{3L}(v_{gd} + 3\omega L i_q - d_d v_o) \\
\frac{di_q}{dt} &= \frac{1}{3L}(v_{gq} - 3\omega L i_d - d_q v_o) \\
\frac{dv_c}{dt} &= \frac{1}{C}(\frac{3}{2}(d_d i_d + d_q i_q) - i_o) \\
v_o &= v_c + R_c(\frac{3}{2}(d_d i_d + d_q i_q) - i_o),
\end{aligned} \tag{3.14}$$

where

i_d, i_q - input currents in dq coordinates,

v_{gd}, v_{gq} - input voltages in dq coordinates,

i_o - output dc current,

v_o - output dc voltage,

d_d, d_q - duty cycle in dq coordinates,

ω - angular frequency,

L - phase inductance,

C - output capacitance,

R_c - capacitor ESR.

A Simulink model derived from these equations is shown in Figure 3.19. The model accepts *dq* voltages, *dq* duty cycles, and dc output current as input variables and supplies dc voltage and *dq* currents as output variables.

The control diagram for the boost rectifier is shown in Figure 3.20. It includes decoupling terms $3\omega L/V_o$ to eliminate cross-coupling between the d and q channels so that they could be controlled independently [15]. Perfect decoupling is achieved at a specified line

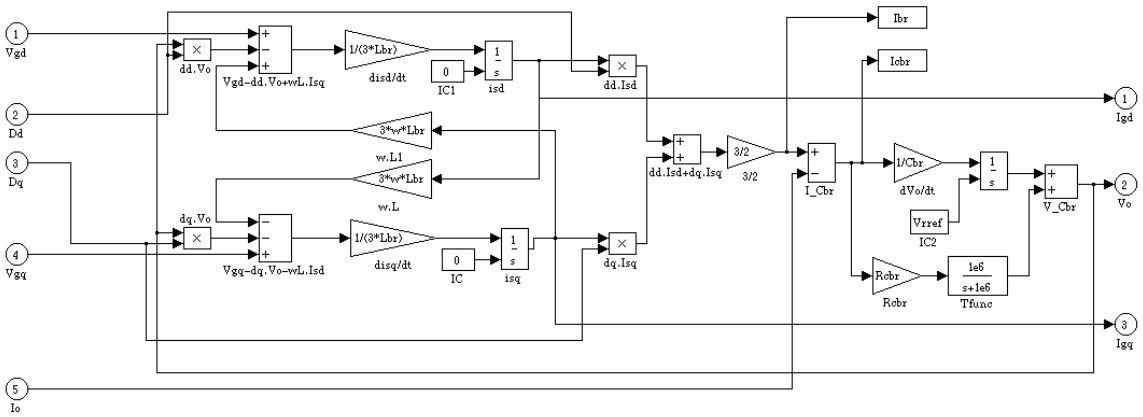

Figure 3.19 Simulink model of the boost rectifier power stage in *dq* coordinates.

frequency and output voltage and is load-independent, which satisfies the conditions of this research.

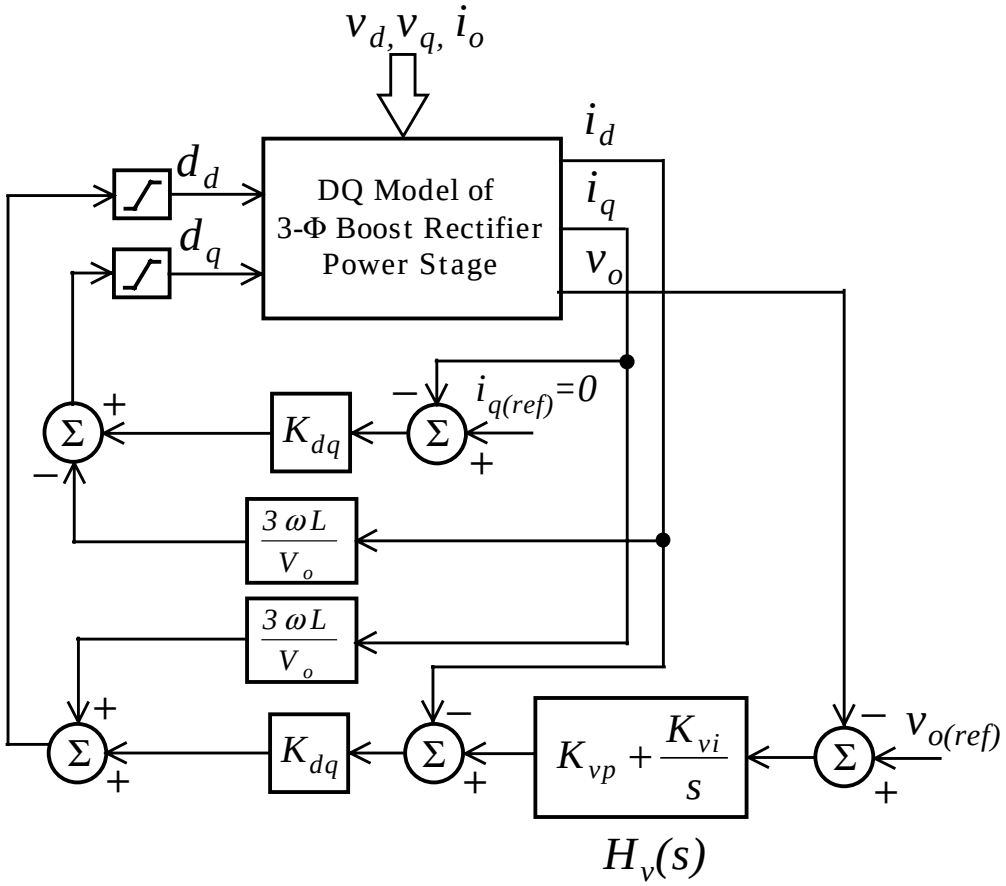

Figure 3.20 Control diagram of the boost rectifier.

The voltage mode feedback control is provided with a feedback voltage loop and two current loops. The current loops control the decoupled channels of the power stage independently by adjusting their duty cycles. They both use proportional controllers with the same gain K_{dq}. The reference signal for the q channel is set to zero since the input currents should be in phase with the input voltages. The reference signal for the d channel is provided by the voltage loop compensator. Closed-loop transfer functions for both current loops are load-independent.

The voltage loop uses a proportional-integral compensator with a transfer function

$$H_v(s) = K_{vp} + \frac{K_{vi}}{s}, \tag{3.15}$$

which provides fast response and no steady-state error in the output voltage. Control-to-output transfer function v_o/i_{dref} significantly depends on the load and direction of the power flow; therefore, the voltage loop compensator can be optimized only for a specific load. In order to use this type of control for the whole range of loads under bidirectional power flow conditions as assumed in this research, a compromise in the compensator design was required. The resulting

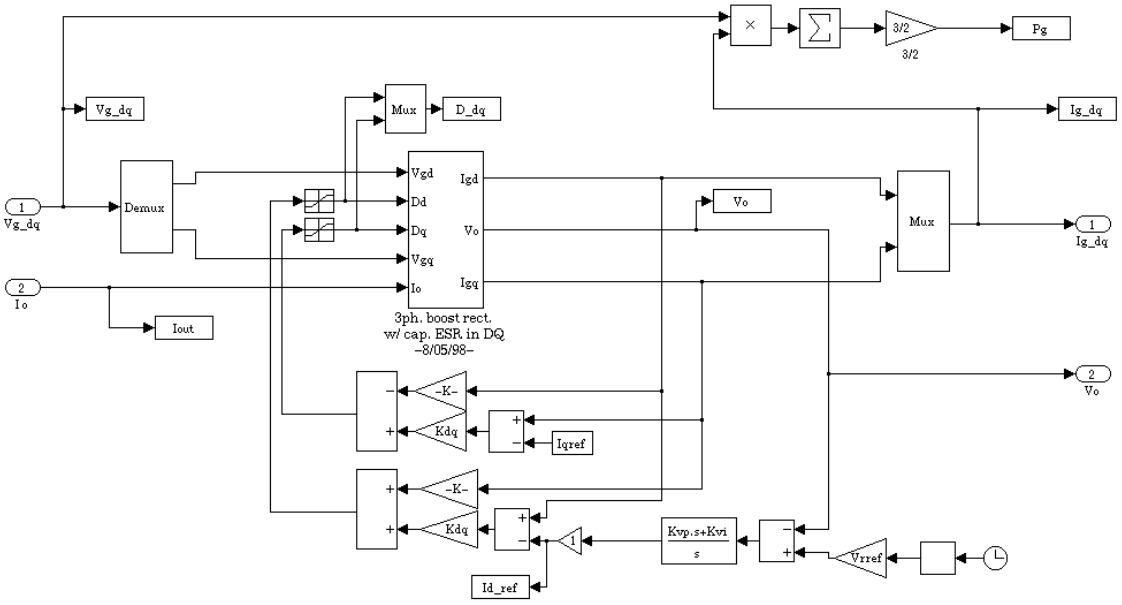

Figure 3.21 Closed-loop Simulink model of the boost rectifier in *dq* coordinates.

design provided a low closed-loop bandwidth yet stable operation and acceptable transient response under all load conditions.

The complete closed-loop Simulink model for the boost rectifier is shown in Figure 3.21. It utilizes the Simulink model of the rectifier power stage as a subsystem.

3.4 Switched Reluctance Generator Modeling

A switched reluctance machine can be used as a starter/generator in the PDS instead of a synchronous generator. This approach eliminates the need in a three-phase-to-dc converter (boost rectifier) discussed above. The switched reluctance generator (SRG) is connected directly to the DC bus through its own inverter, which is a mandatory part of the machine. A schematic of one channel of an SRG developed for aircraft applications is shown in Figure 3.22; the details of its operation and testing results are covered in [16-19]. Another advantage of an SRG compared with a synchronous generator-boost rectifier combination is that the SRG has a simpler rotor design (no windings), which improves its reliability and makes simpler its maintenance. A certain effort was made in the framework of this research in order to develop a Simulink model of the SRG that can be effectively used for simulation and analysis as a part of the global PDS model.

The SRG presents unique challenges in modeling. Like in a synchronous generator, the winding inductances of the SRG depend on the rotor position. In addition, they depend on the phase current because the magnetic flux of a phase always saturates in the aligned position and returns to non-saturated state when the phase goes out of alignment. Therefore, magnetic properties of the material must be taken into account. The phase voltage and current waveforms are not sinusoidal. Unlike the synchronous machine, there is no transformation of variables that could transform the SRG voltages and currents into dc variables. The majority of models built for a switched reluctance machine (for example, [20]) follow a straightforward approach that

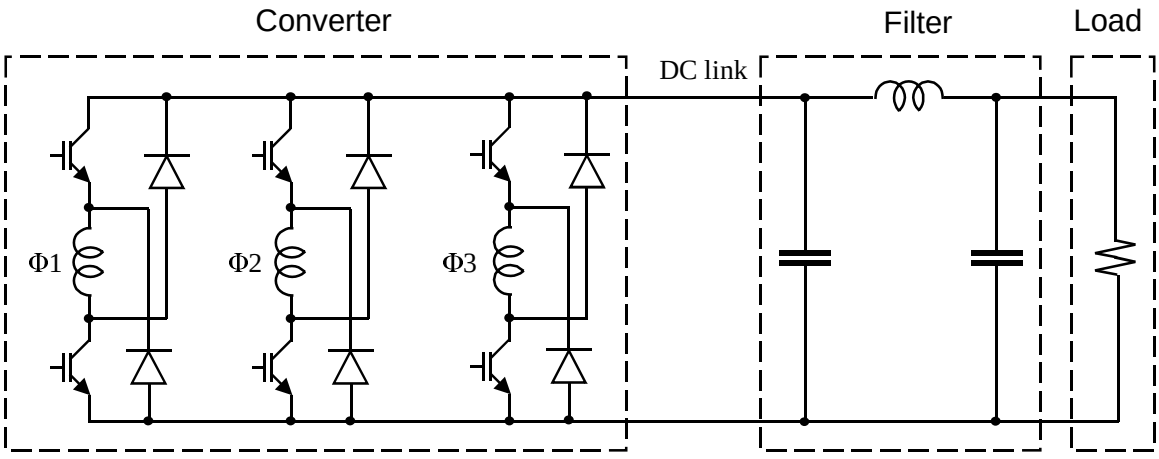

Figure 3.22 Switched reluctance starter/generator circuit diagram.

includes modeling of all details of its operation. This results in a detailed model, which is very complex, computationally intensive, not suitable for control design, and cannot be used as a part of the global PDS model for simulation and analysis.

An average type of model for the SRG could be built based on assumption made in [21]. Figure 3.23 shows how the DC link current is made up of individual phases' currents. With a certain degree of idealization, this current may be viewed as a discrete function of time, in which each step corresponds to the current of the phase active at this moment. This approach results in a discrete average model of a SRG [21] shown in Figure 3.24. In this model, the DC link current

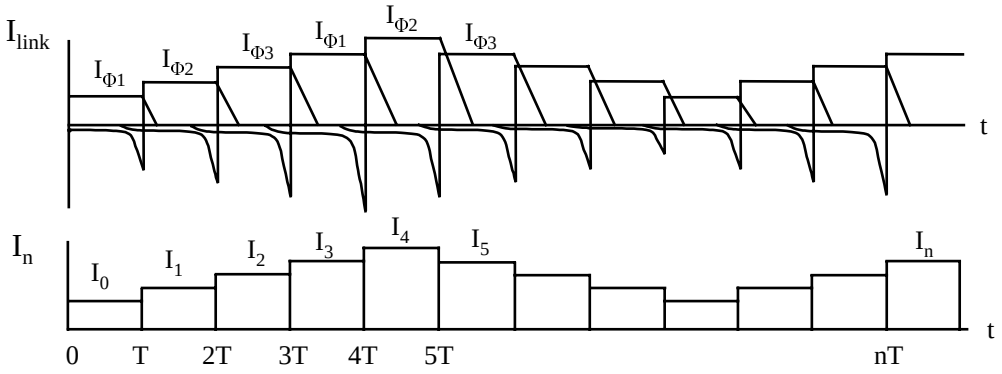

Figure 3.23 Switched reluctance starter/generator discrete average modeling concept, [21].

is represented by a current source controlled with a discrete controller. The rest of the model is a low-pass DC link filter. The value of the current is constant over one electrical cycle but may change from cycle to cycle. The controller adjusts the DC link current in order to maintain the output voltage at a specified level. The discrete controller incorporates two time delays: a constant delay introduced by the microprocessor control, and a variable delay, which comes from a discrete nature of the model and depends on the SRG speed. As shown in [21], the model produced results in good agreement with experimental results.

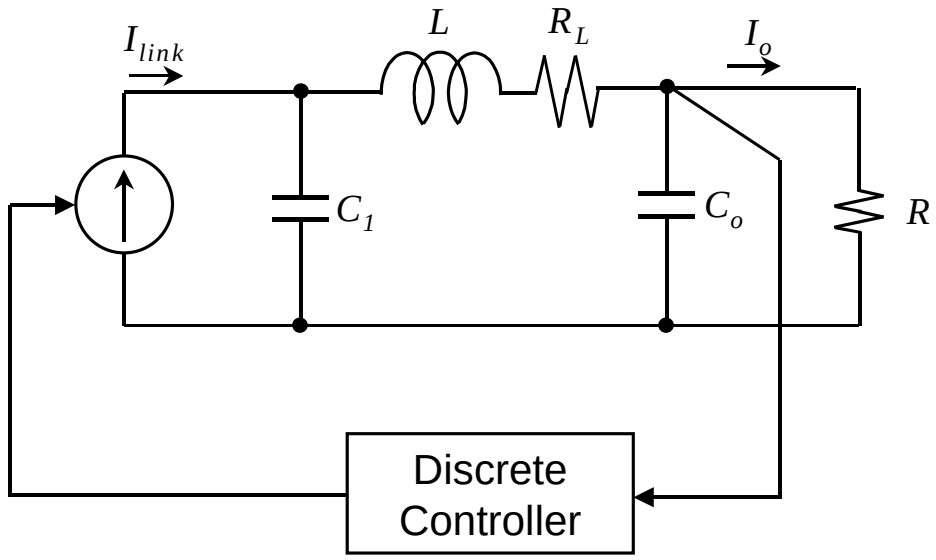

Figure 3.24 Switched reluctance starter/generator discrete average model.

Although the model in Figure 3.24 is a considerable step from the detailed model towards a simple, computationally efficient average model of the SRG, the discrete nature of the model still makes it unsuitable for the purpose of this research. A discrete model of the SRG included into the overall PDS model will make it computationally inefficient because all discrete steps will have to be processed by the integration routine. A discrete model as a part of the PDS will not allow using frequency domain techniques for stability analysis and control design. To overcome these difficulties, a continuous SRG model was built in this research by further developing of the discrete averaging concept presented above.

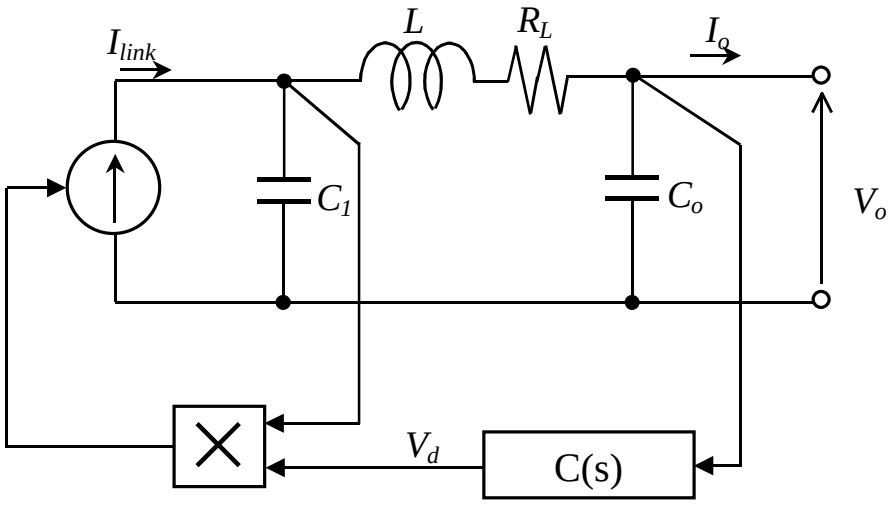

Figure 3.25 Switched reluctance starter/generator continuous average model.

The new model is based on a further simplification of the discrete DC link current waveform shown in Figure 3.23 with an assumption that the current changes continuously. This assumption significantly limits the frequency range in which this model is valid since the lowest phase current frequency, which occurs at ground idle engine speed, is only 5.4kHz. Although different control strategies are possible for the SRG, we assume that output voltage feedback control is used. The model is shown in Figure 3.25. An analog compensator with transfer function C(s) processes the output voltage error and produces the control signal V_d. Voltage across capacitor C_1 is the DC link voltage. As shown in [18], current generated by a phase during its generation period is determined by current built up in the phase during its excitation period (Figure 3.26). The current built up in the phase (the amount of excitation energy) depends both on the time when the switches are closed during the excitation period and the DC link voltage. For an inductor, the current built up in it is proportional to the voltage across the inductor and the time during which the voltage is applied, according to the formula:

$$V = L\frac{\Delta I}{\Delta t}. \tag{3.16}$$

Therefore, the simplest assumption was made that the generated DC link current is equal to the product of the DC link voltage and the feedback control signal V_d as shown in Figure 3.25. This is an analogy with a PWM switch that controls excitation of the phase. V_d is a control signal

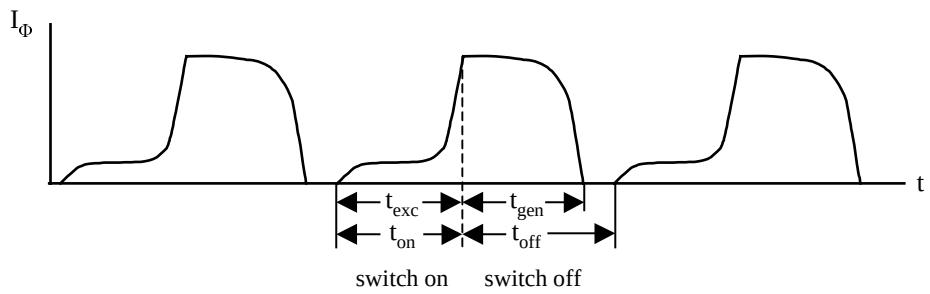

Figure 3.26 Switched reluctance generator phase current waveform, [18].

proportional to the time duration of the excitation switches (Figure 3.22) being closed. It may also be viewed as duty cycle of the switches within the electrical cycle of the phase. It is seen from the model that with constant excitation time (open loop operation) the system may be unstable depending on the load, which agrees with the analysis given in [18]. The model equations are as follows:

$$
\begin{aligned}
& i_{link} = v_{C_1} \cdot v_d \\
& v_d(s) = C(s) v_o(s) \\
& L \frac{di_L}{dt} = v_{C_1} - v_o - R_L i_L \\
& C_1 \frac{dv_{C_1}}{dt} = i_{link} - i_L \\
& C_o \frac{dv_o}{dt} = i_L - i_o
\end{aligned}
\tag{3.17}
$$

where

i_{link} - DC link current,

v_{C1} - DC link voltage,

v_d - control signal,

v_o - output voltage,

i_L - inductor current,

i_o - output current,

L - - filter inductance,

R_L - filter inductor ESR,

C_1 - DC link capacitor,

C_o - output capacitor.

A Simulink block diagram based on the developed continuous model (Figure 3.25) is shown in Figure 3.27.

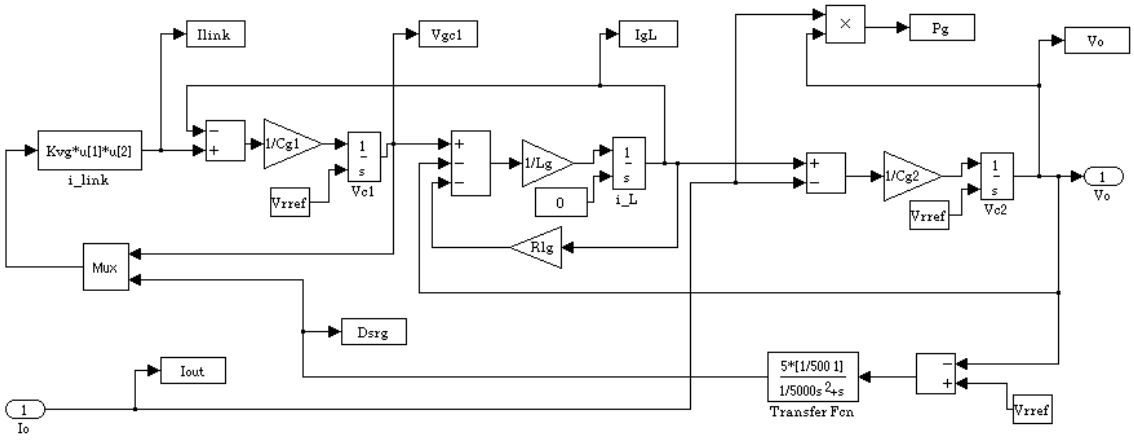

Figure 3.27 Simulink model of the switched reluctance starter/generator.

3.5 Modeling of Flight Actuators

3.5.1 Electromechanical Actuator Modeling

An electromechanical actuator driving an inboard spoiler surface of an aircraft was chosen as an example of a flight actuator being a part of the PDS. A Simulink model of the actuator-surface system was developed by Lockheed Martin Control Systems in Johnson City, New York.

A system diagram of the electromechanical actuator (EMA) is shown in Figure 3.28. It consists of a dc-dc power converter feeding a dc motor, which moves the inboard spoiler surface through a mechanical transmission consisting of a gearbox and a ball screw mechanism. The dc-dc converter is connected to the dc power distribution bus through an input filter, whose purpose is to prevent the switching ripple of the converter from going to the bus. Finally, a multiloop feedback controller is employed to precisely control the surface movement. A typical EMA architecture of a modern aircraft employs a three-phase brushless motor fed by a dc-to-three-phase inverter. However, the model developers came to conclusion that the use of a dc-dc converter and a dc motor models instead will not affect essential features of the subsystem dynamics.

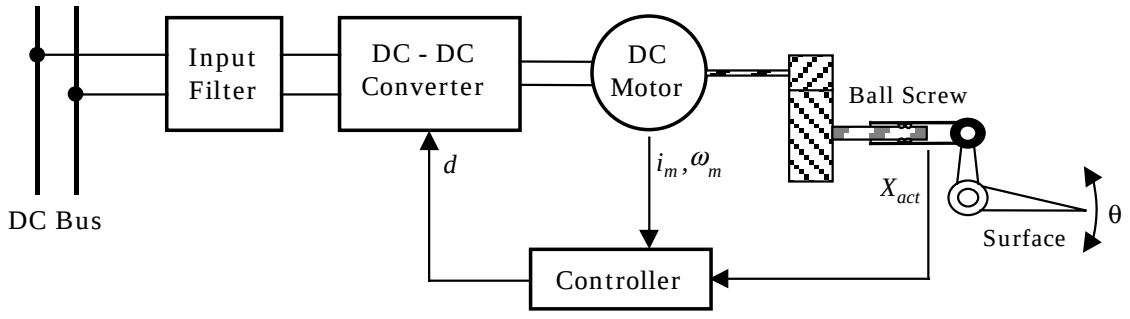

Figure 3.28 Electromechanical actuator system diagram.

A Simulink model for the EMA subsystem (Figure 3.29) follows its structure and consists of six functionally complete modules. The input filter is modeled as an LC filter, whose

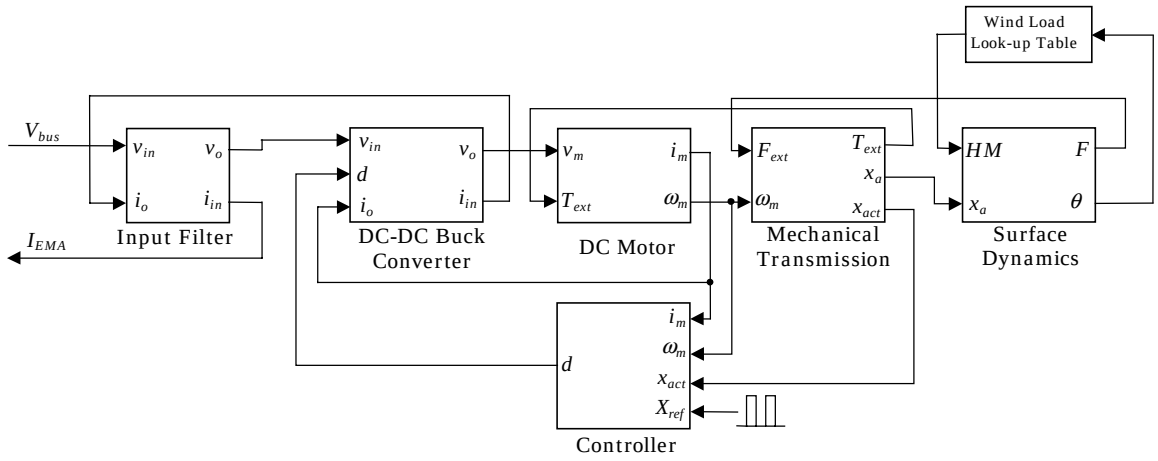

Figure 3.29 Electromechanical actuator Simulink block diagram.

modeling was already discussed above (Figures 3.1 and 3.2). The dc-dc converter module represents a power stage of the buck converter without an output LC filter because its load (dc motor) provides sufficient filtering effect due to its own inductance. Therefore, the average model of the PWM switch shown in Figures 3.4 and 3.5 was used for the dc-dc converter. A Simulink model for a separately excited dc motor is shown in Figure 3.30. The model is derived from the motor equations:

$$\begin{aligned} v_m &= K_e\omega_m + i_m R + L\frac{di_m}{dt} \\ K_t i_m - T_{ex} &= B_m\omega_m + J\frac{d\omega_m}{dt} \end{aligned} \tag{3.18}$$

where

v_m - armature voltage,

i_m - armature current,

ω_m - armature angular speed,

T_{ex} - external (load) torque applied to the shaft,

L - armature inductance,

R - armature resistance,

J_m - armature inertia,

B_m - viscous friction coefficient,

K_e - back-emf constant,

K_t - electromagnetic torque constant.

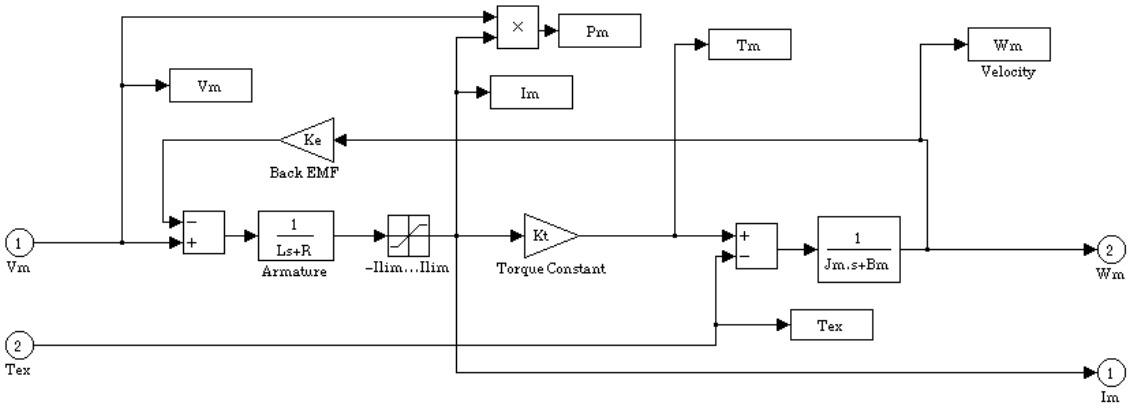

Figure 3.30 Simulink model for a separately excited dc motor.

The mechanical actuator module includes a gearbox and a ball screw mechanism. A Simulink model for the mechanical transmission (Figure 3.31) takes into account inertia, damping, and stiffness of the ball screw mechanism and stiffness of the bearing structure.

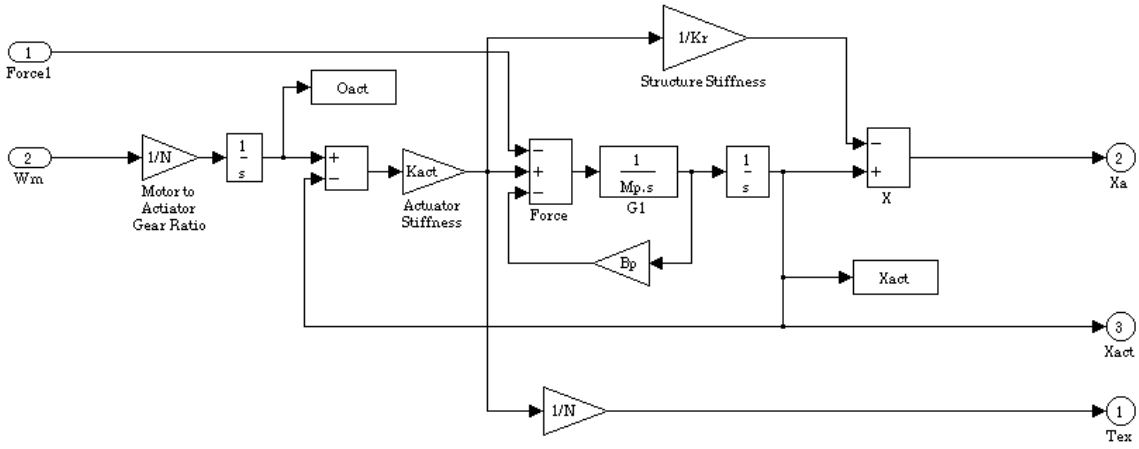

Figure 3.31 Simulink model for the mechanical transmission of the EMA.

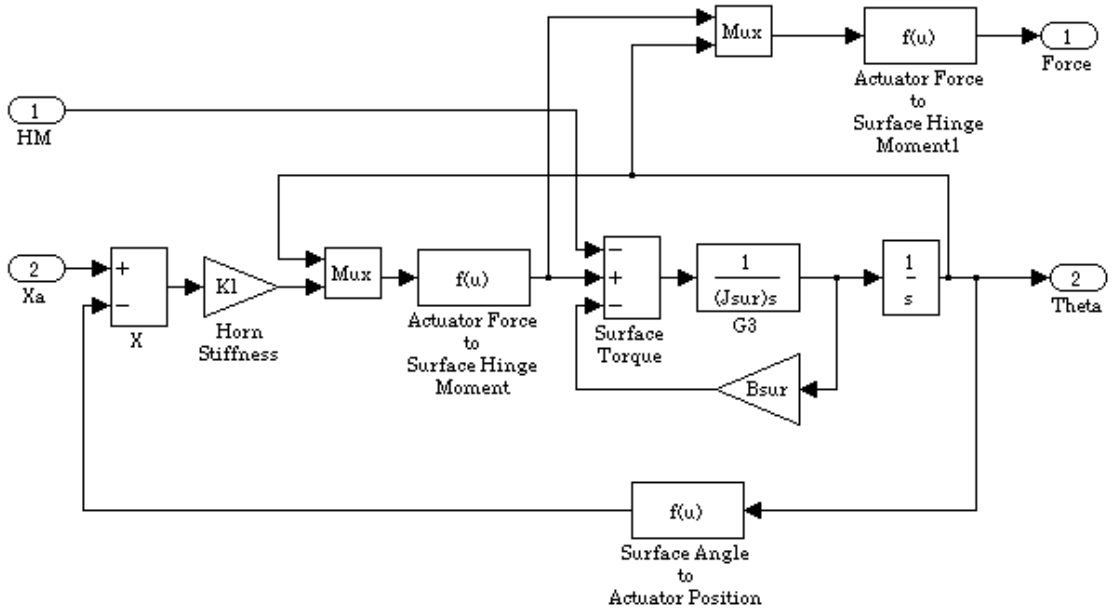

Figure 3.32 Simulink model for the surface dynamics.

A Simulink model for the surface dynamics is shown in Figure 3.32. The model reflects the horn stiffness, surface inertia and damping, and a nonlinear relationship between the mechanical actuator movement and the surface deflection angle.

The feedback controller (Figure 3.33) controls duty cycle of the dc-dc converter according to the actuator position command. The controller employs the motor current, motor speed, and the actuator position feedback loops.

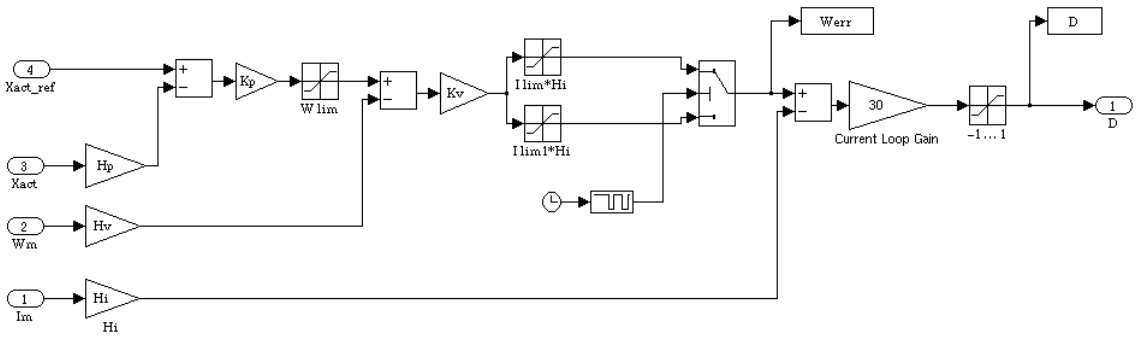

Figure 3.33 Simulink model for the EMA feedback controller.

A part of the EMA model is a Simulink look-up table containing an approximation of the wind load on the spoiler surface as a function of its deflection angle. This table was used in simulations of normal flight conditions. Another possible scenario investigated in this research is testing the system on the ground, which assumes that there is no wind load to the surface.

3.5.2 Electrohydrostatic Actuator Modeling

Another model developed by Lockheed Martin Control Systems as an example of a flight actuator modeling was an electrohydrostatic actuator driving the elevator surface. A system diagram of the actuator is shown in Figure 3.34, and its Simulink model – in Figure 3.35.

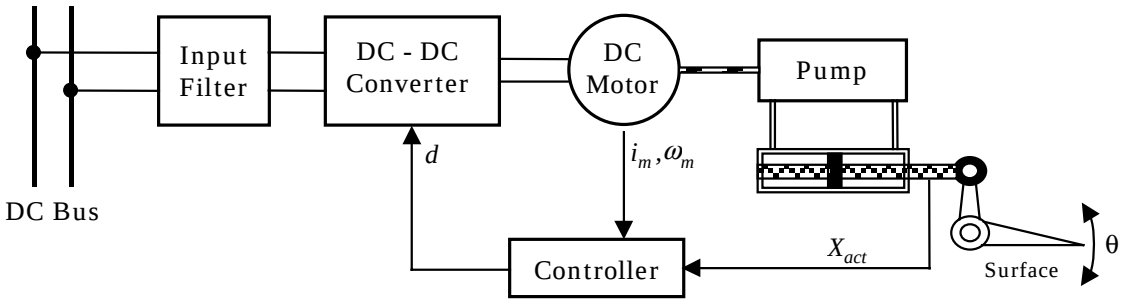

Figure 3.34 Electrohydrostatic actuator system diagram.

The electrohydrostatic actuator (EHA) model is very similar to the EMA model described above. The model employs a hydraulic actuator consisting of a hydraulic pump and a hydro-cylinder instead of a mechanical actuator to convert the motor rotation to the surface movement. A Simulink model of the hydraulic actuator is shown in Figure 3.36. It takes into account the pump leakage, the piston inertia and damping, and the bearing structure stiffness. All the other components of the EHA model have the same structure as the corresponding EMA components but different parameter values. The EHA model was used in simulations in the same way as the EMA model.

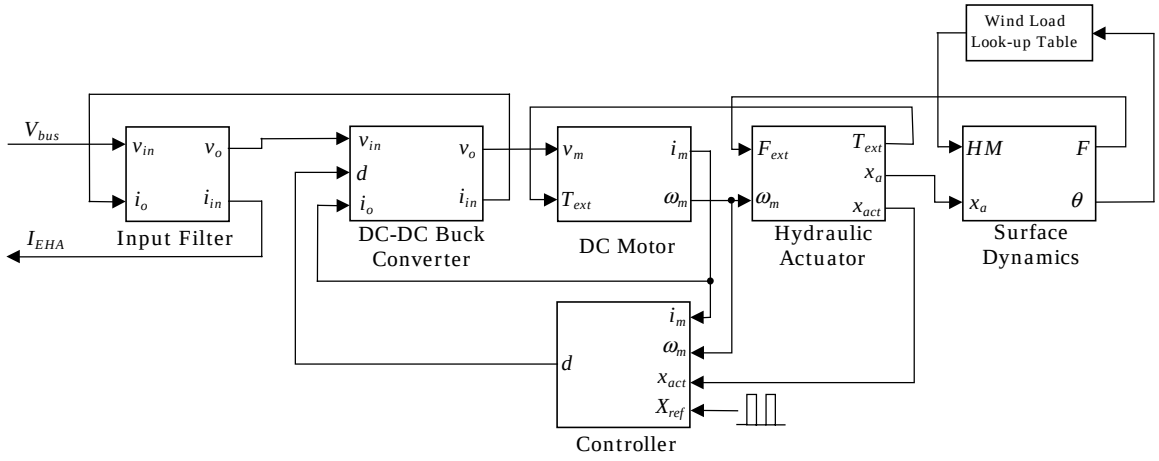

Figure 3.35 Electrohydrostatic actuator Simulink block diagram.

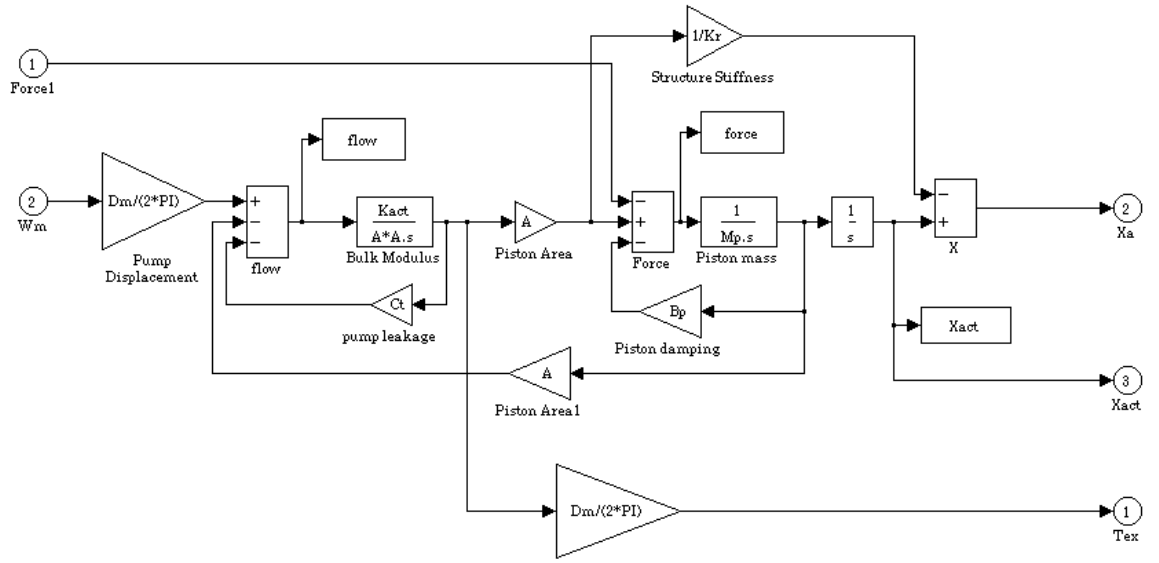

Figure 3.36 Hydraulic actuator Simulink model.

3.6 DC Power Distribution Bus Modeling

The dc bus as viewed in this research consists of wires and cables transmitting dc power between the three-phase-to-dc converters and the loads. These connection elements are characterized by R, L, C parameters distributed along their lengths. Although these parameters are fairly small compared to the corresponding lumped parameters of the subsystems connected to the bus, they do affect the processes in the PDS under certain scenarios of operation and therefore must be taken into account.

Since we are not interested in studying propagation of voltages and currents along the bus, there is no need in modeling it as a transmission line. A much more computationally effective bus model may be obtained by modeling any piece of the bus between two adjacent subsystems connected to it as a network with lumped parameters. In order to account for attenuation and phase delay produced by such a piece a simple LC filter model would suffice. The LC filter network (Figure 3.1) and its Simulink model (Figure 3.2) were already discussed above.

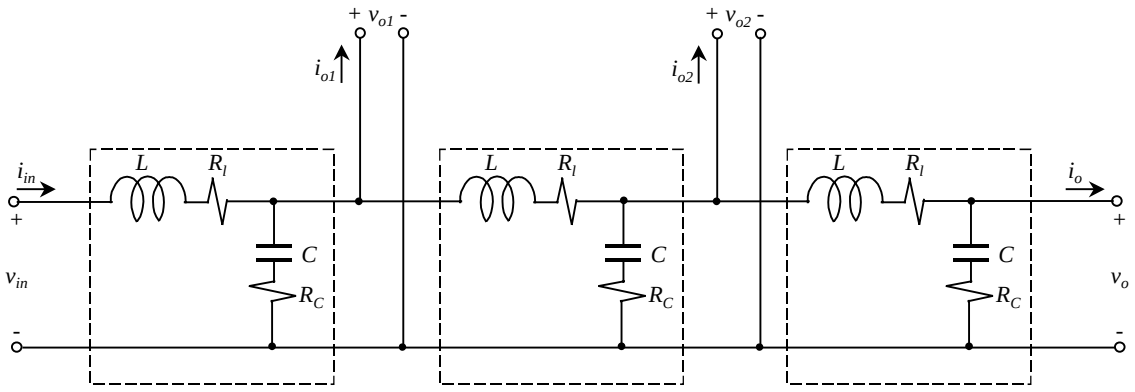

Figure 3.37 Three-section dc bus equivalent circuit.

Figure 3.37 shows a three-section dc distribution bus with two subsystems connected to its ends and two others connected in the middle. Each section is modeled as an LC filter network whose parameters should be determined specifically for each section based on the section length

and the distributed parameter values. The leakage conductance between wires is not modeled since it is negligible for aircraft busses. A corresponding Simulink model shown in Figure 3.38 is based on the LC filter models assembled into a subsystem model according to the interconnection rules.

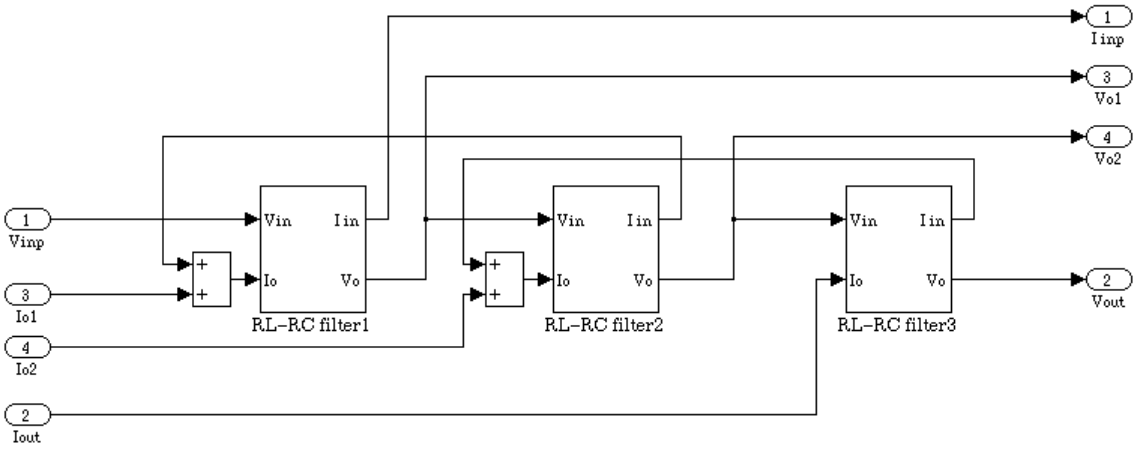

Figure 3.38 Simulink model for a three-section dc bus.

Chapter 4

Stability Analysis of a DC Power Distribution System

4.1 Introduction

Stability in all modes of operation is the first and the most important requirement for a power distribution system. In the PDS containing highly coupled subsystems, possible subsystem interactions complicate the issue. The PDS includes various types of loads, which affect differently the overall system stability. Changes of the load may lead a stable system into instability. Subsystems may be connected and disconnected at any time, thus changing the overall system configuration. In addition, certain loads such as flight actuators may switch into regenerative mode of operation. This condition changes the system configuration as well and opens possibilities for new interactions between its subsystems.

It is expected that up to 75% of the total load in the PDS of a future aircraft will be represented by constant power load [22]. Constant power load is usually a load connected to the DC distribution bus through a voltage regulator. The regulator provides specified voltage and current to the load regardless of voltage disturbances on the bus; therefore, the regulator appears as a load that draws constant power from the bus. Examples of such a load are avionics and flight control actuators. In a flight control actuator, the regulator as a part of the actuator feedback control provides commanded voltage to the motor. A constant power load presents a negative small-signal resistance on the bus, which is known to have a destabilizing effect on the system [23]. Since this is only a small-signal phenomenon (large-signal resistance of a constant power load is positive), possible instability resulting from such a load will not usually cause the

whole system to crash, but will result in undesirable oscillations around the equilibrium point. The bus voltage oscillations can be large enough in magnitude to be a source of EMI, to damage other equipment connected to the bus, and even to create global system instability in a large-signal sense.

The modeling and analysis tools developed in this research can be effectively used to analyze stability of the PDS based on linearization and small-signal analysis techniques. Stability analysis of a PDS with different types of loads including an EMA and a generic constant power load is presented below. This chapter is not intended to be a comprehensive treatment of all possible stability issues in the PDS of a future aircraft but rather an example of using the modeling and analysis tools for stability analysis of the PDS.

4.2 System Configuration and Stability Analysis Techniques

The power distribution system configuration used in this research for stability analysis is shown in Figure 4.1. Power is supplied by a synchronous generator through a three-phase-to-dc boost rectifier to the DC bus loads. The load types considered in this chapter are the EMA and generic resistive and constant power loads. Both single and mixed load types are analyzed.

Stability analysis in this research is based on frequency domain analysis techniques known from linear control theory. The nonlinear PDS model is linearized at certain equilibrium points of interest, then small-signal stability analysis is performed. A positive result of stability analysis would mean that the system is stable for small enough perturbations around the equilibrium point. A small-signal instability could lead to either local instability with oscillations around the equilibrium point, or global instability, when the system states significantly depart from the equilibrium point.

Simulink block diagrams and MATLAB files used for stability analysis are given in Appendix D. It was found convenient to have separate Simulink models for simulation and

linearization. Linearization requires additional elements in the block diagram (input and output ports, switches). Initial values of the system state variables are different for simulation and linearization purposes. Having two separate Simulink block diagrams significantly reduces clutter on the screen, especially for systems with a large number of subsystems.

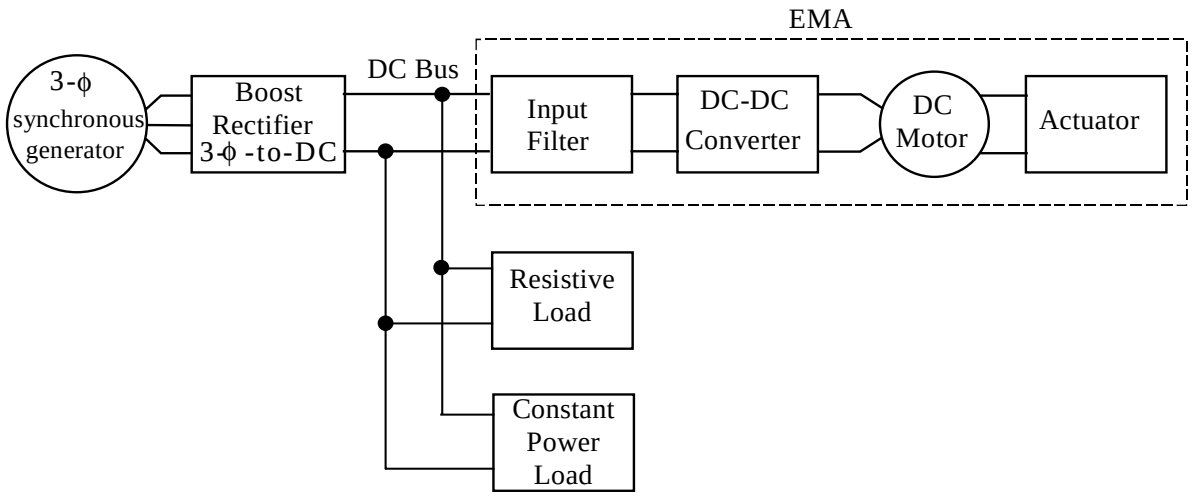

Figure 4.1 Power distribution system configuration for stability analysis.

Linearization of a nonlinear system is performed using MATLAB command `linmod`. Then various transfer functions of interest are extracted from the linearized model and used for stability analysis. For correct results, `linmod` has to be supplied with the state and input vectors at the equilibrium point where linearization is performed. The state and input variables must be arranged within the vectors according to the order that Simulink assigns them within a Simulink model. This order may easily change when the input and output blocks are added to the model for obtaining a particular transfer function. Unfortunately, there is no way to fix this order, and MATLAB does not come with any tool that would automate this rearrangement. As a result, for high order models much work is usually required to set all the variables correctly for each linearization procedure. The analysis tool developed in this research performs this procedure automatically. The state and input variables for an equilibrium solution are stored in a file together with their names. For each linearization procedure, the variables are retrieved from the file and rearranged according to the order of states and inputs in the linearized model.

Obtaining an equilibrium solution for a nonlinear system could also be problematic in MATLAB because it does not have a good enough tool for steady-state analysis. The 'trim' command, intended for this purpose, uses constraint optimization technique, which itself is a complicated mathematical problem without a universal solution. Because of that, numerical algorithm used in 'trim' command often fails to converge when the system order becomes large enough. For this reason, there is no universal technique for obtaining an equilibrium solution for a Simulink model.

As a more practical way, simulation is used in this research to obtain an equilibrium solution. The nonlinear model of the PDS is simulated until it reaches the desired steady state point. Depending on a system configuration, some ingenuity may be required to use this approach successfully. For example, it may be beneficial to introduce into the system some additional damping that does not affect the steady-state solution (placing resistors in series with capacitors) to make simulation converge to the equilibrium point faster. An unstable equilibrium may be obtained with this approach as well if the system is modified such that the equilibrium becomes stable without changing it. For example, unstable equilibria of the PDS with constant power loads in this research were obtained by simulation of the system with equivalent resistive loads.

Another possible approach to obtaining an equilibrium solution for a complex system is using a steady-state model derived from a dynamic Simulink model. Certain circuit-oriented simulators (for example, Spice and Saber) do this procedure automatically by shorting all inductances and opening all branches with capacitors in the model. Although MATLAB does not derive a steady-state model automatically, this procedure can be done manually. This will result in a simplified model, which is easier to solve for an equilibrium. If the resulting model is simplified to such a degree that it does not contain algebraic loops, the equilibrium solutions for the system states and inputs can be calculated manually, one at a time. This technique was also used in this research. If the resulting model does contain algebraic loops, there is still a greater chance that MATLAB would be able to solve it for an equilibrium solution than the original dynamic model. It may be convenient to have a set of three Simulink models for small-signal

analysis of a nonlinear system: a dynamic model for simulation, a model for linearization, and a static model for steady-state analysis.

4.3 Stability Analysis of a PDS with Constant Power Load

At the first stage of analysis, we assume that only a constant power load is applied to the DC bus. The system stability then could be analyzed using loop gain transfer function of the boost rectifier and phase margin test. An alternative approach based on the impedance ratio criterion [23] will be used later.

Figure 4.2 shows the boost rectifier control-to-output voltage transfer functions obtained by linearization of the PDS Simulink model with parameters given in Appendix A. The transfer functions were obtained for constant current load with different power levels ranging from 1kW to 300kW. Constant current load has infinite small-signal input impedance. It does not affect transfer functions of the source but only determines its equilibrium; therefore, it is a good starting point for analysis of dynamic properties of the boost rectifier.

It is seen that both magnitude and phase of the transfer functions in Figure 4.2 significantly change with the power level of the load. A linear compensator for the output voltage feedback loop of the boost rectifier must be optimized for the whole range of possible loads. The compensator

$$C(s) = \frac{s + 3000}{s} \tag{4.1}$$

was designed to provide stable operation of the system for a wide range of load conditions, although with a somewhat slow transient response. As it is seen from the boost rectifier loop gain transfer functions (Figure 4.3), the compensator provides phase margins sufficient for stability with loads of all power levels. However, the bandwidth of the control loop becomes smaller with the increase of the load, which causes slower transient response. A compensator

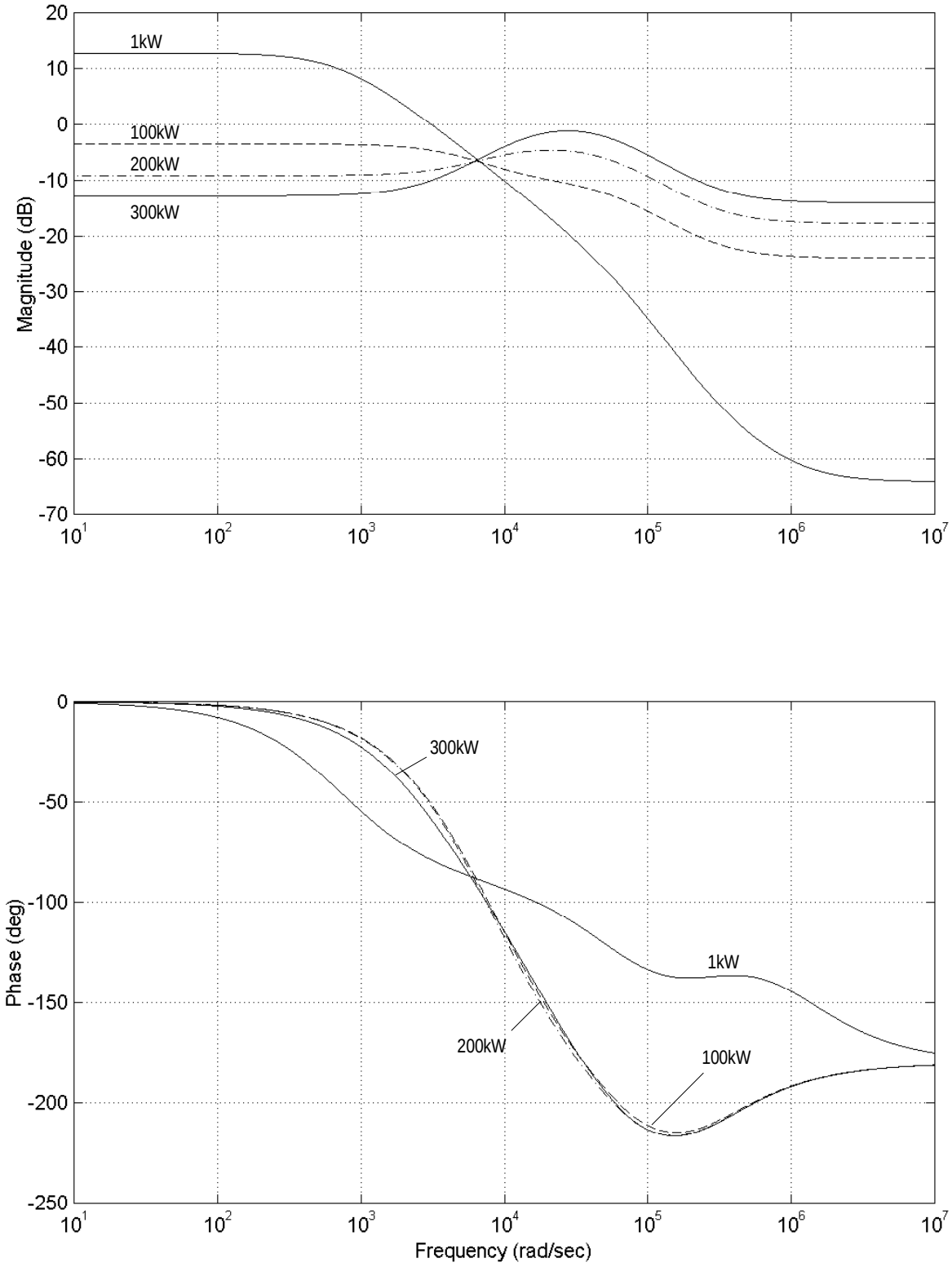

Figure 4.2 Boost rectifier control-to-output transfer functions with constant current load.

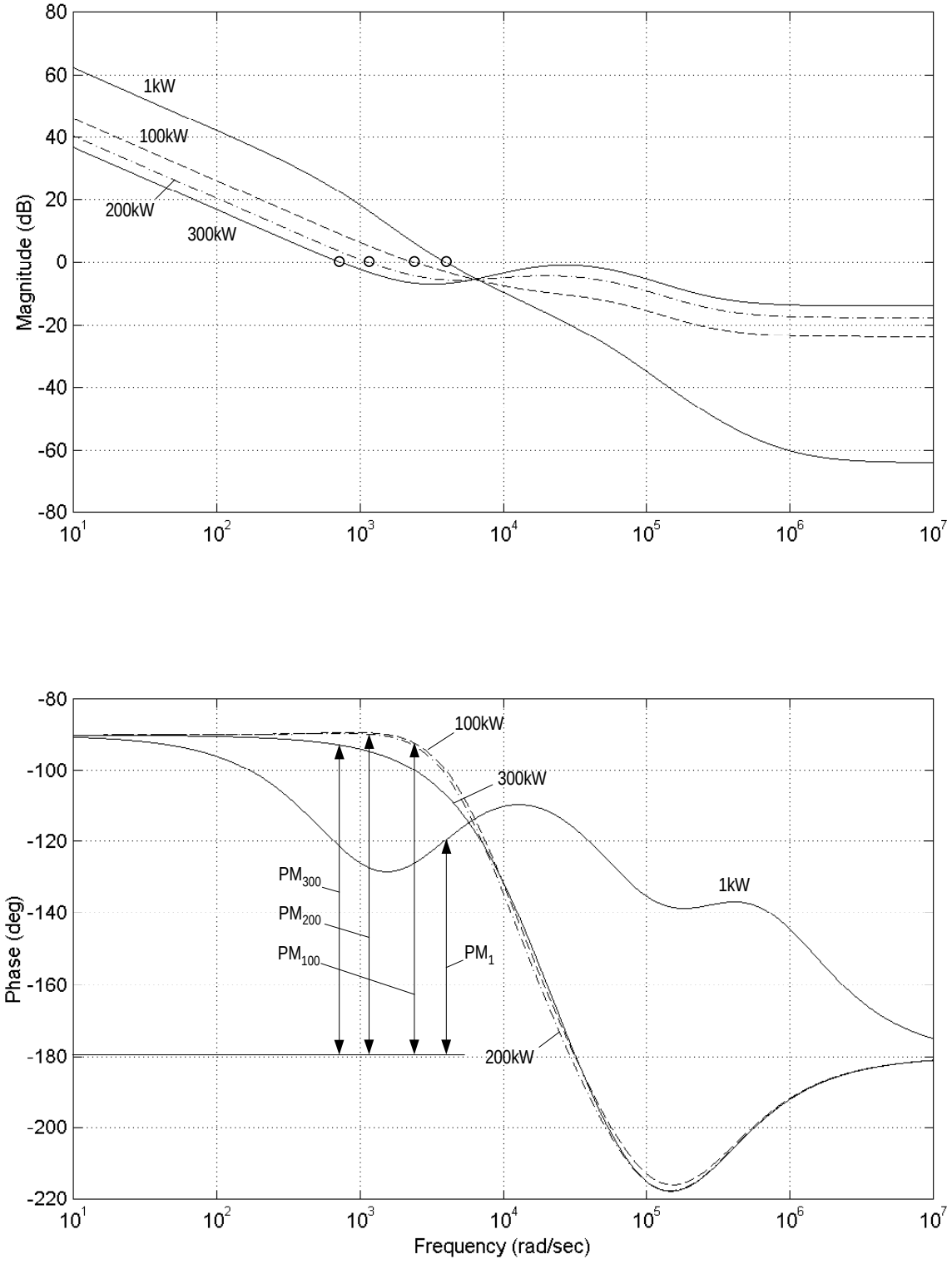

Figure 4.3 Boost rectifier loop gain transfer functions with constant current load.

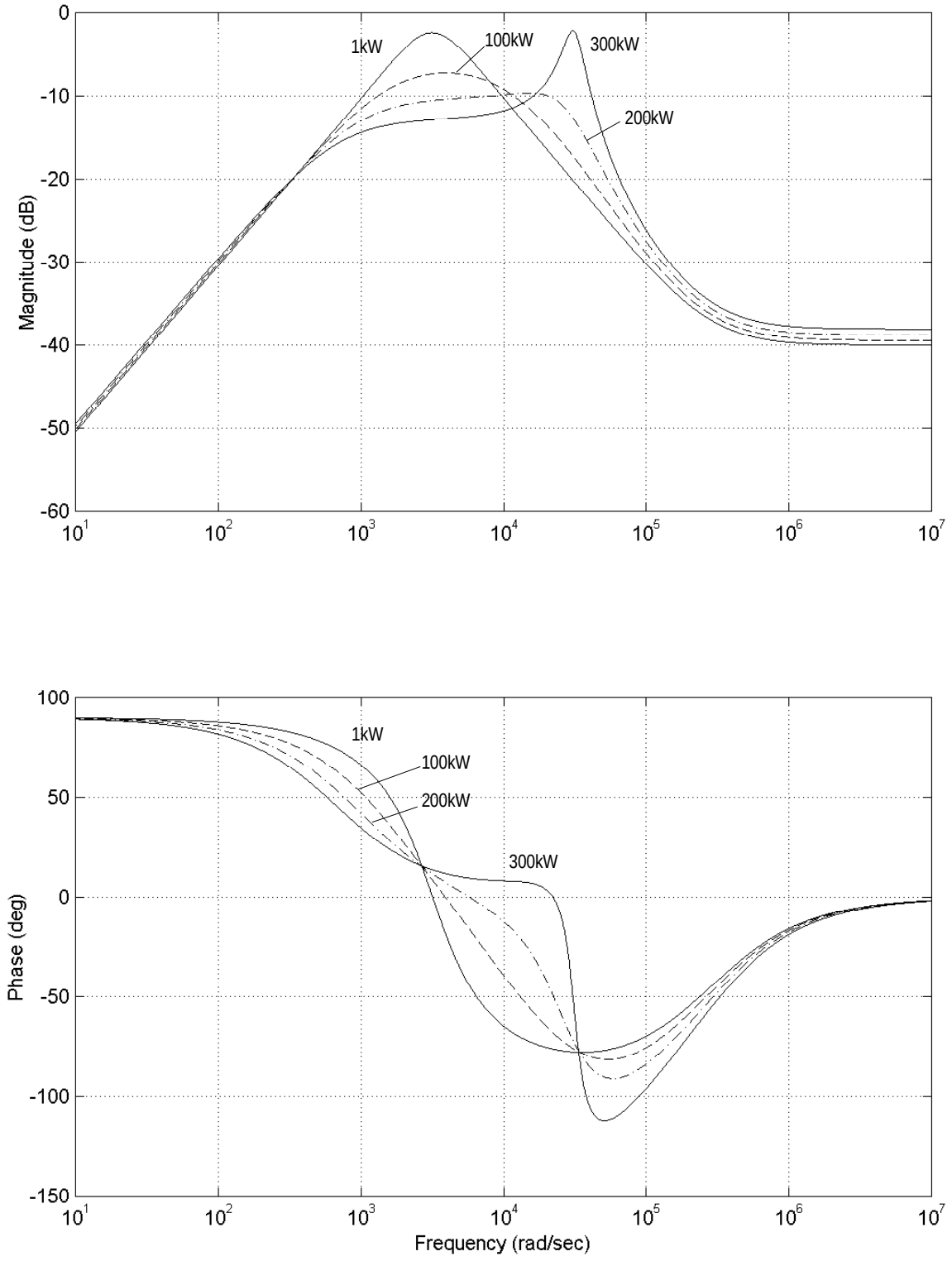

Figure 4.4 Boost rectifier output impedance transfer functions with constant current load.

with gain scheduling would probably be able to eliminate this reduction in the bandwidth, thus making dynamic properties of the boost rectifier better.

Figure 4.4 shows the closed loop output impedance of the boost rectifier with constant current load. This is an important transfer function, which will be used later for stability analysis based on the impedance ratio criterion. It is seen that the output impedance initially decreases with the increase of the load up to about 200kW, after which it increases again.

A bus load may be a constant current load type if it has a regulator designed to deliver a constant current to the load regardless of voltage disturbances on the bus. As mentioned above, constant current load has infinite small-signal input impedance (which may be considered either positive or negative). In practice, however, a load connected to the bus would more likely be either resistive or constant power type. A resistive load has an input impedance equal to its resistance (small-signal resistance if the load is nonlinear) with a phase of zero degrees in the frequency range of interest. A constant power load appears on the DC bus with a large-signal resistance

$$R_{ls} = \frac{V_{bus}^{\ 2}}{P_{const}}, \tag{4.2}$$

and a small-signal resistance

$$R_{ss} = -R_{ls}. \tag{4.3}$$

This load has a small-signal input impedance equal to $|R_{ss}|$ with a phase equal to 180 degrees in the frequency range of interest. Another possible type of load, which will not be considered in this research, is a load with complex input impedance. An RLC-network or a resistive load with an input filter are examples of this type.

Figures 4.5, 4.6, and 4.7 show how the control-to-output, loop gain, and output impedance transfer functions of the boost rectifier are modified in case of resistive and constant power loads in comparison with constant current load of the same power level. The transfer functions are given for two power levels. For resistive loads, the magnitudes of the first two

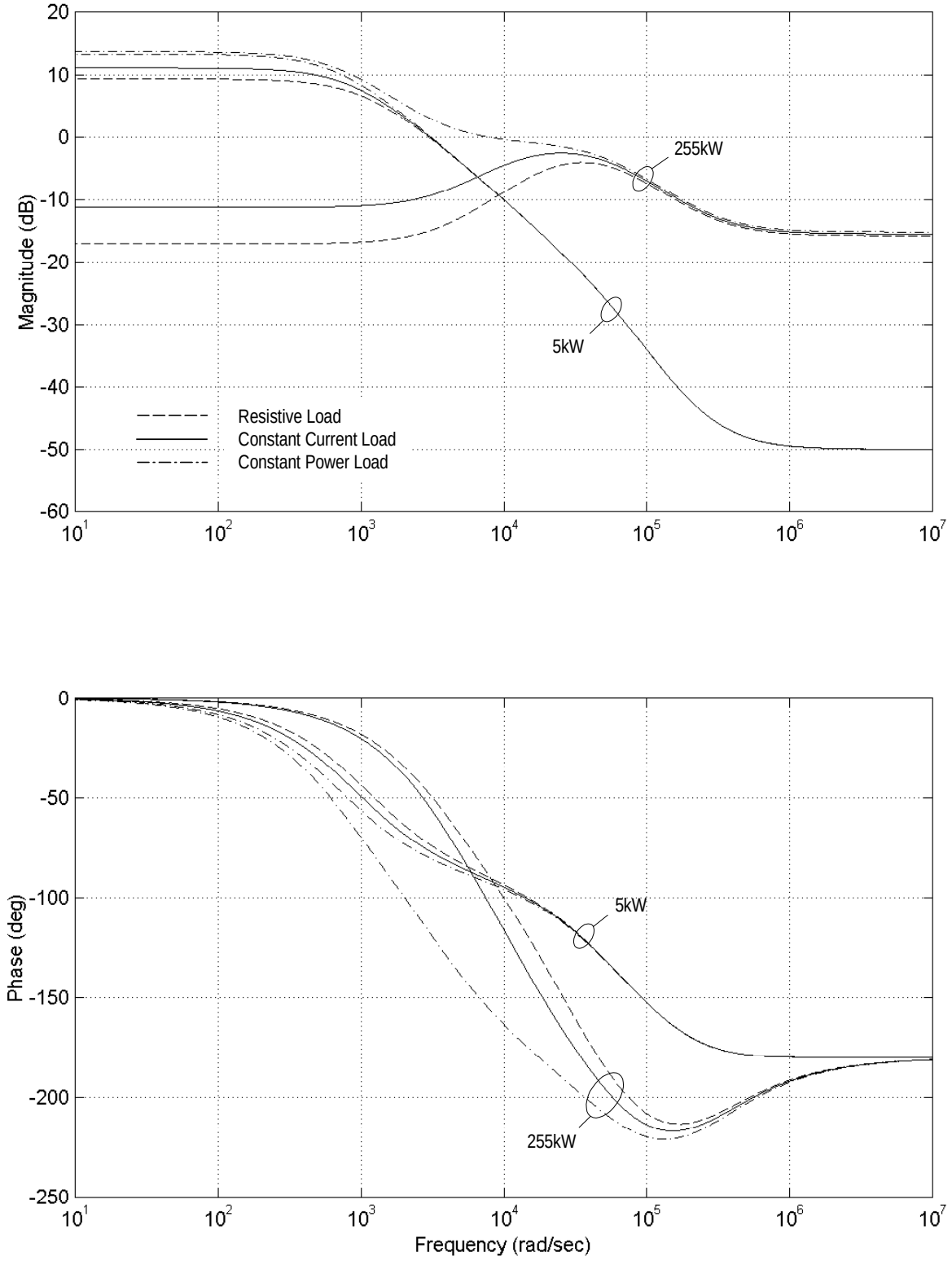

Figure 4.5 Boost rectifier control-to-output transfer functions with different types of load.

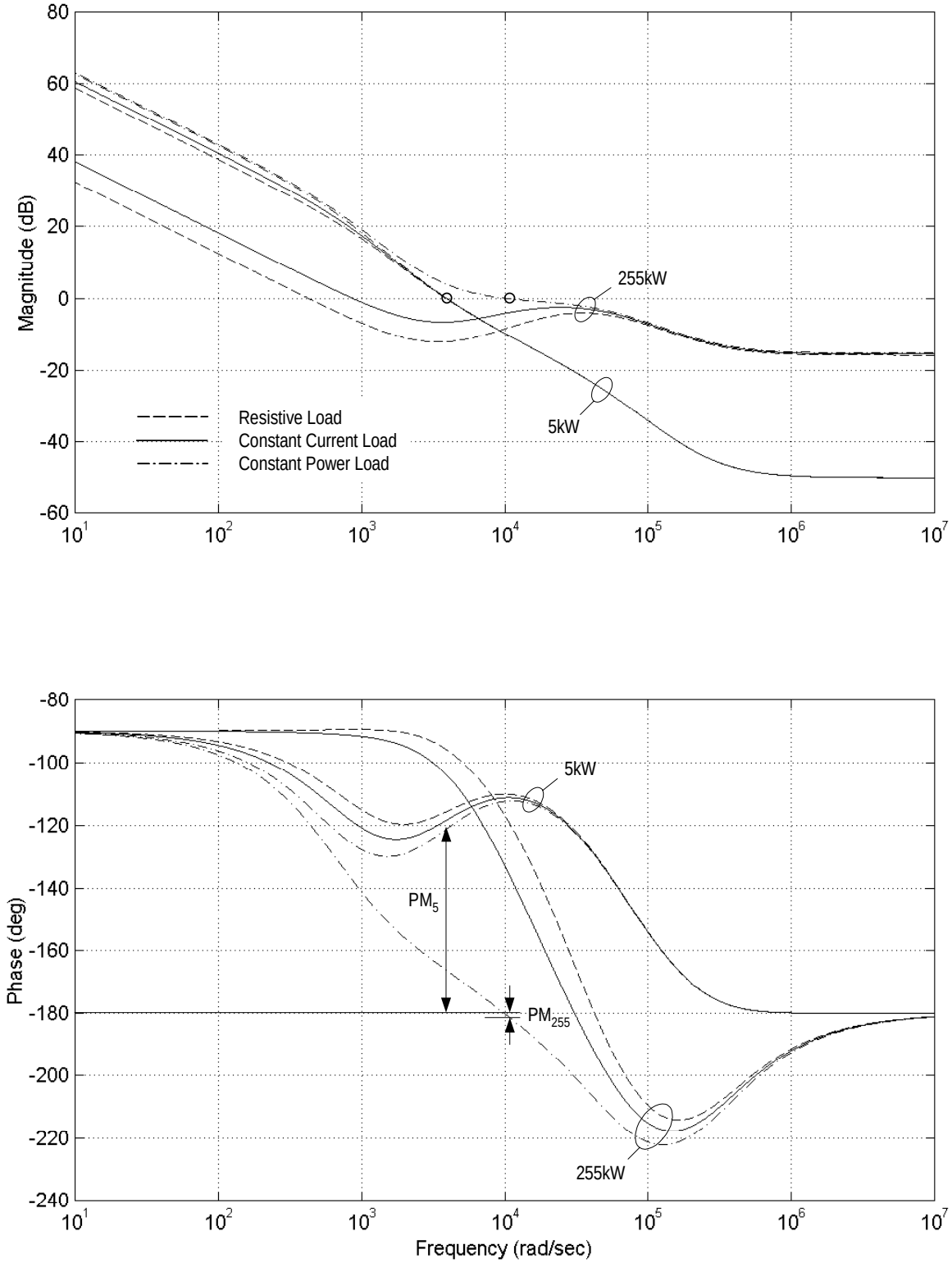

Figure 4.6 Boost rectifier loop gain transfer functions with different types of load.

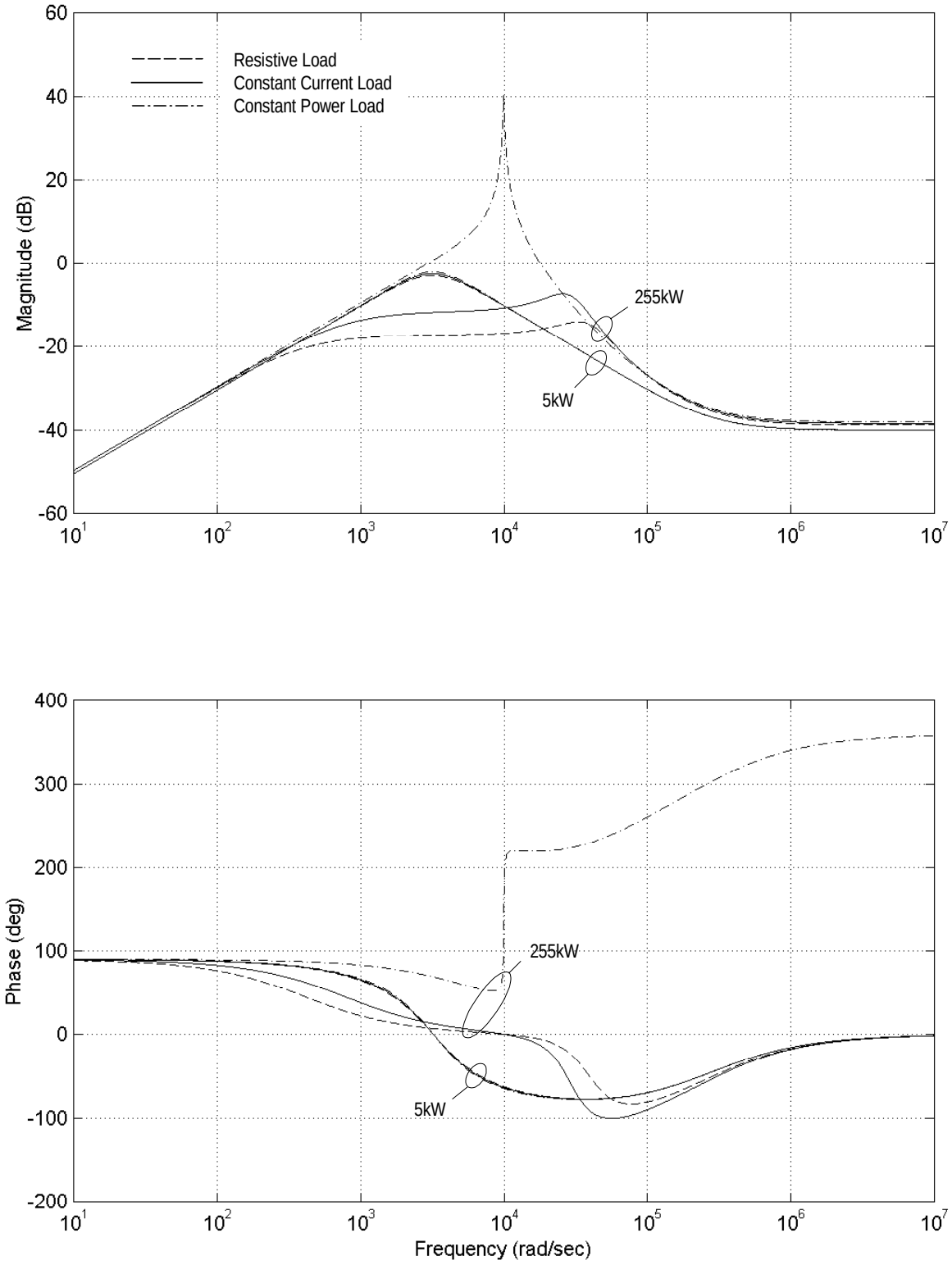

Figure 4.7 Boost rectifier output impedance transfer functions with different types of load.

transfer functions go lower, and the phases – higher than for the respective current loads. It is seen that phase margin with a resistive load is larger than with a current load. With a resistive load, the system is more stable, with higher damping and slower transient response.

The constant power load modifies the transfer functions in the opposite way. For a load of 5kW, the phase margin is reduced compared with the current load at about the same value as it was increased in the case of resistive load. As a result, with the constant power load the system damping is decreased, the system becomes more oscillatory and prone to instability. However, it is still stable enough with a constant power load of 5kW. The other set of transfer functions obtained for 255kW loads shows that with a constant power load of this value the system has even negative phase margin, which indicates instability. This example demonstrates that a constant power load may cause instability in the PDS.

The output impedance transfer functions in Figure 4.7 show that with 255kW constant power load the phase changes its normal shape and passes through 180 degrees. This is an additional indication of instability. The shape of the magnitude curve is significantly modified as well. There is no significant change in output impedance caused by difference in load types at low power levels.

It is convenient to analyze stability of two coupled systems using the approach developed by R. D. Middlebrook [23]. He suggested using the impedance ratio

$$T_1 = \frac{Z_o}{Z_i}, \tag{4.4}$$

where Z_o – output impedance of the source,

Z_i – input impedance of the load,

as a stability test. In order for two coupled systems to be stable, T_1 must not have any roots in the right half-plane. Nyquist stability criterion can be used to check this condition.

The impedance ratio criterion was used in this research to verify the results of stability analysis of the PDS with constant power load presented above and to perform stability analysis

of the system with mixed load. Compared with the boost rectifier phase margin test, the impedance ratio criterion provides helpful insights into conditions required for stability of two coupled systems. The Simulink model was configured for obtaining output impedance of the unloaded boost rectifier and input impedance of the bus load. The output impedance must be obtained with closed control loop and a constant load current such that the equilibrium point set by the actual load is maintained.

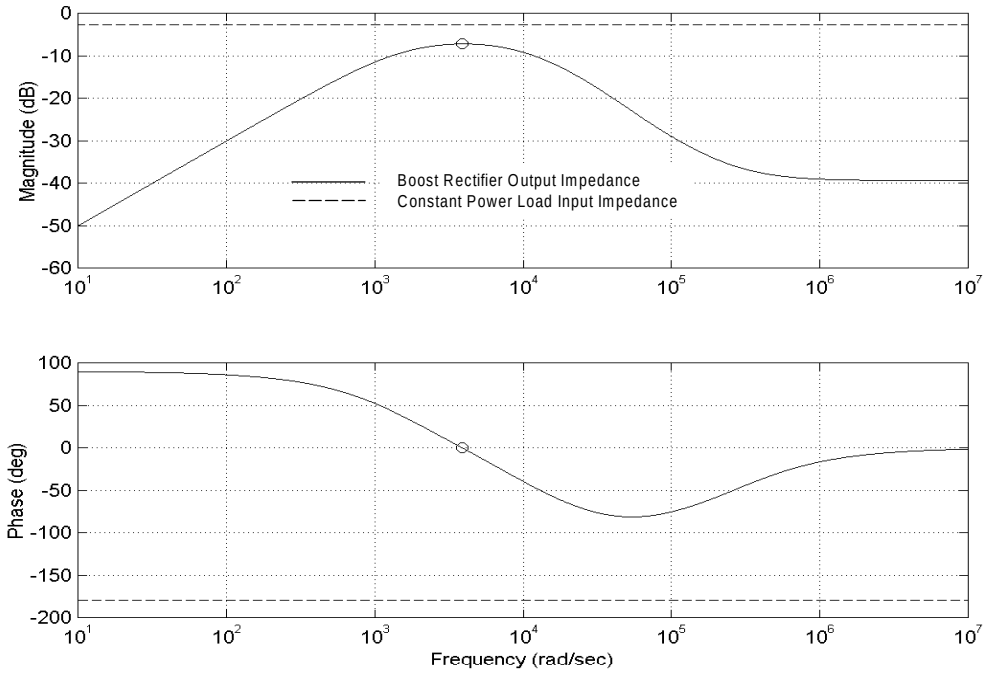

Figure 4.8 Small-signal impedances of the boost rectifier and 100kW constant power load.

Figures 4.8, 4.9, and 4.10 show the boost rectifier output impedance and the bus load input impedance transfer functions obtained for constant power load with three different power levels. As follows from the impedance ratio criterion, instability occurs if magnitude of the load input impedance is lower than magnitude of the boost rectifier output impedance at frequency of the output impedance phase crossing zero. It is seen that the PDS with 100kW constant power load is stable (Figure 4.8); it is close to marginal stability with 253kW load (Figure 4.9), and unstable with 270kW load (Figure 4.10). The same conclusions can be made by examining the respective Nyquist plots in Figure 4.11. The PDS with 253kW load seems to be just stable, being very close to marginal stability. The Nyquist plot for the system with 270kW load

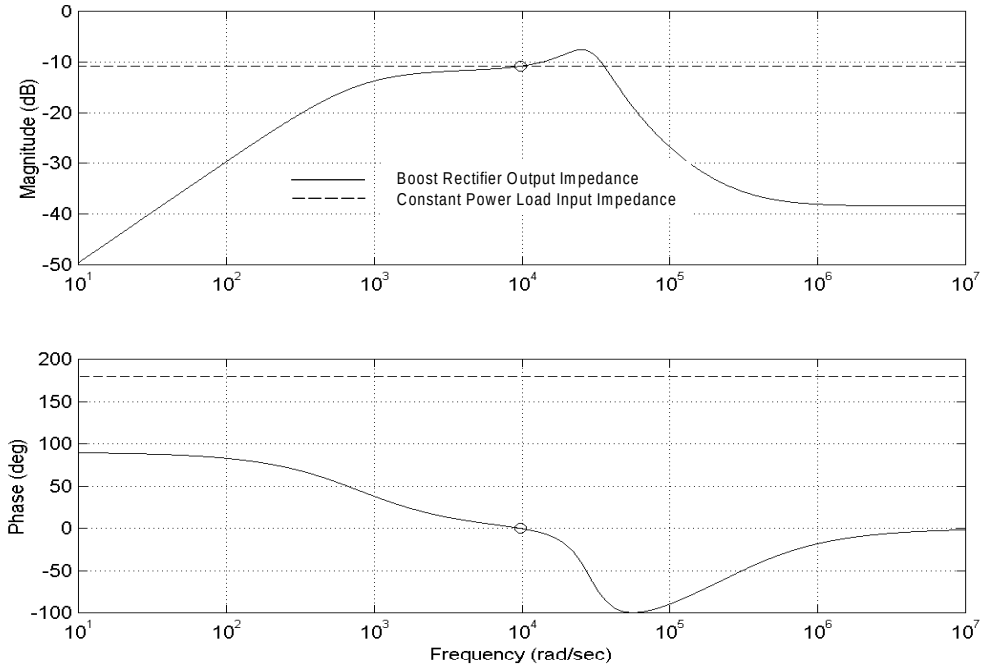

Figure 4.9 Small-signal impedances of the boost rectifier and 253kW constant power load.

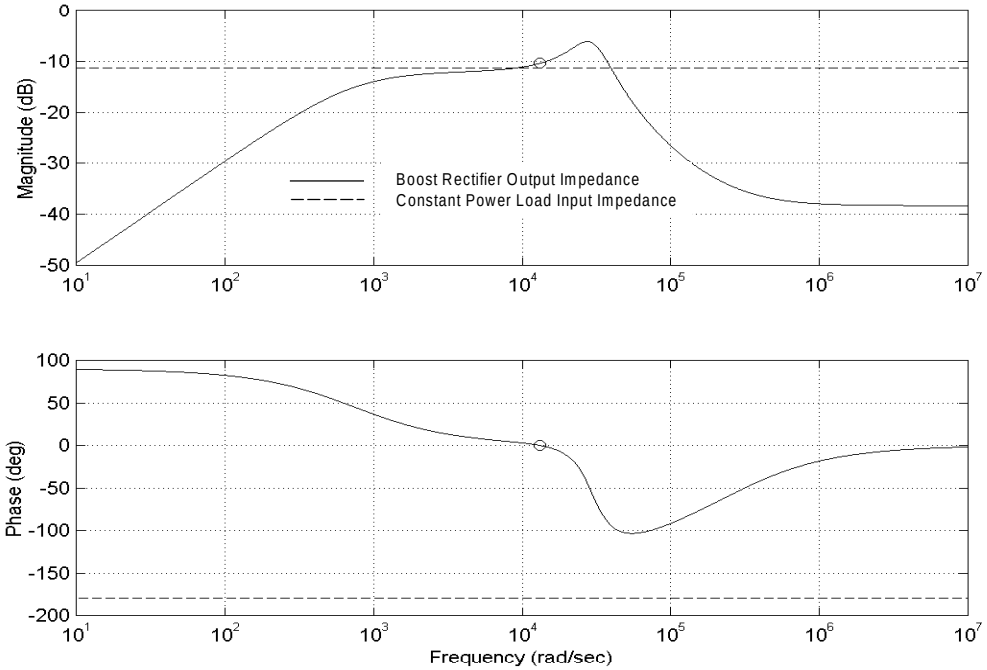

Figure 4.10 Small-signal impedances of the boost rectifier and 270kW constant power load.

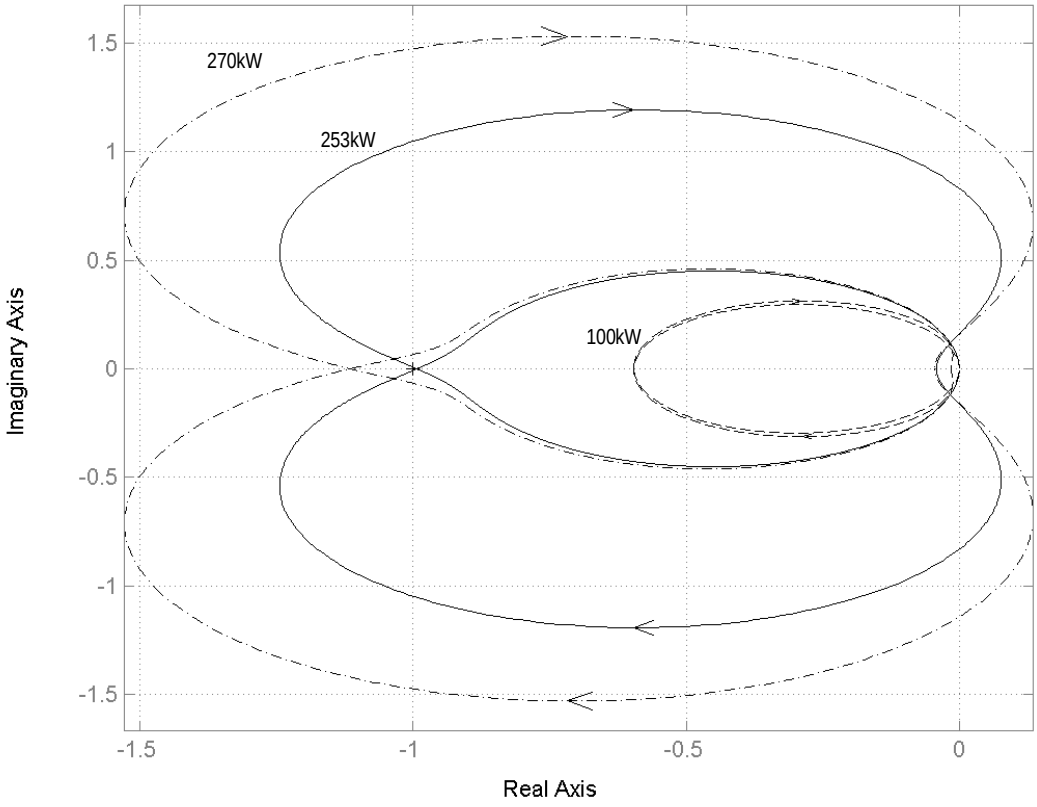

Figure 4.11 Nyquist plots for the PDS with different values of constant power load.

encircles the –1 point, which is an indication of instability. The PDS with 100kW constant power load is stable since the Nyquist plot does not encircle the –1 point. The results of stability analysis made with the impedance ratio criterion completely agree with the results obtained earlier with the use of phase margin test.

Figure 4.12 shows the bus voltage transient response to a step load change. The constant power load was applied to the unloaded bus at the time 0.3s. It is seen that the stable system with 100kW load produces a response with good damping and a very small overshoot. The PDS with 253kW load, after initial transients with a voltage drop caused by saturation in the boost rectifier controller, exhibits a very oscillatory, poorly damped response, typical for a system close to marginal stability. The PDS with 270kW constant power load produces a response with endless nonlinear oscillations. This is a result of stability in large-signal sense with small-signal instability. The frequency of these oscillations is approximately 2200Hz or 13800rad/s, which is

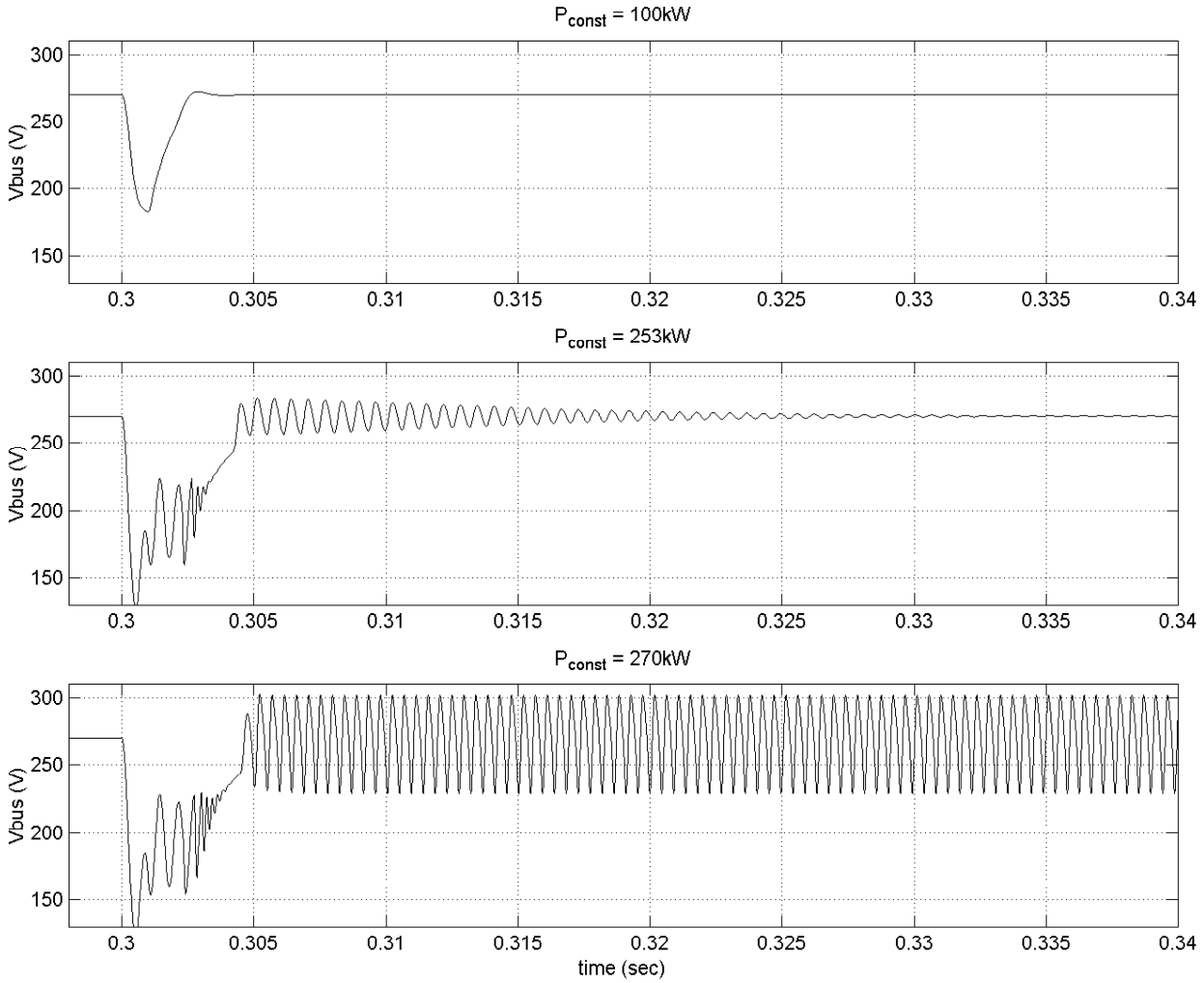

Figure 4.12 Transient response of the DC bus voltage for different values of constant power load.

equal to the phase crossover frequency in Figure 4.10. The magnitude of these oscillations exceeds 300V, which is beyond the limits specified by MIL-STD-704E [8].

According to specifications, the DC bus load in the PDS of a future aircraft will be mixed type with constant power load up to 75% of the total [22]. Therefore, it is important to understand how constant power load will affect dynamic properties of the system in combination with resistive load.

When both resistive and constant power loads are applied to the bus, the operating point of the boost rectifier is determined by the sum of these loads. It can be shown that the equivalent small-signal resistance of the bus will be

$$R_{eq} = \frac{R_n \cdot R_p}{R_n + R_p}, \tag{4.5}$$

where $R_p = \frac{V_{bus}^{\ 2}}{P_{res}}$ – positive small-signal resistance of resistive load P_{res},

$R_n = -\frac{V_{bus}^{\ 2}}{P_{const}}$ – negative small-signal resistance of constant power load P_{const}.

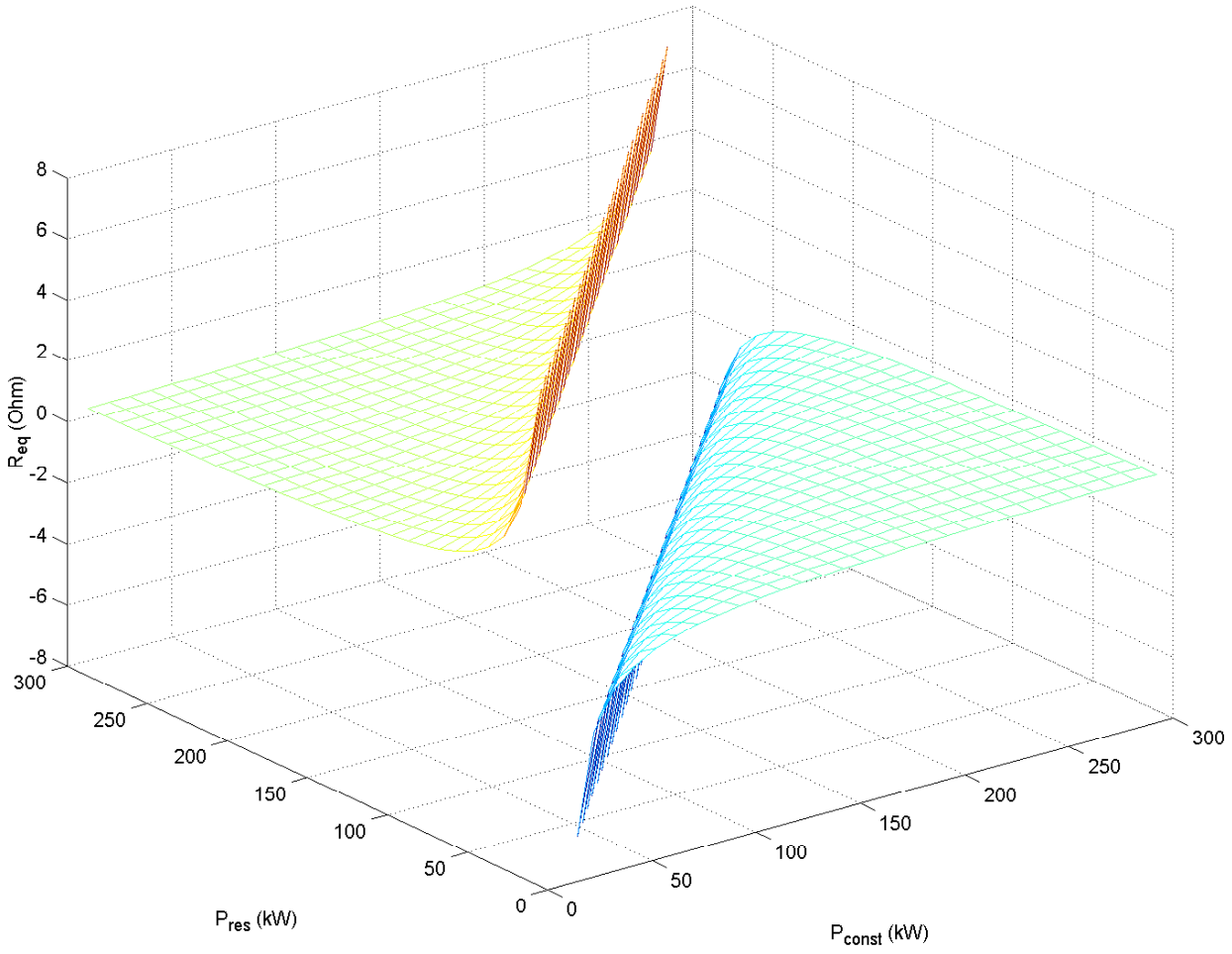

Figure 4.13 Equivalent small-signal resistance of the DC bus with mixed load.

A three-dimensional plot of R_{eq} as a function of P_{res} and P_{const} is shown in Figure 4.13. A potential for unstable interactions in the system exists only when R_{eq} is negative and small enough (close to zero) in magnitude as can be understood from Figures 4.8 through 4.10. This is possible when the mixed load has P_{const} sufficiently larger than P_{res} as seen from Figure 4.13. When P_{const} is equal to P_{res}, the equivalent small-signal resistance goes to infinity (positive or negative), which is the case of constant current load. A mixed load with P_{res} larger than P_{const} has always positive R_{eq}, which increases the system stability as demonstrated above.

Another factor that affects stability of the PDS is magnitude of the boost rectifier output impedance at its phase crossover frequency as shown in Figures 4.8 – 4.10. This is the critical value of the bus load negative resistance at which instability occurs. The output impedance used in the impedance ratio test depends only on the equilibrium point determined by the total bus load. By performing the output impedance analysis for different power levels of the load, the critical values of the load negative resistance were obtained as shown in Figure 4.14.

The load equivalent resistance and its critical values are combined in one plot in order to produce a diagram that shows stability of the system for different load conditions. The part of Figure 4.13 with negative R_{eq} is shown in two dimensions in Figure 4.15, where P_{res} is represented with lines of constant power. R_{eq} is plotted in logarithmic scale against total power of the mixed load. The critical values of load resistance interpolated with cubic splines are plotted with a dashed curve in Figure 4.15 with actual data points shown.

The diagram in Figure 4.15 shows stability conditions for the PDS with mixed load on the DC bus. Any load combination with total power up to 300kW and P_{const} greater than P_{res} has a corresponding point on the diagram. The area below the dashed curve is the region of instability. The PDS with a load point above the dashed line is stable, below – unstable. A load point on the dashed line represents a marginally stable system. For example, point A represents a mixed load with total power 200kW, which includes a 20kW resistive load and a 180kW constant power load. The diagram shows that the negative small-signal resistance of this load is – 6.8dB, or 0.46Ohm. The dashed curve shows that at this total power level the load must have

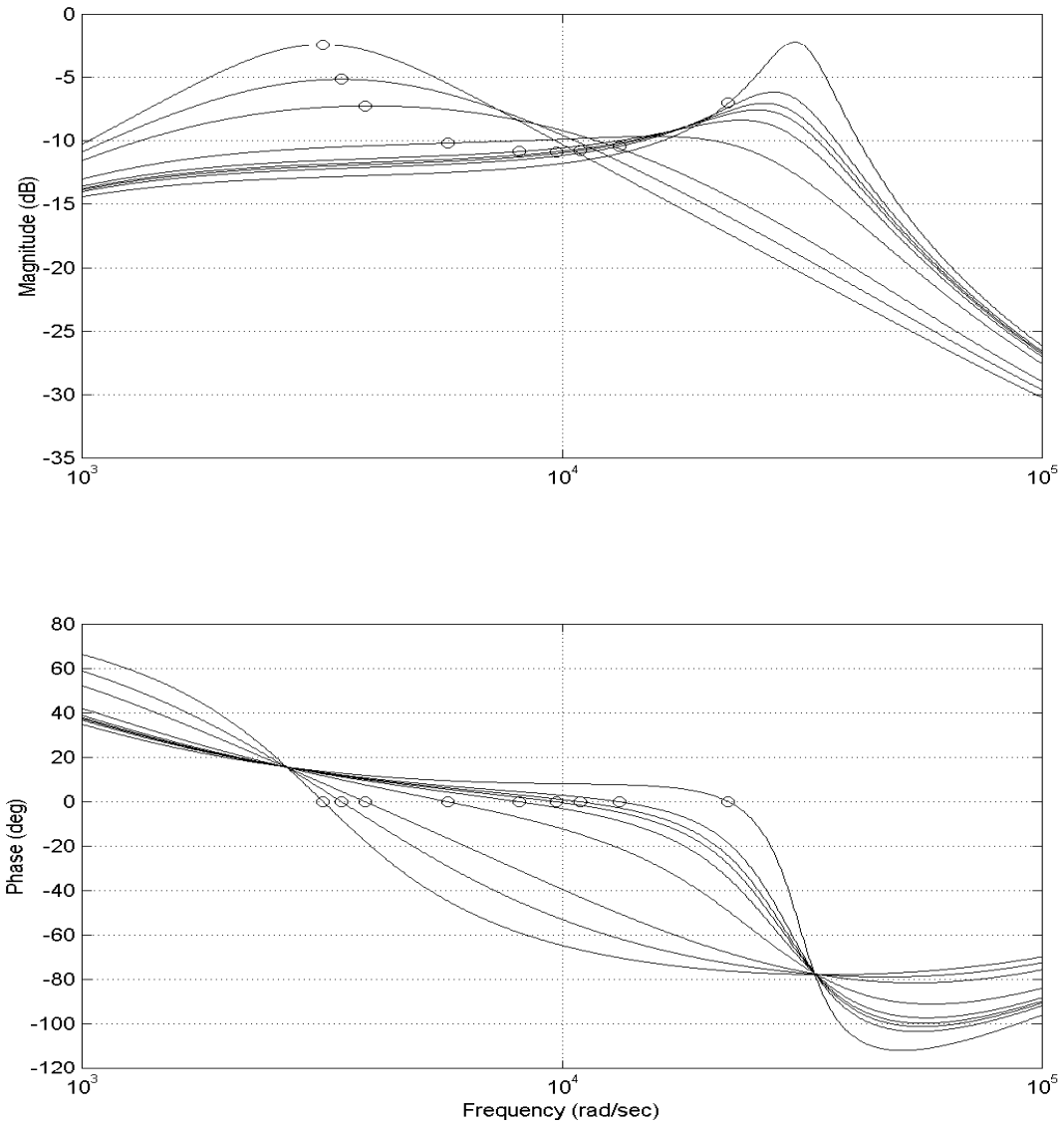

Figure 4.14 Critical negative resistances of the bus load obtained from the boost rectifier output impedance transfer functions for different load powers.

negative resistance lower than –10.2dB (point B), or 0.31Ohm, in order to produce unstable interactions. Therefore, the PDS with the load represented by point A is stable. Similarly, the diagram shows that with the bus load corresponding to point C (40kW resistive load, 250kW constant power load, 290kW total load) the system is unstable.

The dashdot line in Figure 4.15 represents 75% constant power load condition in the mixed resistive/constant power bus load. The area above this line corresponds to load

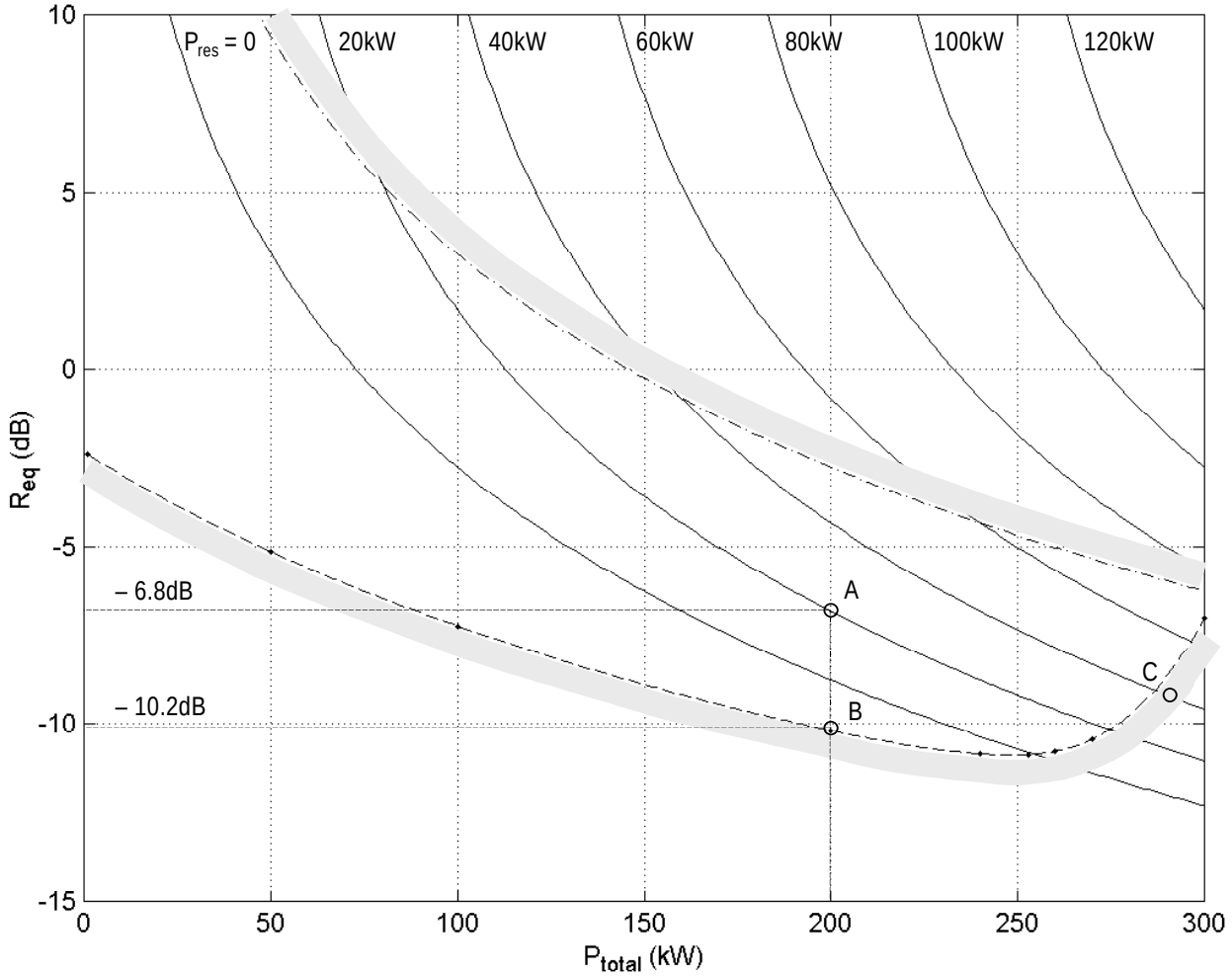

Figure 4.15 The DC bus stability diagram.

combinations where constant power load is less than 75% of the total. The dashed line, limiting the region of instability, is obtained for a particular set of parameters for the generator and boost rectifier. Therefore, it is design-specific. The constant P_{res} lines and the 75% constant power load line are design-independent. For the given generator and boost rectifier design and 300kW total power range, the diagram shows that a bus load satisfying the 75% constant power load condition will not create instability. However, even with the total aircraft constant power load not exceeding 75% of the total aircraft load (assuming the rest of the load to be resistive), it might be possible that during load commutations this condition is temporarily violated, and the PDS may become unstable. With a different generator and boost rectifier design, the area of

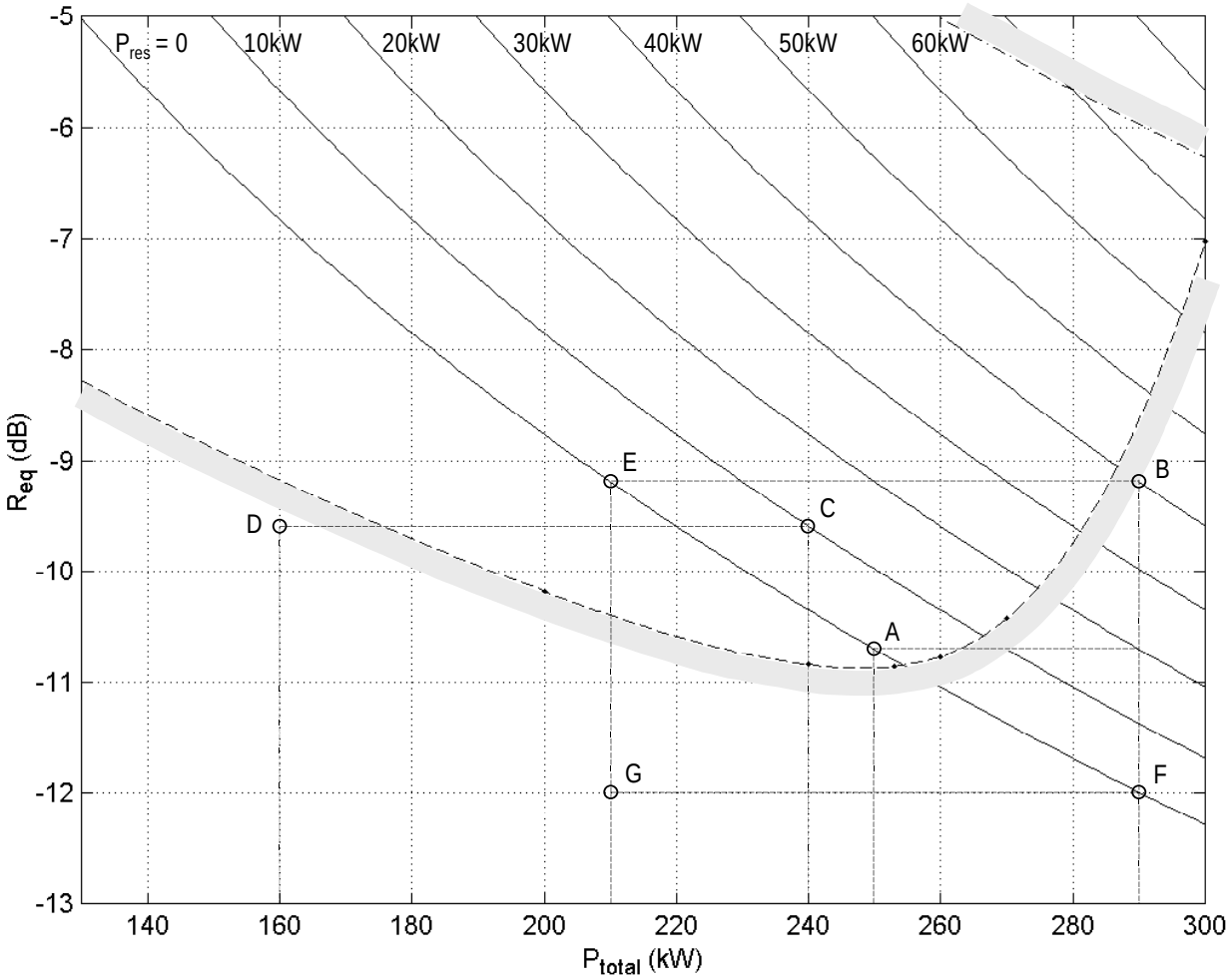

Figure 4.16 Examples of analysis with the DC bus stability diagram.

instability may intersect with the 75% limit area. Therefore, new designs must be checked for this condition to prevent possible instability.

The DC bus stability diagram is a useful tool for stability analysis of the system during load commutations. For example, adding resistive load to the bus with a constant power load usually improves the system stability. However, this is not always the case. Point A on the diagram in Figure 4.16 represents 250kW constant power load on the bus. It was shown earlier that the PDS with this load is stable. When 40kW resistive load is added to the bus, the load point on the diagram moves to point B, which is in the area of instability. The Nyquist plot in

Figure 4.17 obtained for point B proves this conclusion. Transient responses of the bus voltage and current to the step load change are shown in Figure 4.18.

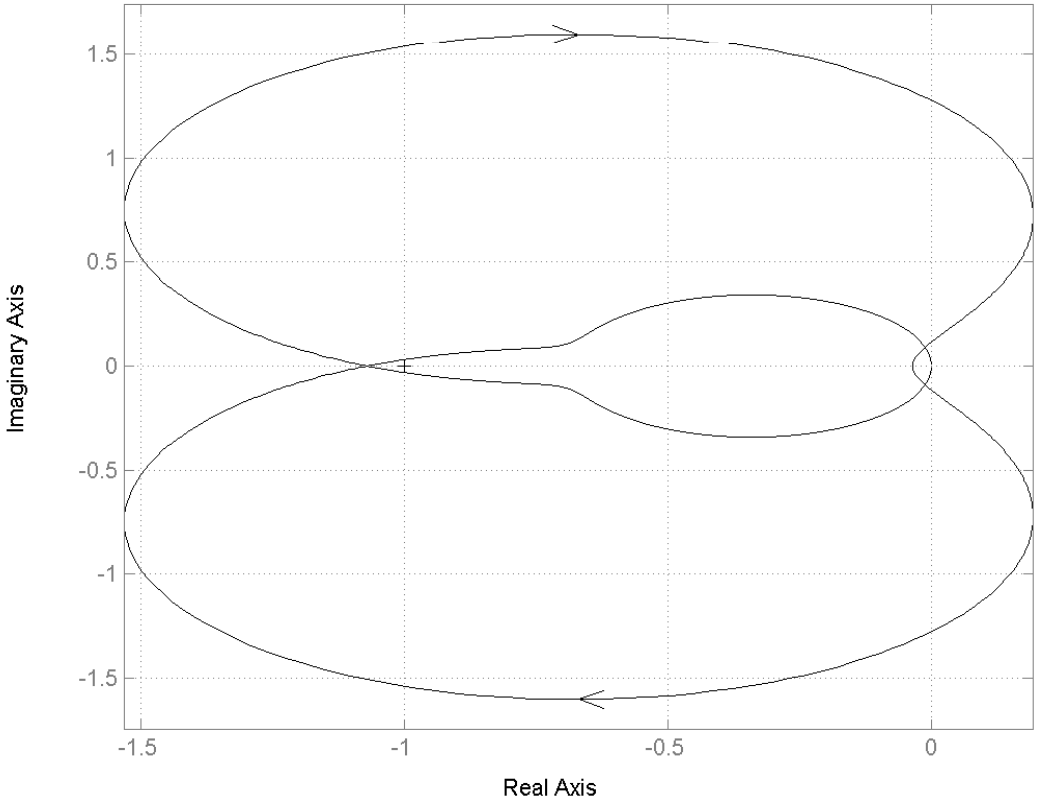

Figure 4.17 Nyquist plot for the PDS with the load represented by point B in Figure 4.16.

It is possible to account for constant current loads in the DC bus stability diagram. A constant current load connected to the bus in addition to resistive and constant power load will not change the total small-signal impedance of the bus, but will change the total load power. Therefore, a constant current load will shift the load point on the diagram horizontally for the amount of the load. The load with positive current will shift the point to the right; the load with negative (regenerative) current will shift the point to the left. The diagram shows that such a shift may lead a stable system into the area of instability, both for positive and for negative currents. For example, point C in Figure 4.16 represents a stable system with 10kW resistive load and 230kW constant power load. An 80kW regenerating constant current load will move the system into point D, which is in the region of instability. The Nyquist plot in Figure 4.19 and simulation results of the system transient response in Figure 4.20 confirm that this initially stable

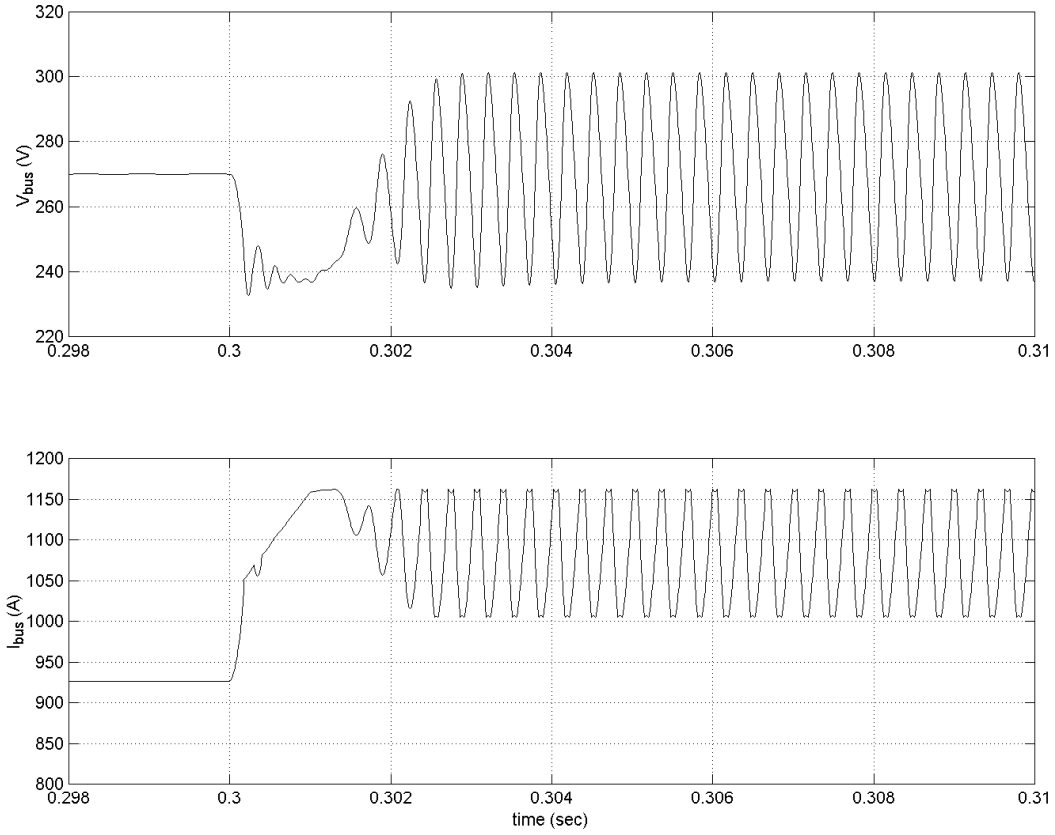

Figure 4.18 Transient responses of the bus voltage and current for a step load change with 40kW resistive load added to 250kW constant power load.

system becomes unstable when the regenerative current is applied to the bus. The resistive and constant power loads are applied to the bus at 0.3s, producing a stable transient response. After that, the regenerative current source is applied at 0.32s, making the system unstable.

The DC bus stability diagram shows that a stable PDS with more than 150 – 200kW total load including more than 75% constant power load may become unstable when sufficiently large regenerative current is applied to the bus. If the critical negative load resistance (the dashed line) continues to increase in the area of negative load powers (this may be a subject of future research), regenerative current may cause instability in the PDS with even smaller loads.

A bus load working in regenerative mode, similarly to its operation in the load mode, may have either positive or negative small-signal resistance. A load may change sign of its

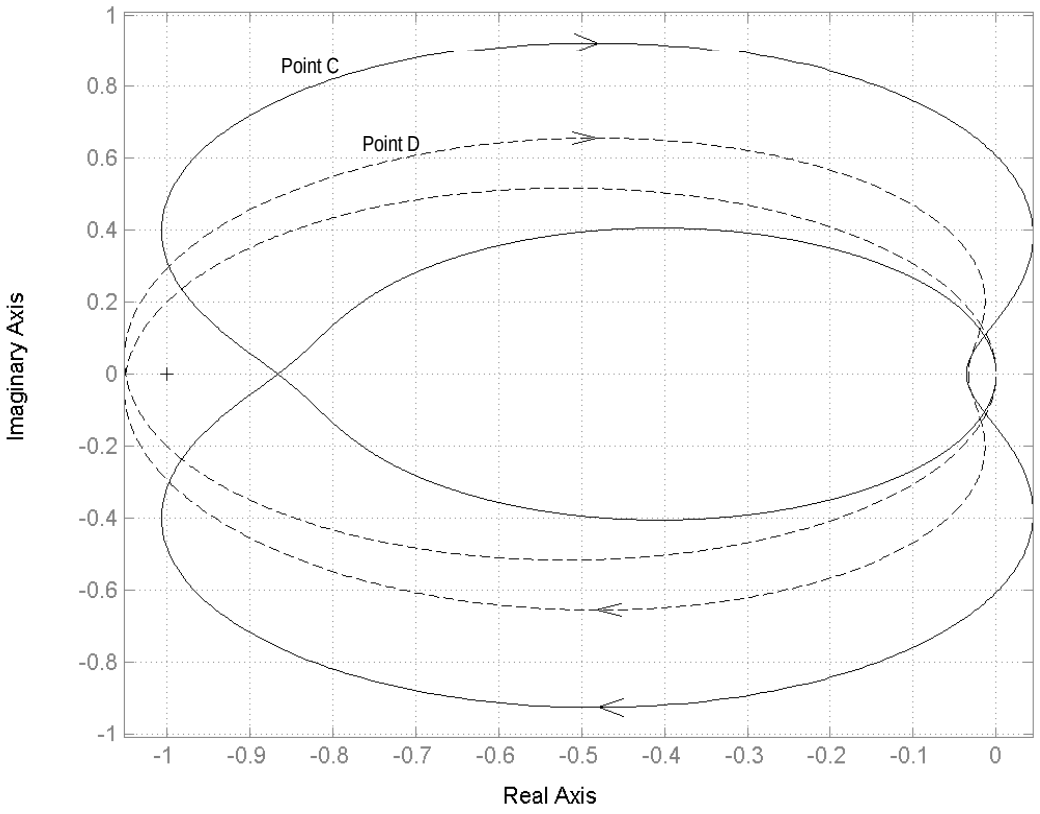

Figure 4.19 Nyquist plots for the PDS with loads represented by points C and D in Figure 4.16.

small-signal resistance when it switches to regenerative mode. For example, a constant power load has a negative small-signal resistance in the load mode and positive in regenerative mode (this will be illustrated later with the EMA example). A load with back-e.m.f. (for example, a battery) exhibits positive small-signal resistance when it receives energy and negative – when it delivers the energy to the bus. It is possible to use the DC bus stability diagram with positive or negative resistance loads working in regenerative mode. Only brief comments are given below concerning the usage of the diagram with such loads; a detailed study of the system stability under regenerative power flow conditions may be a subject of future research.

Any load or source connected to the DC bus affects two parameters determining the bus stability: the bus small-signal resistance and the boost rectifier operating point. The bus small-signal resistance is represented by the vertical coordinate of the load point on the stability diagram; the boost rectifier operating point is represented by the horizontal coordinate of the load

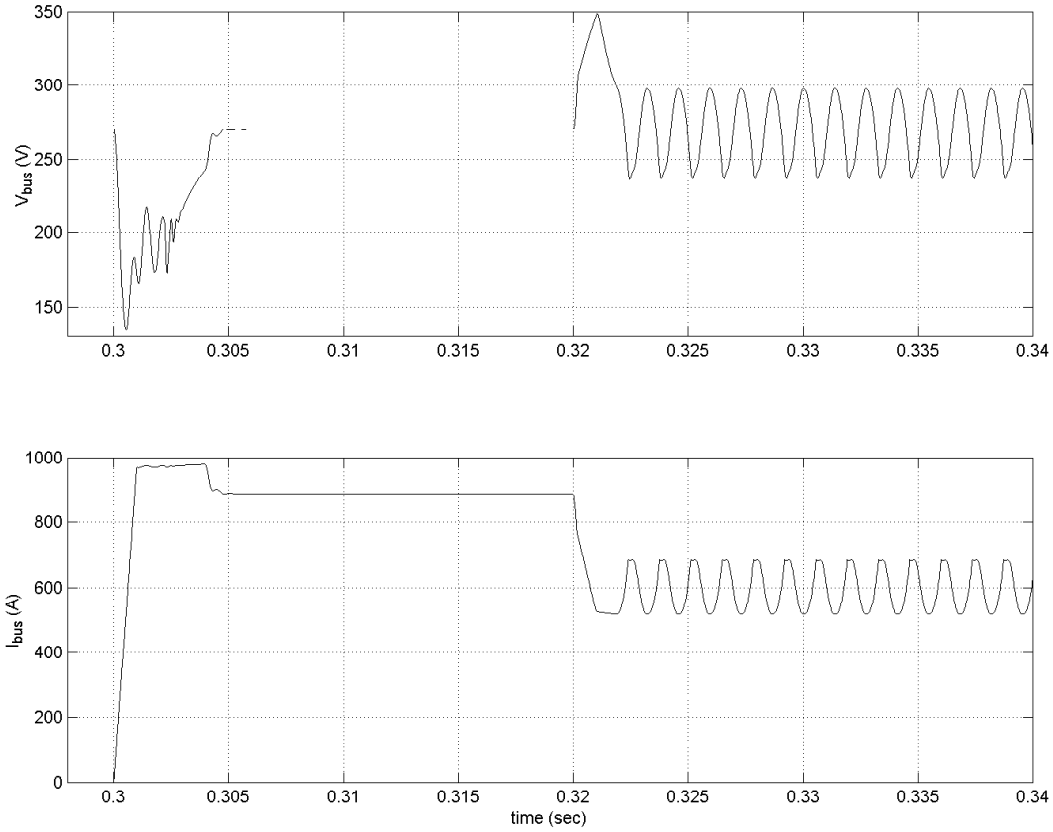

Figure 4.20 DC bus voltage and current transient responses to load changes corresponding to points C and D in Figure 4.16.

point. Therefore, both coordinates must be adjusted to reflect a change produced by connection of a new load.

For any load with small-signal resistance R_{ss}, there can be determined a value of apparent power Pa, with which the load is seen on the bus from small-signal point of view:

$$P_a = \frac{V_{bus}^{\ 2}}{R_{ss}}. \tag{4.6}$$

For a linear load, this power is equal to the actual load power; for a nonlinear load, it may be different. It can be shown that the equivalent small-signal resistance of the bus with a mixed load given by (4.5) can be obtained using the equivalent apparent power of all the loads:

$$P_{eq} = \sum_i P_{a_i} , \tag{4.7}$$

$$R_{eq} = \frac{V_{bus}^{\ 2}}{P_{eq}}, \tag{4.8}$$

where i – number of loads. The actual total load of the bus is calculated as an algebraic sum of all load powers including constant current loads:

$$P_{total} = \sum_i P_i . \tag{4.9}$$

The R_{eq} coordinate on the diagram is adjusted by moving the load point to the 0kW resistive load line at P_{total} equal to the equivalent apparent power obtained from (4.7). After that, the load point is moved horizontally to the point with P_{total} equal to the actual total load power calculated with (4.9). The resulting load point shows stability of the bus with this load.

For example, the system with 250kW constant power load is represented by point A in Figure 4.16. For a 40kW additional resistive load, the first step of adjustment moves the load point to point E with equivalent apparent power 210kW. Then, it moves horizontally to point B with actual total power 290kW. For a regenerative 40kW load with 40kW apparent power (positive small-signal resistance), the load point will stay at point E because the equivalent apparent power in this case is equal to the actual total power. If a 40kW load with –40kW apparent power (negative small-signal resistance) is connected, the load point will move to point F and stay there. However, if this load is regenerative, the bus will operate with 210kW actual total power, and the load point will move to point G. The diagram shows that all these load changes except connecting a regenerative 40kW positive resistance load will make the PDS unstable.

The rules for using the DC bus stability diagram are generalized below.

- The diagram can be used for stability analysis of the PDS with loads having either positive or negative input resistance in the frequency range of the boost rectifier phase crossover point

(Figure 4.14) as a result of their natural properties or feedback action. Loads with complex input impedance are not considered.

- The loads may be linear or nonlinear, with positive or negative input resistance, including constant current loads, sourcing or sinking the bus energy.
- The analysis is performed in the following order.
  1. For each load, identify the small-signal resistance and the actual load power at this operating point.
  2. Calculate the apparent power for each load according to (4.6).
  3. Calculate the equivalent apparent power P_{eq} (4.7) and the actual total power P_{total} (4.9). If P_{eq} is positive, there is no potential for instability if the system is stable with an equivalent constant current load. P_{total} must be positive and within the power range of the diagram in order to use it.
  4. Find a point on the 0kW resistive load line corresponding to the negative P_{eq} taken with positive sign. This point will show R_{eq} of the bus.
  5. Move the point horizontally so that it corresponds to the actual total power P_{total}.
  6. Position of the load point relative to the dashed line will show the system stability at this operating point.

4.4 Stability Analysis of a PDS with an Electromechanical Actuator

The electromechanical actuator system diagram is shown in Figure 4.21. The EMA consists of an input filter, dc-dc converter, dc motor, and a mechanical part with a gearbox, a ball screw mechanism, and a flight control surface deflection system. The converter has feedback control with the actuator position command supplied from a higher-level control system of the aircraft. The feedback makes the converter a typical constant power load in small-signal sense with negative small-signal resistance. The value of the constant power drawn depends on the operating point within the operating cycle. A typical EMA operating cycle for ground testing is shown in Figure 4.22. It shows the motor voltage, current, power, speed, flight control surface

deflection angle, and the ball screw position command. No wind load is applied to the surface in ground testing mode.

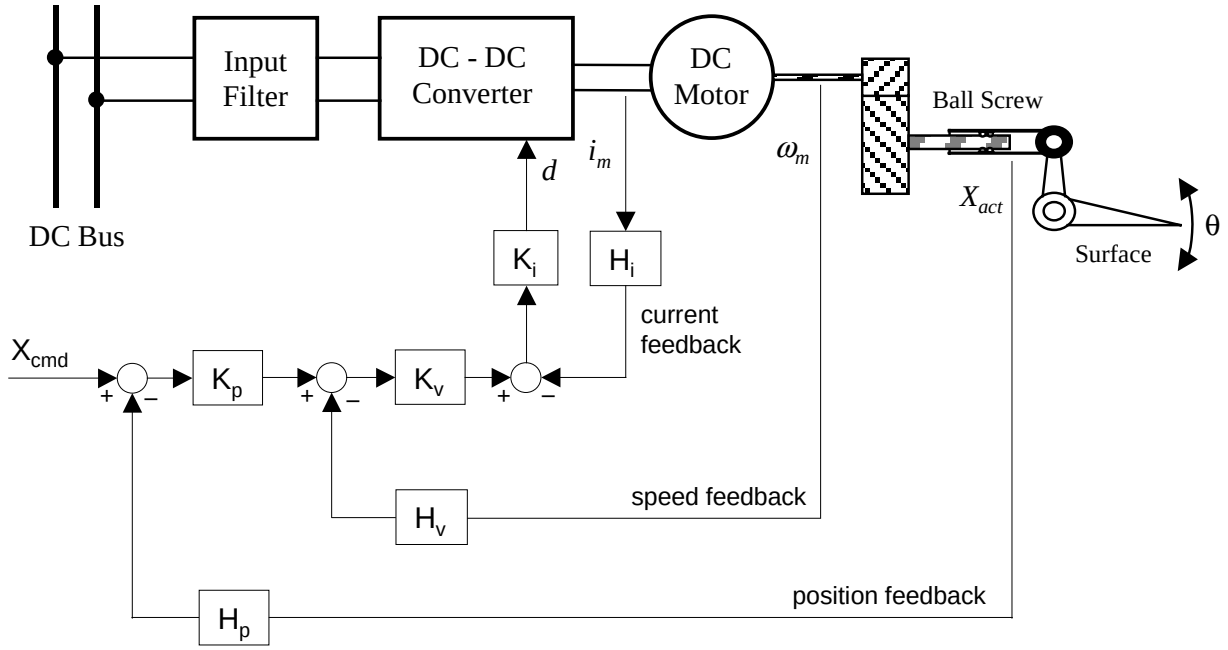

Figure 4.21 Electromechanical actuator system diagram.

The feedback controller provides stability of the feedback loop in all modes of operation. Possible stability problems arise from the input filter, which may produce undesirable interactions with the converter. In addition, the input filter modifies the negative input resistance of the converter such that the EMA as a whole system may have unstable interactions with the boost rectifier. The impedance ratio criterion was used in this research to perform stability analysis of the system.

For stability analysis, the EMA nonlinear model must be linearized in different equilibrium points along its operating cycle, then small-signal analysis is performed. The EMA operating cycle consists of three distinctive periods shown in Figure 4.22: acceleration to the maximum speed (period 1), changing the surface position to the commanded value (period 2), and the surface slowing down with regeneration of energy (period 3). This sequence is repeated with similar waveforms during the second half of the cycle when the surface moves back.

Figure 4.21 shows that the EMA feedback control consists of a ball screw position feedback loop, a motor speed loop, and a motor current loop. The position loop forms a reference signal for the speed loop, which produces a reference for the current loop. The controller is designed such that during period 1 the current loop reference is in saturation, thus producing current limiting for the motor. Because of that, during period 1 the EMA control structure consists of only one current loop from small-signal point of view. Similarly, during period 2 the speed loop reference is in saturation producing speed limiting for the motor. Only current and speed loops are active during period 2 in small-signal sense. All three loops work during period 3.

The existence of the three different periods of operation with different feedback structure makes it possible for the system stability to change significantly from period to period. Therefore, each period must be considered separately in stability analysis; at least one equilibrium point must be examined within each period. The problem is complicated by the fact that there are no true equilibrium points within the operating cycle because certain state variables of the mechanical part of the EMA keep changing slowly over the whole cycle. The only true equilibrium is in the beginning of the cycle when all state variables are equal to zero. No useful stability information can be obtained from this equilibrium point.

In the frequency range of interest where possible oscillations caused by unstable interactions of the input filter with negative input resistance of the converter may occur, slowly changing mechanical state variables may be considered constant for the purpose of small-signal analysis. In this view, they are no longer state variables, but slowly changing time-varying system parameters. Therefore, equilibrium points for stability analysis may be obtained with respect to only state variables produced by voltages and currents. Four equilibrium points OP1 – OP4 in the first half-cycle and similar to them equilibrium points OP5 – OP8 in the second half-cycle as shown in Figure 4.22 were chosen for stability analysis of the system. Two of them were chosen during period 1 in order to trace possible change in the system stability as the power drawn by the system gradually increases. OP4 is chosen at the moment when the motor regenerative current reaches its maximum and its derivative is zero in the beginning of the regeneration period. The equilibrium solutions were obtained by simulating the system until it reaches the respective time moment.

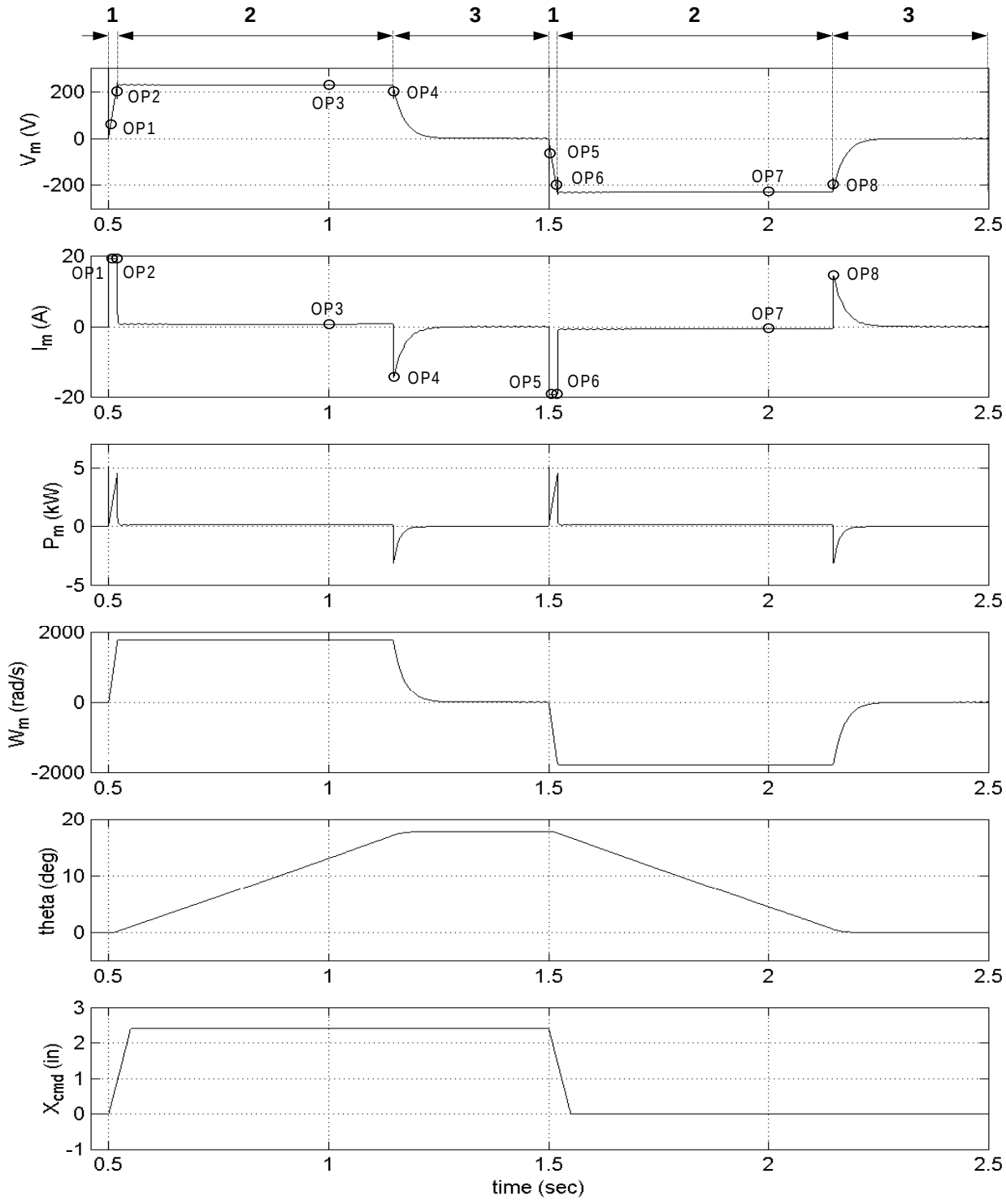

Figure 4.22 Electromechanical actuator operating cycle.

Initially, stability analysis was performed for the EMA fed from an ideal DC bus modeled by 270V ideal voltage source. This approach allows studying interactions within the EMA unaffected by the rest of the PDS. An input filter providing 40dB attenuation of the converter switching ripple at switching frequency 20kHz shown in Figure 23 was used for analysis. An additional damping resistance R_a was added to the filter in order to alleviate possible interactions with the converter. The filter parameters are the following:

$L = 300\mu H,$
$C = 25\mu F,$
$R_l = 0.1\Omega,$
$R_C = 0.01\Omega,$
$R_a = 0.12\Omega.$

The input filter forward voltage transfer function is shown in Figure 4.24.

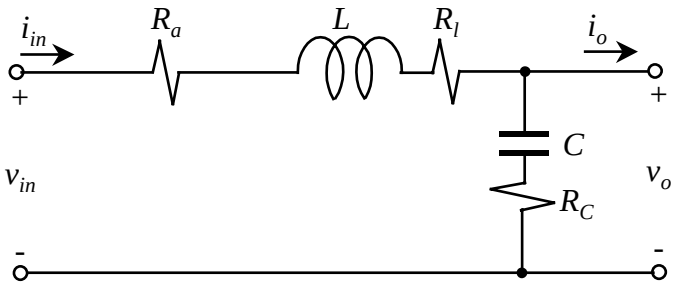

Figure 4.23 Input filter for the electromechanical actuator.

Figure 4.25 shows the input filter output impedance and the converter input impedance transfer functions for the operating point OP1. It is seen that the converter with feedback has negative input resistance within a large frequency range. The magnitude of the input filter output impedance at its phase crossover point is below the magnitude of the closed-loop input impedance of the converter, which indicates that the system is stable at this operating point. Figure 4.26 shows the same transfer functions for the operating point OP2. It is seen that the converter closed-loop input impedance is now lower than the input filter output impedance at the crossover point. This means instability of the system. The results of stability analysis of the operating points OP1 and OP2 show that the system starts its operating cycle as stable and then

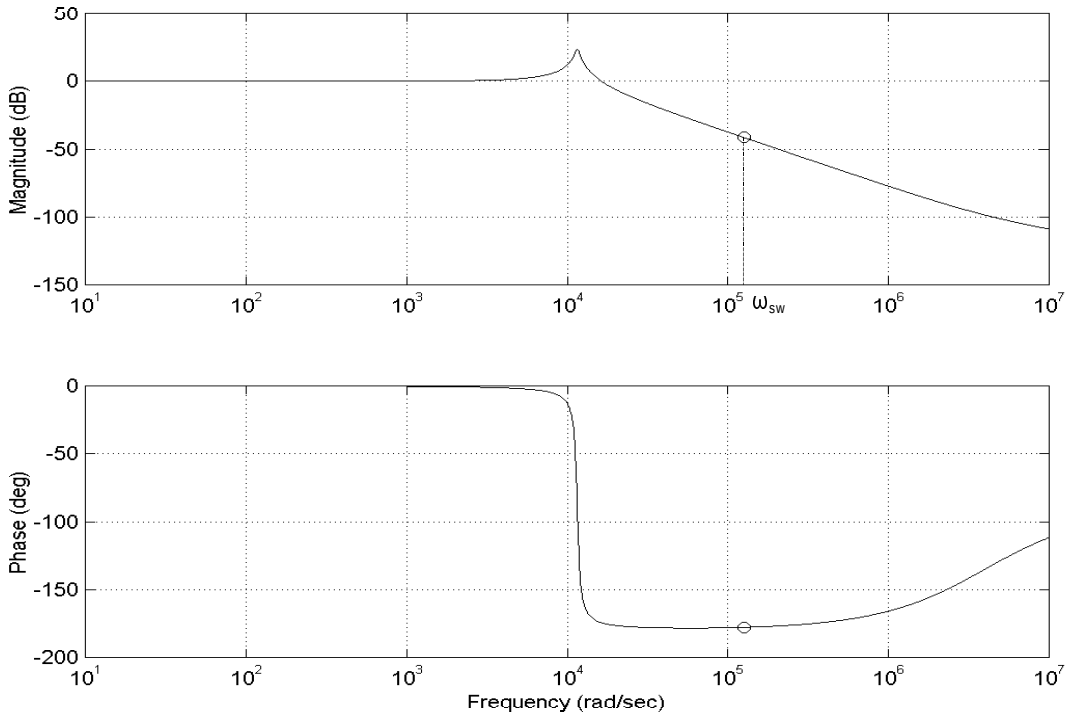

Figure 4.24 Input filter forward voltage transfer function.

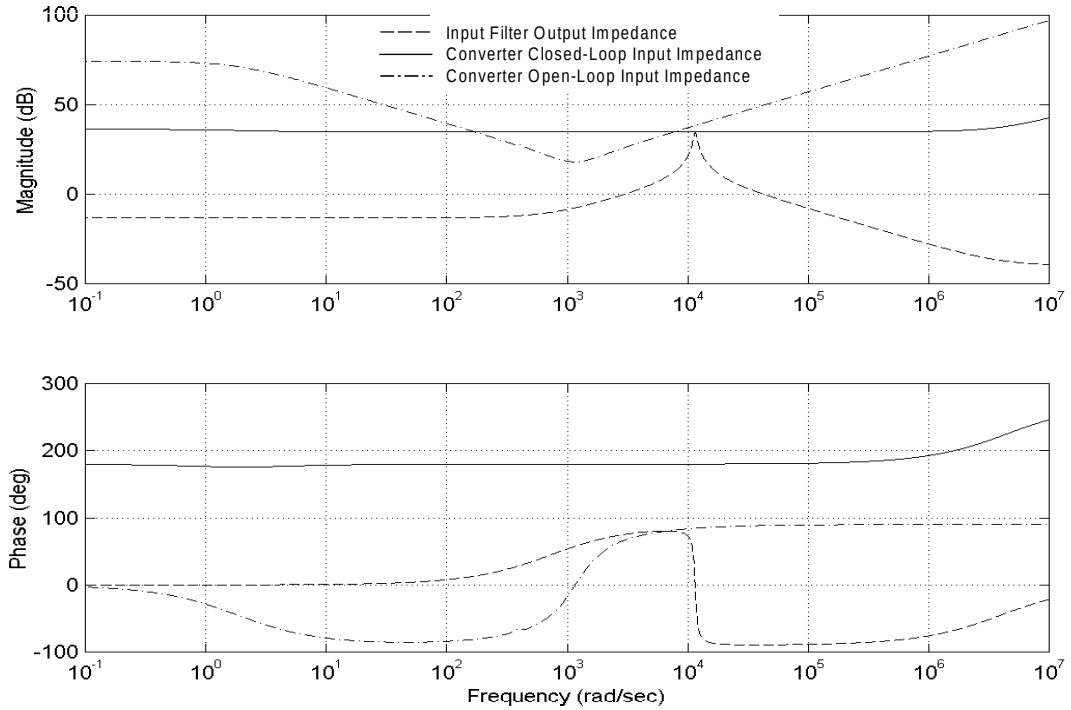

Figure 4.25 Input filter and converter transfer functions at operating point OP1.

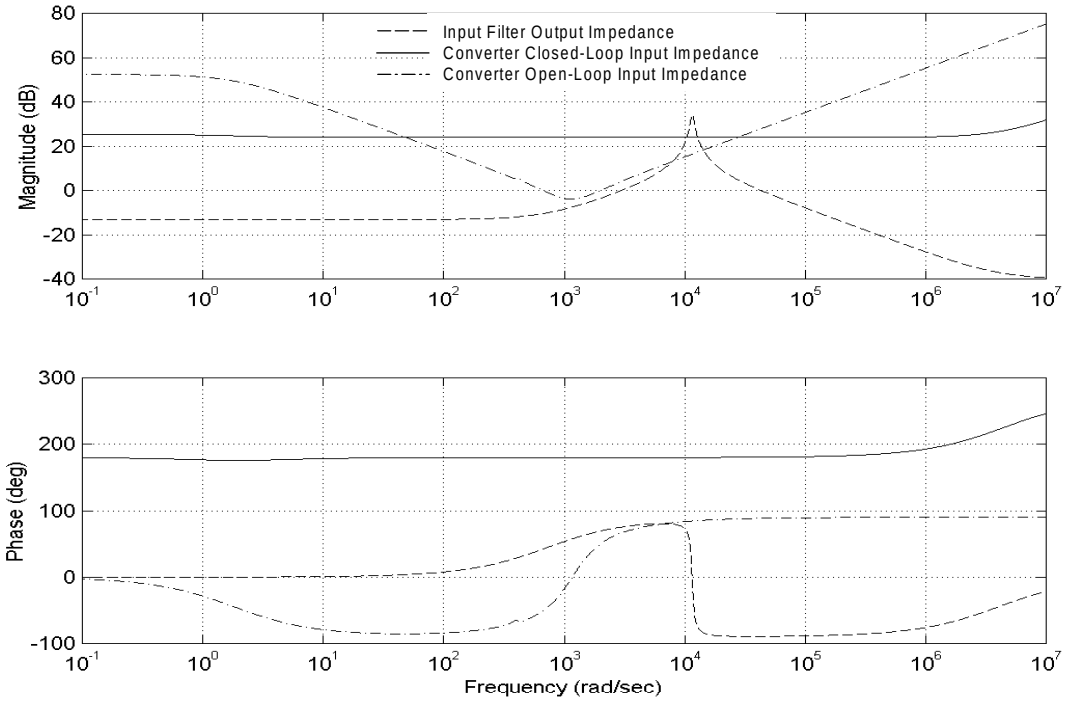

Figure 4.26 Input filter and converter transfer functions at operating point OP2.

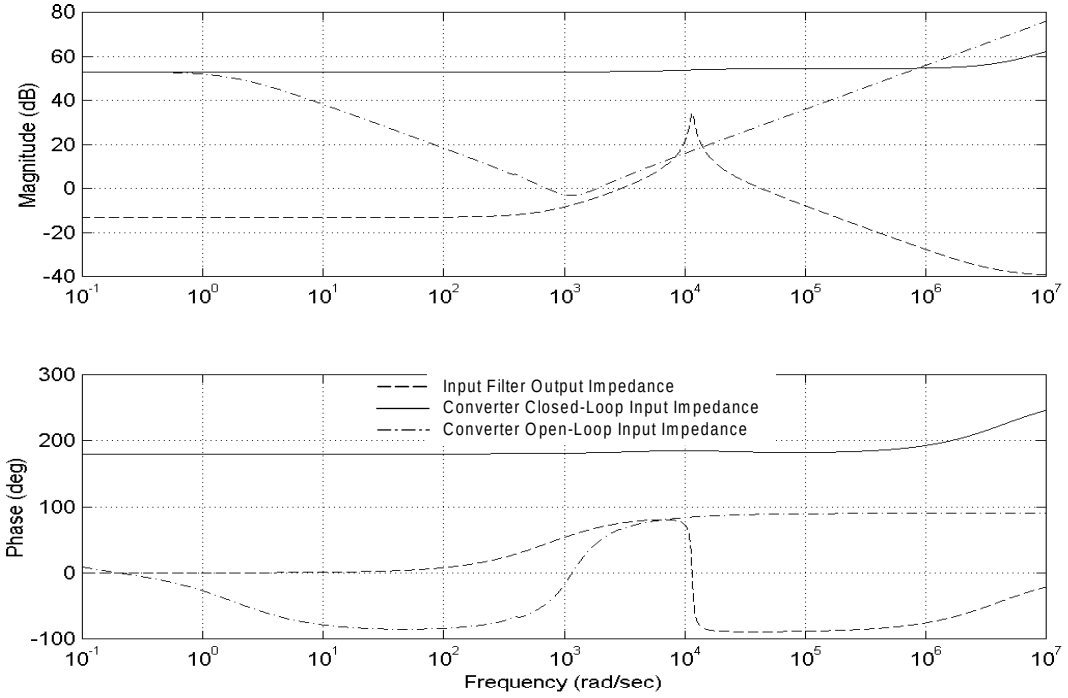

Figure 4.27 Input filter and converter transfer functions at operating point OP3.

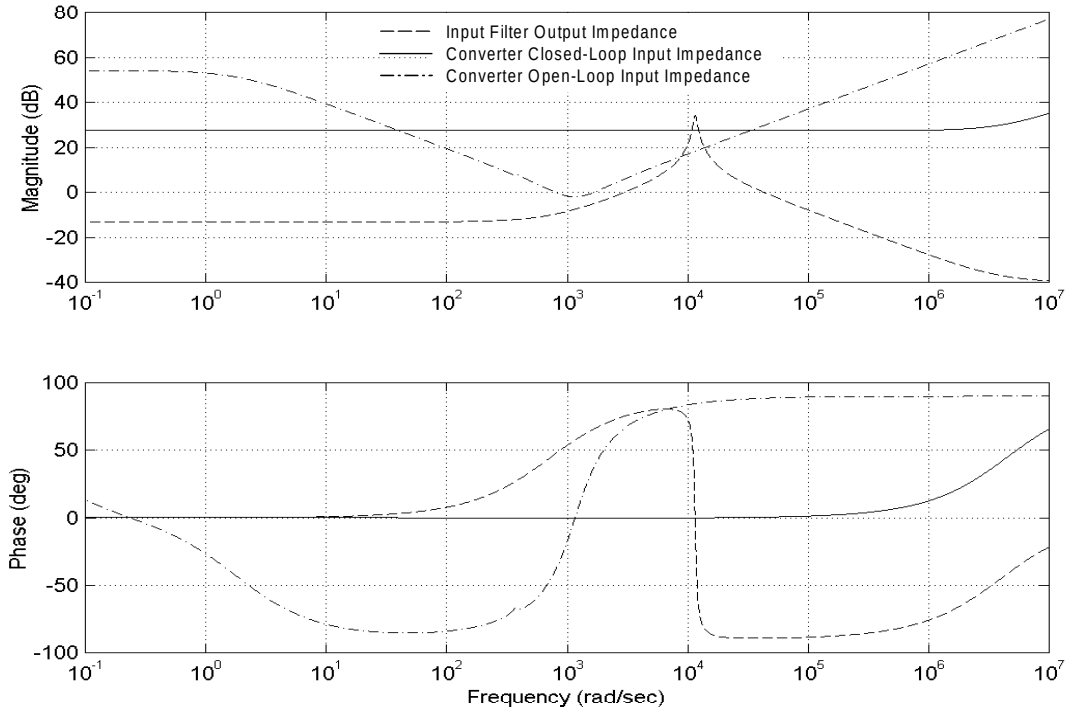

Figure 4.28 Input filter and converter transfer functions at operating point OP4.

becomes unstable as the operating point moves to the end of period 1. The Nyquist diagrams in Figure 4.29 confirm this conclusion.

The transfer functions for operating point OP3 are shown in Figure 4.27. The converter has a higher negative input resistance than for two previous operating points. The system is very stable at this operating point. The motor voltage, current, and speed are maintained constant during the whole period 2, which means that the stability analysis results obtained for OP3 should be valid for the whole period.

Operating point OP4 represents regenerative power flow conditions in the EMA. The transfer functions are shown in Figure 4.28. The phase of the closed-loop input impedance of the converter is zero, which means positive small-signal resistance. A constant power load in regenerative mode of operation has positive small-signal input impedance because positive change in the input voltage results in decrease in magnitude of the negative input current, which

is a positive change as well. The Nyquist plot for OP4 in Figure 4.29 shows that the EMA with regenerative power flow is always stable, which is true for the whole period 3.

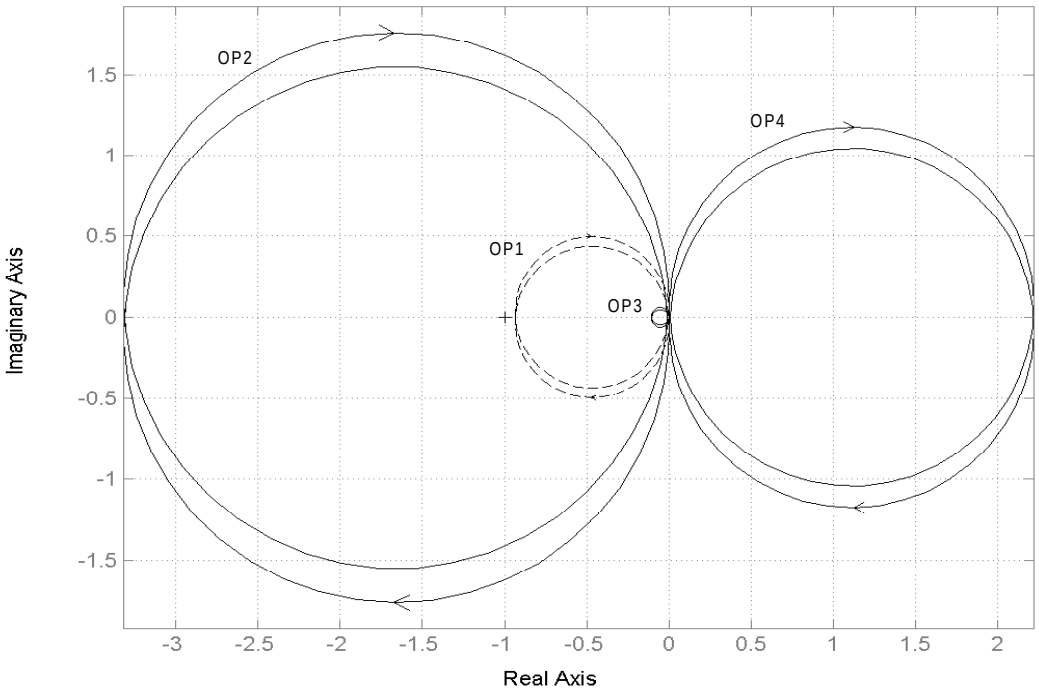

Figure 4.29 Nyquist plots for the EMA and input filter interaction.

Figure 4.30 shows simulation results of the EMA, which confirm the results of small-signal stability analysis. Oscillations caused by instability take place during the last part of period 1. These oscillations are shown in detail in Figure 4.31. Initial oscillations in the beginning of period 1 are caused by a step change in the current loop reference. It is seen that they tend to die out because initially the system is stable, but then they increase again as the system moves into the unstable region of the period. Further growth of the oscillations is limited by saturation of the converter duty ratio as the system moves to the end of period 1. The oscillations die out when the system enters period 2. No instability is observed during periods 2 and 3, which agrees with the stability analysis above. Simulation results in Figure 4.30 confirm that results of stability analysis performed for periods 1, 2, and 3 of the first half of the operating cycle are valid for the second half of the cycle as well.

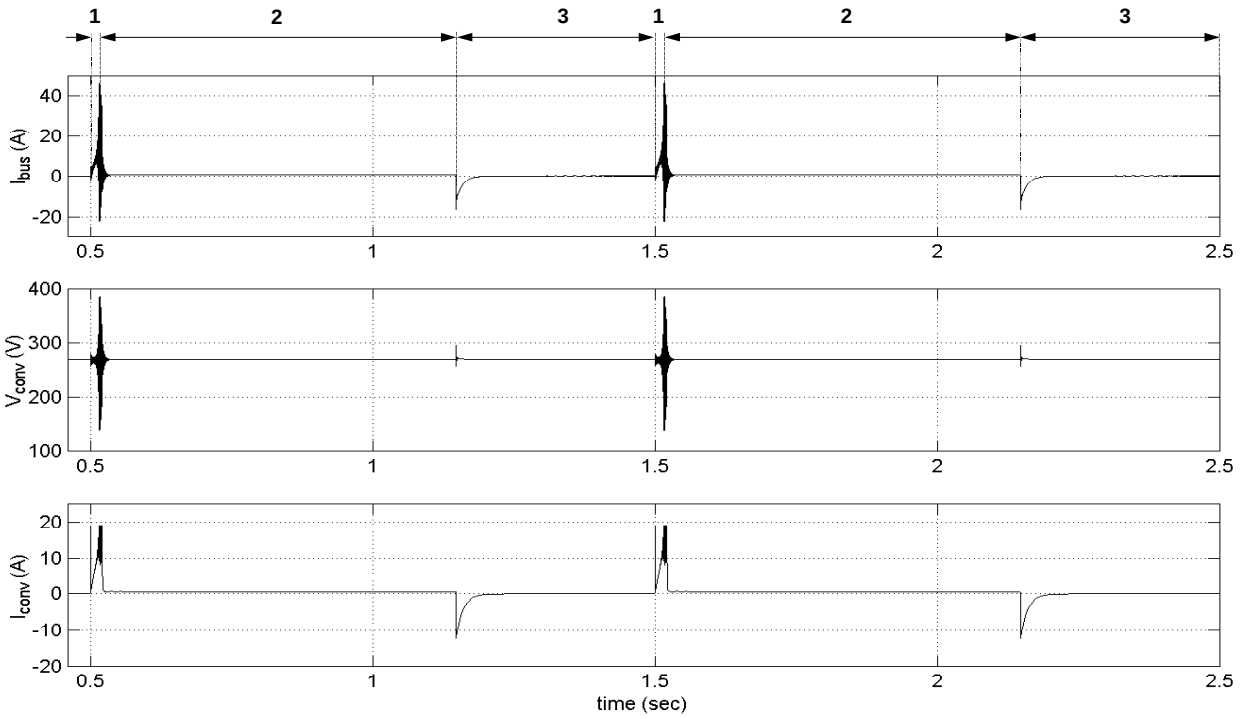

Figure 4.30 Simulation of the EMA with an ideal DC bus for the whole operating cycle.

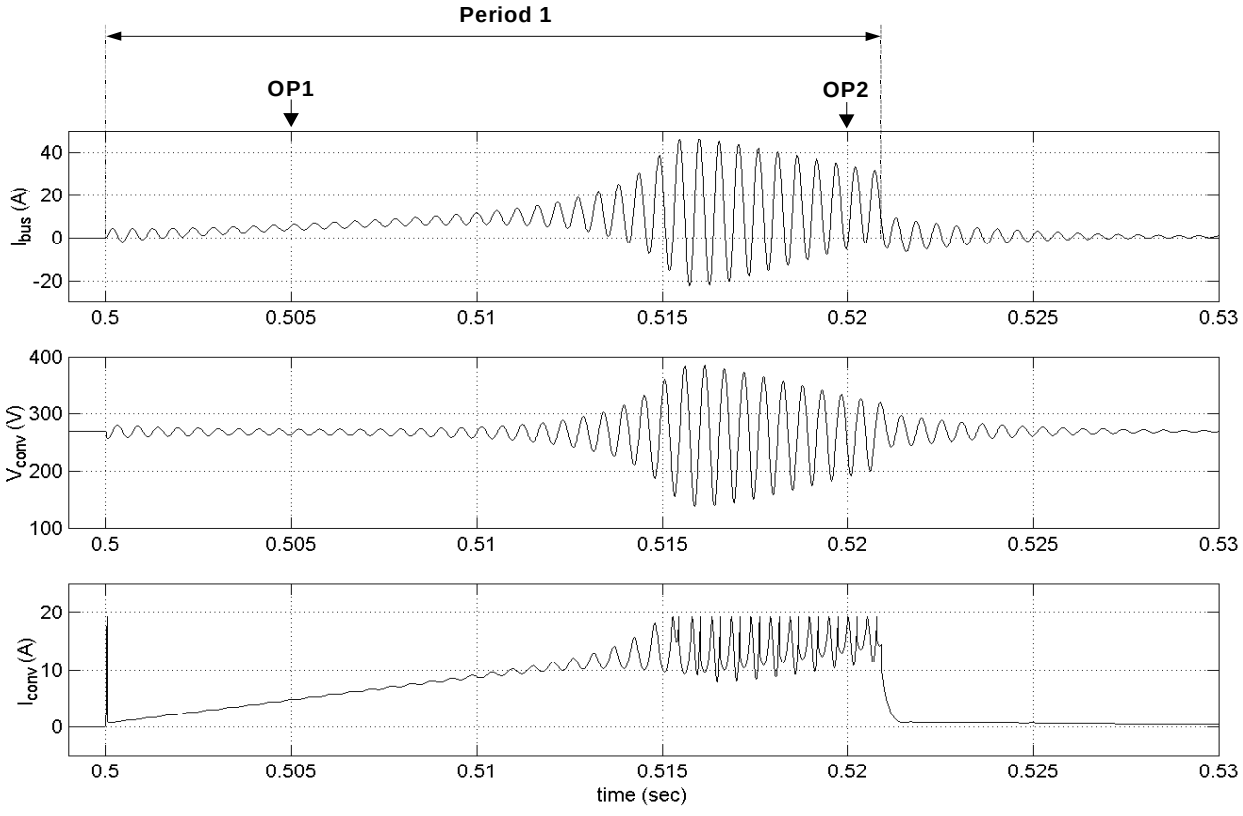

Figure 4.31 Simulation of the EMA with an ideal DC bus.

Non-zero impedance of the real bus compared with an ideal voltage source produces a stabilizing effect on the filter – converter interactions. The following analysis is given for the whole system configuration for the unstable operating point OP2. Figure 4.32 presents a comparison of the input filter output impedance obtained with the ideal and real busses, and the closed-loop input impedance of the converter. The figure shows that the filter output impedance with the real bus has lower peaking at its resonant frequency than with the ideal bus, although the system is still unstable at this operating point. The corresponding Nyquist plots are shown in Figure 4.33. Since there are more than one interface in this example where instability can occur, the system may already be unstable because of instability at another interface. Therefore, open-loop right-half plane (RHP) poles of the impedance ratio were checked to ensure correct interpretation of the Nyquist plots. According to Nyquist stability criterion, the number of closed-loop RHP poles, which determine the closed-loop system stability, is equal to

$$Z = N + P, \tag{4.10}$$

where Z – number of closed-loop RHP poles,

N – number of clockwise encirclements in the Nyquist plot,

P – number of open-loop RHP poles.

Both impedance ratios plotted in Figure 4.33 have no open-loop RHP poles and produce two encirclements, which give two closed-loop RHP poles for both cases. This result means instability for both ideal and real DC bus. It is seen that it should be easier to achieve stability with the real bus by making adjustments in the system.

Instability may also occur on the DC bus as a result of interactions between the boost rectifier and the EMA. Figure 4.34 shows the boost rectifier output impedance and the EMA input impedance transfer functions. The boost rectifier output impedance transfer function has already been discussed earlier. The EMA input impedance appears as the converter input impedance modified by the input filter. It can be observed that at low frequencies the EMA input impedance is formed by negative input resistance of the converter. The EMA input impedance is changed significantly by the input filter at frequencies near and above its resonant frequency. Instability is possible if the EMA input impedance magnitude is lower than the boost rectifier output impedance over a certain frequency range provided that the phases of these

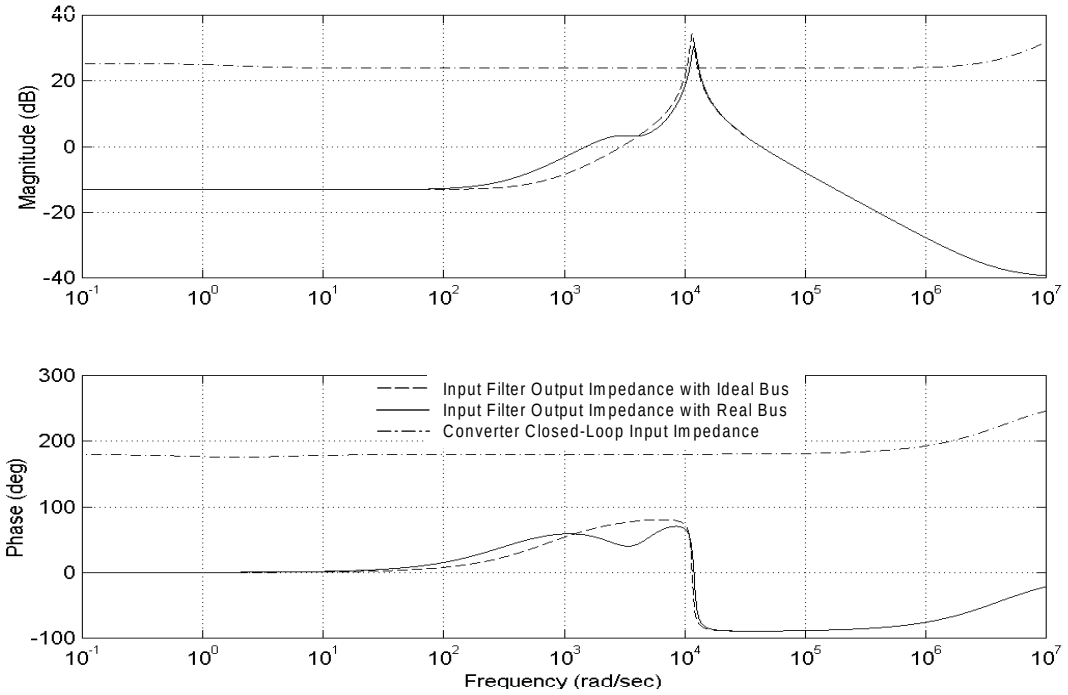

Figure 4.32 Input filter and converter transfer functions.

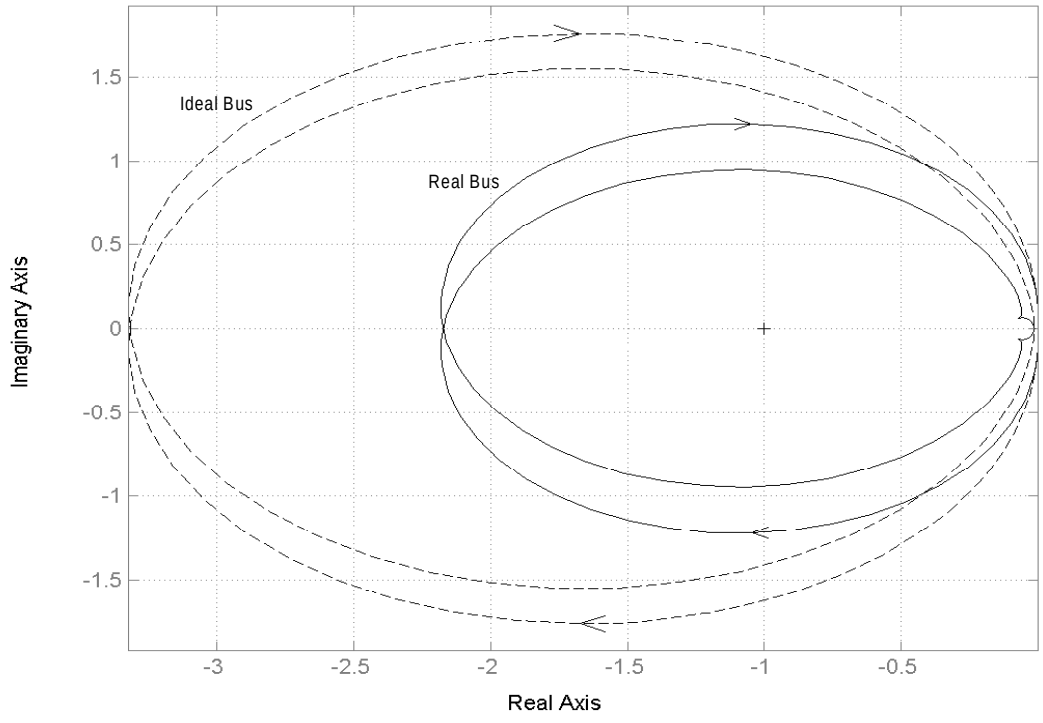

Figure 4.33 Nyquist plots for the input filter and converter interaction with ideal and real bus.

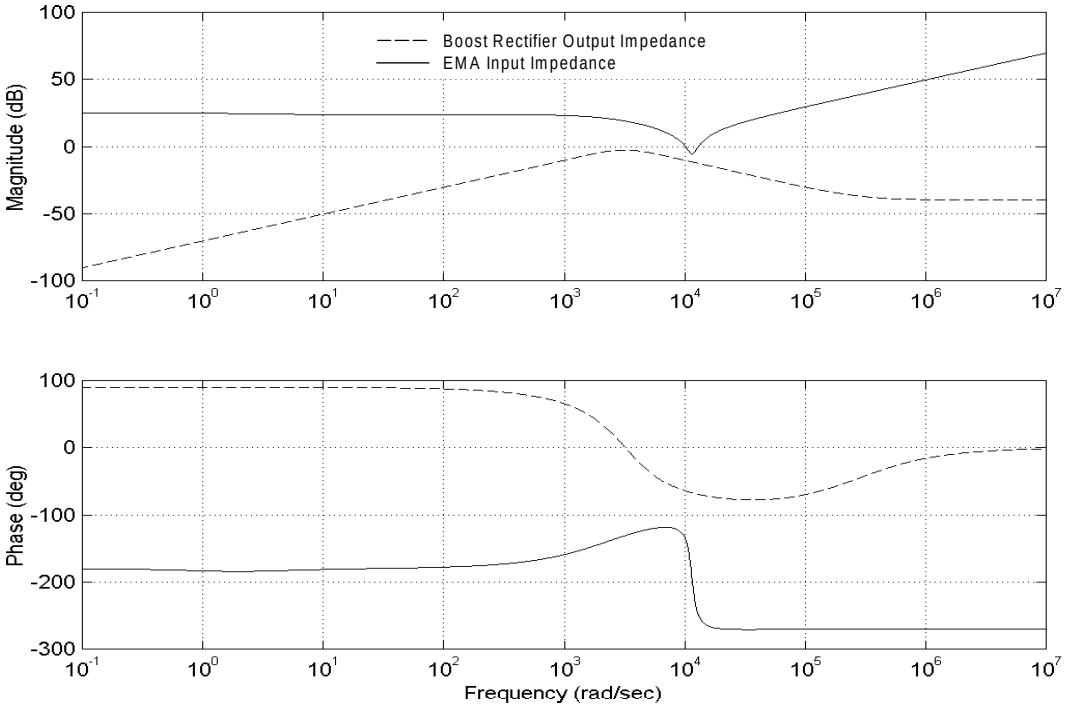

Figure 4.34 Boost rectifier output impedance and the EMA input impedance.

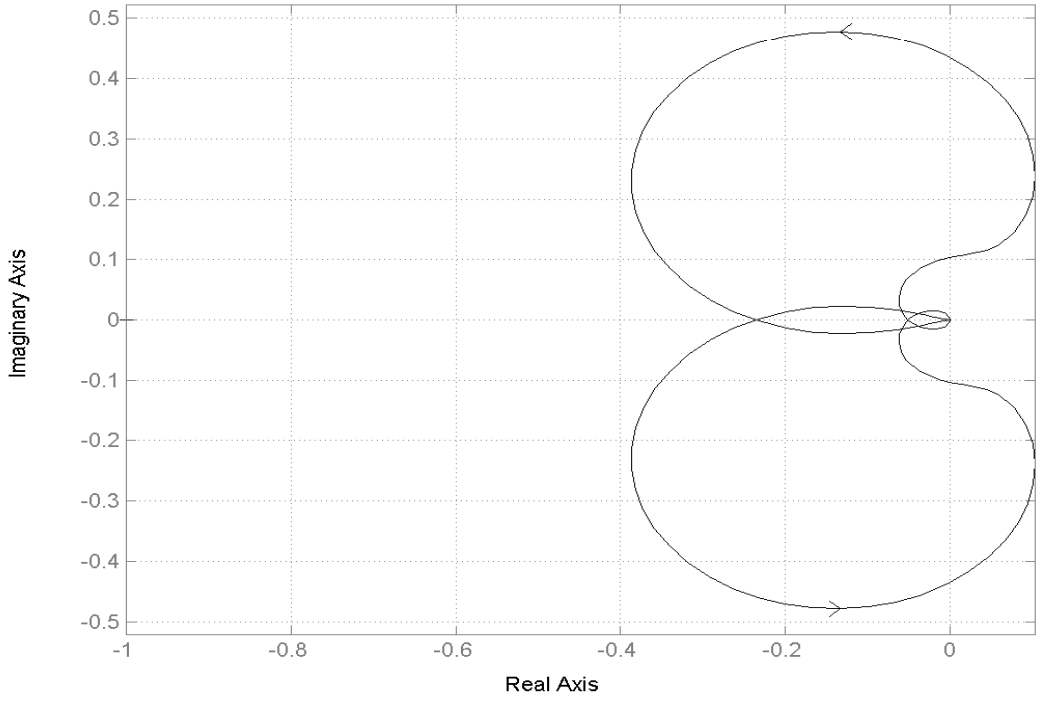

Figure 4.35 Nyquist plot for the boost rectifier and the EMA interaction.

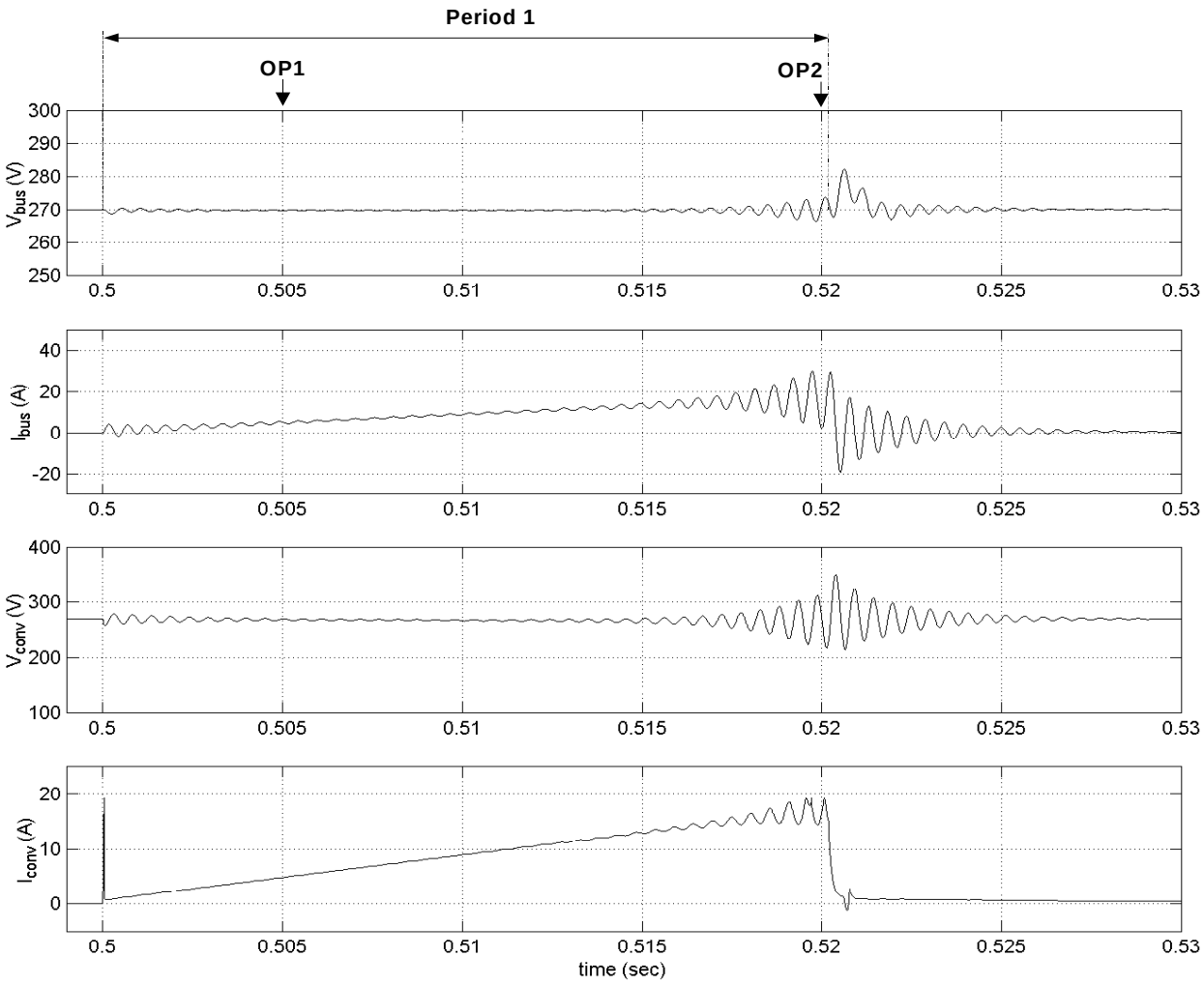

Figure 4.36 Simulation of the EMA with real DC bus.

transfer functions have 180 degrees difference within this range. The Nyquist plot in Figure 4.35 shows that this does not happen in this case. However, it was found that the impedance ratio at this interface has two RHP poles. Since there are no encirclements on the plot, there are two closed-loop RHP poles. They show that the system is unstable at this interface. The instability at the input filter – converter interface creates instability of the whole system, which is confirmed by the analysis above. It can be observed by comparing the converter input impedance in Figure 4.32 and the boost rectifier output impedance in Figure 4.34 that the converter connected directly to the DC bus would not cause any stability problems in the PDS. It is the input filter that causes possible instability both on the DC bus and between itself and the converter.

Figure 4.36 shows simulation results of the EMA with the real bus during period 1. Compared with Figure 4.31, the input filter – converter oscillations are significantly reduced, which is in agreement with the stability analysis based on Figures 4.32 and 4.33.

As a further example of using the modeling and analysis tools for stability analysis of the PDS, a filter with different damping is considered. The damping resistance R_a in the input filter was increased to 0.65Ω in order to achieve stability at operating point OP2. The resulting transfer functions and Nyquist plots are shown in Figures 4.37 and 4.38. The system with the ideal bus is still unstable, but with the real bus is already stable. There are no encirclements and no RHP poles for the impedance ratio with the real bus. This is an indication of stability. The simulation in Figure 4.41 confirms that the system is stable during the whole period 1.

Analysis of the DC bus stability for $R_a = 0.65\Omega$ is performed based on Figures 4.39 and 4.40. The Nyquist plot shows two counterclockwise encirclements; the impedance ratio has two RHP poles. Therefore, the number of closed-loop RHP poles for this interface is

$$Z = N + P = -2 + 2 = 0, \tag{4.11}$$

which indicates that the system is stable. This result is in full compliance with simulation results in Figure 4.41 as mentioned above. Simulation results of the system during the whole operating cycle presented in Figure 4.42 show that the system with $R_a = 0.65\Omega$ is stable during periods 2 and 3 as well.

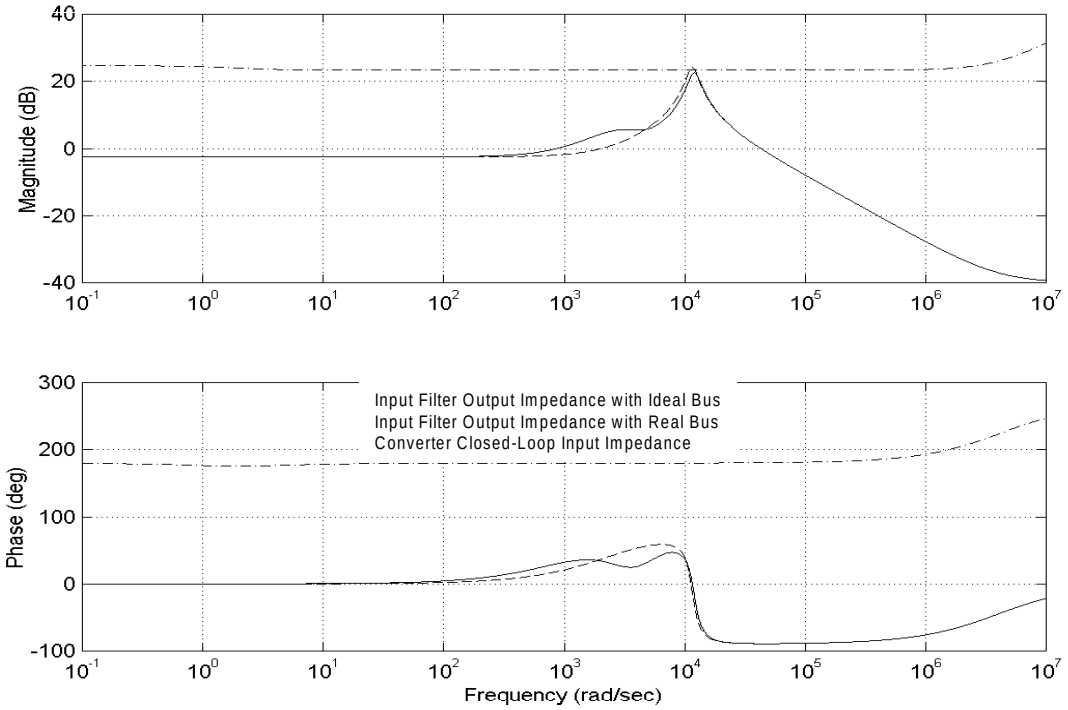

Figure 4.37 Input filter and converter transfer functions with $R_a = 0.65\Omega$.

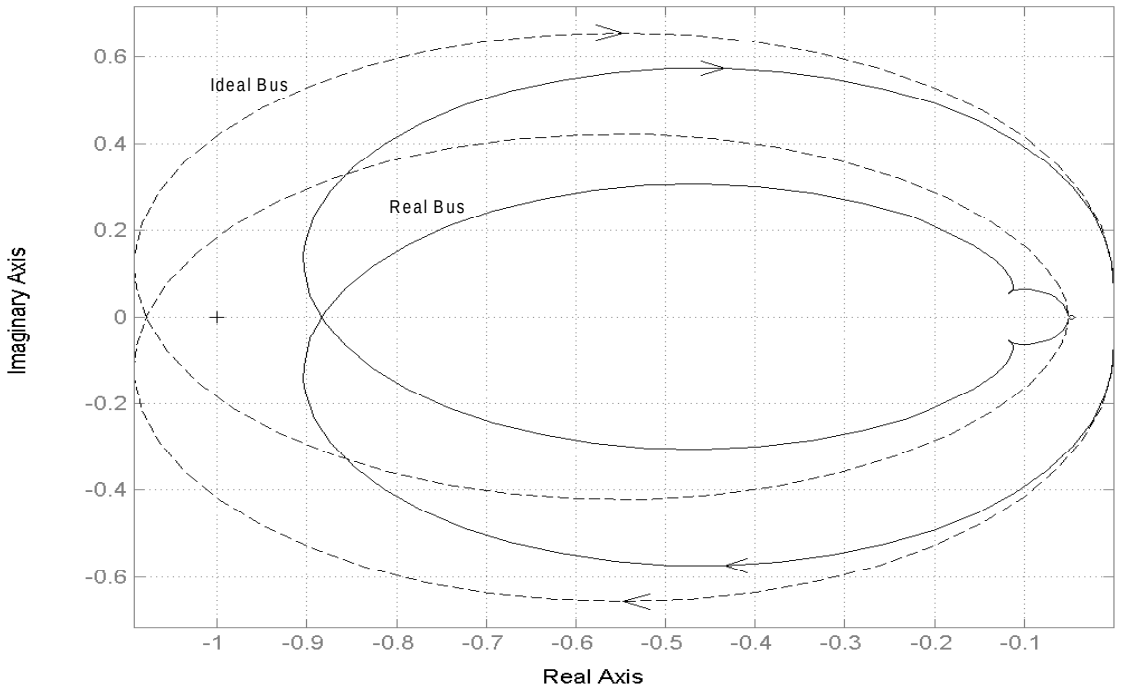

Figure 4.38 Nyquist plots for the input filter and converter interaction with $R_a = 0.65\Omega$.

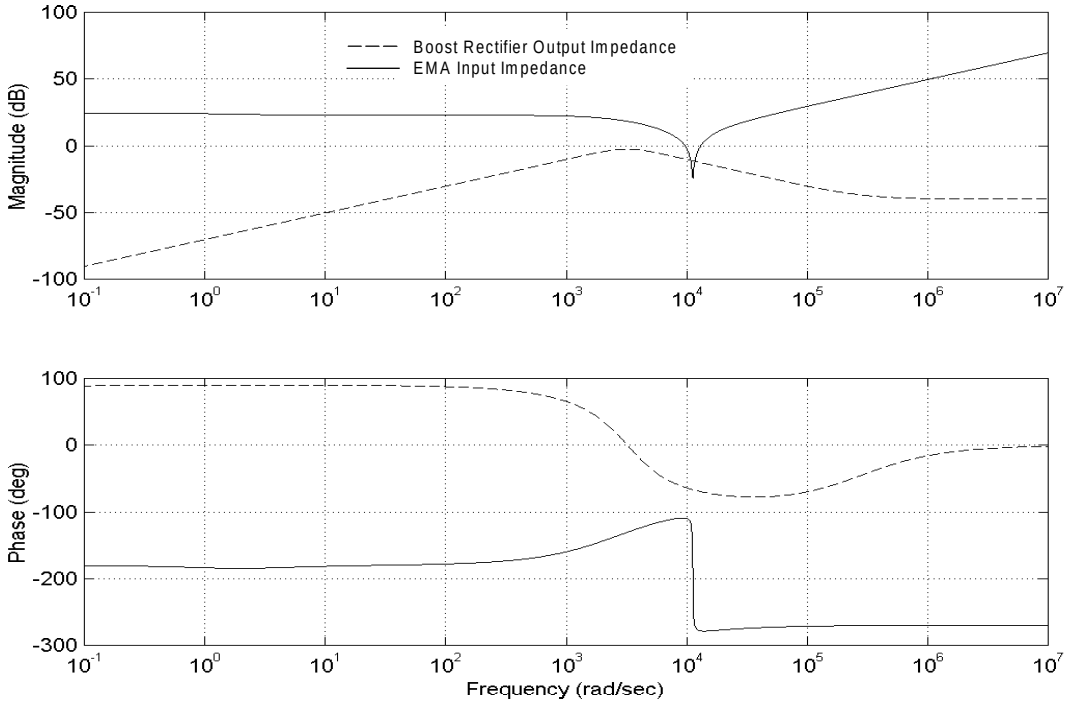

Figure 4.39 Boost rectifier output impedance and the EMA input impedance with $R_a = 0.65\Omega$.

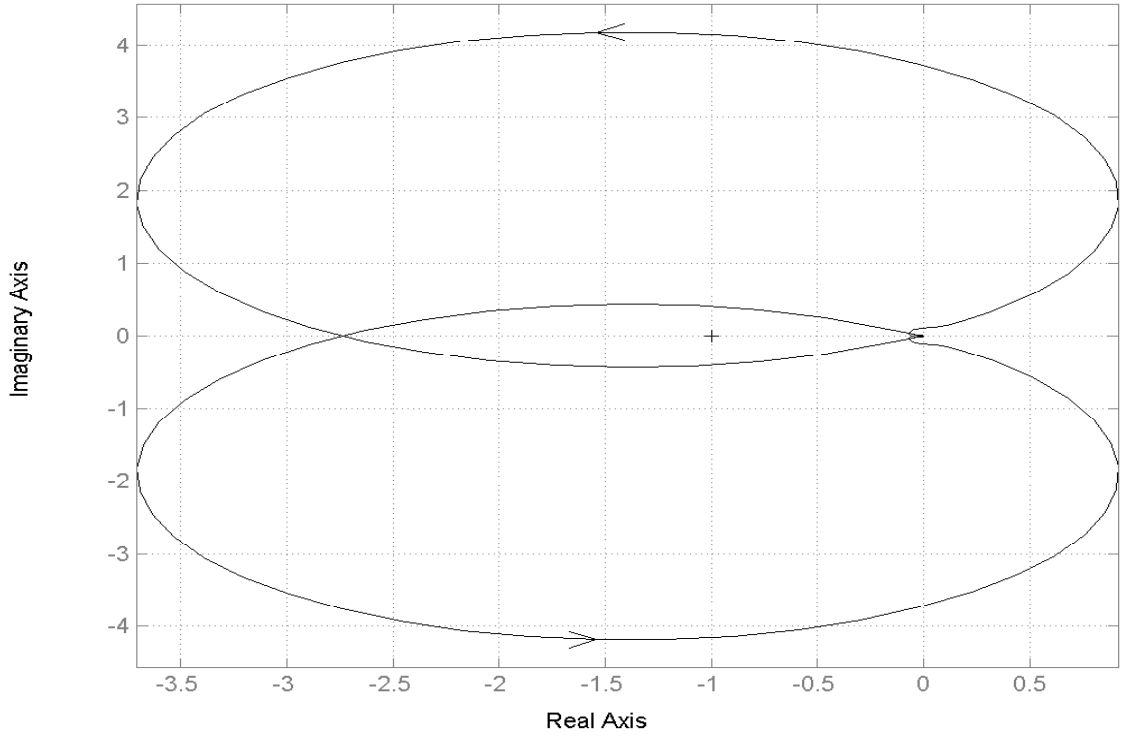

Figure 4.40 Nyquist plot for the boost rectifier and the EMA interaction with $R_a = 0.65\Omega$.

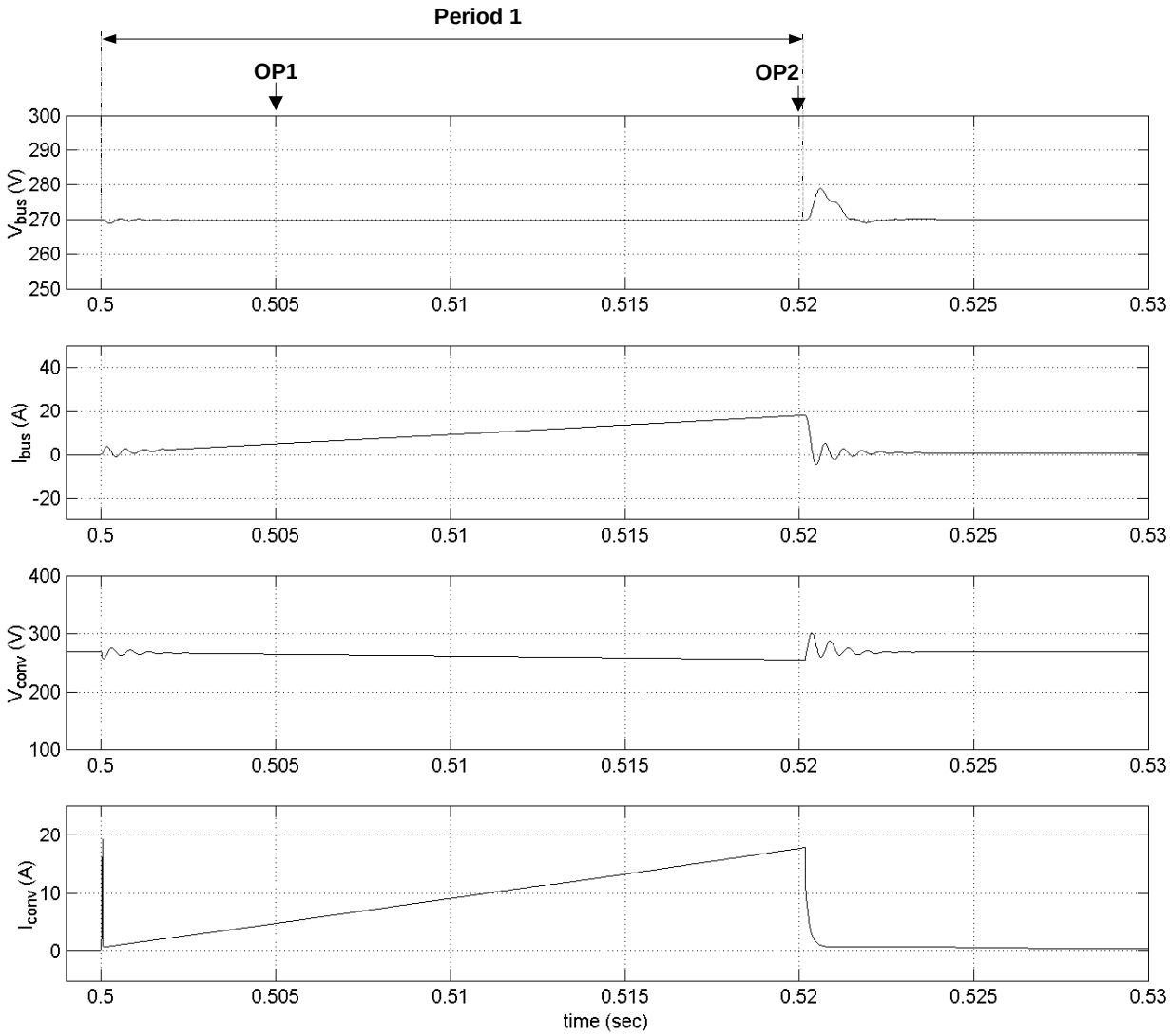

Figure 4.41 Simulation of the whole PDS with $R_a = 0.65\Omega$.

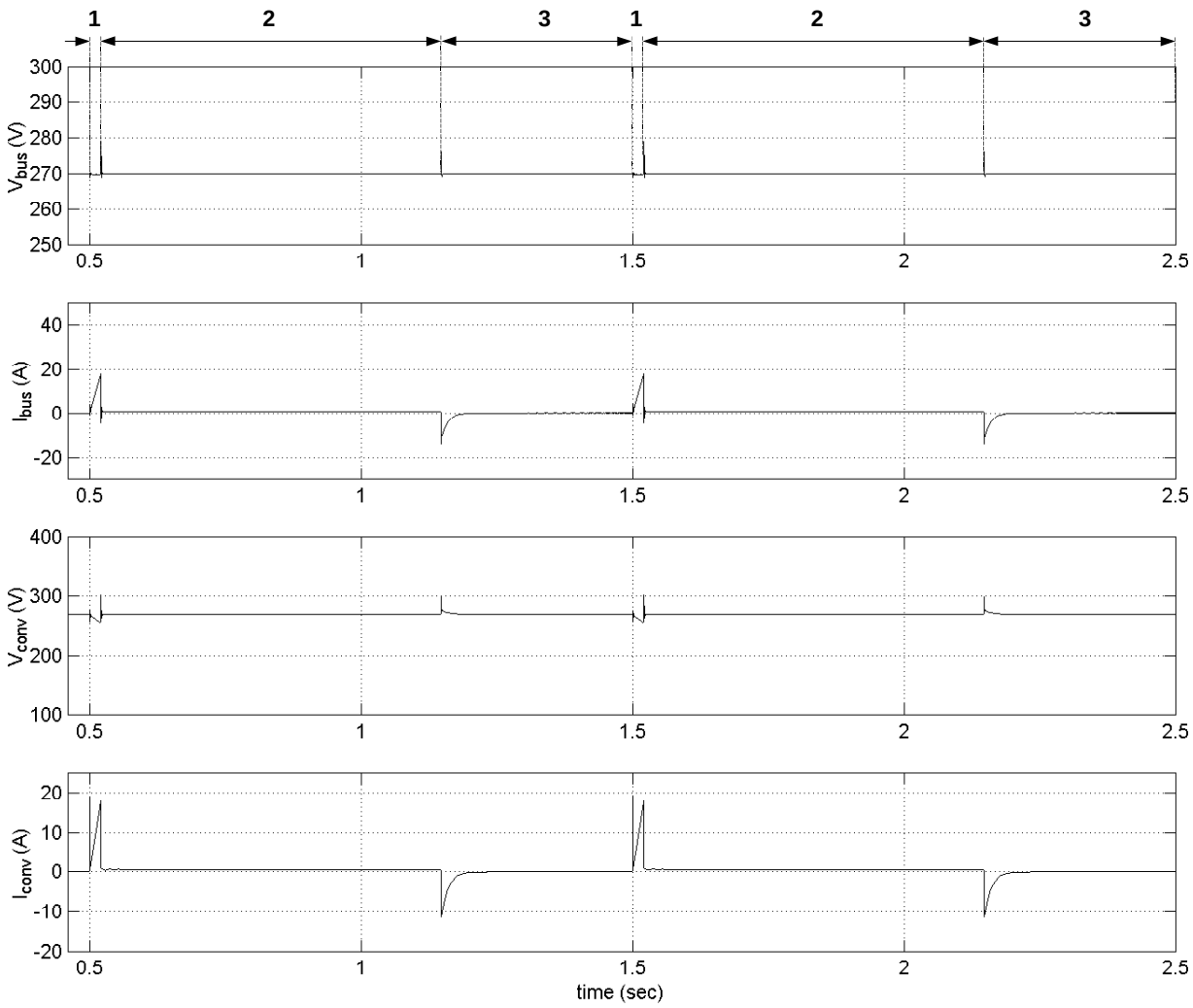

Figure 4.42 Simulation of the whole PDS with R_a = 0.65Ω during the operating cycle.

The examples of stability analysis of the PDS with constant power load and the EMA presented in this chapter show that the modeling and analysis tools developed in this research are very effective for stability analysis of complex nonlinear systems.

Chapter 5

Analysis of Bidirectional Power Flow in a DC Power Distribution System

5.1 Introduction

A prominent feature of the PDS is bidirectional power flow in its subsystems and the DC distribution bus. As opposite to the normal power flow from the sources to the loads, the reverse power flow occurs when certain loads in the system work in regenerative mode. For example, this mode of operation is typical for flight control actuators, which alternate normal and regenerative modes during their operational cycle. This chapter presents an analysis of the effect of regenerative power flow on the overall system performance characteristics such as DC bus power quality and system efficiency.

The energy coming from a regenerating subsystem tends to raise the DC bus voltage unless this energy is utilized by certain means. When no other load with sufficient power consumption is present at the moment of regeneration, and no measures are taken to utilize the regenerative energy, the bus voltage can easily rise beyond allowable limits specified by MIL-STD-704E [8]. This phenomenon may affect normal operation of the PDS and cause damage to the equipment connected to the bus. An attractive solution would be to store this energy in the battery for future use. Unfortunately, the battery charges too slowly to accept the regenerative energy, which usually comes in short transient spikes of high power. Presently, there are several possible ways to deal with regenerative energy in the system:

- dissipate it in resistors connected to the bus at the time of regeneration,

- let it go back to the engine by using the generator and three-phase-to-dc power converter in regenerative mode,
- use large capacitors in order to store the regenerative energy either in the DC bus, or in the regenerating subsystem,
- use a DC bus conditioner (a power converter that stores the extra energy from the bus in a large capacitor and returns the energy to the bus when loads are available).

Currently, industry uses the first approach with damping resistors dissipating the regenerative energy. Unfortunately, the amount of this energy is so high that the resistors require liquid cooling. This solution complicates the system and reduces the benefits of the "more electric approach" in aircraft design. The use of a bus conditioner seems to be too complicated and expensive at this time; it is left for future consideration. This chapter considers utilizing the regenerative energy in the power source (the engine) with the use of additional capacitors in the DC bus and in the regenerating subsystem in order to alleviate transient voltage spikes caused by regenerative power flow.

5.2 System Configuration for Bidirectional Power Flow Analysis

The system configuration shown in Figure 5.1 was used to study the effects of additional capacitors on the DC bus power quality and the system efficiency under bidirectional power flow conditions. The system consists of a three-phase synchronous generator, three-phase-to-dc boost rectifier, the EMA including an input filter, and a constant resistive load on the DC bus, representing all other system loads except the EMA. The system waveforms during one operating cycle of the EMA are shown in Figure 5.2 (operation without the wind load) and Figure 5.3 (operation with the wind load). The analysis is performed for the time period from 0.5s to 2.5s, which corresponds to the full cycle of the EMA. The period from 0 to 0.5s is a "start-up" period; it is used to bring the simulation model to the initial conditions corresponding to the beginning of the cycle. This period is not included into consideration.

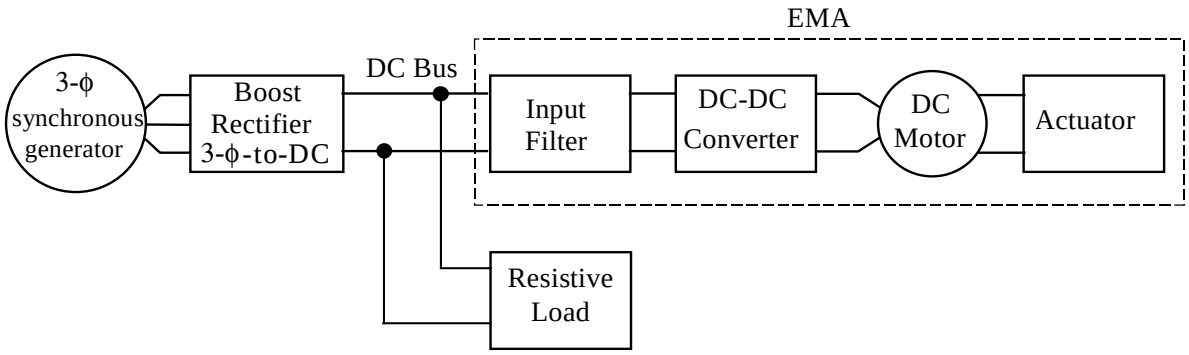

Figure 5.1 System configuration for bidirectional power flow analysis.

Figures 5.2 and 5.3 are typical examples of the system operation with and without the wind load for a certain set of system parameters. The plots show the DC bus voltage and power, the motor current, the flight control surface deflection angle, and the EMA reference signal coming from a higher-level control system. The major phenomena under investigation such as regenerative energy flow and voltage disturbances on the bus occur at times when the actuator reference signal changes abruptly and the actual position of the actuator reaches its commanded value. This causes the actuator motor to speed up or to slow down, thus consuming or regenerating a certain amount of energy, which causes significant current flow in the system and, as a result, voltage disturbances on the DC bus. Regenerative energy flow always occurs in the system when the actuator reference signal causes the actuator moving parts to slow down, and their mechanical energy is converted into electrical. In addition, the wind load produces regenerative energy when the surface moves in the direction of the air flow. In this case, the wind energy is converted into electrical energy. This energy will have to be consumed from the boost rectifier later during the cycle when the actuator reference signal causes the actuator surface to move against the air flow.

What happens to the regenerative energy in this particular system configuration depends primarily on the value of the resistive load on the DC bus. If the load is large enough such that the power that it draws from the bus exceeds the peak value of the actuator regenerative power, the power drawn from the boost rectifier remains positive at all times. The actuator regenerative

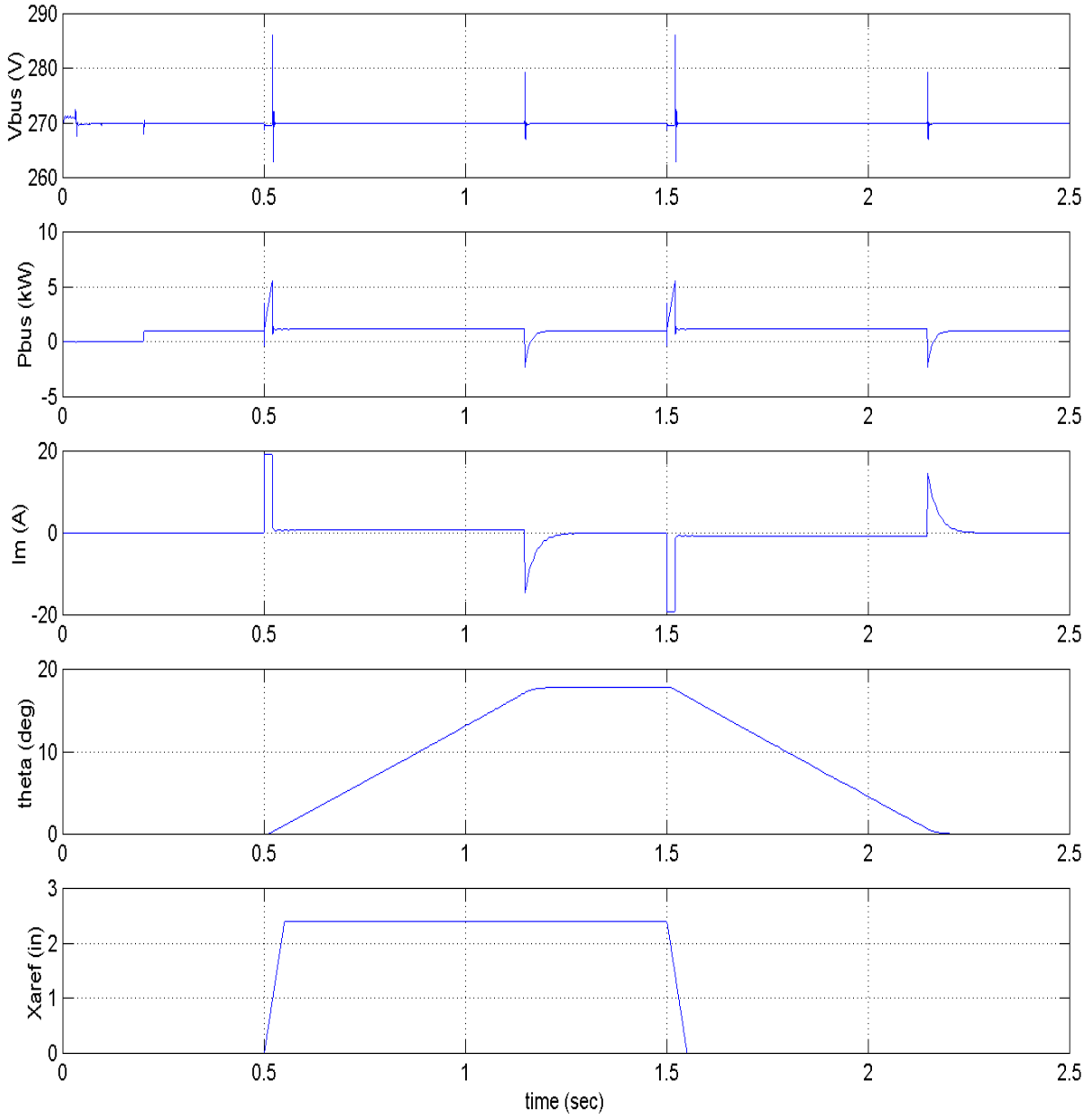

Figure 5.2 System operation without the wind load.

power is completely consumed by the resistive load, thus merely decreasing the power drawn from the boost rectifier. If the peak actuator regenerative power exceeds the load power requirement, the excessive power will be transformed back to the generator by the boost rectifier. This case is shown in Figures 5.2 and 5.3, where the load draws 1kW power from the DC bus. If the rectifier does not possess bidirectional energy flow capability, the excessive amount of

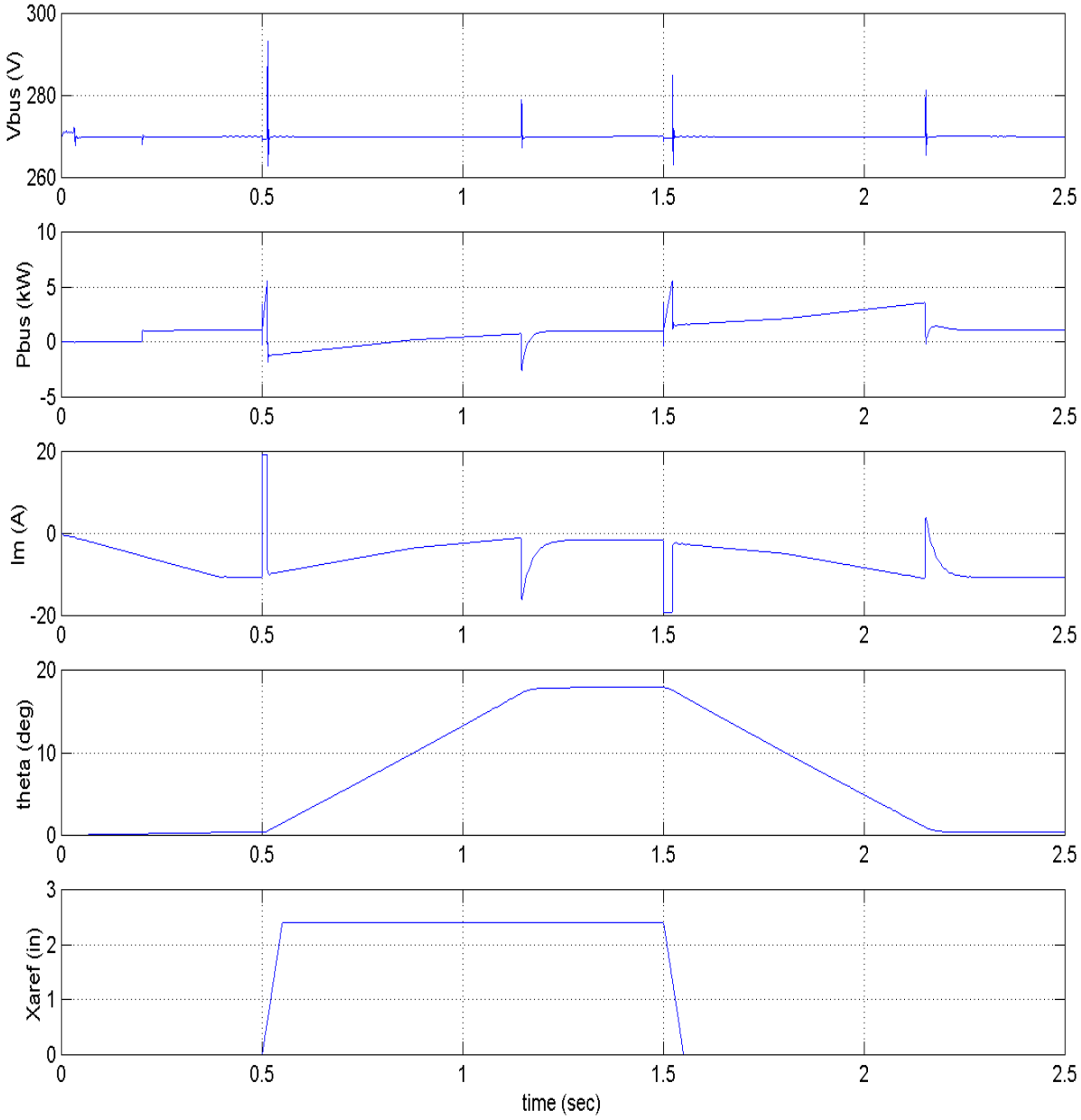

Figure 5.3 System operation with the wind load.

energy will be stored in the rectifier output capacitor and the input filter capacitor, which will cause the DC bus voltage to increase. The amount of this increase will be determined by the capacitor's total value and the amount of energy regenerated. When a bidirectional boost rectifier is used, the capacitors do not store the regenerative energy permanently, but only affect the system transients.

5.3 Overall System Performance Characteristics and Methodology of Bidirectional Power Flow Analysis

The distributed power quality may be characterized by the DC bus voltage disturbances. They are affected by the system damping, which is determined by parameters of both system elements and control structure. In this study of the DC bus power quality, magnitude of voltage spikes on the bus and settling time of the transients were used as performance measures. For the purpose of this research, we defined a "voltage spike" as a voltage disturbance on the DC bus that exceeds an allowable limit $\pm\Delta V$. "Transients" are considered as a series of spikes. We define the "settling time of the transients" as a time interval during which the series of spikes occurs provided that the spikes in the series are separated by time intervals no more than an allowable time Δt. This concept is illustrated in Figure 5.4. The following values for these parameters were assumed:

$\Delta V = 2V$,

$\Delta t = 0.001s$.

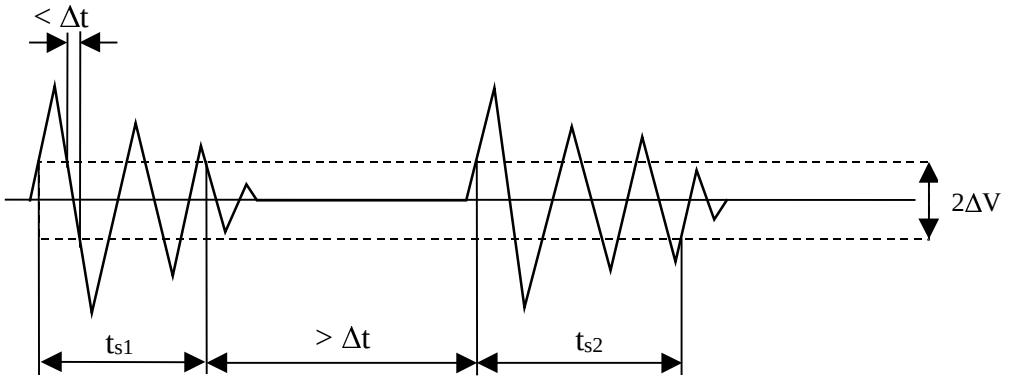

Figure 5.4 Settling time of the transients on the DC bus.

In order to characterize quantitatively the process of energy distribution and regeneration in the sample PDS (Figure 5.1), the complete energy flow analysis was performed. Energy flow in the system is described in terms of energy flow at subsystems boundaries (Figure 5.5). Energy

is computed at each boundary by integrating the corresponding power as a function of time during the EMA operating cycle.

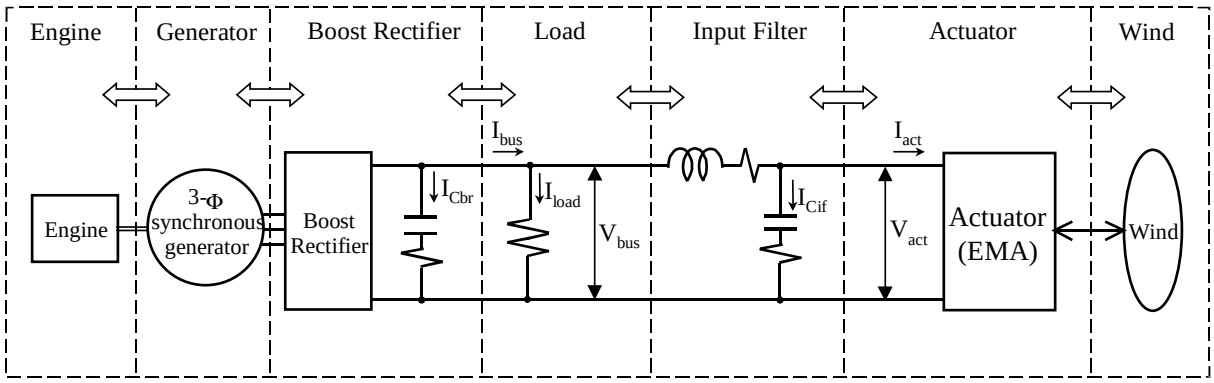

Figure 5.5 Bidirectional energy flow in the system.

The definitions used for energy flow analysis in the system are given below. Mechanical power supplied by the engine to the generator:

$$P_{gm} = P_g + P_{gl}, \tag{5.1}$$

where P_g – power transferred from the generator to the boost rectifier,

P_{gl} – total power losses in the generator.

Power supplied by the generator to the boost rectifier:

$$P_g = 1.5\,(V_{gd}\,I_{gd} + V_{gq}\,I_{gq}), \tag{5.2}$$

where V_{gd}, V_{gq} – generator output voltages in *dq* coordinates,

I_{gd}, I_{gq} – generator output currents in *dq* coordinates.

Generator electrical losses are calculated as a sum of losses in phase windings, damper winding, and the excitation winding. Total generator losses are obtained by multiplying the electrical losses by two to account for magnetic and other types of losses. Total generator losses are used

for calculating mechanical power supplied by the engine to the generator because no engine simulation is involved.

Losses in phase resistances:

$$P_{gls} = 1.5\ (I_{gd}^2 + I_{gq}^2)\ R_s, \tag{5.3}$$

where I_{gd}, I_{gq} – phase currents in *dq* coordinates,

R_s – resistance per phase in the equivalent circuit.

Losses in the damper winding:

$$P_{glk} = 1.5\ (I_{kd}^2\ R_{kd} + I_{kq}^2\ R_{kq}), \tag{5.4}$$

where I_{kd}, I_{kq} – damper winding currents in *dq* coordinates,

R_{kd}, R_{kq} – damper winding resistances in *dq* coordinates.

Losses in the field winding:

$$P_{glf} = I_{fd}^2\ R_{fd}, \tag{5.5}$$

where I_{fd} – field winding current referenced to the stator,

R_{fd} – field winding resistance referenced to the stator.

Total generator losses:

$$P_{gl} = 2\ (P_{gls} + P_{glk} + P_{glf}). \tag{5.6}$$

Power transferred from the boost rectifier to the load:

$$P_{bus} = V_{bus}\ I_{bus}, \tag{5.7}$$

where V_{bus} – DC bus voltage,

I_{bus} – DC bus current.

Power transferred from the load to the input filter:

$$P_{fi} = V_{bus}\ (I_{bus} - I_{load}), \tag{5.8}$$

where I_{load} – load current.

Power transferred from the input filter to the EMA:

$$P_{act} = V_{act}\, I_{act}, \tag{5.9}$$

where V_{act}, I_{act} – input voltage and current of the EMA, respectively.

Power transferred from the actuator to the air:

$$P_{wind} = H_m\, \omega_{sur}, \tag{5.10}$$

where H_m – external moment from the air flow,

ω_{sur} – actuation surface angular speed.

Energy flowing from the left to the right is considered positive, regenerative energy flowing in the opposite direction – negative. Based on energy flow analysis at subsystem interfaces shown in Figure 5.5, the energy balance for each subsystem is calculated.

Energy balance for the engine, which is the net energy coming from the engine to the generator:

$$W_{eng} = W_{gmp} - W_{gmn}, \tag{5.11}$$

where W_{gmp} – positive energy, coming from the engine,

W_{gmn} – negative (regenerative) energy, going back to the engine from the generator.

Energy balance for the generator, equal to the total losses in the generator:

$$W_{gen} = (W_{gmp} - W_{gmn}) - (W_{gp} - W_{gn}), \tag{5.12}$$

where W_{gp} – positive energy, transferred from the generator to the boost rectifier,

W_{gn} – negative (regenerative) energy, going back to the generator from the boost rectifier.

Energy balance for the boost rectifier, equal to its losses:

$$W_{brec} = (W_{gp} - W_{gn}) - (W_{busp} - W_{busn}), \tag{5.13}$$

where W_{busp} – positive energy, transferred from the boost rectifier to the bus,

W_{busn} – negative (regenerative) energy, going back to the boost rectifier from the bus.

Energy balance for the resistive load:

$$W_{load} = (W_{busp} - W_{busn}) - (W_{fip} - W_{fin}), \tag{5.14}$$

where W_{fip} – positive energy, transferred from the bus to the input filter,

W_{fin} – negative (regenerative) energy, going back from the input filter to the bus.

Energy balance for the input filter, equal to its losses:

$$W_{iflt} = (W_{fip} - W_{fin}) - (W_{actp} - W_{actn}), \tag{5.15}$$

where W_{actp} – positive energy, transferred from the input filter to the EMA,

W_{actn} – negative (regenerative) energy, going back from the EMA to the input filter.

Energy balance for the EMA, equal to its losses:

$$W_{actr} = (W_{actp} - W_{actn}) - (W_{windp} - W_{windn}), \tag{5.16}$$

where W_{windp} – positive energy, transferred from the EMA to the air,

W_{windn} – negative (regenerative) energy, going from the air flow to the EMA.

Energy balance for the air flow, equal to the net energy passed by the EMA to the air:

$$W_{wnd} = W_{windp} - W_{windn}. \tag{5.17}$$

Once the losses in the subsystems are calculated, the overall system efficiency is obtained as

$$\eta = \frac{W_{gmp} - (W_{gen} + W_{brec} + W_{iflt} + W_{actr})}{W_{gmp}}. \tag{5.18}$$

Efficiency is calculated for total energy coming from the engine. Total losses include the losses in the generator, boost rectifier, input filter, and the actuator. Energy dissipated in the resistive load, passed to the air by the actuator, and regenerative energy returned into the engine is considered to be usefully spent.

5.4 Effect of the Input Filter Capacitor on the System Characteristics under Bidirectional Power Flow Conditions

At the first stage of analysis, influence of the EMA input filter capacitor on the system performance was studied by using a parametric sweep technique. The system operation was simulated repeatedly for different values of the capacitance, with and without the wind load. The capacitance value range was chosen with the lowest value based on necessary switching ripple attenuation and the highest value approaching 1F. The system performance measures such as energy flow and voltage disturbance characteristics then were analyzed based on the simulation results.

The study showed that voltage spikes on the DC bus produced by the EMA cyclic operation are significantly reduced with the increase of the input filter capacitance C_{if}. For example, Figures 5.2 and 5.3 show the system operation with the lowest value of the capacitance, equal to 63μF. Figures 5.6 and 5.7 show the system waveforms for a capacitance value of 63mF, which is three orders of magnitude larger than the previous value. It is seen that voltage disturbances produced on the bus become lower in magnitude and longer in time with the increase of the capacitance. The EMA waveforms are preserved regardless of the capacitance value due to the EMA feedback control. The results of parametric sweep analysis of voltage disturbances caused by regenerative power flow are shown in Figures 5.8 and 5.9. Figure 5.8 shows the voltage spike magnitude vs. the input filter capacitance. Both positive (above 270V) and negative (below 270V) spikes reduce their magnitude almost to zero when the capacitance becomes extremely large. Figure 5.9 shows settling time of these disturbances vs. input filter capacitance. The figure shows that for low capacitance values, the settling time increases with the increase of the capacitance because the time constant of the circuit increases. At the same time, the magnitude of the disturbances decreases as it is seen from Figure 5.8. When this magnitude falls below the allowable limit $\pm\Delta V$, the settling time becomes zero, according to the definition of the DC bus transients given above. The analysis showed that the same type of dependence is observed for all voltage disturbances on the bus, both regenerative and non-regenerative, during the operating cycle.

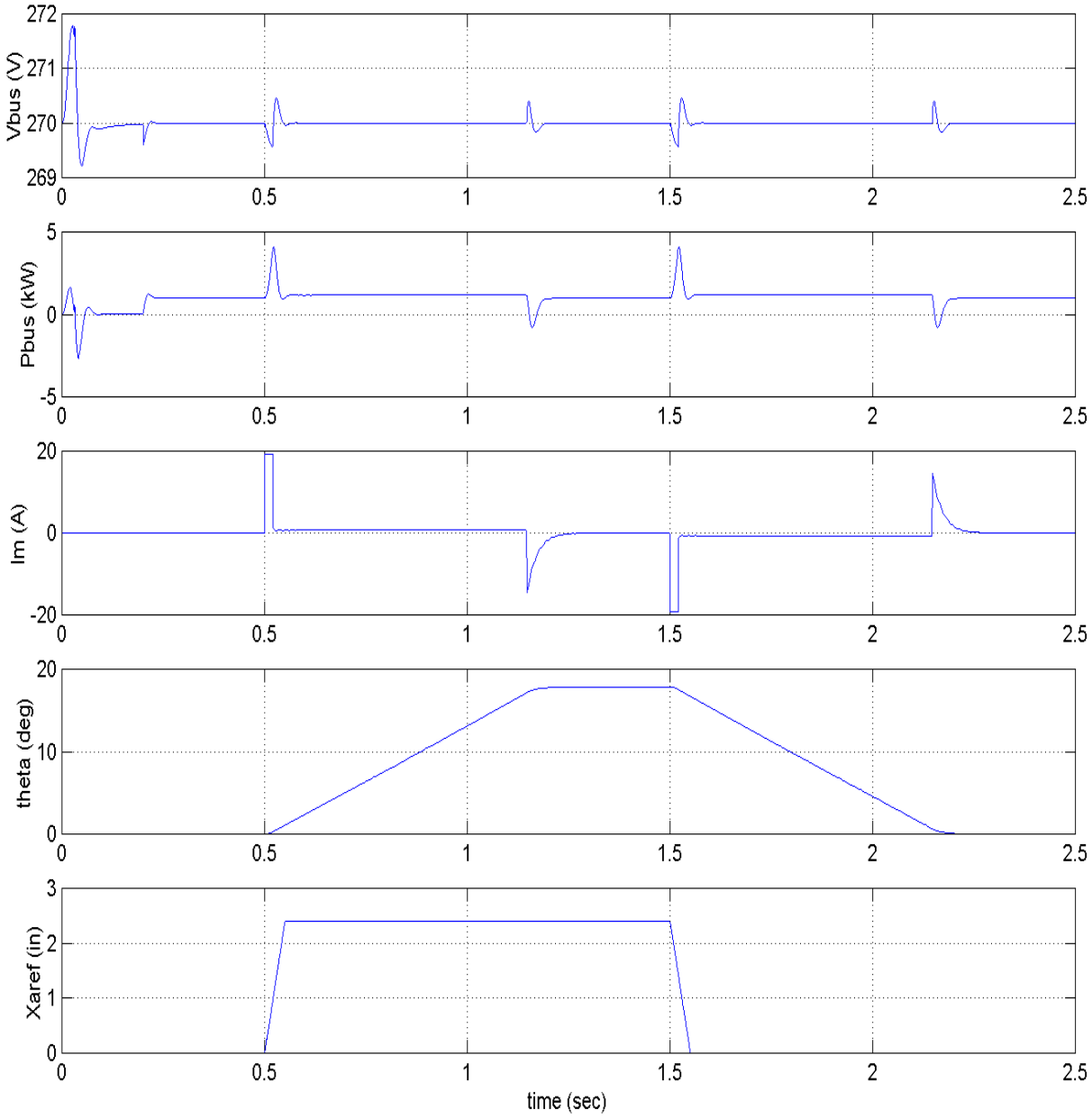

Figure 5.6 System operation without the wind load; C_{if} = 63mF.

The analysis of energy flow in the system shows that the amount of energy drawn by the system from the source (the engine) depends on the input filter capacitance. The results are illustrated in Figures 5.10 and 5.11 for operation without and with the wind load, respectively. The figures show the total energy transferred from the engine to the system, the amount of regenerative energy passed back to the engine, and percentage of the regenerative energy in the

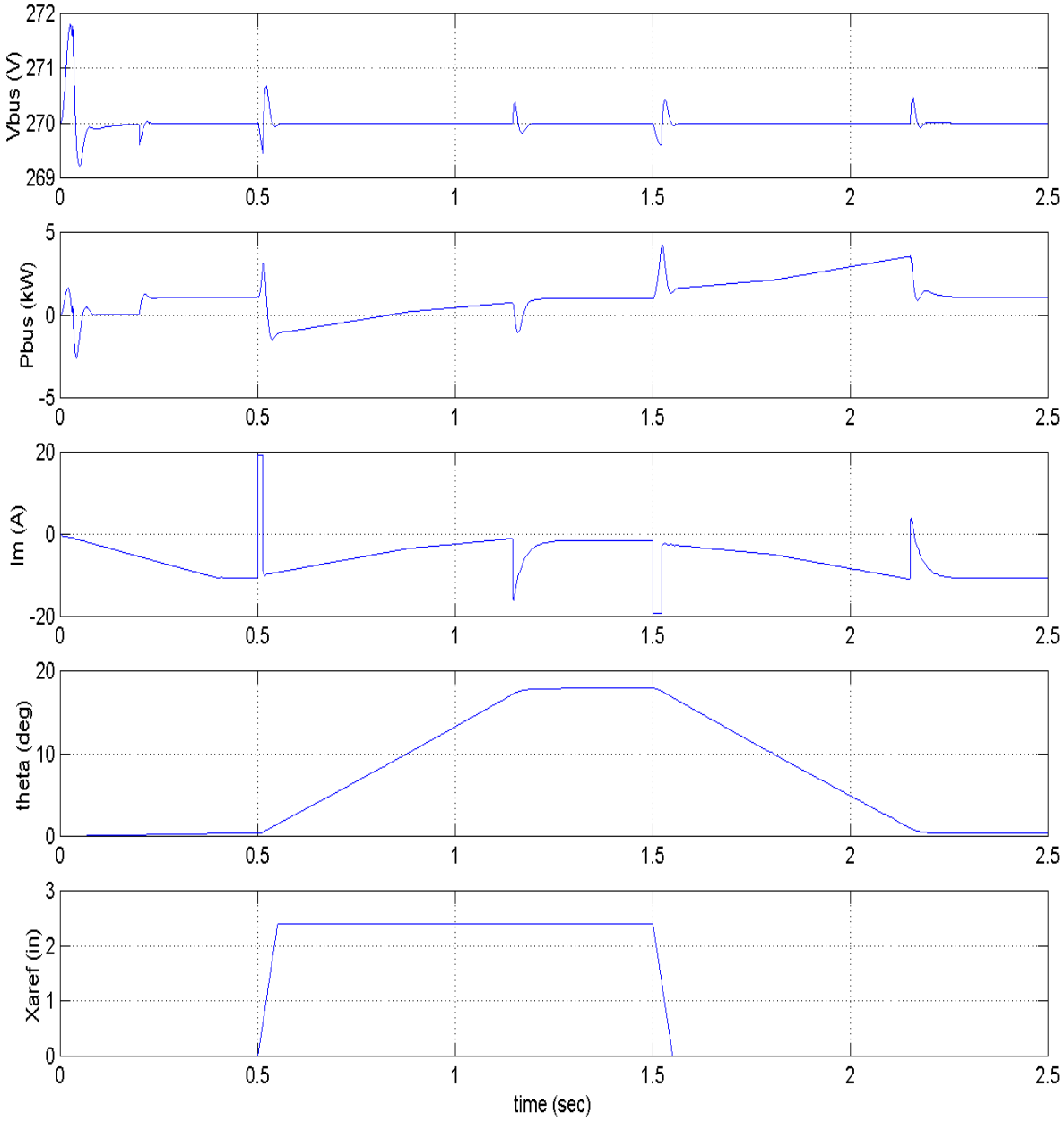

Figure 5.7 System operation with the wind load; C_{if} = 63mF.

total energy drawn by the system. It is seen that there is a global trend for the total energy to decrease when the capacitance becomes very large. At large capacitance values, the regenerative energy is almost fully absorbed by the capacitor without going back to the engine; the transients and associated with them losses are reduced. The amount of regenerative energy going back to the engine at large values of the capacitance decreases to zero for operation without the wind

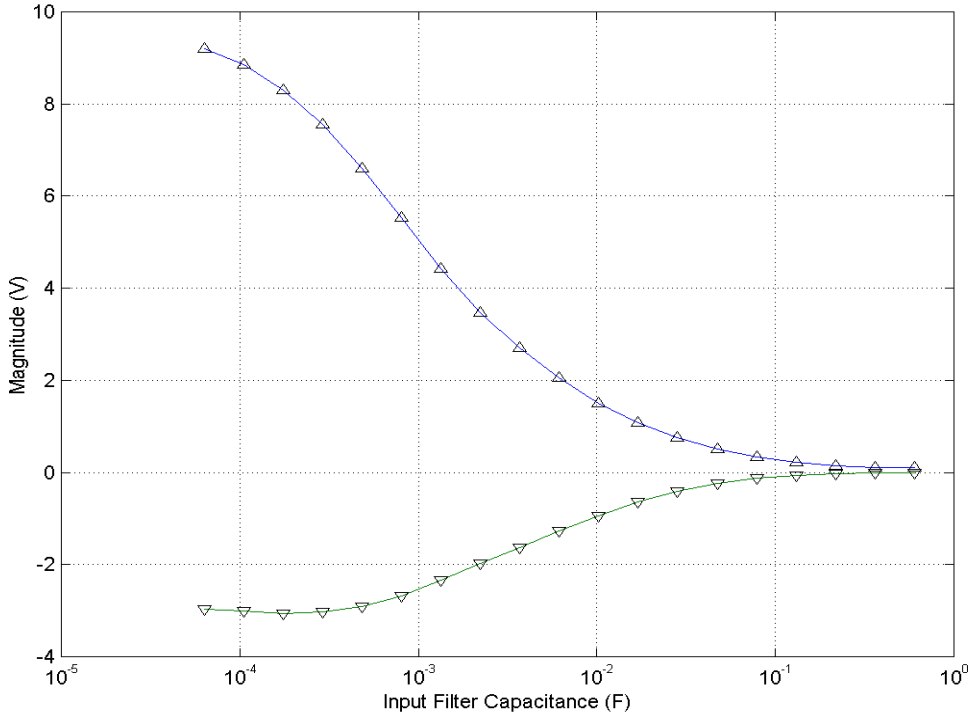

Figure 5.8 Voltage spikes magnitude vs. input filter capacitance.

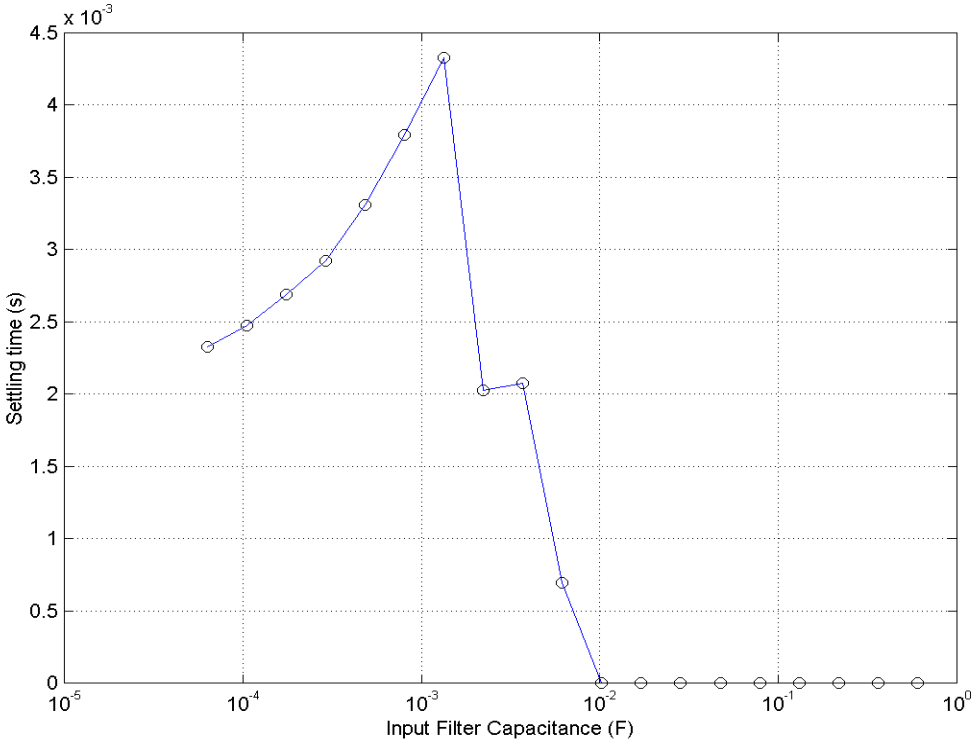

Figure 5.9 Settling time of the transients vs. input filter capacitance.

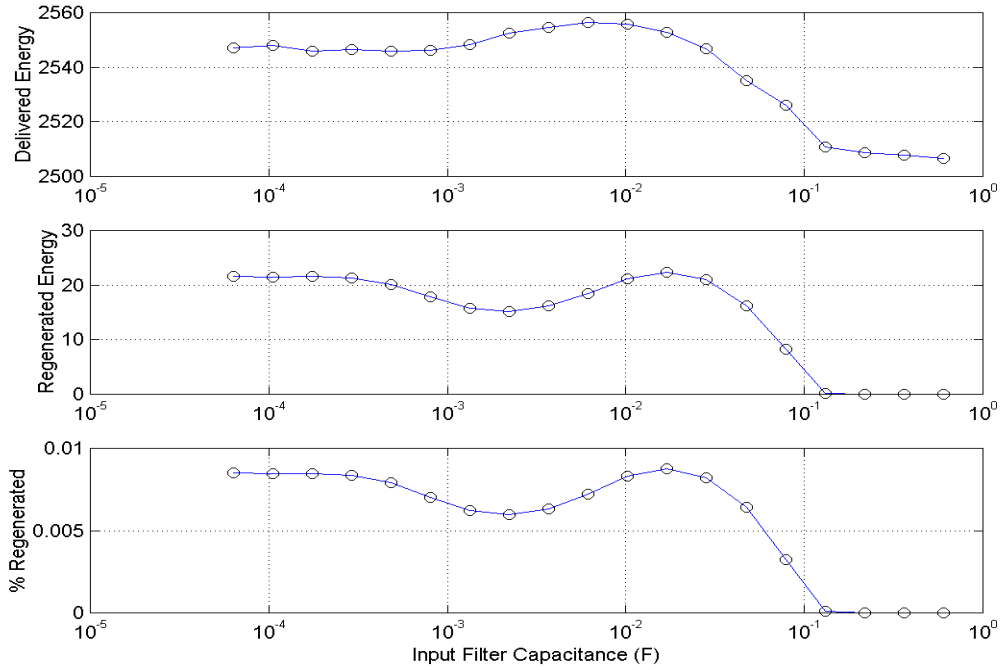

Figure 5.10 Total energy delivered from the engine and regenerated back (J) in the system without the wind load.

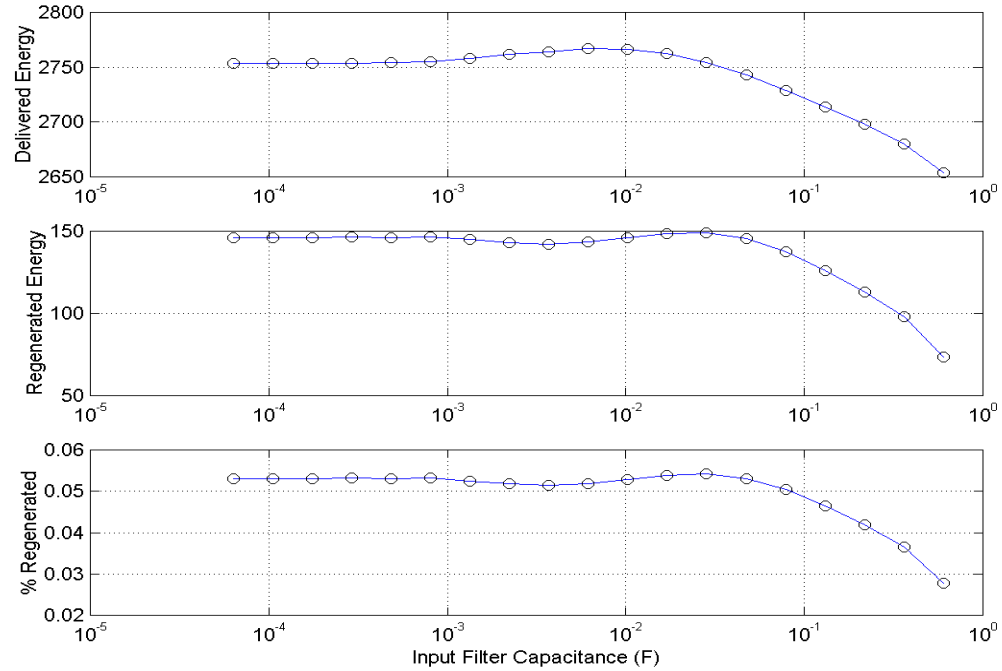

Figure 5.11 Total energy delivered from the engine and regenerated back (J) in the system with the wind load.

load. In the case with the wind load, the amount of regenerative energy is much higher as seen from Figure 5.11. This energy cannot be fully absorbed by the capacitor; however, its amount is reduced significantly. The air flow driving the actuator surface contributes significant amount of regenerative energy to the system. The figures show that the percentage of regenerative energy in the system operating with the wind load is six times higher than in the system operating without the wind load, where regenerative energy is contributed only by moving masses.

Figure 5.12 shows energy balance for subsystems. For the generator, the boost rectifier, the input filter, and the actuator the energy balance represents losses in the respective subsystem. It is seen that for the generator, the boost rectifier, and the input filter the losses tend to decrease at large capacitance values for operation both with and without the wind load. This phenomenon contributes to reduction of the total energy consumed by the system as was shown previously. The actuator losses are not significantly affected by the capacitance value. Although the DC bus voltage transients are affected by the input filter capacitance, the actuator's feedback control makes its operation unaffected by the bus voltage variations. It is seen that losses in the generator, the boost rectifier, the input filter, and the actuator are noticeably higher in case with the wind load, because the extra energy processed by these subsystems is accompanied by extra losses.

The resistive load is considered a payload; its energy balance decreases due to the decrease in the bus voltage rms value when the transients become smaller at large capacitance values. The air flow energy balance represents the net energy passed to the air by the actuator flight control surface. This amount is equal to zero for operation without the wind load. When the system operates with the wind load, this amount is very small and independent of the input filter capacitance.

A special consideration was given to the generator losses, which demonstrate an increase in the middle of the capacitance range. Figure 5.13 shows the losses that constitute the total generator losses. Losses in the phase resistances and field winding are almost constant in the whole range of capacitance with a slight trend to decrease at large capacitance values because of a decrease in the amount of regenerative energy transferred back to the engine. However, losses

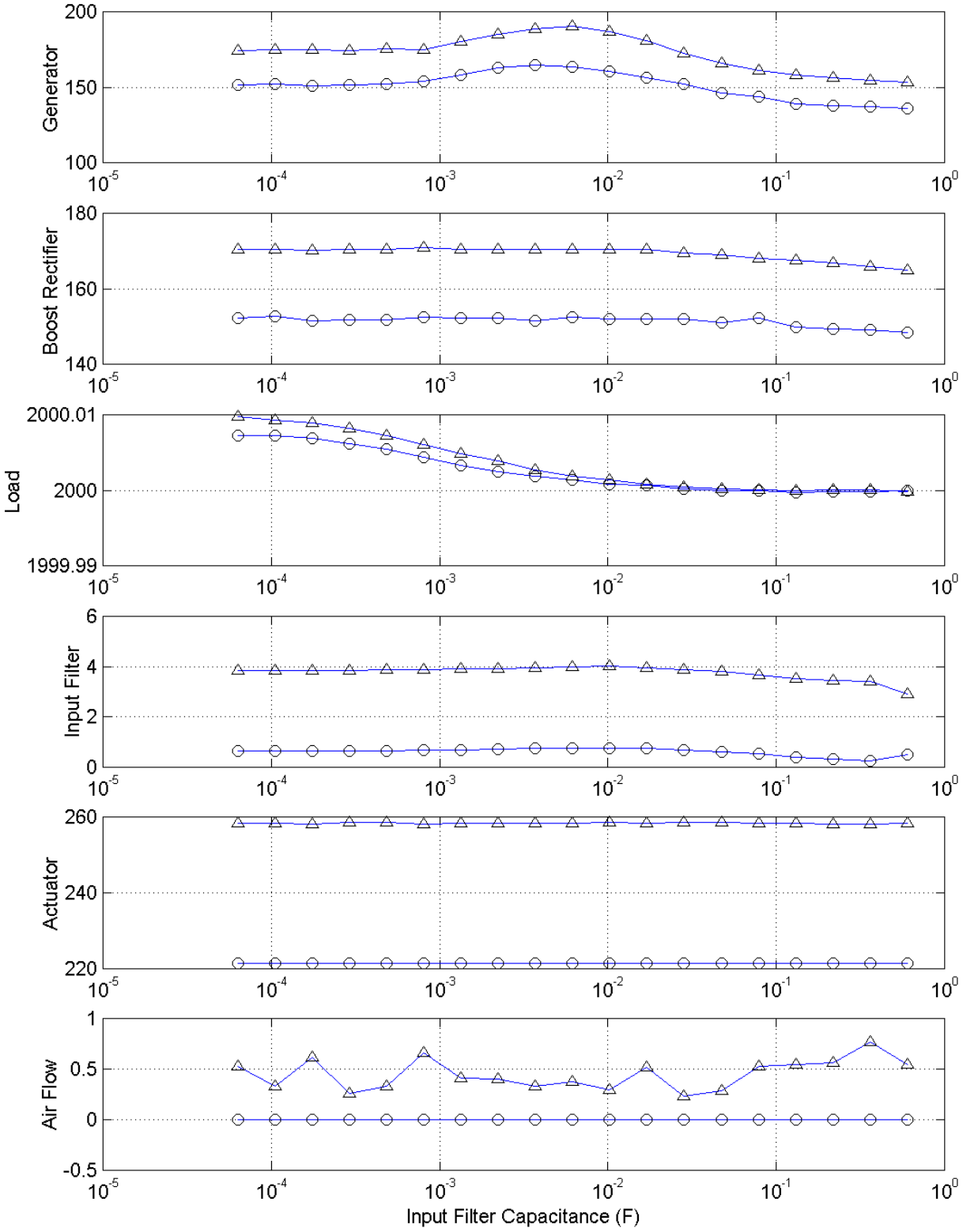

Figure 5.12 Energy balance (J) for subsystems with (Δ) and without (o) the wind load.

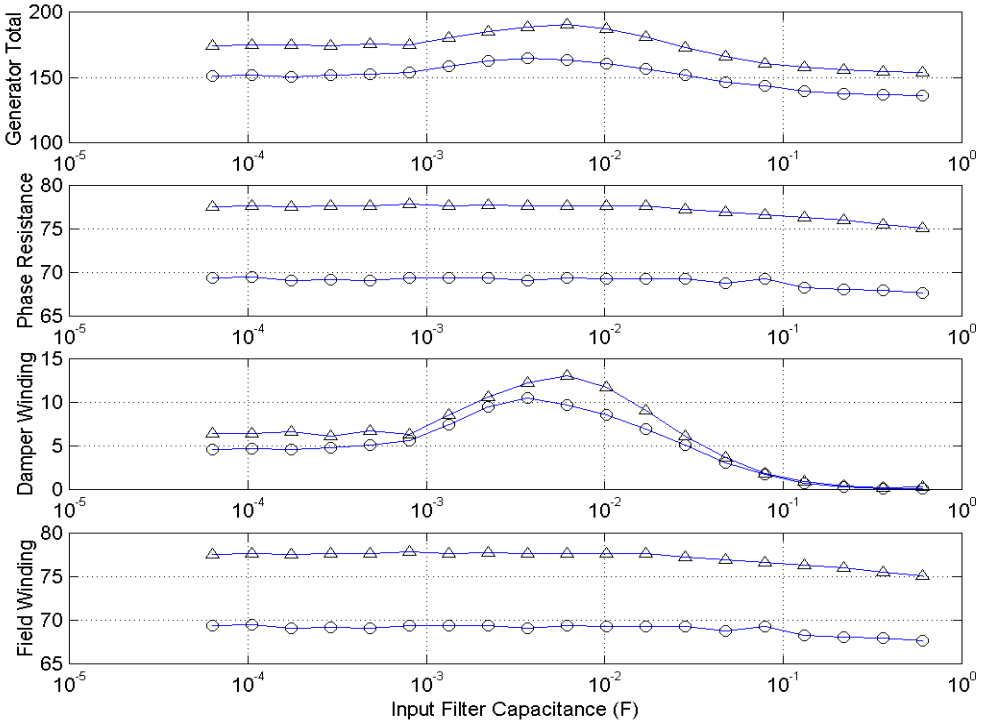

Figure 5.13 Generator losses in the system with (Δ) and without (o) the wind load.

in the damper winding experience an increase in the middle of the capacitance range. It is known that the damper winding does not carry current in steady-state operation of the generator. The purpose of the damper winding is to damp transients by dissipating their energy. For low values of the capacitance, the transients, although high in magnitude, are relatively short in duration, and do not produce much dissipation in the damper winding. For very large capacitance values, the transients become very small. It is in the middle of the capacitance range, when the transients are still relatively high and their duration is long because of the time constant increased by the large capacitance, the damper winding losses experience an increase. This phenomenon explains why the generator losses in Figure 5.12 have an increase in the middle of the range. This increase in losses produces an increase in energy drawn from the engine, as shown in Figures 5.10 and 5.11, and a corresponding decrease in the overall system efficiency.

The overall system efficiency is plotted in Figure 5.14. The variation of the efficiency as a function of the input filter capacitance is very small – within 1% of the initial value. The

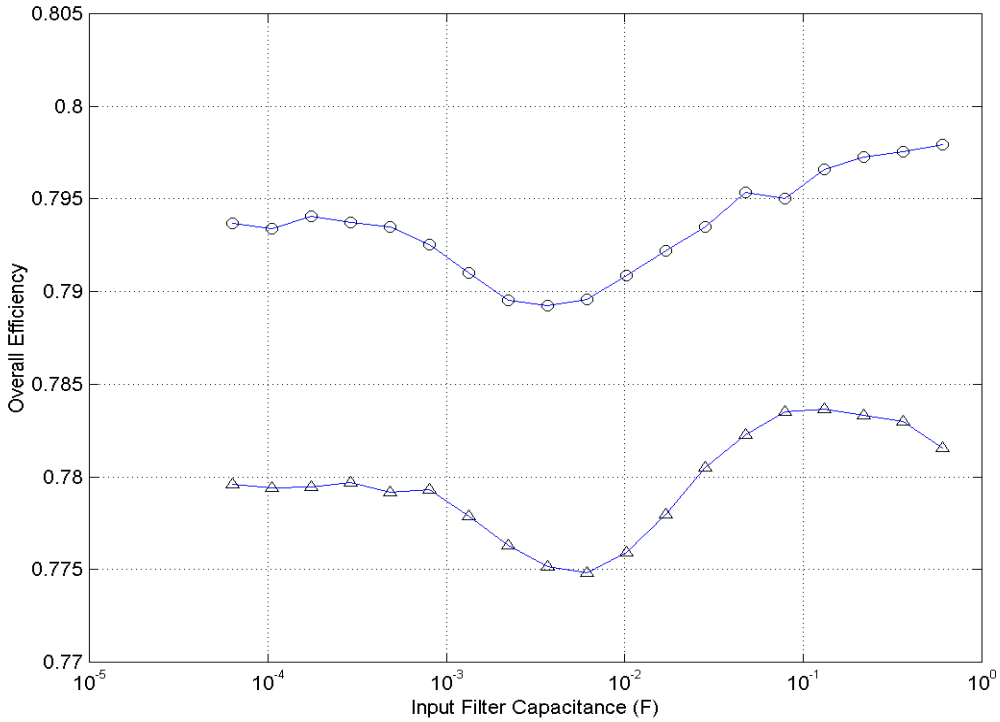

Figure 5.14 Overall efficiency of the system with (Δ) and without (o) the wind load.

increase in the generator losses produces a decrease in the efficiency for operation both with and without the wind load. At the same time, a global trend in increase of the overall efficiency at very high capacitance values can be seen, especially for operation without the wind load. Efficiency of the system operating with the wind load is approximately 1% lower than without the wind load. The results show that there is no advantage in using large capacitors in the input filter in order to improve the overall system efficiency, although the DC bus power quality can be improved.

5.5 Effect of the Boost Rectifier Capacitor on the System Characteristics under Bidirectional Power Flow Conditions

The effect of the boost rectifier capacitor on the bidirectional power flow characteristics was studied by using the parametric sweep technique, similarly to the previous case with the input filter capacitor. The results obtained were similar as well. Figures 5.15 and 5.16 show waveforms of the system operating without and with the wind load, respectively, with the boost rectifier output capacitance C_{br} increased to 350mF. Compared with waveforms of the system

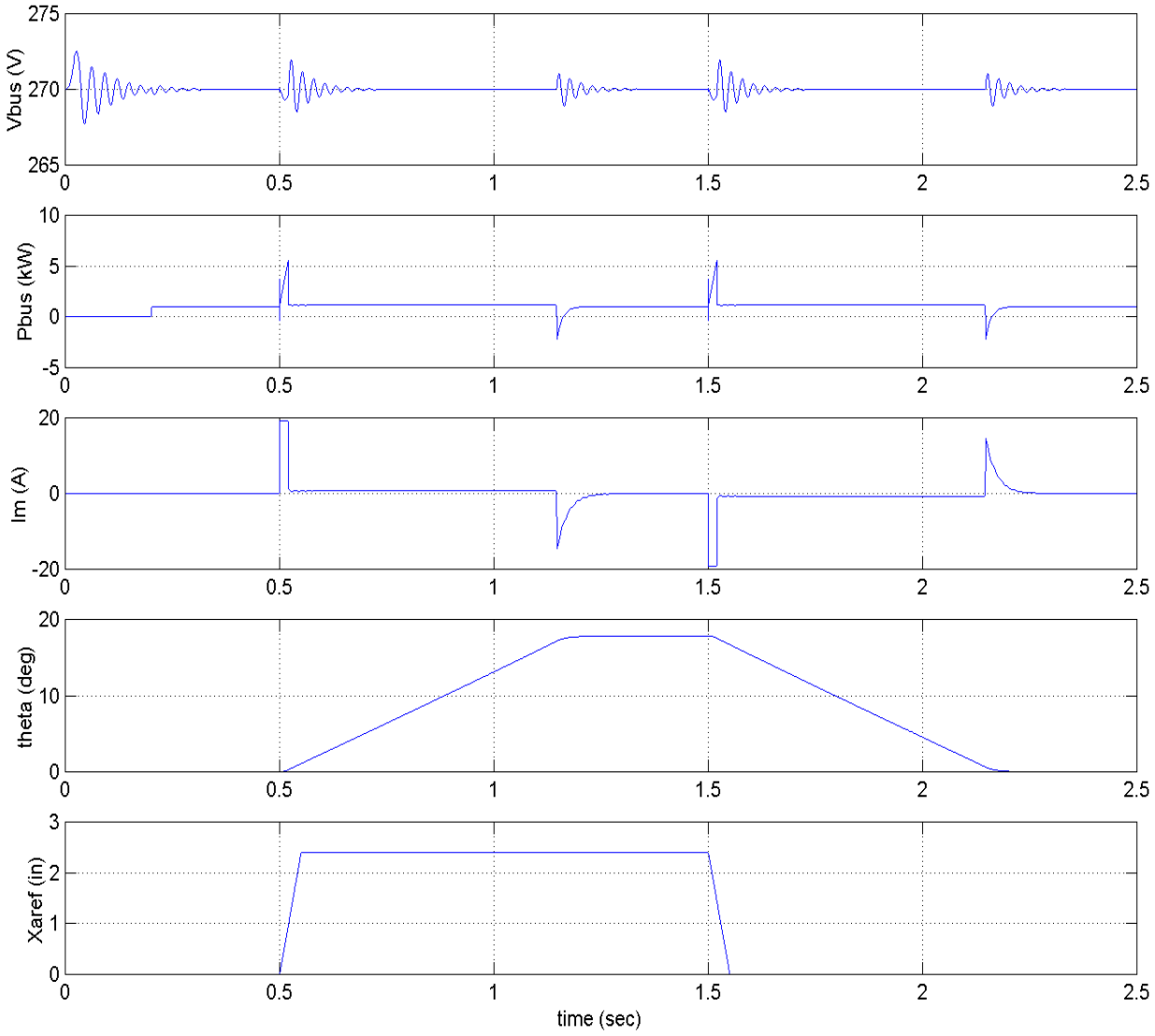

Figure 5.15 System operation without the wind load; C_{br} = 350mF.

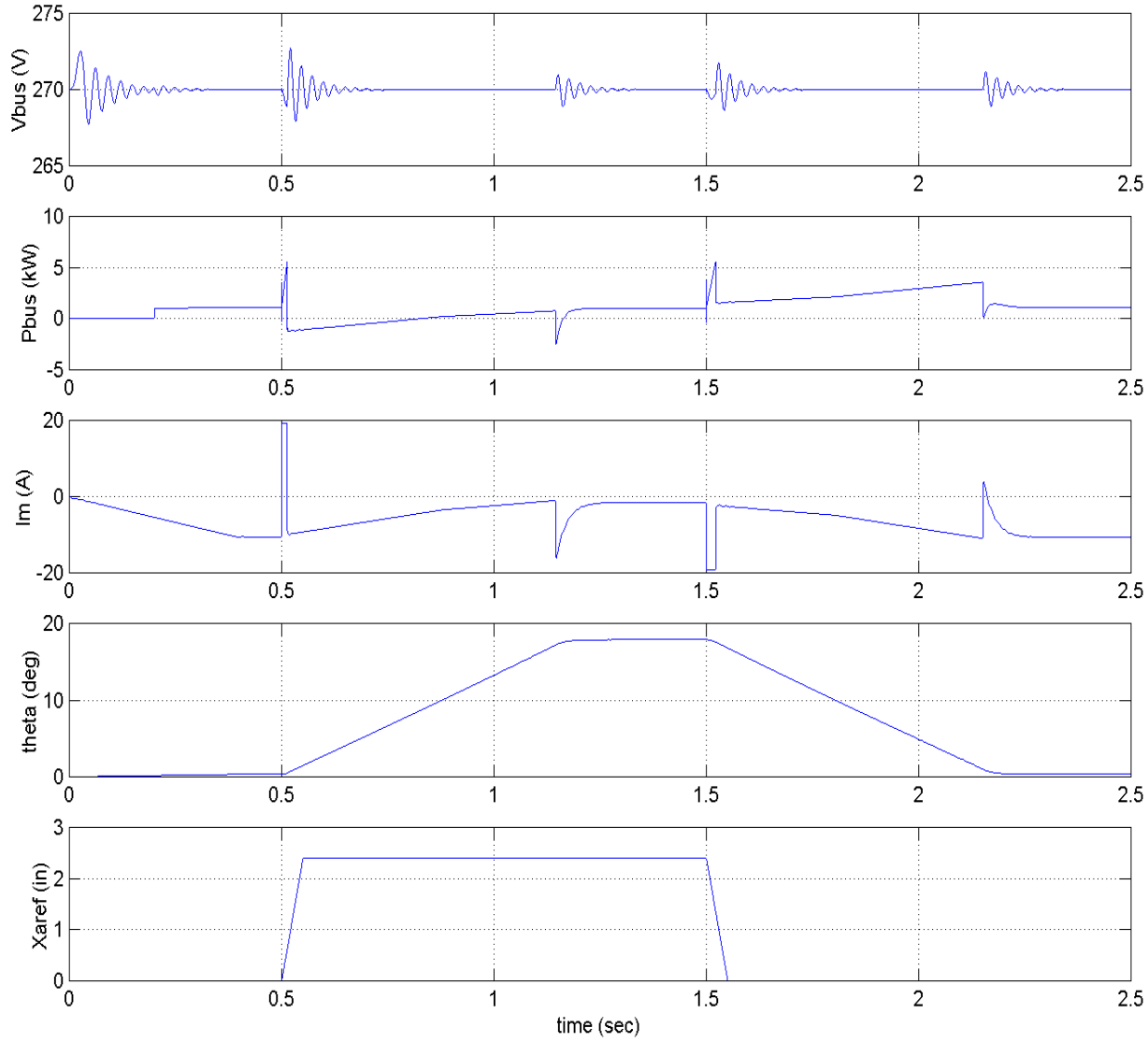

Figure 5.16 System operation with the wind load; C_{br} = 350mF.

with a nominal set of parameters (Figures 5.2 and 5.3), the results show that the DC bus voltage disturbances produced by both direct and regenerative power flow become lower in magnitude and longer in duration with the increase of the capacitance. This effect is illustrated in Figures 5.17 and 5.18, which show the voltage spikes magnitude and settling time of the transients. The figures show the same type of dependence as observed in Figures 5.8 and 5.9 for the case with variation of the input filter capacitance. It is noticeable that the magnitude curve in Figure 5.17 goes down steeper than in Figure 5.8. This is because the boost rectifier capacitor is connected directly to the bus, without an intermediate inductor as in case of the input filter capacitor.

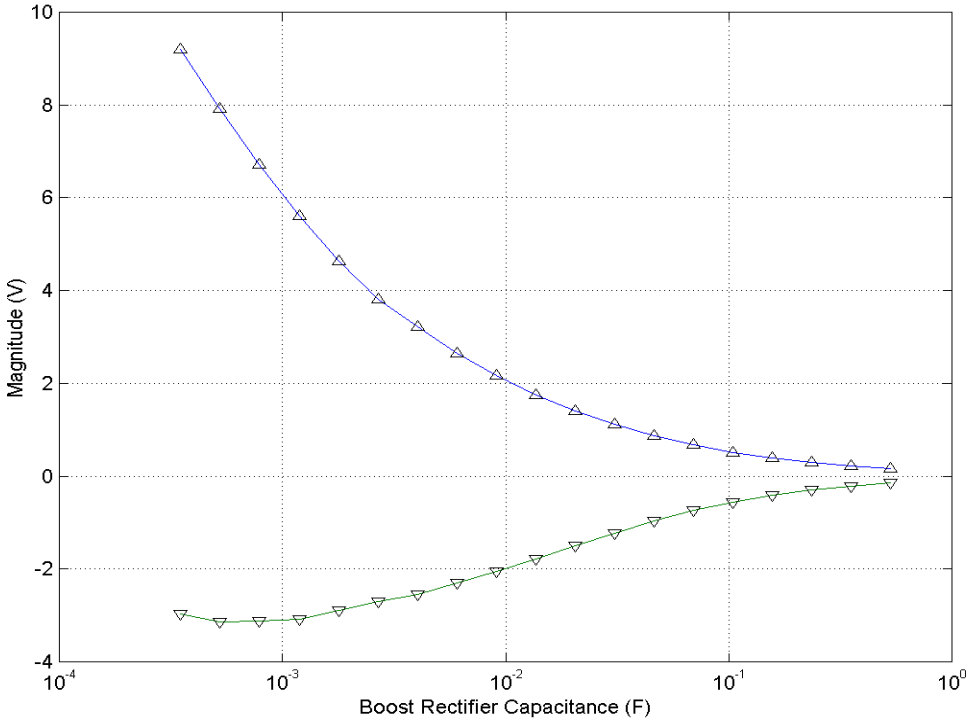

Figure 5.17 Voltage spikes magnitude vs. boost rectifier capacitance.

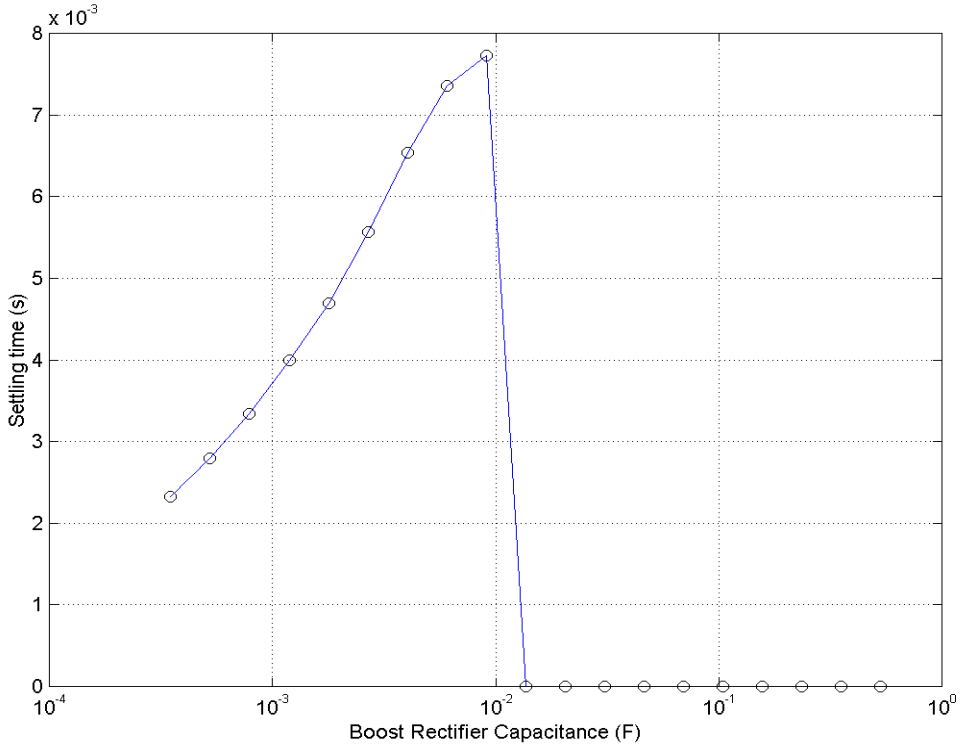

Figure 5.18 Settling time of the transients vs. boost rectifier capacitance.

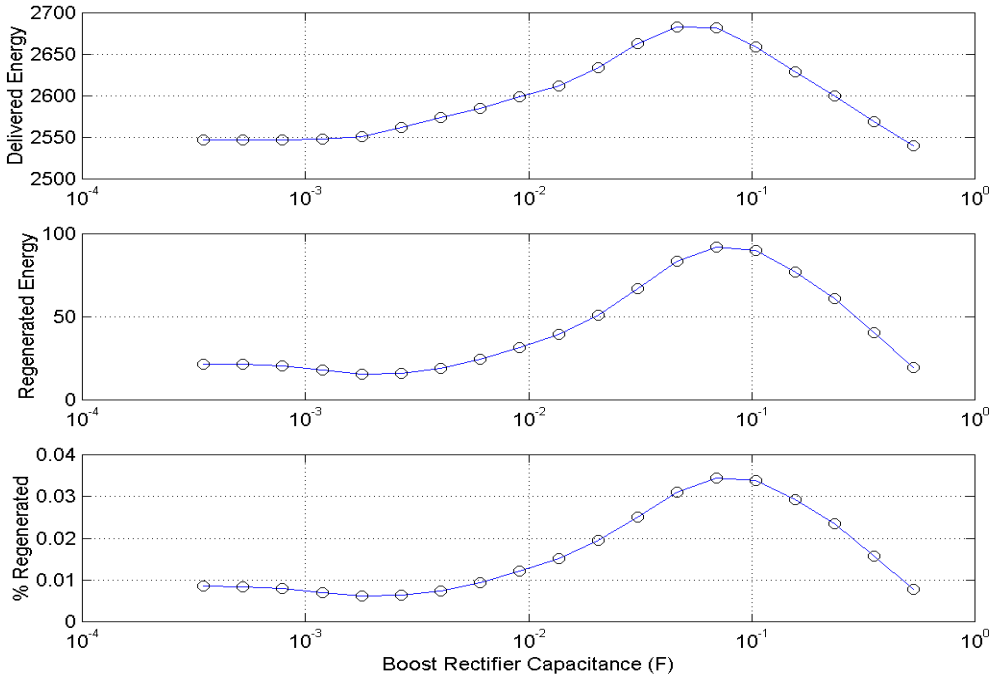

Figure 5.19 Total energy delivered from the engine and regenerated back (J) in the system without the wind load.

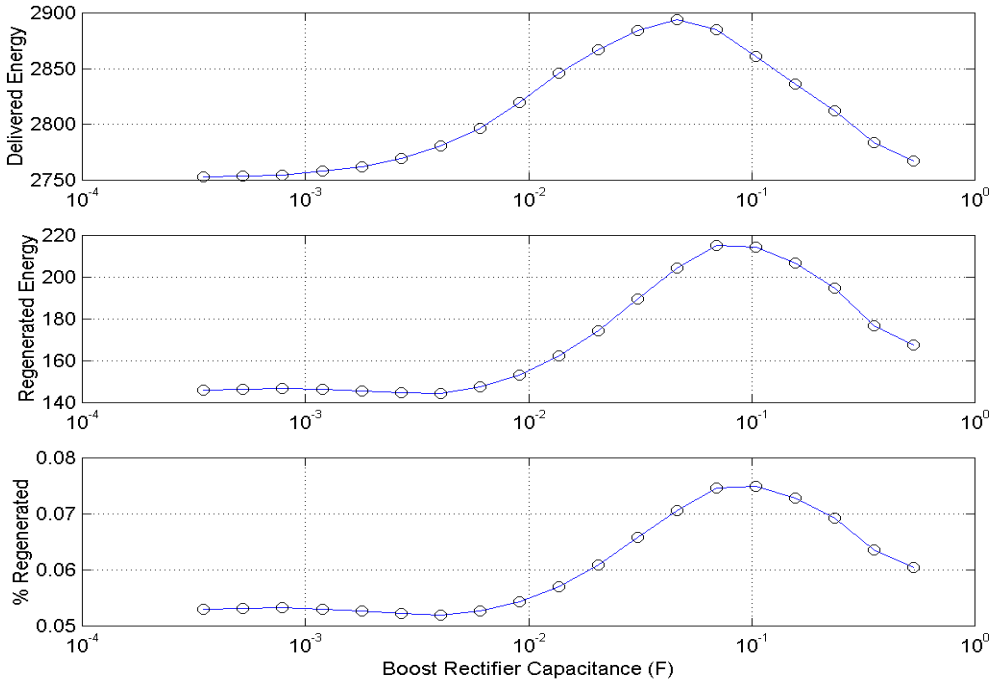

Figure 5.20 Total energy delivered from the engine and regenerated back (J) in the system with the wind load.

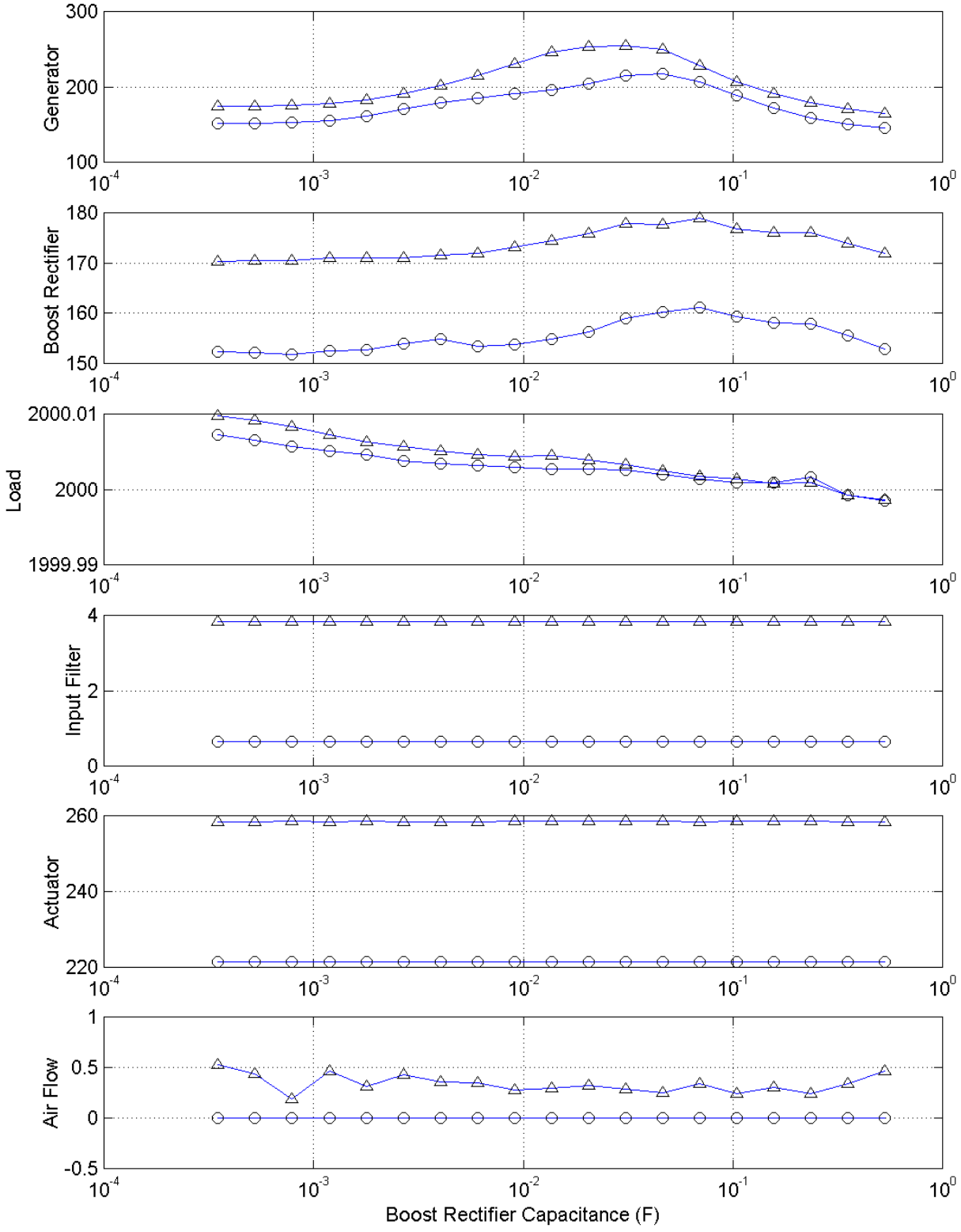

Figure 5.21 Energy balance (J) for subsystems with (Δ) and without (o) the wind load.

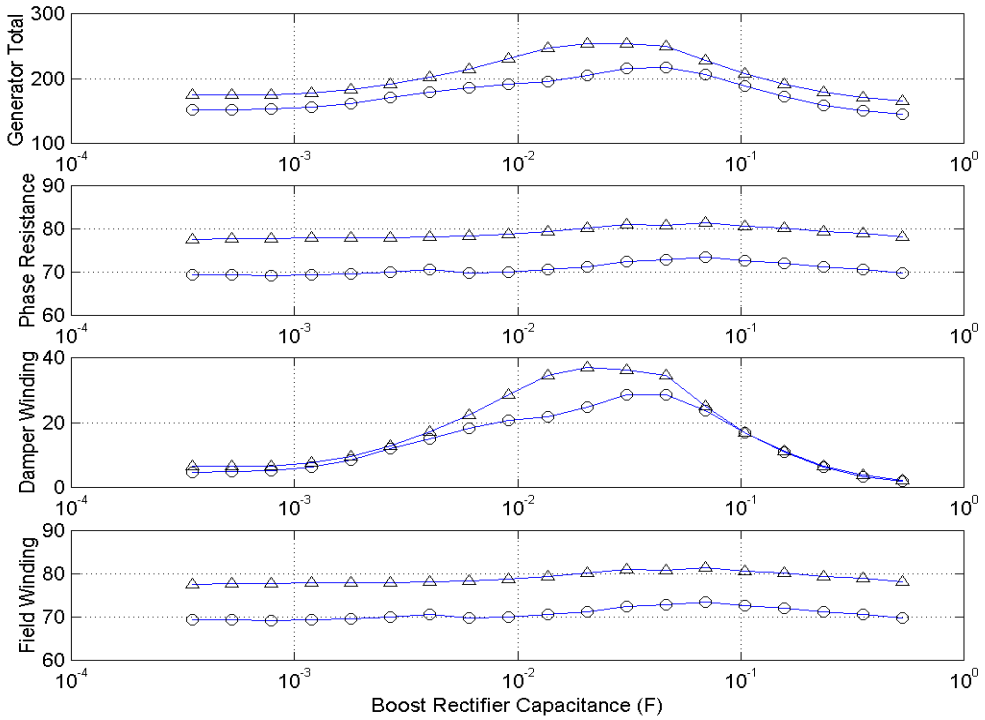

Figure 5.22 Generator losses in the system with (Δ) and without (o) the wind load.

The energy flow analysis yields the results very similar to the case with variation of the input filter capacitance. Figures 5.19 and 5.20 are similar to the corresponding Figures 5.10 and 5.11, although the rise in power consumption in the middle of the capacitance range is more prominent. It is seen from comparing Figures 5.13 and 5.22 that losses in the damper winding in the latter case rise many more times over the initial value than in the former. A comparison of Figures 5.6 and 5.7 with the corresponding Figures 5.15 and 5.16 show that the DC bus transients are more oscillatory with 350mF boost rectifier capacitor than with 63mF input filter capacitor. In the latter case, the input filter inductance with its ESR provides an additional filtering and damping action when the regenerative power flow causes transients on the DC bus. The long, poorly damped oscillations, which occur on the bus when a large boost rectifier capacitor is used, increase rms values of voltages and currents in the generator and the boost rectifier. This effect leads to increased losses in their phase resistances in addition to the increase in the damper winding losses as seen in Figures 5.21 and 5.22. As a result, the overall efficiency curves in Figure 5.23 experience a decrease in the middle of the capacitance range as much as three times larger than the corresponding curves in Figure 5.14. The drop in efficiency

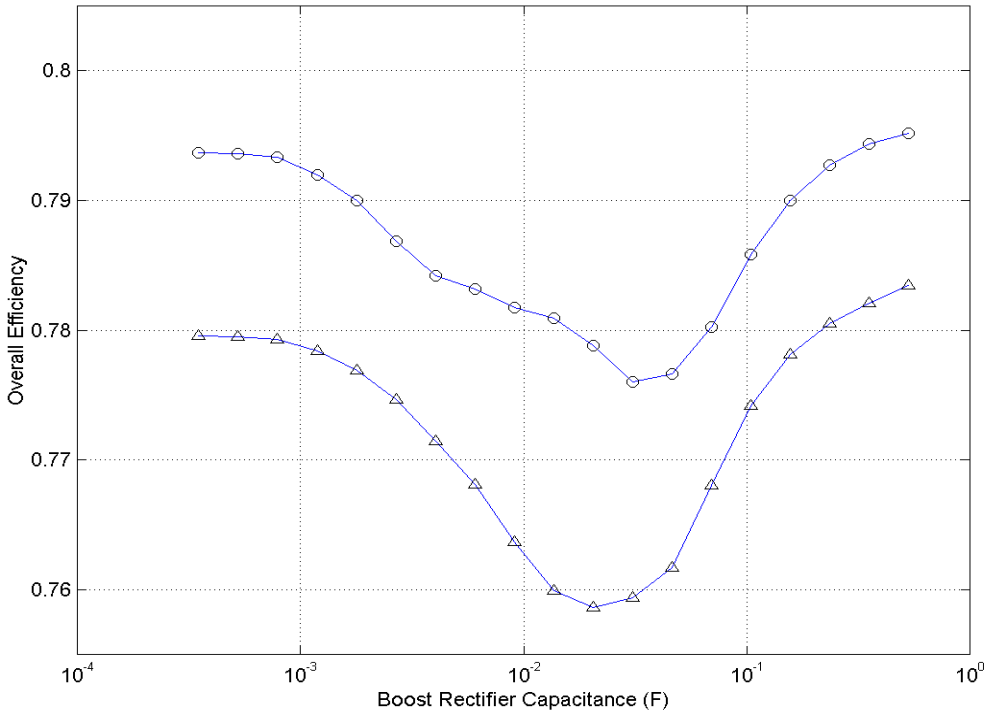

Figure 5.23 Overall efficiency of the system with (Δ) and without (o) the wind load.

is up to 1.5% in case with the wind load, and it is barely recovered with using of very large capacitance values at the end of the range.

The results of bidirectional power flow analysis showed that large capacitors in the input filter and the boost rectifier can be effectively used to reduce the magnitude of voltage spikes on the DC bus. At the same time, the large capacitors do not provide any advantage in utilizing the regenerative power flow in the system. In fact, the overall system efficiency reduces insignificantly when the capacitance values are increased up to two orders of magnitude against their initial values. This is especially noticeable in case of using a large boost rectifier capacitor, which creates long, poorly damped, low-frequency oscillations on the bus. For this reason, it is better to use a larger input filter capacitor than the boost rectifier capacitor in order to reduce the magnitude of voltage spikes on the DC bus.

Chapter 6

Conclusions

This work presents modeling and analysis of a typical DC power distribution system in a 21st century transport aircraft using a set of modeling and simulation tools developed in this research. MATLAB/Simulink was chosen as a software platform. The multi-level modeling concept was used as a modeling approach, which assumes building models of different levels of complexity for each subsystem within the PDS. Three types of models were built: a detailed model, a behavioral model, and a reduced order model. The subsystem models, implemented in Simulink, were combined into the whole PDS model following certain interconnection rules. Subsystem models of different levels were mixed for modeling of different scenarios of operation. Linearization techniques provided by MATLAB were used to obtain linearized models of nonlinear systems for stability analysis and control design. The subsystems modeled in this research included a three-phase synchronous generator, a three-phase boost rectifier, a switched-reluctance starter/generator, DC-DC converters, electromechanical and electrohydrostatic actuators, and different types of the DC bus loads.

The modeling tools were used to investigate different stability issues in the PDS. Dynamic properties of the boost rectifier were studied and then used for analysis of interactions between the boost rectifier and different types of loads. It was found that presence of a constant power load on the DC bus may cause instability in the system. This instability results in oscillations of the DC bus voltage and current, which exceed the allowable limits set by MIL-STD-704E. The DC bus stability diagram was proposed as a convenient tool for predicting stability of the PDS with different types of loads without performing an actual stability test based

on regular stability analysis tools. It was shown that a potential for instability in the PDS exists under both direct and regenerative power flow conditions.

A detailed stability analysis of the PDS with an electromechanical actuator was performed. The actuator's operating cycle was analyzed in order to identify the parts of the cycle with a potential for instability. It was found that the most prone to instability parts of the cycle are those where the EMA draws the maximum power from the DC bus. At these moments, unstable interactions between the EMA input filter and the converter may develop. It was shown that this instability can be eliminated by choosing an appropriate input filter design. The analysis demonstrated that the converter of the EMA operates as a constant power load with negative small-signal input resistance in the motoring mode and as a constant power source with positive small-signal input resistance in the regenerative mode. There is no potential for unstable interactions between the converter and the input filter of the EMA in the regenerative mode of operation.

The EMA converter input impedance as it appears on the DC bus is modified by the input filter, which may lead to unstable interactions between the EMA and the boost rectifier. The analysis showed that there is no instability between the boost rectifier and the EMA with small DC bus loads even when there are unstable interactions within the EMA. However, there is a potential for instability caused by the EMA when there are large loads on the bus, as follows from the DC bus stability diagram.

The PDS model developed in this research was used to study the effects of bidirectional power flow in the PDS, produced by regenerative action of flight actuators, on the DC bus power quality characteristics and energy efficiency of the PDS. The regenerative energy returned to the bus creates voltage disturbances, which may be beyond the allowable limits. The effect of using large energy storage capacitors located in the boost rectifier and the EMA on the voltage disturbances was investigated. It was found that increased values of these capacitors can significantly reduce voltage disturbances on the DC bus. A large input filter capacitor in the EMA was found more suitable for this purpose because a large boost rectifier output capacitor showed a tendency to create poorly damped low-frequency oscillations on the bus.

The analysis showed that large capacitors do not provide any energy savings in the PDS. The overall efficiency of the system remains nearly at the original level when very large capacitors are used. It even decreases up to 2% at intermediate capacitance values due to increased losses in the system produced by the DC bus transients. This effect is more prominent when using a large boost rectifier capacitor. Based on the analysis results, the following observations can be made:

- distribution of losses in the system is frequency-dependent and determined by all dynamic (filtering) components;
- additional capacitors at different places of the system not only redirect the transient energy flow, but also change the spectral characteristics of the disturbance.

As a result, the system efficiency should be determined and the system optimization should be performed taking into account its transient performance, not only the static operating conditions.

The examples of analysis presented in this thesis show that the modeling and simulation tools developed in this research can be effectively used to study different aspects of the DC power distribution system including stability, transient response, and energy transfer issues. The concepts used in this research are versatile enough and can be used for building similar analysis tools for complex systems with closely interacting subsystems.

Appendix A

Parameters of the DC Power Distribution System Components

Table A.1 Synchronous generator parameters.

Parameter	Symbol	Unit	Nominal value
Armature phase resistance	R_s	Ohm	0.09113
Rotor speed	ω	rad/s	376.99
Armature phase leakage inductance	L_{ls}	H	0.9e-3
D axis coupling inductance	L_{md}	H	43e-3
Q axis coupling inductance	L_{mq}	H	21e-3
Field winding resistance (reflected to stator)	R_{fd}	Ohm	0.018
Field winding leakage inductance (refl. to stator)	L_{lfd}	H	3.4e-3
D axis damper winding resistance (refl. to stator)	R_{kd}	Ohm	0.08
Q axis damper winding resistance (refl. to stator)	R_{kq}	Ohm	0.08
D axis damper winding leakage inductance (reflected to stator)	L_{lkd}	H	0.16e-3
Q axis damper winding leakage inductance (reflected to stator)	L_{lkq}	H	0.35e-3
Additional resistance	R_a	Ohm	1e5
Field voltage (reflected to stator)	v_{fd}	V	1

Table A.2 Three-phase boost rectifier parameters.

Parameter	**Symbol**	**Unit**	**Nominal value**
One-phase inductance	L	H	18e-6
Output capacitance	C	F	350e-6
Output capacitor ESR	R_c	Ohm	0.01
Current feedback loops gain	K_{dq}	–	0.0126
Voltage loop proportional gain	K_{vp}	–	1
Voltage loop integral gain	K_{vi}	–	3300
Output voltage reference	$v_{o(ref)}$	V	270

Table A.3 DC bus cable parameters.

Parameter	**Symbol**	**Unit**	**Nominal value**
Resistance per foot	R	Ohm/ft	1.13e-3
Inductance per foot	L	H/ft	1e-9
Capacitance per foot	C	F/ft	1e-12
Capacitance ESR per foot	R_C	Ohm/ft	negligible
Cable length for Inboard Spoilers (EMA)	L_{EMA}	ft	10
Cable length for Elevators (EHA)	L_{EHA}	ft	40

Table A.4 EMA input filter parameters.

Parameter	**Symbol**	**Unit**	**Nominal value**
Inductance	L_i	H	1e-5
Inductor ESR	R_{li}	Ohm	0.1
Capacitance	C_i	F	1e-3
Capacitor ESR	R_{ci}	Ohm	0.01

Table A.5 DC motor parameters.

Parameter	**Symbol**	**Unit**	**Nominal value**
Armature inductance	L	H	4.5e-4
Armature resistance	R	Ohm	0.5
Back emf constant	K_e	V/(rad/s)	0.129
Torque constant	K_t	in-lb/A	1.141
Motor group inertia	J_m	in-lb-s^2	2.43e-4
Motor group damping	B_m	in-lb-s	3.125e-4

Table A.6 Actuator mechanical linkage parameters.

Parameter	Symbol	Unit	Nominal value
Motor to Actuator gear ratio	N	rad/in	249.6π
Actuator stiffness	K_{act}	lbf/in	9.0e5
Piston mass	M_p	lbf-s^2/in	5.43e-3
Piston damping	B_p	lbf-s/in	15
Surface load inertia	J_{sur}	in-lb-s^2	36.2
Surface load damping	B_{sur}	in-lb-s	1702
Horn radius	h	in	4.9
Horn stiffness	K_l	in-lb/rad	1.0e6
Structure stiffness	K_r	in-lb/rad	5.0e5
Gear efficiency	N_{mech}	–	0.85

Table A.7 EMA feedback controller parameters.

Parameter	Symbol	Unit	Nominal value
Motor current limit	–	A	19.3
Position forward gain	K_p	V/V	76
Velocity command limit	W_{lim}	V	+/–6.8
Velocity forward gain	K_v	V/V	122.5
Position feedback gain	H_p	V/in	1.6
Velocity feedback gain	H_v	V/(rad/s)	3.82e-3
Current feedback gain	H_i	V/A	0.25
Current forward gain	K_i	V/A	30

Appendix B

MATLAB Function for DQ-to-ABC Transformation

```
function [abc] = dq2abc(dq,w,t)
%DQ2ABC  DQ-to-ABC transformation.
%   [ABC] = DQ2ABC(DQ,W,T)  performs DQ-to-ABC transformation for
%     a balanced three-phase system as follows:
%
%               [cos wt          -sin wt        ]
%       [ABC] = [cos (wt-2pi/3)  -sin (wt-2pi/3)] [DQ],
%               [cos (wt+2pi/3)  -sin (wt+2pi/3)]
%
%     where T - time vector, W - angular frequency,
%     DQ - two-column matrix of a variable values in DQ coordinates,
%     ABC - three-column matrix of corresponding values in ABC
%     coordinates. The number of rows of DQ and ABC must be equal to
%     LENGTH(X).
%
%   See also ABC2DQ.

%   K.P. Louganski 1-05-98
%   VPEC, Virginia Tech

error(nargchk(3,3,nargin));

wt=w*t;
phi=2*pi/3;

abc(:,1)= dq(:,1).*cos(wt)-dq(:,2).*sin(wt);
abc(:,2)= dq(:,1).*cos(wt-phi)-dq(:,2).*sin(wt-phi);
abc(:,3)= dq(:,1).*cos(wt+phi)-dq(:,2).*sin(wt+phi);
```

This function was developed for conversion of simulation results produced in *dq* coordinates into three-phase *abc* coordinates. It may be used with variable-step integration routines. The time vector *t* must be saved during the simulation along with the two-column matrix of the time history of the variable of interest in *dq* coordinates. After the simulation, an

auxiliary equally spaced vector *x* spanning the range of *t* is created. The vector *x* should have a sufficient number of elements in order to accommodate the most rapid changes of the *abc* components. The two-column *dq* matrix is then converted into a three-column *abc* matrix by applying the "dq2abc" function to the *dq* values interpolated along *x*. An example below illustrates usage of the function for plotting *dq* simulation results in *abc* reference frame.

```
%  t    – time vector obtained from simulation,
%  V_dq – two-column matrix of a variable in DQ coordinates

x=[0:0.001*max(t):max(t)]';
figure
V_abc=dq2abc(interp1(t,V_dq,x),w,x);
plot(x,V_abc)
```

Appendix C

State-Space Model for a Synchronous Generator

In order to present the generator equations (3.11) in the standard state-space form, it is necessary to solve them for the state derivatives and collect the input and state variables into matrices. The five equations of (3.11) containing the state derivatives may be represented as follows:

$$\begin{bmatrix} a_{11} & 0 & a_{13} & 0 & a_{15} \\ 0 & a_{22} & 0 & a_{24} & 0 \\ a_{31} & 0 & a_{33} & 0 & a_{35} \\ a_{41} & 0 & a_{43} & 0 & a_{45} \\ 0 & a_{52} & 0 & a_{54} & 0 \end{bmatrix} \begin{bmatrix} x_1 \\ x_2 \\ x_3 \\ x_4 \\ x_5 \end{bmatrix} = \begin{bmatrix} b_1 \\ b_2 \\ b_3 \\ b_4 \\ b_5 \end{bmatrix}, \qquad \text{(C.1)}$$

where the auxiliary variables are

$$x_1 = \frac{di_{sd}}{dt} \qquad a_{11} = -(L_{ls} + L_{md})$$

$$a_{13} = L_{md}$$

$$x_2 = \frac{di_{sq}}{dt} \qquad a_{15} = L_{md}$$

$$b_1 = -R_a i_d + (R_a + R_s) i_{sd} - \omega(L_{ls} + L_{mq}) i_{sq} + \omega L_{mq} i_{kq}$$

$$x_3 = \frac{di_{kd}}{dt}$$

$$x_4 = \frac{di_{kq}}{dt} \qquad a_{22} = -(L_{ls} + L_{mq})$$

$$a_{24} = L_{mq}$$

$$x_5 = \frac{di_{fd}}{dt} \qquad b_2 = -R_a i_q + (R_a + R_s) i_{sq} + \omega(L_{ls} + L_{md}) i_{sd} - \omega L_{md} i_{fd} - \omega L_{md} i_{kd}$$

$$a_{31} = -L_{md} \qquad a_{41} = -L_{md} \qquad a_{52} = -L_{mq}$$
$$a_{33} = L_{md} \qquad a_{43} = L_{lkd} + L_{md} \qquad a_{54} = L_{lkq} + L_{mq}$$
$$a_{35} = L_{lfd} + L_{md} \qquad a_{45} = L_{md} \qquad b_5 = -R_{kq} i_{kq}$$
$$b_3 = v_{fd} - R_{fd} i_{fd} \qquad b_4 = -R_{kd} i_{kd}$$

Solving the equation (C.1) symbolically in terms of the circuit parameters would be too cumbersome, and it is unnecessary because the parameters do not change during simulation. The solution is obtained by inverting the matrix of coefficients numerically:

$$X = A^{-1} \cdot B, \tag{C.2}$$

where

$$X = \begin{bmatrix} x_1 \\ x_2 \\ x_3 \\ x_4 \\ x_5 \end{bmatrix}, \qquad A = \begin{bmatrix} a_{11} & 0 & a_{13} & 0 & a_{15} \\ 0 & a_{22} & 0 & a_{24} & 0 \\ a_{31} & 0 & a_{33} & 0 & a_{35} \\ a_{41} & 0 & a_{43} & 0 & a_{45} \\ 0 & a_{52} & 0 & a_{54} & 0 \end{bmatrix}, \qquad B = \begin{bmatrix} b_1 \\ b_2 \\ b_3 \\ b_4 \\ b_5 \end{bmatrix}.$$

It can be seen that

$$\begin{bmatrix} b_1 \\ b_2 \\ b_3 \\ b_4 \\ b_5 \end{bmatrix} = \begin{bmatrix} R_a + R_s \\ \omega(L_{ls} + L_{md}) \\ 0 \\ 0 \\ 0 \end{bmatrix} \cdot i_{sd} + \begin{bmatrix} -\omega(L_{ls} + L_{mq}) \\ R_a + R_s \\ 0 \\ 0 \\ 0 \end{bmatrix} \cdot i_{sq} + \begin{bmatrix} 0 \\ -\omega L_{mq} \\ 0 \\ -R_{kd} \\ 0 \end{bmatrix} \cdot i_{kd} + \begin{bmatrix} \omega L_{mq} \\ 0 \\ 0 \\ 0 \\ -R_{kq} \end{bmatrix} \cdot i_{kq} + \begin{bmatrix} 0 \\ -\omega L_{md} \\ -R_{fd} \\ 0 \\ 0 \end{bmatrix} \cdot i_{fd} +$$
$$\begin{bmatrix} -R_a \\ 0 \\ 0 \\ 0 \\ 0 \end{bmatrix} \cdot i_d + \begin{bmatrix} 0 \\ -R_a \\ 0 \\ 0 \\ 0 \end{bmatrix} \cdot i_q + \begin{bmatrix} 0 \\ 0 \\ 1 \\ 0 \\ 0 \end{bmatrix} \cdot v_{fd} = B_1 \cdot \begin{bmatrix} i_{sd} \\ i_{sq} \\ i_{kd} \\ i_{kq} \\ i_{fd} \end{bmatrix} + B_2 \cdot \begin{bmatrix} i_d \\ i_q \\ v_{fd} \end{bmatrix}, \tag{C.3}$$

where

$$B_1 = \begin{bmatrix} b_{11} & b_{12} & 0 & b_{14} & 0 \\ b_{21} & b_{22} & b_{23} & 0 & b_{25} \\ 0 & 0 & 0 & 0 & b_{35} \\ 0 & 0 & b_{43} & 0 & 0 \\ 0 & 0 & 0 & b_{54} & 0 \end{bmatrix}, \qquad B_2 = \begin{bmatrix} b_{16} & 0 & 0 \\ 0 & b_{27} & 0 \\ 0 & 0 & b_{38} \\ 0 & 0 & 0 \\ 0 & 0 & 0 \end{bmatrix},$$

$$\begin{aligned} b_{11} &= b_{22} = R_a + R_s \\ b_{21} &= \omega(L_{ls} + L_{md}) \\ b_{12} &= -\omega(L_{ls} + L_{mq}) \\ b_{23} &= -\omega L_{mq} \\ b_{43} &= -R_{kd} \\ b_{14} &= \omega L_{mq} \\ b_{54} &= -R_{kq} \\ b_{16} &= b_{27} = -R_a \\ b_{38} &= 1. \end{aligned}$$

From equations (C.2) and (C.3) it is seen that

$$\frac{d}{dt}\begin{bmatrix} i_{sd} \\ i_{sq} \\ i_{kd} \\ i_{kq} \\ i_{fd} \end{bmatrix} = A^{-1} \cdot B_1 \cdot \begin{bmatrix} i_{sd} \\ i_{sq} \\ i_{kd} \\ i_{kq} \\ i_{fd} \end{bmatrix} + A^{-1} \cdot B_2 \cdot \begin{bmatrix} i_d \\ i_q \\ v_{fd} \end{bmatrix} = A_g \cdot \begin{bmatrix} i_{sd} \\ i_{sq} \\ i_{kd} \\ i_{kq} \\ i_{fd} \end{bmatrix} + B_g \cdot \begin{bmatrix} i_d \\ i_q \\ v_{fd} \end{bmatrix}, \qquad \text{(C.4)}$$

which is the state equation of the model. The output equation is obtained from the two equations of (3.11) containing the output variables. The state variables are obtained as well by adding them to the vector of output variables.

$$\begin{bmatrix} v_d \\ v_q \\ i_{sd} \\ i_{sq} \\ i_{kd} \\ i_{kq} \\ i_{fd} \end{bmatrix} = \begin{bmatrix} R_a & 0 & 0 & 0 & 0 \\ 0 & R_a & 0 & 0 & 0 \\ 1 & 0 & 0 & 0 & 0 \\ 0 & 1 & 0 & 0 & 0 \\ 0 & 0 & 1 & 0 & 0 \\ 0 & 0 & 0 & 1 & 0 \\ 0 & 0 & 0 & 0 & 1 \end{bmatrix} \begin{bmatrix} i_{sd} \\ i_{sq} \\ i_{kd} \\ i_{kq} \\ i_{fd} \end{bmatrix} + \begin{bmatrix} -R_a & 0 & 0 \\ 0 & -R_a & 0 \\ 0 & 0 & 0 \\ 0 & 0 & 0 \\ 0 & 0 & 0 \\ 0 & 0 & 0 \\ 0 & 0 & 0 \end{bmatrix} \begin{bmatrix} i_d \\ i_q \\ v_{fd} \end{bmatrix} = C_g \begin{bmatrix} i_{sd} \\ i_{sq} \\ i_{kd} \\ i_{kq} \\ i_{fd} \end{bmatrix} + D_g \begin{bmatrix} i_d \\ i_q \\ v_{fd} \end{bmatrix}$$

Appendix D

MATLAB Code for Stability Analysis of the DC Power Distribution System

D.1 Simulink Models for Stability Analysis of the PDS

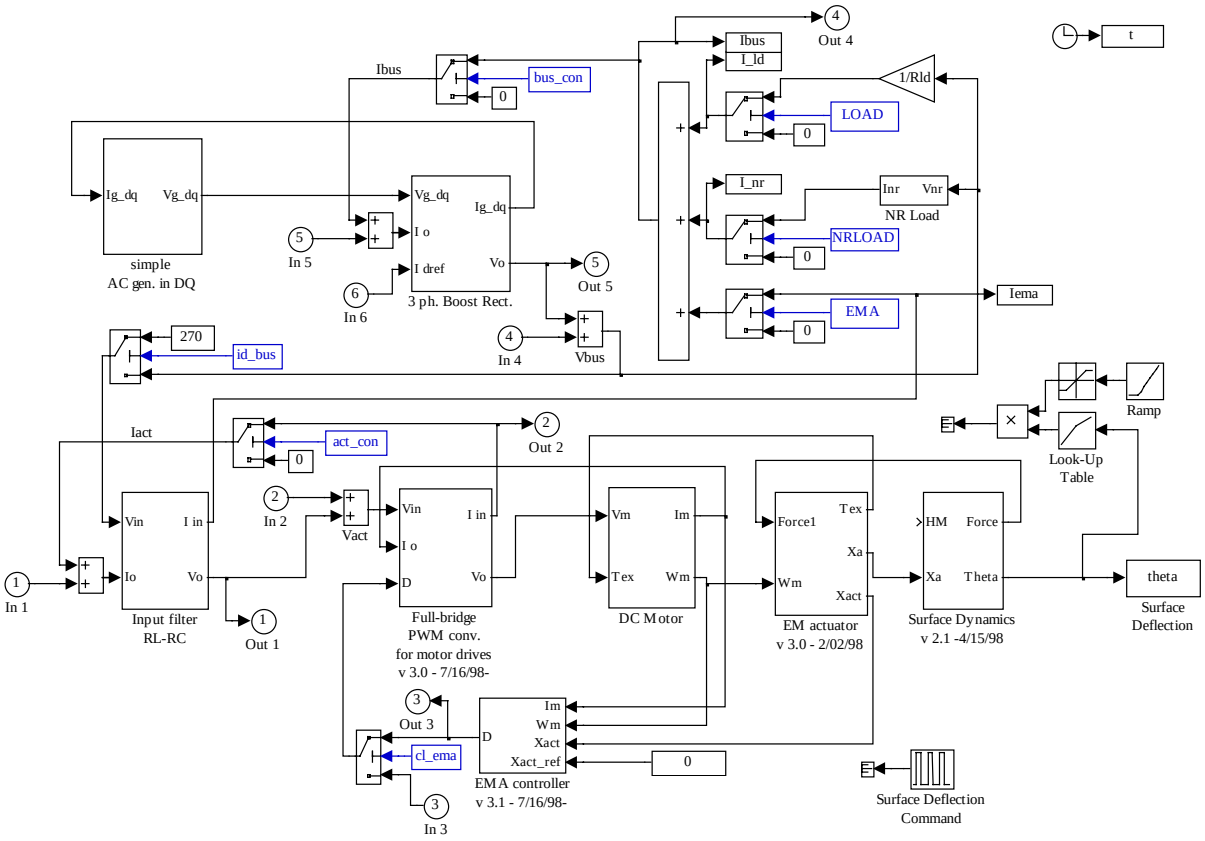

Figure D.1 Simulink model for linearization of the PDS.

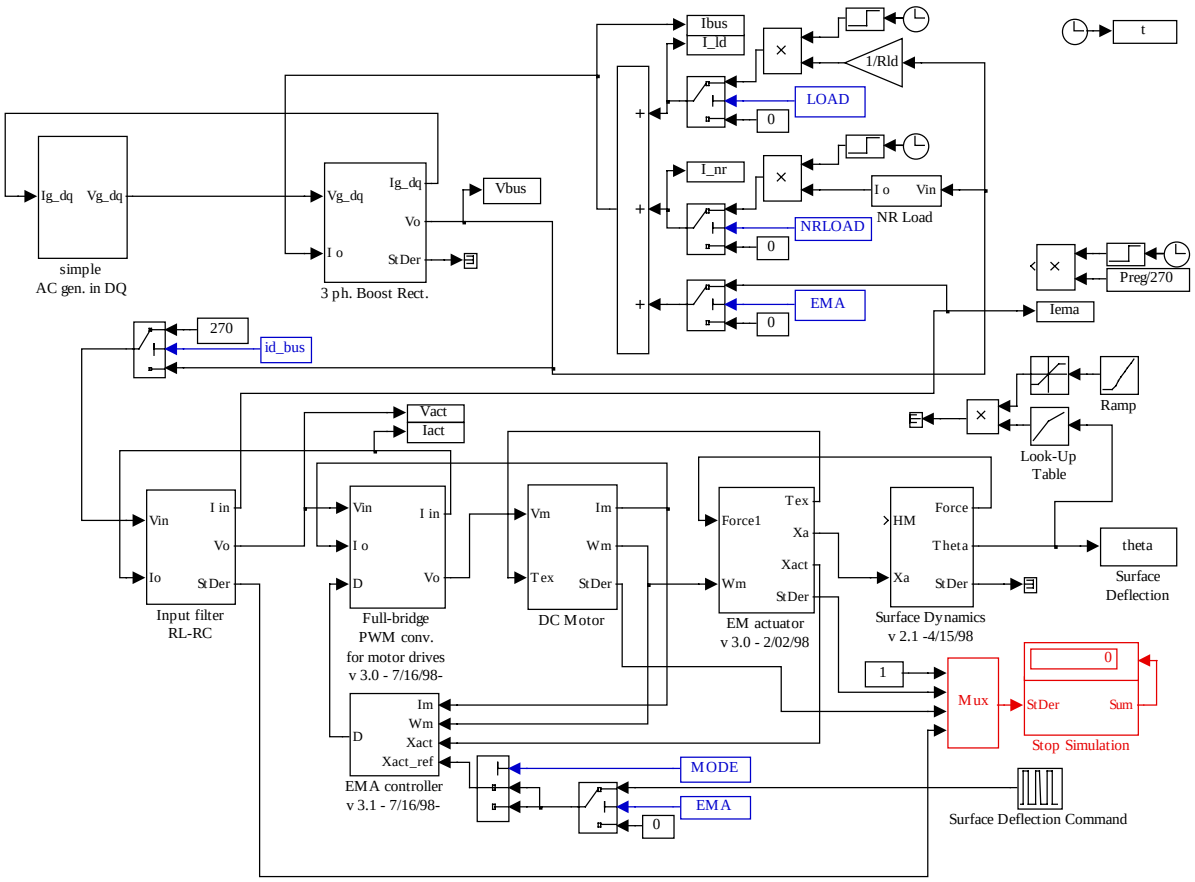

Figure D.2 Simulink model for simulation of the PDS.

D.2 MATLAB Files for Stability Analysis of the PDS

"analsys.m" – master m-file for analysis

```
% DC Power Distribution System analysis and simulation
% Stability Analysis

% Required supplementary files:
%   sysg.mdl       - Simulink model for simulation
%   sysg_lin.mdl   - Simulink model for linearization
%   emaparam.m     - EMA & DC motor parameter m-file
%   plotsimul      - m-file for plotting the simulation results
%   operpoint      - m-file for preparing oper. point info for 'linmod' command


% SYSTEM PARAMETERS
% =================

% Simple generator in DQ

Eg_d = 200;
Eg_q = 0;
Rg = 0.01;         % one phase resistance
w = 2*pi*60;       % Generator frequency

% Three-phase - to - DC bidirectional converter

Vrref   =   270;
Lbr     =   18e-06;
Cbr     =   350e-06;   % Output filter Capacitance
Rcbr    =   0.01;      % Output cap. ESR
fs      =   20e3;      % switching frequency
Kdq = 0.5*3*Lbr*2*pi*fs/Vrref;
Kpbr    =   1;         % Compensator - proportional gain
Kibr    =   3000;      % Compensator - integral gain
Iqref   =   0;         %

%% RESISTIVE (positive) LOAD %%

Po = 160e3;        % nominal output power (resistive load)
Rld = Vrref^2/Po;

%% NEGATIVE RESISTANCE (CONSTANT POWER) LOAD %%

Pnr = 200e3;       % 200kW const. power load (R = -Vbus^2/Pnr)

%% EMA INPUT FILTER %%

Li = 300e-6;
Ci = 25e-6;
Rli = 0.22;
Rci = 0.01;

% EMA parameters

emaparam       % EMA & DC motor parameters m-file
Preg = 80e3;   % current source load

% Simulation parameters
decim = 1;     % output to workspace decimation
dur = 25e-1;

% TYPE OF ANALYSIS:    MODE = 1   - time-domain simulation
%                             2   - obtaining an equilibrium point by simulation
%                             3   - linearization
```

```
sim_model = 'sysg';           % Simulink model for simulation
lin_model = 'sysg_lin';       % Simulink model for linearization

format compact
%%%%%%%%%%%%%%%%%%%%%%%%  ANALYSIS SPECIFICATIONS  %%%%%%%%%%%%%%%%%%%%
eq_file   = 'sysg001_022_eq01';   % ".MAT" file for saving an equilibr. point

MODE     = 3

LOAD    = 0        % 0/1 - off/on
NRLOAD  = 0
EMA     = 1        % 0/1 - off/on
id_bus  = 0        % 0/1 - real bus/ideal bus (270V)

% Switches work only for linearization:
cloop      = 0;    % 0/1 - open/closed BR Vo feedback loop
bus_con    = 0;    % 0/1 - disconnected/connected Ibus and BR Io
act_con    = 0;    % 0/1 - disconnected/connected Iact and IF Io
cl_ema     = 0;    % 0/1 - open/closed EMA control loop
ema_op12   = 1;    % EMA current loop
ema_op3    = 0;    % EMA speed loop

if  MODE == 2, dur=0.5005;
end
% OP1=0.505; OP2=0.52; OP3=1.0; OP4=1.1471;
%%%%%%%%%%%%%%%%%%%%%%%%%%%%%%%%%%%%%%%%%%%%%%%%%%%%%%%%%%%%%%%%%%%%%%%%%%%
format loose

INP=input('Proceed with analysis? ("y"=yes)  ','s');
if INP ~= 'y' & INP ~= 'Y'
error('OK. Parameters loaded.')
end


switch MODE

case {1,2}     % SIMULATION

% Simulation options
    set_param(sim_model,'SaveFinalState','on');
    set_param(sim_model,'FinalStateName','xFinal');
    options1 = simset('Solver','ode15s','RelTol',1e-5,'AbsTol',1e-7);
    [t] = sim(sim_model,dur,options1);

if MODE == 2       % EQUILIBRIUM POINT

% Save the order of states in the Simulink model:

    [sizes,xinit,xstring] = eval(sim_model);
    storder = char(xstring);
    [nrows,ncols] = size(storder);
    st_ord = storder(:,length(sim_model)+1:ncols);

% Save the equilibrium point (states and inputs)

    st_vect = xFinal';
    Iact_0  = Iact(length(t));
    Vact_0  = Vact(length(t));
    D_0     = D(length(t));
    Vbus_0  = Vbus(length(t));
    Ibus_0  = Ibus(length(t));
    Idref_0 = Idref(length(t));

    save (eq_file, 'sim_model', 'dur', 'st_ord', 'st_vect', '*_0')

end    % end of 'if MODE == 2' statement


% Plotting the time history

plotsimul      % run m-file for plotting the simulation results
```

```
%%%%%%%%%%%%%%%%%%%%%%%%%%%%%%%%%%%%%%%%%%%%%%%%%%%%%%%%%%%%%%%%%%%%%%%

case 3         % LINEARIZATION

%%%%%%%%%%%%%%%%%%%%%%%%%%%%%%%%%%%%%%%%%%%%%%%%%%%%%%%%%%%%%%%%%%%%%%%

% Obtaining the state vector and input vector for linearization

operpoint      % calling m-file

wv = logspace(-1,7,8*400);% frequency range for plotting t.f.

% Set the input vector according to the "lin_model":
% Vbus must be connected to BR Vo
% Set to zero dc values of the inputs supplied from other parts of the system

if cl_ema == 1, D_0 = 0; end         % don't care
Vbus = 0;                            % important!
if bus_con == 1,   Ibus_0 = 0; end   % important!
if cloop == 1, Idref_0 = 0; end      % don't care

% Obtaining a linearized model:

input_vect = [Iact_0 Vact_0 D_0 Vbus_0 Ibus_0 Idref_0]';

[Af2,Bf2,Cf2,Df2] = linmod(lin_model,st_vect1,input_vect);
system = ss(Af2,Bf2,Cf2,Df2);

%%%%%%%%%%%%%%%%% MODELING SCENARIO w/o EMA %%%%%%%%%%%%%%%%%%%%%%%%%
%%%%%%%%%%%%%%%%%%%%%%%%%%%%%%%%%%%%%%%%%%%%%%%%%%%%%%%%%%%%%%%%%%%%%%%
% Zobr must be obtained w/ current load (not resistive);
% Ibus must be disconnected to obtain Zibus correctly.

if EMA == 0,       % modeling scenario w/o EMA

if cloop == 0,     % open loop (BR feedback)
if bus_con == 0,       % Ibus disconnected
  Yi_bus = system(4,4); [num,den] = tfdata(Yi_bus);
  Zi_bus = tf(den,num);   %%% Zi of the bus looking from BR (incl. EMA and all connected loads)

  vo_idref = system(5,6);     %%% BR vo/idref t.f. (current load) %%%
  Tbr = vo_idref*tf([Kpbr Kibr],[1 0]);  %%% BR Loop Gain t.f. (current load)%%%
  figure
  [magn,phas] = bode(vo_idref,wv);
  magdb=wv; magdb(:)=20*log10(magn(1,1,:));  phase=wv; phase(:)=phas(1,1,:);
  [magn,phas] = bode(Tbr,wv);
  magdb1=wv; magdb1(:)=20*log10(magn(1,1,:));  phase1=wv; phase1(:)=phas(1,1,:);
  subplot(211)
  semilogx(wv,magdb,'-',wv,magdb1,'--'); grid on
  ylabel('Magnitude (dB)'); title('BR vo/idref t.f. (-), BR Loop Gain t.f. (--) (current load)');
  subplot(212)
  semilogx(wv,phase,'-',wv,phase1,'--'); grid on
  ylabel('Phase (deg)');  xlabel('Frequency (rad/sec)')

  Zo_ol = -system(5,5);       %%% BR output impedance w/ current load (open loop)
  Zo_br = Zo_ol/(1+Tbr);  %%% Cl. Loop BR Output Imped. (analytically)
  figure
  [magn,phas] = bode(Zi_bus,wv);  %% Zi_bus obtained with bus_con=0 %%
  magdb=wv; magdb(:)=20*log10(magn(1,1,:));  phase=wv; phase(:)=phas(1,1,:);
  [magn,phas] = bode(Zo_br,wv);
  magdb1=wv; magdb1(:)=20*log10(magn(1,1,:));  phase1=wv; phase1(:)=phas(1,1,:);
  subplot(211)
  semilogx(wv,magdb,'-',wv,magdb1,'--'); grid on
  ylabel('Magnitude (dB)'); title('Bus (Loads only) Zi (-), BR Closed Loop Zo (--)');
  subplot(212)
  semilogx(wv,phase,'-',wv,phase1,'--'); grid on
  ylabel('Phase (deg)');  xlabel('Frequency (rad/sec)')

  figure          %%% Nyquist Plot of the Impedance Ratio %%%
```

```
  nyquist(Zo_br/Zi_bus,wv); grid
  title('BR -- Impedance Ratio T1 = Zo br / Zi bus');
else                  % Ibus connected
  % Currently nothing is specified here
end    % end 'if bus_con'

else       % closed loop (BR feedback)
if bus_con == 0,       % bus disconnected
  Yi_bus = system(4,4); [num,den] = tfdata(Yi_bus);  %the same as w/ open loop
  Zi_bus = tf(den,num);   %%% Zi of the bus looking from BR (incl. EMA and all connected loads)

  Zo_br = -system(5,5);       %%% BR output impedance w/ current load (closed loop)
  figure
  [magn,phas] = bode(Zi_bus,wv);
  magdb=wv; magdb(:)=20*log10(magn(1,1,:));  phase=wv; phase(:)=phas(1,1,:);
  [magn,phas] = bode(Zo_br,wv);
  magdb1=wv; magdb1(:)=20*log10(magn(1,1,:));  phase1=wv; phase1(:)=phas(1,1,:);
  subplot(211)
  semilogx(wv,magdb,'-',wv,magdb1,'--'); grid on
  ylabel('Magnitude (dB)'); title('Bus (Loads only) Zi (-), BR Closed Loop Zo (--)');
  subplot(212)
  semilogx(wv,phase,'-',wv,phase1,'--'); grid on
  ylabel('Phase (deg)');  xlabel('Frequency (rad/sec)')

  figure          %%% Nyquist Plot of the Impedance Ratio %%%
  nyquist(Zo_br/Zi_bus,wv); grid
  title('BR -- Impedance Ratio T1 = Zo br / Zi bus');
else                  % Ibus connected
  % Currently nothing is specified here
end    % end 'if bus_con'

end    % end 'if cloop'
end    % end 'if EMA == 0'


%%%%%%%%%%%%%%%%% MODELING SCENARIO with EMA %%%%%%%%%%%%%%%%%%%%%%%%%
%%%%%%%%%%%%%%%%%%%%%%%%%%%%%%%%%%%%%%%%%%%%%%%%%%%%%%%%%%%%%%%%%%%%%%
%
if EMA == 1,       % modeling scenario with EMA

if id_bus==0, bus_con=1; cloop=1; end %if real bus, close all BR switches
Zo_if = -system(1,1);     %%% IF Zo; 'minus' to get positive impedance
Yi_ema = system(2,2); [num,den] = tfdata(Yi_ema);
Zi_ema = tf(den,num);         %%% EMA Zi (w/o input filter)
figure                    %%% Filter Zo and Actuator Zin t.f. %%%
[magn,phas] = bode(Zi_ema,wv);
magdb=wv; magdb(:)=20*log10(magn(1,1,:));  phase=wv; phase(:)=phas(1,1,:);
[magn,phas] = bode(Zo_if,wv);
magdb1=wv; magdb1(:)=20*log10(magn(1,1,:));  phase1=wv; phase1(:)=phas(1,1,:);
subplot(211)
semilogx(wv,magdb,'-',wv,magdb1,'--'); grid on
ylabel('Magnitude (dB)');
  if cl_ema==0, title('Filter Z_o and Actuator Z_i_n (Open Loop)');
  else title('Filter Z_o and Actuator Z_i_n (Closed Loop)');
  end
subplot(212)
semilogx(wv,phase,'-',wv,phase1+360,'--'); grid on
ylabel('Phase (deg)');  xlabel('Frequency (rad/sec)')

if cl_ema == 0,
  T = system(3,3);    %%% EMA Control-to-Duty Cycle (-Loop gain) t.f. %%%
  figure
  [magn,phas] = bode(T,wv);
  magdb=wv; magdb(:)=20*log10(magn(1,1,:));  phase=wv; phase(:)=phas(1,1,:);
  subplot(211)
  semilogx(wv,magdb,'-'); grid on
  ylabel('Magnitude (dB)');  title('Control-to-Duty Cycle t.f.');
  subplot(212)
  semilogx(wv,phase,'-'); grid on
  ylabel('Phase (deg)');  xlabel('Frequency (rad/sec)')
```

```
  Av_if = system(1,4); % IF forward voltage (reverse current) t.f.
  figure                  %%% IF Forward Voltage t.f. (unloaded) %%%
  [magn,phas] = bode(Av_if,wv);
  magdb=wv; magdb(:)=20*log10(magn(1,1,:));  phase=wv; phase(:)=phas(1,1,:);
  wsw = 2*pi*20e3;
  subplot(211)
  semilogx(wv,magdb,'-',wsw,interp1(wv,magdb,wsw),'ro'); grid on
  ylabel('Magnitude (dB)');  title('Forward Voltage t.f.');
  subplot(212)
  semilogx(wv,phase,'-',wsw,interp1(wv,phase,wsw),'ro'); grid on
  ylabel('Phase (deg)');  xlabel('Frequency (rad/sec)')

  vo_idref = system(5,6);     %%% BR vo/idref t.f. %%%
  Tbr = vo_idref*tf([Kpbr Kibr],[1 0]);  %%% BR Loop Gain t.f. %%%
  figure
  [magn,phas] = bode(vo_idref,wv);
  magdb=wv; magdb(:)=20*log10(magn(1,1,:));  phase=wv; phase(:)=phas(1,1,:);
  [magn,phas] = bode(Tbr,wv);
  magdb1=wv; magdb1(:)=20*log10(magn(1,1,:));  phase1=wv; phase1(:)=phas(1,1,:);
  subplot(211)
  semilogx(wv,magdb,'-',wv,magdb1,'--'); grid on
  ylabel('Magnitude (dB)'); title('BR vo/idref t.f. (-), BR Loop Gain t.f. (--)');
  subplot(212)
  semilogx(wv,phase,'-',wv,phase1,'--'); grid on
  ylabel('Phase (deg)');  xlabel('Frequency (rad/sec)')

  Yi_bus = system(4,4); [num,den] = tfdata(Yi_bus);
  Zi_bus = tf(den,num);       % Zi of the bus looking from BR
                              % (incl. EMA and all connected loads)
  Zo_ol = -system(5,5);       % BR output impedance (open loop)
  Zo_br = Zo_ol/(1+Tbr);  % Cl. Loop BR Output Imped. (analytically)
  figure
  [magn,phas] = bode(Zi_bus,wv);
  magdb=wv; magdb(:)=20*log10(magn(1,1,:));  phase=wv; phase(:)=phas(1,1,:);
  [magn,phas] = bode(Zo_br,wv);
  magdb1=wv; magdb1(:)=20*log10(magn(1,1,:));  phase1=wv; phase1(:)=phas(1,1,:);
  subplot(211)
  semilogx(wv,magdb,'-',wv,magdb1,'--'); grid on
  ylabel('Magnitude (dB)'); title('Bus (Loads + IF only) Zi (-), BR Closed Loop Zo (--)');
  subplot(212)
  semilogx(wv,phase,'-',wv,phase1,'--'); grid on
  ylabel('Phase (deg)');  xlabel('Frequency (rad/sec)')

else       % closed loop
  figure
  nyquist(Zo_if/Zi_ema,wv); grid
  title('EMA -- Impedance Ratio T1 = Zo if / Zi ema');

end    % end 'if cl_ema == 0'
end    % end 'if EMA == 1'

end    % end of 'switch MODE' operator
```

“emaparam.m” – EMA and DC Motor Parameters

```
% EMA parameters file (by Lockheed Martin Control Systems)
%
% Inboard Spoiler Surface Parameters

Kp      = 76;          % V/V
wlim    = 6.8;         % V

Kv      = 122.5;       % V/V
Hp      = 1.6;         % V/in
Hv      = 0.00382;     % V/(rad/sec)
Jm      = 2.43e-4;     % in-lb-sec^2
Bm      = 3.125e-4;    % in-lb-sec
N       = 249.6*pi;    % rad/in
Kact    = 9e5;         % lbf/in
Mp      = 5.43e-3;     % lbf-sec^2/in
Bp      = 15;          % lbf-sec/in
Jsur    = 36.2;        % in-lb-s^2
Bsur    = 1702;        % in-lb-s
h       = 4.9;         % in
Kl      = 1e6;         % in-lb/rad
Kr      = 5e5;         % in-lb/rad

% BDC Motor Parameters

Ka      = 20;          % V/V
L       = 0.00045;     % H
R       = 0.5;         % Ohms
Kt      = 1.141;       % in-lbf/amp
Ke      = 0.129;       % V/(rad/sec)
Ilim    = 19.3;        % Amp
Hi      = 0.25;        % V/A
Nmech   = 0.85;
```

“plotsimul.m” – Plotting Simulation Results

```
% Plotting simulation results

% SYSTEM
    figure
    spmax=4;
    subplot(spmax,1,1)
    plot(t,Vbus);  grid
    ylabel('Vbus (V)')
    title('Boost Rectifier and DC Bus')

    subplot(spmax,1,2)
    plot(t,Ibus);  grid
    ylabel('Ibus (A)')

    subplot(spmax,1,3)
    plot(t,D_dq,t,D);  grid
    ylabel('D dq, D')

    subplot(spmax,1,4)
    plot(t,Pg/1000,t,Vbus.*Ibus/1000);  grid
    ylabel('Pg, Pbus (kW)')
    xlabel('time (sec)')
    zoom

if EMA == 1,   % EMA
    figure
    spmax=5;
    subplot(spmax,1,1)
    plot(t,Vm,t,Vact);  grid
```

```
    ylabel('Vm, Vact (V)')
    title('Electromechanical Actuator')

    subplot(spmax,1,2)
    plot(t,Im,t,Ibus);  grid
    ylabel('Im (A), Ibus (A)')

    subplot(spmax,1,3)
    plot(t,Vm.*Im/1000);  grid
    ylabel('Pm (kW)')

    subplot(spmax,1,4)
    plot(t,Wm);  grid
    ylabel('Wm (rad/s)')

    subplot(spmax,1,5)
    plot(t,theta*180/pi);  grid
    ylabel('theta (deg)')
    xlabel('time (sec)')
    zoom
end    % end 'if EMA'
```

"operpoint.m" – obtaining the operating point for linearization

```
% Obtaining the state vector and input vector saved in file
% for linearization of the model 'lin_model'


clear  st_ord st_vect st_vect1 *_0

load (eq_file)        % load equilib. point into the workspace

% Obtain the order of states in the model for linearization:

    [sizes,xinit,xstring] = eval(lin_model);
    storder = char(xstring);
    [nrows,ncols] = size(storder);
    st_ord1 = storder(:,length(lin_model)+1:ncols);

% Sort the state variables according to the new order:

    for xrow1 = 1:nrows,
      for xrow = 1:nrows,
          if st_ord1(xrow1,:) == st_ord(xrow,:)
            st_vect1(xrow1) = st_vect(xrow); break
          elseif xrow == nrows
            error('ERROR !!!  MODELS OR BLOCK NAMES ARE NOT IDENTICAL !!!')
          end  % end of the 'if' statement
      end      % end of the 'for xrow' statement
    end        % end of the 'for xrow1' statement

    st_vect1 = st_vect1';
```

Appendix E

MATLAB Code for Bidirectional Power Flow Analysis in the DC Power Distribution System

E.1 Simulink Model for Parametric Sweep Analysis of the PDS

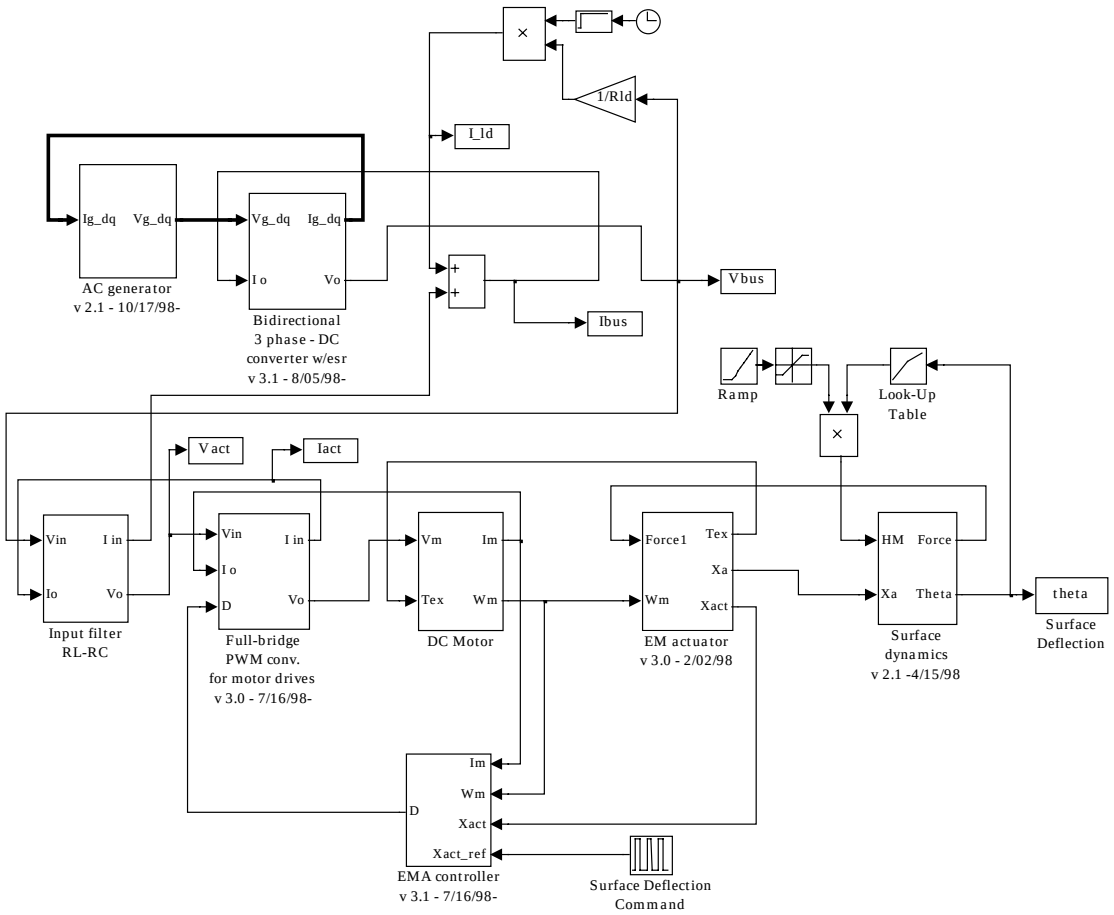

Figure E.1 Simulink model for bidirectional power flow analysis in the PDS.

E.2 MATLAB Files for Parametric Sweep Analysis of the PDS

"sweepsys.m" – Running the Simulation

```
% Parametric sweep simulation
% Bidirectional Power Flow Analysis

% Required supplementary files:
%   model_name.mdl - Simulink model of the system
%   sysgen_par.m   - synchronous generator parameter m-file
%   emaparam.m - EMA & DC motor parameter m-file
%   spikes.m   - simulation results analysis
%   syspower.m - power flow analysis

clear all      % clear the workspace
close all      % close all windows

% SYSTEM PARAMETERS
% =================

% Synchronous Generator

syngen_par         % gen. parameters m-file
Vgref=100;
Kgref=1000;

% Three-phase - to - DC bidirectional converter

Vm  =   200;           % input voltage
Vrref   =   270;
Lbr =   18e-06;
Rbr =   0.2;           % BR inductor ESR in DQ
Cbr =   350e-06;       % Output filter Capacitance
Rcbr    =   0.01;      % Output cap. ESR
fs  =   20e3;          % switching frequency
Kdq = 0.5*3*Lbr*2*pi*fs/Vrref;
Iqref   =   0;

%% INPUT FILTER %%

Li  = 1e-5;
Rli = 0.1;
Ci  = 63e-6;
Rci = 0.01;

%% RESISTIVE LOAD %%

Rld = 72.9;% 1kW load

% EMA parameters

emaparam       % EMA & DC motor parameters m-file

% PARAMETRIC SWEEP SIMULATION
% ===========================

% Data for analysis
deltav = 2;% allowable bus voltage deviation for settling time calc.
Vbref = Vrref;
Vsp1max=[]; Vsp1min=[]; ts1=[];      % voltage spikes magn. and settling time
Vsp2max=[]; Vsp2min=[]; ts2=[];
Vsp3max=[]; Vsp3min=[]; ts3=[];
Vsp4max=[]; Vsp4min=[]; ts4=[];

Wbusp=[]; Wbusn=[]; buseff=[];
Wldp=[];  Wldn=[];  loadeff=[];
```

```
Wactp=[]; Wactn=[]; acteff=[];
Wbrp=[];  Wbrn=[];  breff=[];
Wcifp=[]; Wcifn=[]; cifeff=[];
Wifp=[];  Wifn=[];  ifeff=[];
Wcbrp=[]; Wcbrn=[]; cbreff=[];
Wwindp = []; Wwindn = [];
Wactel = [];
Wactm = [];

Wgmp=[];  Wgmn=[];
Wgp=[];  Wgn=[];
Wfip=[];  Wfin=[];
Wtot=[];
Wgls=[]; Wglk=[]; Wglf=[]; Wgl=[];

% Sweep parameter

par_name = 'Cbr';  % specify here the parameter to be swept
beg_val = 350e-06;
end_val = 0.8;
num_val = 20;

par_vect = logspace(log10(beg_val),log10(end_val),num_val);
par_vect = str2num(num2str(par_vect));

%pltype = 0;   % plotting with a linear x-scale
pltype = 1;    % plotting with a logarithmic x-scale

% Simulation parameters
dur=25e-1;
decim = 1;     % output to workspace decimation

cycle_number = 0;

    for par_val = par_vect;
    cycle_number = cycle_number+1
    assignin('base',par_name,par_val);
    eval(par_name)

    options1 = simset('Solver','ode15s','RelTol',1e-3,'AbsTol',1e-4);
    sim('sysgen11a',dur,options1);

    spikes
    syspower2

% PLOTTING THE RESULTS
% ====================

    figure
    spmax=5;
    subplot(spmax,1,1)
    plot(t,Vbus)
    grid
    ylabel('Vbus (V)')

    subplot(spmax,1,2)
    plot(t,Vbus.*Ibus/1000)
    grid
    ylabel('Pbus (kW)')

    subplot(spmax,1,3)
    plot(t,Im)
    grid
    ylabel('Im (A)')

    subplot(spmax,1,4)
    plot(t,theta*180/pi)
    grid
   ylabel('theta (deg)')

    subplot(spmax,1,5)
```

```
    plot(t,Xaref)
    grid
    ylabel('Xaref (in)')

    xlabel('time (sec)')
    zoom on

    end

 % Saving the data for future use

save brcap20 par_name par_vect cycle_number pltype Vsp* Vbref ts* Wtot Wg* Wbus* Wfi*…
       Wact* Wwind*
```

"syngen_par.m" – Synchronous Generator Parameters

```
% Synchronous generator parameter file
% Parameters in DQ coordinate frame

Rs      = 0.09113;     % armature phase resistance
Lls     = 0.9e-3;      % armature phase leakage inductance

Lmd     = 43e-3;       % d axis coupling inductance
Lmq     = 21e-3;       % q axis coupling inductance

Rfd     = 0.018;       % field winding resistance (refl. to stator)
Llfd    = 3.4e-3;      % field winding leakage inductance (refl. to stator)

Rkd     = 0.08;        % d axis damper winding resistance (refl. to stator)
Rkq     = 0.08;        % q axis damper winding resistance (refl. to stator)
Llkd    = 0.16e-3;     % d axis damper winding leak. induct. (refl. to stator)
Llkq    = 0.35e-3;     % q axis damper winding leak. induct. (refl. to stator)

w       = 2*pi*60;     % rotor speed
Ra      = 1e5;         % additional resistance
Vfd     = 1;           % field voltage (refl. to stator)

% State space matrices

Agtmp=zeros(5);

Agtmp(1,1) = -Lls-Lmd;
Agtmp(1,3) = Lmd;
Agtmp(1,5) = Lmd;
Agtmp(2,2) = -Lls-Lmq;
Agtmp(2,4) = Lmq;
Agtmp(3,1) = -Lmd;
Agtmp(3,3) = Lmd;
Agtmp(3,5) = Llfd+Lmd;
Agtmp(4,1) = -Lmd;
Agtmp(4,3) = Llkd+Lmd;
Agtmp(4,5) = Lmd;
Agtmp(5,2) = -Lmq;
Agtmp(5,4) = Llkq+Lmq;

Bg1 = zeros(5);

Bg1(1,1) = Ra+Rs;
Bg1(1,2) = -w*(Lls+Lmq);
Bg1(1,4) = w*Lmq;
Bg1(2,1) = w*(Lls+Lmd);
Bg1(2,2) = Ra+Rs;
Bg1(2,3) = -w*Lmd;
Bg1(2,5) = -w*Lmd;
Bg1(3,5) = -Rfd;
Bg1(4,3) = -Rkd;
Bg1(5,4) = -Rkq;
```

```
Bg2 = zeros(5,3);

Bg2(1,1) = -Ra;
Bg2(2,2) = -Ra;
Bg2(3,3) = 1;

Ag = inv(Agtmp)*Bg1;
Bg = inv(Agtmp)*Bg2;

Cg = zeros(7,5);
Cg(1,1) = Ra;
Cg(2,2) = Ra;
Cg(3:7,:) = eye(5);

Dg = zeros(7,3);
Dg(1,1) = -Ra;
Dg(2,2) = -Ra;
```

"emaparam.m" – EMA and DC Motor Parameters

```
% EMA parameters file (by Lockheed Martin Control Systems)
%
% Inboard Spoiler Surface Parameters

Kp      = 76;          % V/V
wlim    = 6.8;         % V

Kv      = 122.5;       % V/V
Hp      = 1.6;         % V/in
Hv      = 0.00382;     % V/(rad/sec)
Jm      = 2.43e-4;     % in-lb-sec^2
Bm      = 3.125e-4;    % in-lb-sec
N       = 249.6*pi;    % rad/in
Kact    = 9e5;         % lbf/in
Mp      = 5.43e-3;     % lbf-sec^2/in
Bp      = 15;          % lbf-sec/in
Jsur    = 36.2;        % in-lb-s^2
Bsur    = 1702;        % in-lb-s
h       = 4.9;         % in
Kl      = 1e6;         % in-lb/rad
Kr      = 5e5;         % in-lb/rad

% BDC Motor Parameters

Ka      = 20;          % V/V
L       = 0.00045;     % H
R       = 0.5;         % Ohms
Kt      = 1.141;       % in-lbf/amp
Ke      = 0.129;       % V/(rad/sec)
Ilim    = 19.3;        % Amp
Hi      = 0.25;        % V/A
Nmech   = 0.85;
```

"spikes.m" – Calculation of the DC Bus Power Quality Characteristics

```
% Analysis of voltage spikes on DC bus obtained from simulation
%
%       t    -- time vector
%       Vbus -- DC bus voltage

t1beg = 0.5;                  % beginning of the time interval #1
t1end = 0.8;                  % end of the time interval #1
ind1 = find(t>=t1beg & t<=t1end)';       %vector of indices in the time span
Vsp1max = [Vsp1max max(Vbus(ind1))]; % max voltage during the transient
Vsp1min = [Vsp1min min(Vbus(ind1))]; % min voltage during the transient
ind1pos = find(Vbus(ind1)>(Vbref+deltav))';
ind1neg = find(Vbus(ind1)<(Vbref-deltav))';
ind1pn = [ind1pos ind1neg];
if isempty(ind1pn), ind1pn = 0; end
ts1 = [ts1 t(min(ind1)+max(ind1pn))-t(min(ind1)+min(ind1pn))];  % settling time

t2beg = 1.0;                  % beginning of the time interval #2
t2end = 1.4;                  % end of the time interval #2
ind2 = find(t>=t2beg & t<=t2end)';       %vector of indices in the time span
Vsp2max = [Vsp2max max(Vbus(ind2))];
Vsp2min = [Vsp2min min(Vbus(ind2))];
ind2pos = find(Vbus(ind2)>(Vbref+deltav))';
ind2neg = find(Vbus(ind2)<(Vbref-deltav))';
ind2pn = [ind2pos ind2neg];
if isempty(ind2pn), ind2pn = 0; end
ts2 = [ts2 t(min(ind2)+max(ind2pn))-t(min(ind2)+min(ind2pn))];  % settling time

t3beg = 1.5;                  % beginning of the time interval #3
t3end = 1.8;                  % end of the time interval #3
ind3 = find(t>=t3beg & t<=t3end)';       %vector of indices in the time span
Vsp3max = [Vsp3max max(Vbus(ind3))];
Vsp3min = [Vsp3min min(Vbus(ind3))];
ind3pos = find(Vbus(ind3)>(Vbref+deltav))';
ind3neg = find(Vbus(ind3)<(Vbref-deltav))';
ind3pn = [ind3pos ind3neg];
if isempty(ind3pn), ind3pn = 0; end
ts3 = [ts3 t(min(ind3)+max(ind3pn))-t(min(ind3)+min(ind3pn))];  % settling time

t4beg = 2.0;                  % beginning of the time interval #4
t4end = 2.4;                  % end of the time interval #4
ind4 = find(t>=t4beg & t<=t4end)';       %vector of indices in the time span
Vsp4max = [Vsp4max max(Vbus(ind4))];
Vsp4min = [Vsp4min min(Vbus(ind4))];
ind4pos = find(Vbus(ind4)>(Vbref+deltav))';
ind4neg = find(Vbus(ind4)<(Vbref-deltav))';
ind4pn = [ind4pos ind4neg];
if isempty(ind4pn), ind4pn = 0; end
ts4 = [ts4 t(min(ind4)+max(ind4pn))-t(min(ind4)+min(ind4pn))];  % settling time
```

"syspower2.m" – Bidirectional Power Flow Analysis

```
% Analysis of power flow in the system obtained from simulation
%

tmin = 0.5;% beginning of the actuator operating cycle
tmax = 2.5;% end of the actuator operating cycle

ind = find(t>=tmin & t<=tmax);    %vector of indices in the time span
tnew = t(ind);

%%%%%%%%%%%%%%%%%%%%%%%%%%%%%% GENERATOR %%%%%%%%%%%%%%%%%%%%%%%%%%
% Generator losses

Pgls=(Ig_dq(:,1).^2 + Ig_dq(:,2).^2)*Rs*3/2; %losses in phase resistances
```

```
Pglk=((Ik_dq(:,1).^2)*Rkd + (Ik_dq(:,2).^2)*Rkq)*3/2; %losses in damper winding
Pglf=Ifd.^2*Rfd;                        % losses in the field winding
Pgl = (Pgls + Pglk + Pglf)*2;           % total generator losses
                                        % x2 to account for other types of losses
Pnew = Pgls(ind);
Wgls = [Wgls trapz(tnew,Pnew)];       % energy lost in phase resistances
Pnew = Pglk(ind);
Wglk = [Wglk trapz(tnew,Pnew)];       % energy lost in damper winding
Pnew = Pgls(ind);
Wglf = [Wglf trapz(tnew,Pnew)];       % energy lost in field winding
Pnew = Pgl(ind);
Wgl = [Wgl trapz(tnew,Pnew)];     % total energy lost in generator

% Energy coming from the engine   %***
Pgm = Pg + Pgl;                         % mech. power delivered to the generator
Pnew = Pgm(ind); Ppos = Pnew.*(Pnew>0); Pneg = Pnew.*(Pnew<0);
Wgmp = [Wgmp trapz(tnew,Ppos)];       %***    % positive energy
Wgmn = [Wgmn -trapz(tnew,Pneg)];      %***    % negative (regenerated) energy

%%%%%%%%%%%%%%% BOOST RECTIFIER %%%%%%%%%%%%%%%
% Energy flowing into the boost rectifier %***

Pnew = Pg(ind); Ppos = Pnew.*(Pnew>0); Pneg = Pnew.*(Pnew<0);
Wgp = [Wgp trapz(tnew,Ppos)];         %***    % positive energy
Wgn = [Wgn -trapz(tnew,Pneg)];        %***    % negative (regenerated) energy

% Energy coming from the boost rectifier to the load %***

Pbus = Vbus.*Ibus;
Pnew = Pbus(ind); Ppos = Pnew.*(Pnew>0); Pneg = Pnew.*(Pnew<0);
Wbusp = [Wbusp trapz(tnew,Ppos)];     %***    % positive energy
Wbusn = [Wbusn -trapz(tnew,Pneg)];    %***    % negative (regenerated) energy

%%%%%%%%%%%%%%%%%%%%%%% INPUT FILTER  %%%%%%%%%%%%%%%%%%%%%
% Energy coming into the filter from the DC bus  %***

Pfi = Vbus.*(Ibus-I_ld);
Pnew = Pfi(ind); Ppos = Pnew.*(Pnew>0); Pneg = Pnew.*(Pnew<0);
Wfip = [Wfip trapz(tnew,Ppos)];       %***    % positive energy
Wfin = [Wfin -trapz(tnew,Pneg)];      %***    % negative (regenerated) energy

%%%%%%%%%%%%%%%%%%%%%%%% ACTUATOR %%%%%%%%%%%%%%%%%%%%%%%%
% Energy coming from the input filter %***

Pact = Vact.*Iact;
Pnew = Pact(ind); Ppos = Pnew.*(Pnew>0); Pneg = Pnew.*(Pnew<0);
Wactp = [Wactp trapz(tnew,Ppos)];     %***    % positive energy
Wactn = [Wactn -trapz(tnew,Pneg)];    %***    % negative (regenerated) energy

%%%%%%%%%%%%%%%%%%%%%%%% AIR FLOW %%%%%%%%%%%%%%%%%%%%%%%%
Pwind = hm.*Wsur;
Pnew = Pwind(ind); Ppos = Pnew.*(Pnew>0); Pneg = Pnew.*(Pnew<0);
Wwindp = [Wwindp trapz(tnew,Ppos)];   % positive energy (passed to the wind)
Wwindn = [Wwindn -trapz(tnew,Pneg)];  % negative energy (received from the wind)
```

References

[1] J. A. Weimer, "Power Management and Distribution for the More Electric Aircraft," Proceedings of the 30th Intersociety Energy Conversion Engineering Conference, 1995, pp. 273-277.

[2] M. L. Maldonado, N. M. Shah, K. J. Cleek, P. S. Walia, G. Korba, "Power Management and Distribution System for a More Electric Aircraft (MADMEL) – Program Status," Proceedings of the 31st Intersociety Energy Conversion Engineering Conference, 1996, pp. 148-153.

[3] J. S. Cloyd, "A Status of the United States Air Force's More Electric Aircraft Initiative," Proceedings of the 32nd Intersociety Energy Conversion Engineering Conference, 1997, pp. 681-686.

[4] M. E. Elbuluk, M. D. Kankam, "Motor Drive Technologies for the Power-by-Wire (PBW) Program: Options, Trends, and Tradeoffs," Proceedings of the IEEE 1995 National Aerospace and Electronics Conference, NAECON'95, pp. 511-522.

[5] G. L. Fronista and G. Bradbury, "An Electromechanical Actuator for a Transport Aircraft Spoiler Surface," Proceedings of the 32nd Intersociety Energy Conversion Engineering Conference, 1997, pp.694-698.

[6] K.C. Reinhardt, M. A. Marciniak, "Wide-Bandgap Power Electronics for the More Electric Aircraft," Proceedings of the 31st Intersociety Energy Conversion Engineering Conference, 1996, pp. 127-132.

[7] R. A. Smith, H. J. Van Horn, "The J/IST of Improving JSF," Aerospace America, November 1997, pp. 20-22.

[8] "MIL-STD-704E. Aircraft Electric Power Characteristics." Military standard.

[9] J. G. Kassakian, M. F. Schlecht, G. C. Verghese, "Principles of Power Electronics," Addison-Wesley, 1991.

[10] The MathWorks, Inc., "MATLAB User's Guide,' The MathWorks, Inc., Natick, Mass., 1993.

[11] The MathWorks, Inc., "Simulink User's Guide,' The MathWorks, Inc., Natick, Mass., 1993.

[12] The MathWorks, Inc., “Control System Toolbox User’s Guide,” The MathWorks, Inc., Natick, Mass., 1993

[13] P. C. Krause, “Analysis of Electrical Machinery,” McGraw Hill, 1987.

[14] S. Hiti, D. Borojevic, “Small-Signal Modeling and Control of Three-Phase PWM Converters,” IEEE 1994 IAS Annual Meeting Proceedings, pp. 1143-1150.

[15] S. Hiti, D. Borojevic, “Control of Front-End Three-Phase Boost Rectifier,” APEC’94, pp. 927-933.

[16] E. Richter and C. Ferreira, “Performance Evaluation of a 250kW Switched Reluctance Starter/Generator,” IEEE 1995 IAS Annual Meeting Proceedings, pp. 434-440.

[17] A. V. Radun, C. A. Ferreira, E. Richter, “Two-Channel Switched Reluctance Starter/Generator Results,” IEEE Transactions on Industry Applications, vol. 34, no. 5, pp. 1026-1034.

[18] A. Radun, “Generating with the Switched Reluctance Motor,” IEEE APEC 1994 Annual Meeting Proceedings, pp. 41-47.

[19] A. Radun, J. Rulison, and P. Sanza, “Switched Reluctance Starter/Generator,” SAE Technical Papers, 1995, Paper No. 921974.

[20] C. R. Elliott, J. M. Stephenson, and M. J. McClelland, “Advances in Switched Reluctance Drive System Dynamic Simulation.” EPE 1995 Annual Meeting Proceedings, pp. 622-626.

[21] A. V. Radun and Y. Q. Xiang, “Switched Reluctance Starter/Generator System Modeling Results,” SAE Technical Papers, 1995, Paper No. 951407.

[22] C. A. Ferreira and W. D. Jones, “Detailed Design of a 30-kW Switched Reluctance Starter/Generator System for a Gas Turbine Engine Application,” IEEE Industry Applications Society Annual Meeting Proceedings, 1993, pp. 97-105.

[23] R. D. Middlebrook, “Input Filter Considerations in Design and Application of Switching Regulators,” IEEE Industry Applications Society Annual Meeting Proceedings, 1976, pp. 366-382.

[24] T. L. Skvarenina, S. Pekarek, O. Wasynczuk, P. C. Krause, “Simulation of a More-Electric Aircraft Power System Using an Automated State Model Approach,” Proceedings of the Intersociety Energy Conversion Engineering Conference, 1996, pp. 133-136.

[25] W. A. Tabisz, M. M. Jovanovic, F. C. Lee, “Present and Future of Distributed Power Systems,” Proceedings of the Applied Power Electronics Conference, 1992, pp. 11-18.

[26] B. H. Cho and B. Choi, “Analysis and Design of Multi-Stage Distributed Power Systems,” Proceedings of the Virginia Power Electronics Conference, 1991, pp. 55-62.

[27] D. M. Sable, B. H. Cho, and F. C. Lee, “Spacecraft Power System Compatibility and Stability for the NASA EOS Satellite,” Proceedings of the Intersociety Energy Conversion Engineering Conference, 1992.

[28] Y. V. Panov and F. C. Lee, ”Stability of a DC Power System with Solid State Power Controllers,” Proceedings of the Virginia Power Electronics Conference, 1995.

[29] C. M. Wildrick, F. C. Lee, B. H. Cho, B. Choi, “A Method of Defining the Load Impedance Specifications for a Stable Distributed Power System,” Proceedings of the Power Electronics Specialist Conference, 1993, pp. 826-832.

[30] Z. Mihailovic, “Modeling and Control Design of VSI-fed PMSM Drive Systems with Active Load,” M.S. Thesis, Blacksburg, VPI&SU, 1998.

[31] N. Mohan et al., “Simulation of Power Electronic and Motion Control Systems – An Overview,” IEEE Proceedings, August 1994, vol. 82, pp. 1287-1302.

Vita

The author, Konstantin P. Louganski, was born in Tuapse, Russia in 1964. He received his Electrical Engineer's degree in Electromechanics from Rostov Institute for Railroad Engineering, Rostov-on-Don, Russia in 1986. After graduation, he worked for railroad industry as a process engineer and a maintenance engineer of electrical and electronic equipment. In 1994, he enrolled in a post-graduate Electrical Engineering program in Moscow Automechanical Institute, Russia, where he worked on modeling and simulation of electric vehicles.

The author joined Virginia Power Electronics Center at Virginia Tech in 1997. As a graduate research assistant, he worked in the area of modeling and analysis of a DC power distribution system using MATLAB/Simulink software. He is planning to graduate with a Master of Science degree in Electrical Engineering in October 1999.